Applying unconventional secretion for the export of bivalent Sars-CoV2 nanobodies in *Ustilago maydis*

Inaugural Dissertation

For the attainment of the **title of doctor**
In the **Faculty of Mathematics and Natural Sciences**
At the **Heinrich Heine University Düsseldorf**

Presented by
Magnus Philipp
From Coesfeld, Germany
Düsseldorf, April 2022

From the Institute for Microbiology
in the Faculty of Mathematics and Natural Sciences
of the Heinrich Heine University Düsseldorf

Published by the permission of the
Faculty of Mathematics and Natural Sciences at
Heinrich Heine University Düsseldorf

Supervisor: Prof. Dr. Michael Feldbrügge
Institute for Microbiology
Heinrich Heine University Düsseldorf

Co-supervisor: Prof. Dr. Julia Frunzke
Institute for Bio- and Geosciences 1: Biotechnology
Forschungszentrum Jülich, Heinrich Heine University Düsseldorf

Date of oral examination: 14.07.2022

The research detailed in this thesis was conducted from July 2018 until April 2022 in Düsseldorf at the Heinrich Heine University Düsseldorf in the Institute for Microbiology under the supervision of Prof. Dr. Michael Feldbrügge.

Statutory declaration

I hereby declare that this dissertation is the result of my own work, taking into account the "Rules and principles for Saveguarding and Good Scientific Practice at Heinrich Heine University Düsseldorf". No other persons' work has been used without due acknowledgement. Further I assure that I did not use any other literature than the ones specified and cited. This dissertation has not been submitted in the same or similar form to other Institutions. I have not previously failed a doctoral examination procedure.

Eidesstattliche Erklärung

Ich versichere an Eides Statt, dass die Dissertation von mir selbstständig und ohne unzulässige fremde Hilfe unter Beachtung der „Grundsätze zur Sicherung guter wissenschaftlicher Praxis an der Heinrich-Heine-Universität Düsseldorf" erstellt worden ist. Keine andere Person wirkte an der Arbeit ohne entsprechende Nennung mit. Darüber hinaus versichere ich, dass keine Literatur außerhalb der genannten und zitierten Quellen genutzt wurde. Die Dissertation wurde in ihrer jetzigen oder ähnlichen Form noch bei keiner anderen Hochschule eingereicht. Ich habe zuvor keine erfolglosen Promotionsversuche unternommen.

Magnus Philipp

Düsseldorf, den 07.09.2022

Abstract

With an ever-rising demand for biopharmaceuticals, a versatile repertoire of protein production platforms to enable supply of tailor-made solutions for products is needed. Biosynthesis and secretion of functional biopharmaceuticals has previously been established in the microbial model *Ustilago maydis*. This was achieved by hitchhiking the unconventional secretion mechanism of chitinase Cts1. The pathway allows for the export of unglycosylated proteins circumventing the endomembrane system, which can be advantageous for bacterial targets or biopharmaceuticals to be used in humans. A positive side-effect of using Cts1 as a carrier is its ability to bind chitin which can be exploited for target protein purification or surface immobilization. However, yields of the expression system are not competitive and application of the immobilization capability has not been fully exploited, yet. In this study two strategies were followed towards utilizing of unconventional secretion for protein production and target-oriented application:

i) To enhance the repertoire of exported targets, a novel protein export carrier was established. Recent insights into the secretory mechanism of Cts1 revealed the putative anchoring factor Jps1 not only as a crucial player for Cts1 localization and secretion but also as a potential secretion target itself. To this end, Jps1 secretion was confirmed using β-glucuronidase as an established reporter, revealing up to 2.7-fold increased secretion compared to Cts1-mediated export. These findings were combined with the previously established inducible secretion system, further enhancing secretory yield. Additionally, export of functional luciferase and bivalent synthetic anti-Sars-CoV2 nanobodies was achieved with Jps1 as a carrier.

ii) With the aim to combine Sars-CoV2 detection and chitin immobilization of Cts1, further unconventionally secreted anti-Sars-CoV2 nanobody variants were studied in depth, starting with characterization of their production and export using Cts1 as a carrier. Two functional Cts1-fusions were tested for their capability of Sars-CoV2 capture and neutralization, revealing one construct capable of both. Subsequently an ELISA type Sars-CoV2 antigen test based on a chitin surface was successfully established, allowing for detection of Sars-CoV2 receptor binding domain in the nanomolar range. To further improve the virus detection system *U. maydis* derived nanobody variants were functionalized for direct detection utilizing peroxidase Apex2.

In summary, secretory yield and target variety could be increased utilizing Jps1 and functionalization of a chitin surface and nanobody-Cts1 fusions resulted in the development of a novel type of virus detection system.

Zusammenfassung

Durch die stetig steigende Nachfrage an biopharmazeutischen Proteinen, wird ein vielseitiges Repertoire an Proteinproduktionsplattformen benötigt, um die Versorgung maßgeschneiderte Produkte sicherzustellen. Biosynthese und Sekretion funktioneller biopharmazeutischer Proteine wurde bereits im mikrobiellen Modellorganismus *Ustilago maydis* etabliert. Dazu wurde der unkonventionelle Sekretionsmechanismus der Chitinase Cts1 ausgenutzt. Dieser Sekretionsweg ermöglicht den Export unglykosylierter Proteine, indem das Endomembransystem umgangen wird. Dies kann von Vorteil für den Export bakterieller- und biopharmazeutischer Proteine mit dem Ziel der Nutzung im Menschen sein. Eine weitere vorteilhafte Eigenschaft von Cts1 ist der Fakt, dass Cts1 Chitin bindet. Diese Eigenschaft kann für direkte Proteinaufreinigung und Immobilisierung genutzt werden. Allerdings ist die Ausbeute des Systems bis jetzt nicht kompetitiv und die Möglichkeiten der Cts1 Immobilisierung wurden noch nicht ausgeschöpft. In dieser Arbeit wurden zwei Strategien verfolgt, um unkonventionelle Sekretion für die Produktion und zielorientierte Anwendung von Proteinen zu nutzen:

i) Um das verfügbare Repertoire exportierbarer Ziele zu erhöhen, wurde ein neues Exportprotein etabliert. Neuste Erkenntnisse haben den potenziellen Ankerfaktor Jps1, nicht nur als notwendigen Bestandteil für die Lokalisierung und Sekretion von Cts1, sondern auch als potentiell sekretiertes Protein, identifiziert. Um diesen Aspekt näher zu beleuchten, wurde β-Glucuronidase mit Jps1 sekretiert, wodurch unkonventionelle Sekretion und 2.7-fach höhere Ausbeute im Vergleich zum Export mit Cts1 nachgewiesen werden konnten. In Kombination mit vorher etablierten induzierbaren Sekretionsstämmen konnte die Ausbeute weiter erhöht werden. Außerdem, konnten aktive Luciferase und ein bivalenter, synthetischer anti-Sars-CoV2 Nanokörper als Jps1 Fusionen sekretiert werden.

ii) Mit dem Ziel Sars-CoV2 Detektion mit Nanokörpern und Immobilisierung von Cts1 zu verbinden, wurden weitere mit Cts1 sekretierte anti-Sars-CoV2 Nanokörper Varianten grundlegend auf ihre Produktions- und Sekretionseigenschaften untersucht. Zwei funktionelle Cts1-Fusionsporteine wurden weiter auf ihre Fähigkeit Sars-CoV2 zu Binden und Neutralisieren untersucht, wobei ein Nanokörper beide Kriterien erfüllte. Basierend auf diesen Ergebnissen wurde ein ELISA-artiger Sars-CoV2 Antigentest auf eine Chitinoberfläche etabliert. Um dieses System weiter zu verbessern, wurden unkonventionell sekretierte Nanokörper Varianten mit der Peroxidase Apex2 fusioniert, um direkte Detektion des Antigens zu ermöglichen.

Zusammenfassend konnte die sekretorische Ausbeute erhöht und das Repertoir sekretierbarer Zielproteine durch die Nutzung von Jps1 erweitert werden. Des Weiteren konnte durch Verbindung einer Chitinoberfläche und Nanokörper-Cts1 Fusionen ein neuartiges Virusdetektionssystem etabliert werden.

Abbreviations

µg	Microgram	**M**	Molar
µl	Microliter	**mAb**	Monoclonal Antibody
µM	Micromolar	**Mers-CoV**	Middle eastern respiratory syndrome corona virus
ABC	ATP binding cassette	**Mg**	milligram
ACE2	Angiotensin-converting enzyme	**Min**	Minute
Ara	Arabinose	**Ml**	Milliliter
ATP	Adenosine triphosphate	**mM**	Mill molar
BfRAM	Bundesinstitut für Arzneimittel und Medizinprodukte	**mRNA**	Messenger ribonucleic acid
BSA	Bovine serum albumin	**Ng**	Nanogram
CBD	Chitin binding buffer detergent	**nM**	Nanomolar
cbx	Carboxin	**Nm**	Nanometer
CE	Cell extract	**NTA**	Nitrilotriacetic acid
C_H	Constant heavy domain	**NTD**	N-terminal domain
C_L	Constant light domain	**OD_{600}**	Optical density 600 nm
CM	Complete medium	**ORF**	Open reading frame
CoV	Corona virus	**PAGE**	Polyacrylamide gel electrophoresis
COVID-19	Coronavirus disease 2019	**PBS**	Phosphate buffered saline
CT	Cycle threshold	**PBS-T**	Phosphate buffered saline-Tween
Ctrl	Control	**PCR**	Polymerase chain reaction
DNA	Deoxyribonucleic acid	**Pdi**	Protein disulphide isomerase
DDP4	Dipeptidyl peptidase 4	**PMSF**	Phenylmethylsulfonylfluorid
DTT	Dithiothreitol	**PTS**	Peroxisomal targeting sequence
EDTA	Ethylenediaminetetraacetic acid	**RBD**	Receptor binding domain
EMEA	European Medicines agency	**RFU**	Relative fluorescence units
ER	Endoplasmic reticulum	**RNA**	Ribonucleic acid
Fab	Antigen binding Fragment	**RPC**	Relative photon count
FDA	Food and Drug administration (USA)	**RT-PCR**	Reverse transcriptase polymerase chain reaction
Fig.	Figure	**Sars**	Severe acute respiratory syndrome
Fluc	Firefly luciferase	**scFv**	Single chain variable fragment
FR	Framework	**SDS**	Sodium dodecyl sulfate
g	Gram	**SHH**	Streptavidin-Histidine-Hemagglutinin
GEF	Guanine nucleotide exchange factor	**SNARE**	Soluble NSF attachment receptor
Gfp	Green fluorescent protein	**SP**	Signal peptide
Glc	Glucose	**SRP**	Signal recognition particle
Golgi	Golgi apparatus	**Strep**	Streptavidin
GST	Glutathione S-transferase	**Sup.**	Supplementary
GTP	Guanosine Triphosphate	**Sybody**	Synthetic nanobody
Gus	β-glucuronidase	**TCA**	Trichloroacetic acid
h	Hour	**TCLD**	Tissue culture infection dose

HA	Hemagglutinin	**TRIS**	Tris(hydroxymethyl)aminomethane
HcAb	Heavy chain antibody	**UMAG**	*Ustilago maydis* gene
His	Histidine	**UPR**	Unfolded protein response
HRP	Horseradish peroxidase	**UV**	Ultra violet
HSP	Heat shock protein	**v/v**	Volume for volume
IgG	Immunoglobulin	**VH**	Variable heavy domain
IMAC	Immobilized metal affinity chromatography	**VHH**	Heavy chain variable domain (in HcAbs)
kb	Kilo base	**VL**	Variable light domain
kDa	Kilo Dalton	**VP16**	Alpha-gene trans activating factor
L	Liter	**w/v**	Weight for volume
LacZ	β-lactamase	**WHO**	World health organization
LFIA	Lateral flow immunoassay	**× g**	Times gravity

Table of contents

1 Introduction

1.1 Heavy chain antibodies – potent biopharmaceuticals

1.1.1 Protein biopharmaceuticals

The term "biopharmaceutical" is often used to describe any form of biologically derived medical product, including both, products generated by recombinant host organisms and naturally occurring compounds extracted from living systems. However, the definition is not clear and the word often only refers to products produced by recombinant technologies (Rader 2008). For the purpose of this thesis the term biopharmaceutical will be defined as a biological product, derived by recombinant production and used as drug and/or medical analysis tool. Biopharmaceuticals include recombinant enzymes for the treatment of genetic conditions, monoclonal antibodies (mAbs), bio-similars and nucleic acid based technology, such as RNA vaccines (Walsh 2018). Of these classes mAbs still hold the largest market share with over 40 % (Walsh 2018). The use of mAb therapeutics is quickly expanding since 2014, as seen by the number of pharmaceutical mAbs entering phase 3 trials rising from 52 mAbs in review in 2017 to 115 in 2021 alone (Reichert 2017, Kaplon and Reichert 2021).

The biopharmaceutical market constitutes a significant part of the wider biotechnology market. The biotechnology market has an estimated net worth of 1,006.7 billion US dollars of which 330.7 billion US dollars are estimated to encompass the biopharmaceutical market (Grand View Research 2021, Research and Markets 2021). An important part of the biopharmaceutical market is the market for recombinant proteins valuing 139.4 billion US dollars in 2021 (Mordor Intelligence 2021).

1.1.2 Composition and biochemical properties

The most commonly employed type of antibody to this date both for analytics and in medicine are mAbs (Walsh 2018). IgG antibodies or Immunoglobulins are serum glycoproteins involved in the immune response as a defensive mechanism (Salvador et al. 2019). The structure of these antibodies is highly conserved in mammals and made up of two heavy and two light chains, which are linked by disulphide bridges. The heavy chain consists of four domains, C_H2 and C_H3, which make up the immunoglobulin scaffold and C_H1 which links the variable VH domain to the scaffold. The light chain consists of the conserved C_L domain and the variable VL domain. The linked VH and VL domains

form the variable fragment that facilitates target specific binding. This structure gives the antibodies their well-known "Y" shape (Padlan 1994). Variable linked regions together with their constant regions (VH, VL and C_H1, C_L) can be identified as an antigen binding fragment (Fab) and the linked variable regions without their constant regions as a single chain variable fragment (scFv) (Ruigrok et al. 2011) (Fig. 1.1). Another type of antibody that has recently come to attention is the heavy chain only antibody (HcAb) that is found in the sera of *camilidae* (e.g. camels, llamas and alpacas) and *selachii* (e.g. nurse sharks, wobbegong) (Hamers-Casterman et al. 1993, Flajnik and Kasahara 2010). While surprisingly similar in structure it is to note that these two types of HcAbs evolved convergently (Flajnik et al. 2011). HcAbs show a simplified structure when compared to mAbs. Like mAbs they are made up of two heavy chains, however they lack a light chain and their heavy chain is simplified, consisting only of the C_H2/C_H3 scaffold and a single dedicated variable domain referred to as VHH which forms the functional equivalent of the Fab from mAbs (Muyldermans 2013). The VHH domain can be used to form a single domain antibody that is commonly referred to as a nanobody (Fig 1.1).

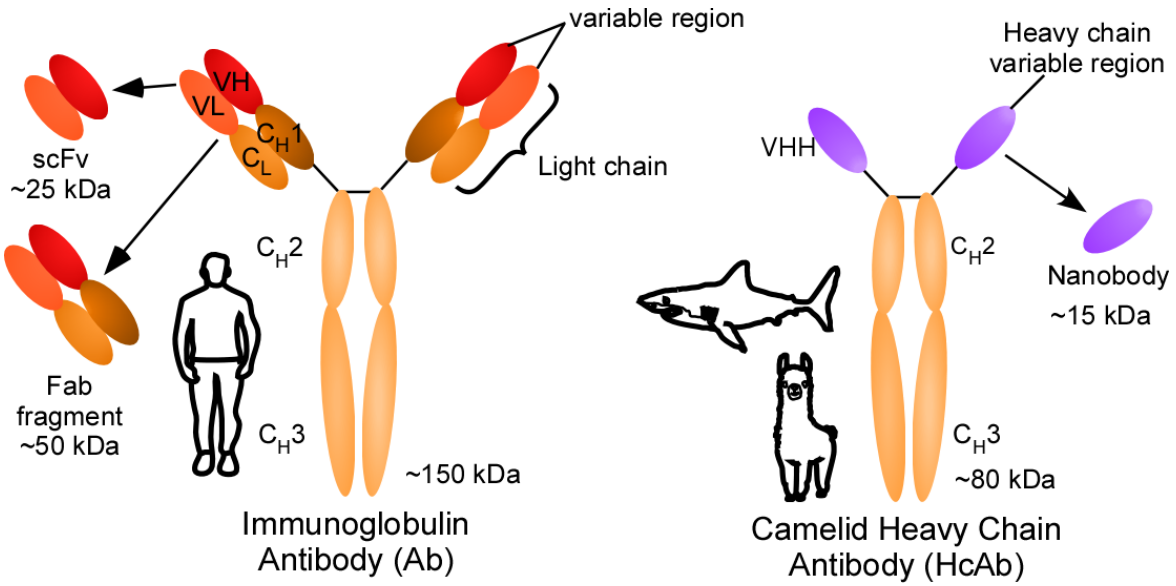

Figure 1.1: Schematic representation of Abs and HcAbs. Human Ab formed of heavy chain scaffold (C_H3 and C_H2), continuing into two C_H1 (stabilizing domain, brown) and VH (variable region, red) with two light chains attached made up of C_L (stabilizing domain, light brown) and VL (variable region, orange). Heavy chain and light chain variable region can be identified together with their respective stabilizing domains as a Fab-fragment or without them as a single-chain-variable-fragment (scFv). The heavy chain antibody (HcAb), as found in *camilidae* and *selachii* families, is formed of a heavy chain scaffold (C_H3 and C_H2), carrying only a heavy chain variable domain (VHH). The heavy chain variable domain can be expressed alone as a nanobody. Figure based on Muyldermans (2013).

The VHH consists of three hypervariable regions that are surrounded by a conserved framework (FR). The V domains secondary structure comprises nine β-strands, organized into two β-sheets that are connected by loops that contain the hypervariable regions. Further stability is provided by a conserved disulphide bond. Thus the N-terminal part of the VHH, containing the hypervariable loops, forms a complementary surface to its respective epitope named complementary-determining region (CDR) while the β-sheets are more conserved and form the FR of the domain (Muyldermans et al. 2009). Compared to the VH from mAbs the structural organization of the VHH is similar, however, in the region known as FR2 that would be linking VH and VL in a mAb, usually highly conserved large and hydrophobic amino acids are replaced by smaller hydrophilic amino acids (Vu et al. 1997).

These differences in structure and size give nanobodies interesting properties as an alternative to classical mAbs. Nanobodies directly obtained from libraries often show dissociation constants to their respective ligands in the low nanomolar or even picomolar ranges, making them comparable or superior binders, when compared to mAbs (Koide et al. 2007, Vuchelen et al. 2009). Due to the folding of its H3 loop and the hydrophilic content of FR2 they are highly water soluble and not prone to aggregation (Salvador et al. 2019). Furthermore, nanobodies have been shown to be very stable with antigen binding activity being preserved after storage on 4 °C for months and even on 37 °C for several weeks (Arbabi Ghahroudi et al. 1997). Moreover, most nanobodies only denature at 60 to 80 °C with some even reaching up to 90 °C before denaturation (Arbabi Ghahroudi et al. 1997, Dumoulin et al. 2002). Additionally, nanobodies have also been shown to be stable in the presence of proteases, extreme pH and detergents (Dumoulin et al. 2002). Interestingly, their binding can be improved via multimerization either to facilitate stronger binding to a single antigen or to allow for bivalent binding of two antigens at once (Robert et al. 1999, Sedykh et al. 2018). In addition, they can be expressed as functionalized fusion proteins with enzymes or fluorescent markers (Wang et al. 2015, Tränkle and Rothbauer 2017). Their small size gives them another advantage over conventional mAbs as they have been shown to have an enhanced intercellular diffusion rate and are also cleared from the bloodstream faster, preventing possible toxicity effects. Thus, making them not only interesting biopharmaceuticals for analytics, but also as drugs (Kijanka et al. 2015).

1.1.3 Generation and production

Besides their interesting biochemical properties, nanobodies have further advantages over mAbs that lie in their generation and production. The history of antibody generation and production goes back

decades, starting with the preparation of crude polyclonal antibody mixes, derived from immunized animals by bloodletting and antibody isolation. However, this practice has been largely replaced by the generation of specific monoclonal antibodies by RNA isolation from immunized animals that is followed by antibody identification and subsequent recombinant production in heterologous expression hosts (Houen 2022). Nonetheless, this process can be difficult, as antibody gene clusters are complex and transcription of several open reading frames is needed to obtain all RNA components that lead to translation and assembly of the heavy- and light chain components that constitute a functional mAb (Hood et al. 1975, Muyldermans 2013). Thus, selection and production of smaller and simpler mAb components like scFvs or Fabs is preferable (Skerra 1993). Due to their single domain nature, however, nanobodies show a huge advantage over scFvs and Fabs in selection. VH and VL need to be individually amplified during selection and pairs become scrambled during random assembly, lowering antigen specificity and quality in scFv libraries, when compared to VHH libraries (Yau et al. 2005, Asaadi et al. 2021). This fast selection process has given rise to several nanobody generation and selection methods. The most commonly used method is immunization of *camelidae* species like camels, alpacas or llamas, followed by RNA isolation from lymphocytes, library cloning by PCR and nanobody selection via phage display based ELISA (Liu et al. 2018) (Fig 1.2). Generally, two to three rounds of phage display are sufficient to obtain suitable binders (Salvador et al. 2019).

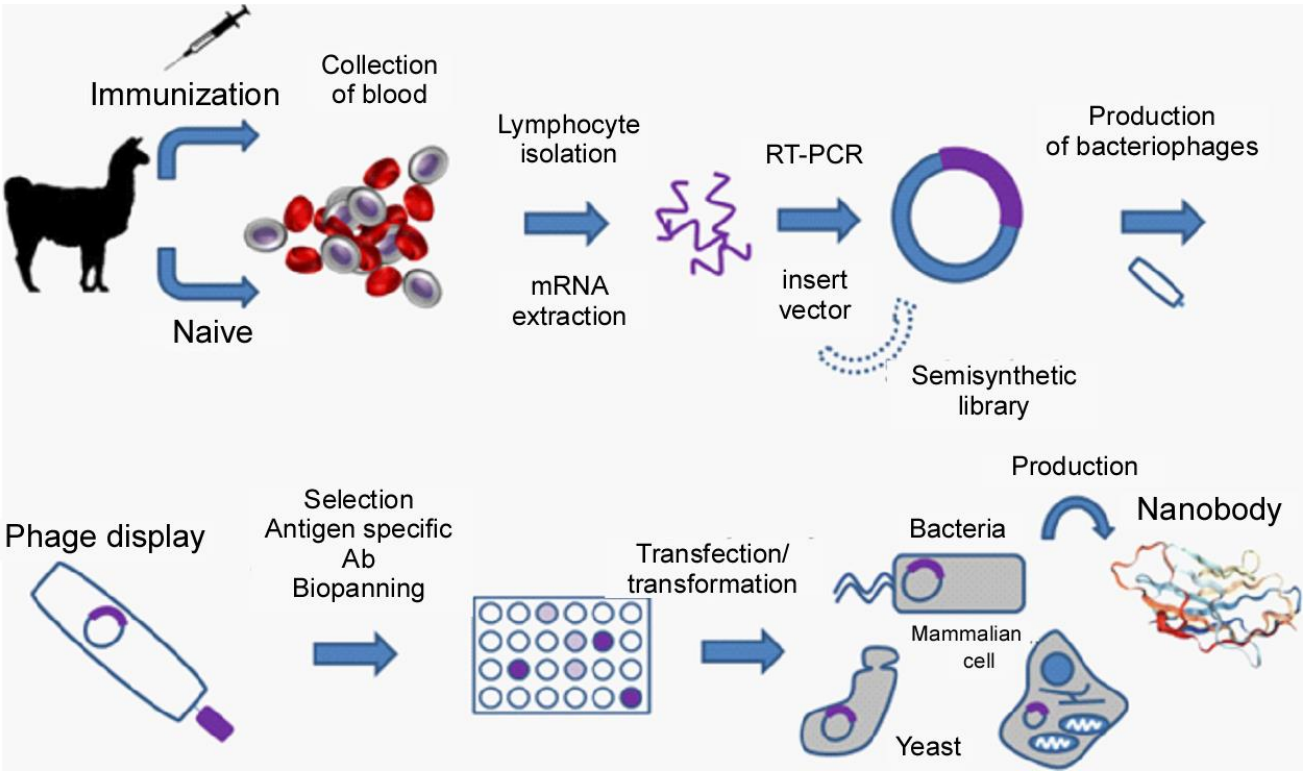

Figure 1.2: Schematic overview of nanobody generation protocol. *Camelidae* are immunized with antigen. Afterwards lymphocytes are isolated, mRNA is extracted, reverse transcribed and cloned into library vectors. These vectors are then transfected into bacteriophages and selected via phage-display ELISA, allowing for immunogenic detection and subsequent DNA isolation of positive candidates. Positive candidate plasmids can then be directly transformed into production hosts or VHH gene can be amplified and cloned into suitably expression vector before transformation/transfection. Modified from Salvador et al. (2019).

Additionally, methods like ribosome or yeast-display and bacterial two-hybrid can be used instead of, or in combination with phage-display for selection (Pellis et al. 2012, Wagner et al. 2018, Oloketuyi et al. 2021). However, nanobodies can also be directly generated from large naïve synthetic libraries allowing for generation without animal harm (Monegal et al. 2009). Nonetheless, generation from naïve libraries can be tedious as they require large library sizes and a higher number of selection rounds (Wagner et al. 2018). Thus, more sophisticated synthetic and semisynthetic libraries have been generated that require smaller library sizes and selection rounds (Wang et al. 2016). This has led to the development of protocols for the generation of fully synthetic nanobodies in timeframes as short as three weeks by the combination of a synthetic library, ribosome- and phage-display (Zimmermann et al. 2020). Furthermore, nanobodies generated via one of the methods described above can be further enhanced by maturation approaches such as error-prone PCR coupled with ribosome-display and alanine scanning based mutations for the identification from amino acids critical for affinity to the respective antigen (Yau et al. 2005, Koide et al. 2007).

Following generation and selection, nanobodies can be produced in a variety of hosts. Successful nanobody expression has been shown for *Escherichia coli*, mammalian cell lines, different yeast species, insect cells and even plants (Muyldermans 2013, Liu and Huang 2018, Asaadi et al. 2021, De Greve 2022). Especially production in microbial hosts offers cheap production at high titers when compared to conventional mAb production in mammalian cell lines which are expensive to maintain and often offer lower titers than their microbial counterparts (Rettenbacher 2021). The most commonly used expression host for nanobodies is *E. coli* (Muyldermans 2013). However, while yielding high titers bacterial expression of nanobodies has distinct drawbacks. Disulphide bridge formation is not achievable in commonly used cytoplasmic expression and instead requires translocation of proteins to the periplasm, lowering yield and complicating purification (Berlec and Strukelj 2013). Furthermore, secretion to the supernatant is not as readily available in *E. coli* as in e.g. mammalian cells or yeasts (Berlec and Strukelj 2013). Several genetic engineering approaches have been undertaken to improve the system. Thus, cytoplasmic formation of disulphide bridges in nanobody production has been made

possible by co-expression of sulfhydryl oxidase and an isomerase (de Marco 2022) and secretion has been enabled via the type I secretion system (Schwarz et al. 2012).

Nonetheless, expression and secretion in yeasts and filamentous fungi is of high interest for recombinant protein and nanobody production. Yeasts like *Pichia pastoris* and *Saccharomyces cerevisiae,* and filamentous fungi such as *Aspergillus niger* and *Trichoderma reesei* offer the possibility to produce and secrete complex eukaryotic proteins with proper folding at high titers (Spadiut et al. 2014, Wang et al. 2020b). Secretion is generally preferred to intracellular production due to easier downstream processing (Sun and Su 2019). To this end efficient expression and secretion of various nanobodies at high titers has been reported in *P. pastoris* (Matsuzaki et al. 2022). Furthermore, a secretion system for nanobodies in *S. cerevisiae* has been established, albeit at lower yield (Harmsen et al. 2022). Thus, nanobodies can be easily generated and expressed in a variety of heterologous hosts.

1.2 Sars-CoV2 and the COVID-19 pandemic

1.2.1 Significance

A recent development that has highlighted the need for novel biopharmaceuticals, was the outbreak of the COVID-19 pandemic which has severely impacted societies and economies across the world. The most immediate consequences of the viral outbreak were constituted by the health concerns posed by the disease, first reported in December 2019 and declared as a global pandemic in March 2020 (Zhu et al. 2020a, Sarkodie and Owusu 2021). This in turn lead to on the one hand heightened investment into healthcare and research systems and on the other hand to quarantine and lock down situations (Hale et al. 2021, Sarkodie and Owusu 2021). These measures proved effective, for example reducing projected case numbers by up to 65% in Hubei province, China (Fang et al. 2020). However, global health systems were severely burdened by severe COVID-19 cases and long COVID. With reported case rates of 3.21 to 6.3% for severe COVID-19 and 2.3% for long COVID that lasted for over 12 weeks before vaccinations were available, high infection incidences overburdened health care systems on several occasions, for example in Italy in early 2020 (Orfali 2020, McKeigue et al. 2021, Sudre et al. 2021). Moreover, global economies were severely impacted by lock down measures, health crises and the resulting high unemployment rates, evident for example by the European Union's economy contracting by 8.3% in 2020 and an estimated cost of two trillion dollars for the global economy in 2021 alone (European Commission 2020, Kaye et al. 2021). Thus, research to understand and combat the spread,

severity and mortality of COVID-19 is crucial and has become a major effort since the beginning of the pandemic.

1.2.2 Biology of the Sars-CoV2 virus

The causative agent of COVID-19 is the Sars-CoV2 virus (Huang et al. 2020a). Sars-CoV2 belongs to the genus beta coronavirus and is most closely related to two other corona viruses isolated from bats. Its closest genetic relative affecting humans is the Sars-CoV virus (Lu et al. 2020). Thus far six groups of human Corona viruses have been identified: H-CoV 229-E, H-CoV OC-43, HCoV HKU-1, H-CoV NL-63, Sars-CoV and Mers-CoV, with the first four groups generally causing mild respiratory disease, while the latter two groups are known to be able to cause severe symptoms with fatality rates of 6 % to 36 % (Marra et al. 2003, Zaki et al. 2012, de Groot et al. 2013). The novel Sars-CoV2, belonging to the latter category, has been classified as the seventh member of the H-CoV group (Huang et al. 2020b). Like other *coronaviridae* Sars-CoV2 is a positive-sense single-stranded RNA virus and has a genome size of 29.8 kb (Yang and Leibowitz 2015, Lu et al. 2020). Its genomic organization is similar to that of other coronaviruses which genomes are generally ordered into 6 to 11 open reading frames (ORFs) (Song et al. 2019). The first 67% as seen from the 5'-terminus are constituted by 1-2 ORFs which encode for non-structural proteins, while the ORFs at the 3'-terminus encode for the structural spike-, envelope-, membrane- and nucleocapsid proteins, as well as accessory proteins (Cui et al. 2019). The key differences observed for Sars-CoV2 are a larger number of eight accessory protein encoding ORFs at the 3'terminus when compared to other H-CoVs, resulting in 14 ORFs overall. Furthermore, when compared to its closest H-CoV relative Sars-CoV on the amino acid level, 380 amino acids are substituted and the accessory protein 8a is missing entirely, while several other accessory proteins vary in the length of their respective amino acid sequence (Wu et al. 2020). Interestingly, several non-structural and structural proteins like the envelope and membrane protein remain entirely conserved between Sars-CoV and Sars-CoV2, while the spike protein complex (Spike) alone shows 27 substitutions (Wu et al. 2020). The Spike of corona viruses belongs to the class I viral membrane fusion proteins that are also present in influenza, HIV and Ebola viruses (Eckert and Kim 2001, Li 2016). The general structure consisting of S2 and S1 subunits and a C-terminal receptor binding domain (RBD) located atop the outward protruding S1 subunit is conserved among corona viruses (Belouzard et al. 2012). However, the hosts target protein of its RBD is not. While Mers-CoV for example recognizes the serine peptidase dipeptidyl peptidase 4 (DDP4), H-CoV NL-63, Sars-CoV and Sars-CoV2 recognize the angiotensin-converting enzyme ACE2 (Li et al. 2003, Raj et al. 2013, Zhou et al. 2020).

The Sars-CoV2 spike is formed of a trimer of S2 domains each anchoring one S1 domain, made up of RBD, NTD, SD1 and SD2 subdomains, to the viral envelope via three stable long helices (Walls et al. 2020). It has been shown that the S1 domains are able to freely rotate around the hinge like structure of the S2 subunit (Turonova et al. 2020). The spike protein can exist in two confirmations: open (RBD up) and closed (RBD down) (Walls et al. 2020, Wrapp et al. 2020b) (Tölzer et al. 2020). However, this confirmation change describes only one of the three RBDs actually opening up, while the other two remain in the down state (Korber et al. 2020). At physiological pH 68% of spike were shown to be in the open confirmation (Pramanick et al. 2021) (Fig 1.3).

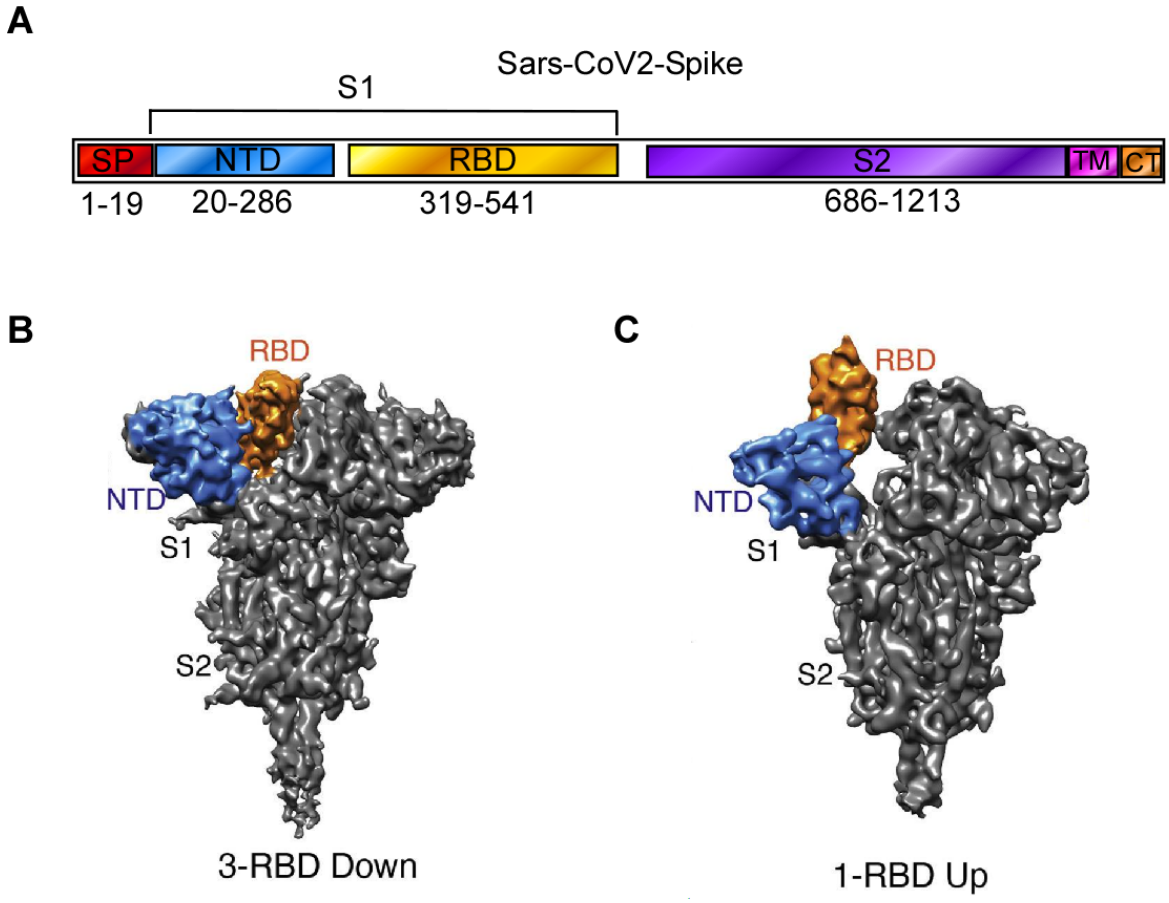

Figure 1.3: Structure of the Sars-CoV2 Spike. (A) Organisation of the Spike protein. The first 19 amino acid form a signal peptide (SP) followed by the NTD domain from amino acid positions 20-286. Together with the receptor binding domain (RBD) at positions 319-541 the NTD makes up the S1 part of the Spike. This is followed by the S2 subdomain at positions 686-1213. **(B)** Structure of the Sars-CoV2 Spike trimer in the RBD down (closed) confirmation. S1 trimer on top is anchored via the S2 trimer in the lower part of the protein complex. RBD domain is closed down next to the NTD domain. **(C)** Structure of the Sars-CoV2 Spike trimer in the RBD (up) confirmation. S1 trimer on top is anchored via the S2 trimer in the lower part of the Spike complex. One of the three RBD domains is up in the ready state for Ace2 binding. Modified from Wang et al. (2020a) and Pramanick et al. (2021).

Sars-CoV2 RBD binds human ACE2 via 21 distinct residues of which 13 are shared with its closest H-CoV relative Sars-CoV which possesses 16 binding residues. More importantly, these changes result in an approximately 4-fold higher binding affinity (Wang et al. 2020a).

In other coronaviruses like Sars-CoV, Mers-Cov and HCoV HKU1 it has been shown that protease cleavage between the S1 and S2 domain upon membrane fusion is necessary for transformation into an elongated post-fusion state and thereby starting the viral infection cascade (Belouzard et al. 2009, Millet and Whittaker 2014, Kirchdörfer et al. 2016). Interestingly it could be observed under laboratory conditions that this does not seem to be the case for Sars-CoV2. While Sars-CoV pseudovirions were only able to form syncytia upon trypsin cleavage, Sars-CoV2 formed syncytia even in the absence of trypsin, possibly explaining the fast transmissibility of the virus (Ou et al. 2020). Subsequently to RBD to ACE2 fusion, the viral envelope fuses with the host cell and viral RNA is released into the host for translation and formation of viral progeny (Walls et al. 2020). Due to the high binding affinity to ACE2, Sars-CoV2 is able to infect all cells expressing the protein, including type-2 alveolar cells in the lungs and upper part of the esophagus, enterocytes in the colon, urothelial cells in the urinary bladder, cardiac myocytes and cells in the oral cavity (Xu et al. 2020a). This explains the symptoms of Sars-CoV2 infection ranging from mild disease of the upper respiratory tract, to severe pneumonia, diarrhea and cardiac disorders, such as myocarditis, further manifesting the Spike protein as a crucial component for the Sars-CoV2 life cycle (Astuti and Ysrafil 2020, Al-Kindi and Zidar 2022) (Walls et al. 2020, Pramanick et al. 2021). Moreover, the Spike seems to be especially prone to accumulate mutations (Saputri et al. 2020).

Since the beginning of the pandemic 34 variants of Sars-CoV2 have emerged that have been categorized into variants under monitoring, variants of interest and variants of concern in order of impact on transmissibility by the WHO (Khateeb et al. 2021, Torjesen 2021). The five variants of concern in order of appearance were classified as B.1.1.7 (Alpha, now classified as de-escalated), B.1.351 (Beta), P.1 (Gamma), B.1.617.2 (Delta) and B.1.1.529 (Omicron). All carried mutations within the Spike complex, especially in the RBD and S1/S2 junction region, that enhanced their transmissibility, immune avoidance and in case of all but Omicron also the severity of disease (https://www.ecdc.europa.eu/en/covid-19/variants-concern) (Davies et al. 2021, Khateeb et al. 2021, Mahase 2021, Sabino et al. 2021, VanBlargan et al. 2022). Hence, the Spike protein, which has been used for the generation of biopharmaceuticals against other *coronaviridae* as well, has become a key target for the generation of vaccines and antibodies (Du et al. 2009, Elshabrawy et al. 2012, Jiang et al. 2014, Kumar et al. 2021).

1.2.3 Biopharmaceuticals for COVID-19 treatment and diagnostics

From a pharmaceutical standpoint the response to the pandemic can be broadly ordered into three categories: Direct disease prevention, disease treatment and indirect disease prevention. Direct disease prevention aims at breaking up infection for example by vaccination while disease treatment constitutes the administration of drugs to patients already being infected with Sars-CoV2, and indirect disease prevention is achieved by population-wide regular testing to identify and quarantine infected individuals before the onset of symptoms and importantly, viral transmission (EuropeanCommision 2021).

First vaccines have thus been developed and applied on a massive scale in the form of mRNA vaccines by Moderna and BionTech/Pfizer and in the form of vector-based vaccines by Johnson & Johnson, Astra Zeneca, Sinopharm and Sputnik V (Callaway 2020, Fernandes et al. 2022). This initial set of vaccines has grown and by now 33 vaccines have been approved in at least one country (Kudlay and Svistunov 2022).

Biopharmaceuticals for treatment have predominantly been applied in the form of mAbs. Therapeutic mAb products such as bamlanivimab, etesevimab, casirivimab, imdevimab, strovimab, cilgavimab and tixagevimab have been approved by the FDA in the USA, are actively used to treat COVID-19 patients and are mostly targeted against the Spike protein and/or its RBD (Hwang et al. 2022). However, other targets such as the nucleocapsid protein and non-structural proteins involved in viral assembly within the host cell are currently under research (Kwarteng et al. 2020, Raj 2021).

Testing for viral infection was first established by RT-PCR (Corman et al. 2020). This testing method is very sensitive but has clear drawbacks in its cost and the fact that it has to be conducted in a laboratory by a trained person (Corman et al. 2020, Hsiao et al. 2021). To this end antigen tests have been developed and made widely available for quick viral detection and use by untrained persons (Hsiao et al. 2021). These assays are built on the lateral flow immunoassay (LFIA) architecture, which has been available since 1984 (Andryukov 2020). LFIA tests generally consist of a sample pad used for adsorption of the sample from which it moves along the flow chamber towards the conjugation pad. Here the sample is bound by a secondary antibody that is conjugated to a colorimetric or fluorescent reporter particle. Further along the flow chamber primary antibodies against the sample antigen are immobilized and trap the conjugate of sample and secondary antibody, forming a positive test line. Behind the test line immobilized primary antibodies directed against the secondary antibody trap residual secondary antibody and form the control line (Cheng 2020). Thus, they allow fast and easy detection within 15 minutes, are sensitive enough to detect regular Sars-CoV2 infection about one day

before the onset of symptoms and can be applied in large scale (Mercer and Salit 2021). This has led to the development of 605 different antigen testing products and over a billion individual tests being conducted until 2022 in Germany alone (BfRAM 2022). Such numbers place enormous strain on production of testing kits and antibodies alike, highlighting the need to further improve existing antibody technology and find novel potent protein production platforms. One candidate that is currently being engineered towards a competitive expression platform, is *Ustilago maydis*.

1.3 The microbial model organism *Ustilago maydis*

Ustilago maydis belongs to the family of *Ustilaginales* and the division of *Basidiomycota.* It was first discovered and described as the causative agent of the corn smut disease. The biotrophic pathogen infects only maize (*Zea mays*) and its ancestor Teosinte (*Zea mays* subsp. *parviglumis*) (Christensen 1963, Banuett 1992, Martinez-Espinoza et al. 2002). *U. maydis* possesses a biphasic and dimorphic life cycle, consisting of a saprotrophic and a biotrophic phase. The saprotrophic, yeast phase constitutes the vegetative growth stage of the fungus in which it proliferates by budding. Upon recognition of a compatible mating partner, cells form conjugation tubes, fuse, and form dikaryotic hypha, which are then able to penetrate and colonize the maize plant (Banuett and Herskowitz 1989, Feldbrügge et al. 2004). Subsequently, tumors are formed within the host plant that are filled with teliospores (Feldbrügge et al. 2004, Döhlemann et al. 2008, Brefort et al. 2009). The life cycle is completed by spore release and germination in which spores undergo meiosis and thus form new haploid yeast cells (Feldbrügge et al. 2006).

In recent years *U. maydis* has achieved relevance as a microbial model organism for additional fields like cell biology and importance for exploitation in biotechnology (Vollmeister et al. 2012, Feldbrügge et al. 2013, Müntjes et al. 2021, Wierckx et al. 2021). It was discovered early on in the 1960s and 1970s that *U. maydis* can be cultivated in the form of its haploid yeast form both in submerged axenic culture and on solid media, enabling its establishment as a eukaryotic model organism (Christensen 1963, Holliday 1974b). Early research was focused especially on homologous recombination and DNA repair mechanisms, leading to the discovery of the Holliday junction and key components of the eukaryotic DNA repair machinery (Holliday 1964, Holliday 1974a). More recently long-range endosome coupled mRNA transport along the microtubule cytoskeleton has come into focus (Pohlmann et al. 2015, Niessing et al. 2018, Jankowski et al. 2019, Olgeiser et al. 2019, Müntjes et al. 2021). Further current cell biology research topics include the elucidation of extracellular vesicle content, transcriptional and post-transcriptional regulation, as well as cell cycle regulation (Feldbrügge et al. 2008, Ruiz-Herrera

et al. 2020, Kijpornyongpan and Aime 2021, Kwon et al. 2021). Since smut fungi cause substantial losses for agriculture each year, *U. maydis* has also become a model for plant pathogen interaction (Martinez-Espinoza et al. 2002, Brefort et al. 2009, Djamei and Kahmann 2012, Göhre et al. 2012, Perez-Nadales et al. 2014, Matei and Döhlemann 2016). As a consequence of the increasing interest, the entire *U. maydis* genome has been sequenced (Kämper et al. 2006) and a plethora of microbiological methods for strain generation and molecular techniques for *in vivo* analysis and the formation of genetic switches, comprising a sophisticated molecular toolbox has emerged. On the one hand microbiological tools include the possibility of stable strain generation via efficient homologous recombination, a cassette type golden-gate cloning system for plasmid generation, clearly mapped integration loci for heterologous gene expression, a variety of (recyclable) resistance cassettes and the recent addition of CRIPR/Cas9 based genome editing (Spellig et al. 1996, Brachmann et al. 2001, Brachmann et al. 2004, Khrunyk et al. 2010, Stock et al. 2012, Terfrüchte et al. 2014, Wege et al. 2021). Application of these tools has led to the identification or generation of a variety of strains applicable for research. These range from a library of available wildtype isolates as a basis for strain engineering to solo pathogenic strains, strains capable of inducible hyphal growth such as AB33, protease deficient strains and secondary metabolite producers (Banuett and Herskowitz 1989, Bölker et al. 1995, Brachmann et al. 2001, Hewald et al. 2006, Geiser et al. 2013, Sarkari et al. 2014, Geiser et al. 2016, Terfrüchte et al. 2018). Molecular techniques on the other hand include generation and application of strong synthetic as well as inducible promoters and the use of 2A peptides for polycistronic eukaryotic gene expression (Hartmann et al. 1999, Zander et al. 2018, Aschenbroich et al. 2019, Müntjes et al. 2020, Hussnätter et al. 2021).

1.3.1 *U. maydis* in biotechnology

One interesting aspect about *U. maydis* when addressing biotechnological application is its status as an organism that is regarded as safe for consumption by several countries including Mexico and Switzerland, having been consumed as food in the form of infected maize combs termed “huitlacoche” since at least the time of the Aztecs (Juarez-Montiel et al. 2011, Valdez-Morales et al. 2016). However, the core interest in the fungal model comes from its capability to produce interesting value-added compounds such as glycolipids, organic acids, triglycerides, carbohydrate active enzymes and biopharmaceuticals (Feldbrügge et al. 2013, Paulino et al. 2017, Wierckx et al. 2021). The production of these compounds has been driven as much by above mentioned strain generation methods as by cultivation optimization and process engineering. *U. maydis* can be cultivated at lab scale in microtiter

plates for efficient large-scale screening of cultures via online monitoring, in conventional shake flasks and in large scale stirred tank bioreactors for scale up of production (Dütz et al. 2000, Terfrüchte et al. 2018, Hosseinpour Tehrani et al. 2019, Dinger et al. 2022). Another possibility for online monitoring during process development was applied to *U. maydis* in the form of the respiration activity monitoring system (RAMOS), allowing for online measurement of dissolved oxygen tension and pH in shake flasks (Anderlei et al. 2004, Terfrüchte et al. 2018).

Furthermore, *U. maydis* is a producer of secondary metabolites such as cellobiose lipids in the form of ustilagic acid, mannosylerythritol lipids (MEL) and itaconic acid (Hewald et al. 2006, Teichmann et al. 2007, Geiser et al. 2016). Efforts in strain engineering have led to enhanced production of MEL and ustilagic acid by the expression of crucial MEL-cluster genes *emt1*, *mac1* and *mac2* via a polycistronic 2A-peptide based mRNA and upregulation of the transcription factor gene *rua1*, respectively (Teichmann et al. 2010, Müntjes et al. 2020). Furthermore, production of MELs with altered and predictable fatty acid profiles has been enabled by generation of strains expressing heterologous variants of acyl-transferases Mac1 and Mac2 (Becker et al. 2021). Itaconic acid production has recently been driven by both genetic engineering and process design. A strain producing only itaconic acid without byproducts such as MELs, ustilagic acid or triaglycerides was engineered by deletion of *cyp3*, abolishing conversion of itaconic acid to (S)-2-hydroyparaconate, MEL and ustilagic acid gene clusters and the deletion of diacylglycerol acyltransferase gene *dgat* (Becker et al. 2020). Deletion of the *fuz7* gene and engineering of built-in drop out by crystallization into the bioprocess led to itaconic acid titers of 220 g/L (Hosseinpour Tehrani et al. 2019). Additionally, *U. maydis* has been applied as a whole cell biocatalyst to produce itaconic acid on brewers spent grain and in a co-culture bioprocess with *Trichoderma reesei* to produce itaconic acid from cellulose (Schlembach et al. 2020, Weiermüller et al. 2021).

Due to its plant pathogenic nature, *U. maydis* is capable of secreting carbohydrate active enzymes. However, most of these are only expressed in its hyphal form which is disadvantageous for bioprocesses. Nonetheless genetic activation by exchanging the respective native promoters with strong constitutive promoters led to expression of intrinsic endopolygalacturonase, endo-1,4-β-xylanase, endoglucanase and β-glucanase in respective expression strains, and further complementation with exo- and endopolygalacturonases from both fungal and bacterial hosts, thereby enabling degradation of and proliferation on xylan, cellobiose and polygalacturonic acid (Geiser et al. 2013, Geiser et al. 2016, Stoffels et al. 2020). Additional enzymes of interest e.g., include an α-L-

arabinofuranosidase, a CalB-type lipase and an AA3_2 glucose oxidoreductase that was shown to be mainly active on gentobiose (Bürth et al. 2014, Paesani et al. 2021, Wijayanti et al. 2021).
However, conventional secretion of carbohydrate active enzymes is only one mode of protein production in *U. maydis*. It also possesses an unconventional secretion pathway which has been recently utilized for the production of biopharmaceuticals (Stock et al. 2012, Sarkari et al. 2014, Terfrüchte et al. 2017).

1.4 Unconventional protein secretion

1.4.1 Conventional and unconventional secretion mechanisms

When talking about eukaryotic protein secretion, it is crucial to first define the difference between conventional and unconventional secretion. Conventional secretion generally describes the endomembrane pathway that leads from protein folding and modification in the endoplasmic reticulum (ER) to post translational modification in the Golgi apparatus to exocytosis and is facilitated via an N-terminal signal peptide (Viotti 2016). Unconventional secretion on the other hand describes all pathways of protein secretion that circumvent the Golgi network (Rabouille 2017).
The conventional secretion pathway starts during translation of the mRNA by the ribosome. Most polypeptides get co-translationally imported into the lumen of the ER (Palade 1975). This co-translational secretion is mediated by signal recognition particles (SRPs) (Walter and Johnson 1994, Bui and Strub 1999). The SRPs binds the hydrophobic end of the nascent polypeptide chain, which is subsequently cleaved by signal peptide peptidases. The polypeptide chain is then delivered to the Sec61 complex and thereby directly imported into the ER lumen (Chirico et al. 1988, Kalies et al. 1994). Polypeptides that are not co-translated into the ER are guided by Ssa heat shock proteins that act as chaperones to maintain the polypeptide chain to the Sec62/63 complex and subsequently transported into the ER lumen (Arnold and Wittrup 1994, Ng et al. 1996). This mechanism has thus been described for most eukaryotic organisms, including mammalian cells (Benham 2012). In the ER the oxidative environment allows for disulphide bond formation, post-translational modification and processing and protein folding (Lee et al. 2004, Csala et al. 2012). These processes are catalyzed by a variety of chaperones and enzymes, such as the protein disulphide isomerase (Pdi) which facilitates oxidation and reduction of disulphide bonds and the endoplasmic reticulum oxireductin which serves as a refueling oxidant for the Pdi (Gross et al. 2004, Wilkinson and Gilbert 2004, Ellgaard and Ruddock 2005). The HSP70 protein BiP is a key player within the ER aiding translocation from the cytosol into the ER lumen, binding hydrophobic regions of polypeptide chains to prevent aggregation and

facilitating protein folding Besides disulphide bond formation, posttranslational modification includes *N*-glycosylation which is facilitated by luminal glycosyltransferases and glycosidases (Csala et al. 2012). Following folding and posttranslational modification proteins are transported to the Golgi apparatus (Lee et al. 2004, Benham 2012). The Golgi apparatus is organised into layered compartments called Golgi stacks (Nakamura et al. 2012). In the Golgi apparatus more posttranslational modifications like O-glycosylation, acetylation, sulfation, phosphorylation, methylation, palmitoylation and proteolytic cleavage of inactive protein forms take place (Stanley 2011, Potelle et al. 2015). Subsequently proteins are incorporated into v-SNARE coated vesicles that are shuttled to the plasma membrane, recognized by t-SNAREs and released into the extracellular space via exocytosis (Delic et al. 2013).

In contrast to the highly conserved conventional secretion pathway, unconventional secretion can occur via several different pathways and does not follow one specific conserved route (Rabouille 2017). Unconventional secretion can be categorized into either vesicular mechanisms based on intracellular transport of vesicular structures and membrane bound intermediates that facilitate protein release, or non-vesicular mechanisms that rely on direct plasma membrane translocation either via membrane transports or self-induced pore formation (Nickel 2010, Rabouille 2017). These can be further categorized into type I-IV unconventional secretion. Type I describes direct translocation via pore formation, Type II categorizes ATP binding cassette (ABC) transporter based release, Type III encompasses all vesicular transport that completely bypasses ER and Golgi and Type IV describes a special case of unconventional secretion pathway of proteins that do harbor a signal peptide and enter the ER but bypass the Golgi apparatus (Rabouille 2017). A basic overview of these mechanisms is depicted in Fig 1.4.

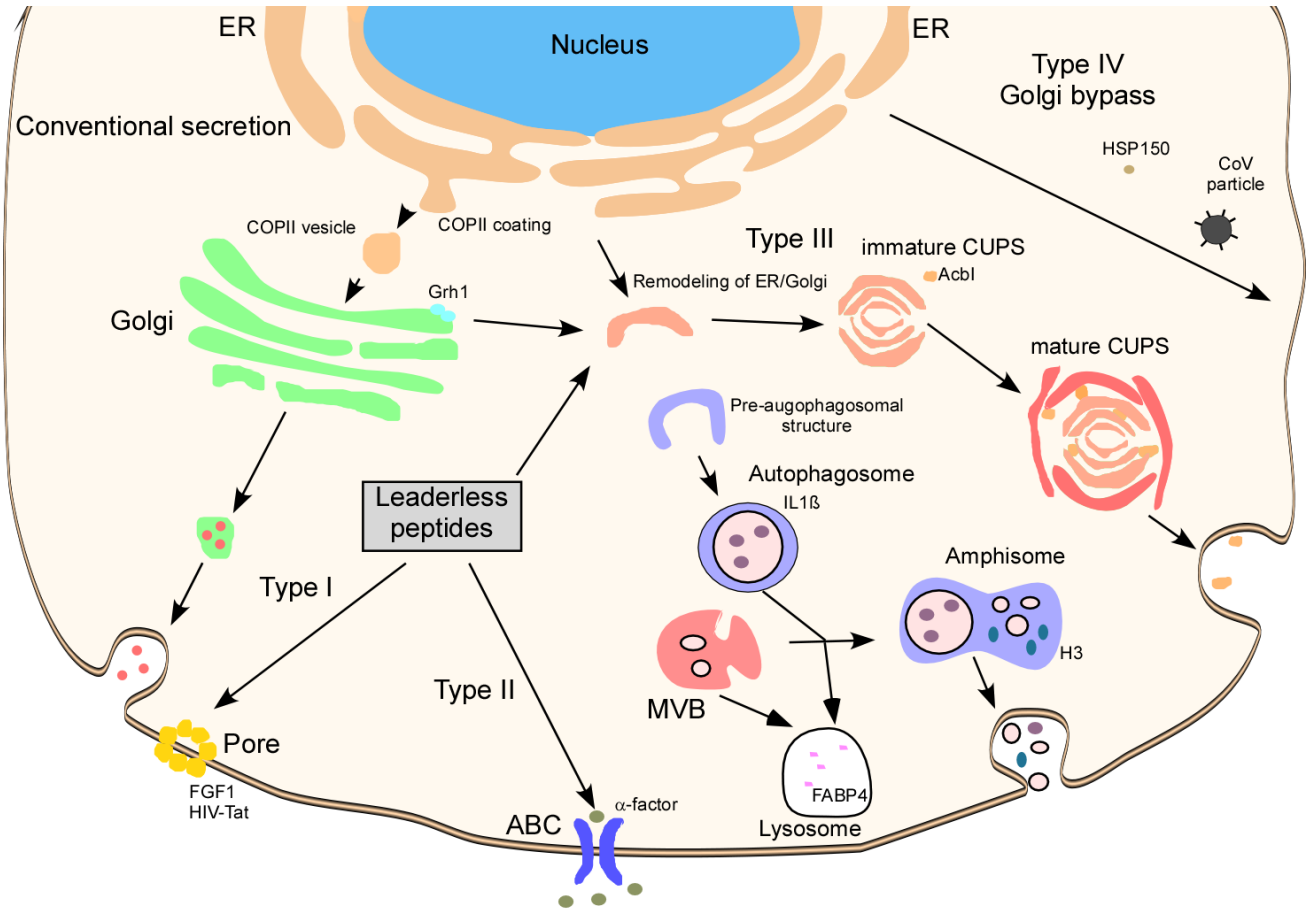

Figure 1.4: Unconventional secretion pathways. Conventional secretion (left side): Polypeptide chains carrying N-terminal signal peptides are translocated into the ER (brown) where protein folding occurs and subsequently transported via COPII carrying vesicles to the Golgi apparatus (light green). After further post-translational modification proteins are delivered to the plasma membrane via v-SNARE carrying vesicles and released via t-SNARE interaction. Translocation of leaderless peptides via Type I-III unconventional secretion: Type I (bottom left): Proteins like FGF1 and HIV-Tat form pores in the plasma membrane, resulting in self-translocation. Type II (bottom middle): Proteins like the *S. cerevisieae* α-factor are transported across the plasma membrane by ATP binding cassette (ABC) transporters. Type III (middle to bottom right): Proteins like AcbI and IL1β are secreted via Autophagosomes, Amphisomes and CUPS that form during starvation or inflammation conditions. CUPS form from remodeled ER structures and release their cargo via direct membrane fusion. Autophagosomes form from pre-autophagosomal structures and can either directly fuse with the plasma membrane to release their cargo (IL1β), fuse with multivesicular bodies to form amphisomes for release (H3) or deliver their cargo, like other multi vesicular bodies into lysosomes (FABP4). Type IV: Proteins such as HSP150 and parts of CoV viruses that carry an N-terminal signal peptide enter the ER but are directly transported to the plasma membrane. In case of CoVs the proteins are assembled to viral particles first and then secreted bypassing the Golgi apparatus. Figure based on Abrahamsen and Stenmark (2010), Rabouille (2017), Cohen et al. (2020) and Saraste and Prydz (2021).

Type I translocation has been described for the mammalian fibroblast growth factor I (FGFI) and occurs as a heat shock or starvation response (Jackson et al. 1992, Shin et al. 1996). FGFI has been

shown to dimerize and interact with membrane phospholipids and Cu^{2+} thus destabilizing the plasma membrane and translocating across the lipid bilayer (Prudovsky et al. 2013). Of note, FGF2 is also unconventionally secreted via Type I but in a distinctly different mechanism that involves cysteine residue dependent binding to phosphatidylinositol 4,5-bisphosphate (PiP2) and Tec kinase phosphorylation of FGF2 mediating pore formation and translocation (Steringer et al. 2012, La Venuta et al. 2015). Another example of Type I translocation is the viral transcription factor HIV Tat which is released from infected cells and taken up by uninfected cells (Chang et al. 1997). Similar to FGF2 its pore formation mechanism is also dependent on PiP2 binding (Zeitler et al. 2015).

Type II secretion was first described for the *S. cerevisiae* mating pheromone α-factor that is secreted by the ATP binding cassette (ABC) transporter Ste6 (McGrath and Varshavsky 1989). Another potentially Type II secreted protein class are heat shock proteins (HSP70) from mammalian cells which are released upon heat shock into the extracellular space (Mambula and Calderwood 2006). However, the exact mode of secretion is still discussed (Cohen et al. 2020).

Type III translocation constitutes the largest amount of individual transport mechanisms described to date, including translocation via microvesicles, compartments for unconventional secretion (CUPS), autophagosomes. lsyosomes and amphisomes (Cohen et al. 2020). Secretion via lysosomal vesicals occurs by fusion of the lysosome to the plasma membrane and has been described in metazoans and yeasts (Li and Kane 2009). One example is the fatty acid binding protein 4 (FABP4) which is a lipid chaperone linked to type 2 diabetes (Furuhashi et al. 2014). Lacking a signal peptide, it is likely translocated directly into the lysosome in an unfolded form and secreted upon lipolysis-mediated signaling (Mita et al. 2015, Villeneuve et al. 2018). Autophagosomal secretion is induced when autophagosomes form during a starvation-induced process that is involved in breaking down cellular components (Cohen et al. 2020). An example for this mechanism is the cytokine IL-1β which is processed by Caspase-I into its active form during inflammation and released via autophagosomes. This cascade is triggered by a multi-protein complex described as the inflammasome (Martin-Sanchez et al. 2016). When autophagosomes fuse with multivesicular bodies the structure is called an amphisome (Klionsky et al. 2014). Histone H3 is unconventionally secreted via amphisomes. It was found in vesicular structures carrying both autophagosomal marker L3 and the multi vesicular body marker CD63 that release H3 into the extracellular space via fusion with the plasma membrane in a non-vesicular form (Jeppesen et al. 2019). CUPS on the other hand are multivesicular bodies that are formed by remodeling of the ER, Golgi and endosomal membranes under starvation conditions. This has been shown by tracing of the migration of Golgi protein Grh1 that translocates from ER exit sites

and early Golgi to distinct vesicular structures upon starvation (Cruz-Garcia et al. 2014). The Acetyl-CoA-binding protein (Acb1) has been shown to be secreted unconventionally from *S. cerevisiae* in CUPS. Under starvation conditions Acb1 is recruited to CUPS by a complex cascade including autophagy proteins, the above described Grh1 and multivesicular body proteins Vps23 and Snf7 (Curwin et al. 2016). Secretion likely occurs via direct fusion with the plasma membrane, as it is dependent on t-SNARE protein Sso1 (Duran et al. 2010).

Type IV secretion is clearly differentiated from Type I to III unconventional and conventional secretion, since proteins still carry an N-terminal signal peptide but are nonetheless secreted, when ER-Golgi transport is inhibited for example by brefeldin A (Grieve and Rabouille 2011). An example for Type IV secretion is the soluble yeast glycoprotein HSP150. While carrying an N-terminal signal peptide its correct localization to the cell surface could still be shown, when COPII coat components Sec13 and Sec24 were missing (Fatal et al. 2004). Of note the cellular exit mechanism of *coronaviridae* seems to be similar to Type IV secretion. It was shown that corona viruses assemble by budding into the intermediate compartment at the ER-Golgi interface with the nucleocapsid protein attaching directly to viral RNA and spike-, envelope and membrane-protein being folded in the endoplasmic reticulum first. After assembly in the intermediate compartment, viral particles bypass the Golgi apparatus and are directly translocated to the plasma membrane in saccular intermediate compartment elements that function as transport carriers (Saraste and Prydz 2021).

1.4.2 Unconventional secretion in *U. maydis* – mechanism and biotechnology

Unconventional secretion in *U. maydis* is facilitated by a mechanism recently described as lock-type secretion (Reindl et al. 2019). The discovery of this novel pathway started with the detection of chitinase Cts1 in *U. maydis* supernatants, even though it did not carry a N-terminal signal peptide (Koepke et al. 2011). Cts1 is a GH18 type chitinase and part of the chitinolytic machinery of *U. maydis* that consists of chitinases Cts1 to Cts4 (Koepke et al. 2011, Langner et al. 2015). Interestingly, only Cts1 is secreted unconventionally while Cts2 to 4 all carry N-terminal signal peptides (Langner et al. 2015). Unconventional secretion of Cts1 was confirmed by fusion of Cts1 to the bacterial β-glucuronidase reporter enzyme (Gus) (Stock et al. 2012). By chance, Gus carries an *N*-glycosylation site that is unaffected when expressed in bacteria but glycosylated when conventionally secreted in eukaryotic hosts, rendering it largely inactive (Farrel and Beachy 1990). When Gus was fused to the N-terminus of Cts1, however, activity was detectable extracellularly (Stock et al. 2012). Cts1 localizes to the fragmentation zone between mother and daughter cell during late stages of cytokinesis but in the

cytoplasm in single cells (Langner et al. 2015, Aschenbroich et al. 2019). Separation of mother and daughter cell and thus formation of the fragmentation zone is initiated by the construction of primary and secondary septa (Weinzierl et al. 2002). This involves the formation of a contractile actomyosin ring in which the Cdc42-Guanine exchange factor Don1 and the Ste20-like protein kinase Don3 are key players (Böhmer et al. 2008, Böhmer et al. 2009). Furthermore, all three key players are co-localized with Cts1 in the fragmentation zone during the late stages of cytokinesis (Sandrock et al. 2006, Böhmer et al. 2009, Schink and Bölker 2009). It was also shown that Don3 itself is unconventionally secreted using the Gus reporter, albeit at low amounts (Aschenbroich et al. 2019). Moreover, loss of Don1 and Don3 results in a strong cytokinesis defect, resulting in tree like structures that lack a secondary septum (Weinzierl et al. 2002, Aschenbroich et al. 2019). Interestingly Cts1 secretion is strongly diminished in these strains but not in other cytokinesis defect strains that still form a secondary septum. Additionally, cell cycle inhibitor experiments indicated that Cts1 secretion is linked to the cell cycle and formation of the secondary septum while cell separation is not required (Aschenbroich et al. 2019). A genetic screen identified three unconventional secretion mutants. Interestingly all three mutants carried mutations in the open reading frame *umag_03776* resulting in expression of truncated versions of the UMAG_03776 protein which was then named Jps1 (jammed in protein secretion screen 1). Further studies revealed co-localization of Jps1 and Cts1 in the fragmentation zone and that Cts1 localization was dependent on Jps1 but not vice versa. Thus, Jps1 was proposed as an anchoring factor for Cts1 in the fragmentation zone (Reindl et al. 2020b).

The current model for unconventional secretion (Fig 1.5) involves the translocation of Cts1 to the fragmentation zone under guidance of Jps1 in the late stages of cytokinesis. Formation of the secondary septum is induced by Don1, Don3 and Cdc42 and upon completion of the fragmentation zone Cts1 and Don3 are released.

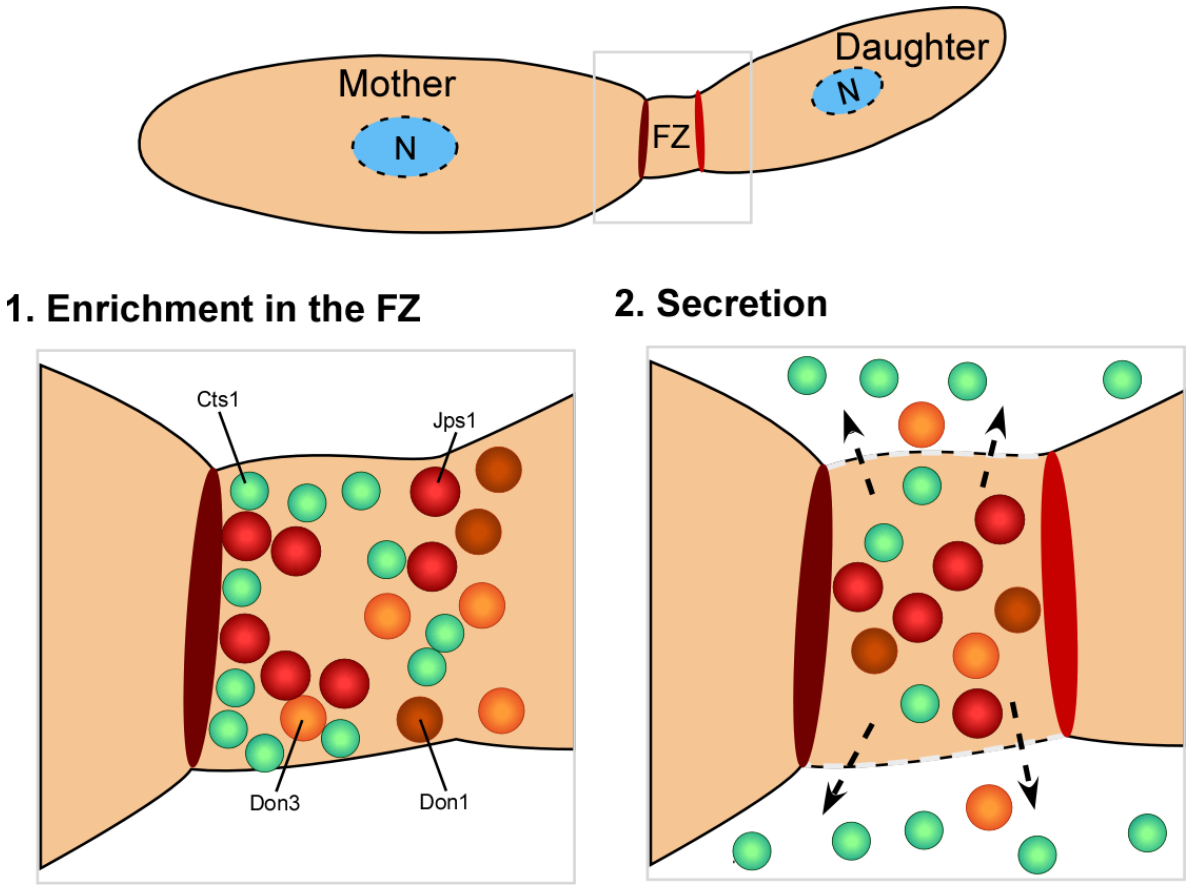

Figure 1.5: Model of lock-type unconventional secretion. Jps1 likely acts as an anchoring factor for Cts1 at the vicinity of the primary septum of the yet unfinished fragmentation zone upon the late stages of the cell cycle. Don1 and Don3 act in formation of the secondary septum and upon completion of the fragmentation zone are secreted into the supernatant. Modified from Wierckx et al. (2021).

Importantly, unconventional secretion of Cts1 can be hitchhiked for the secretion of several active proteins, a process that harbors some interesting advantages. First of all, *N*-glycosylation is avoided which is favorable for the production of biopharmaceuticals since protein based drugs carrying fungal *N*-glycosylation can trigger severe immune responses in patients (Gerngross 2004). Furthermore, protein stability can be decreased by glycosylation and bacterial enzymes can be completely inactivated (Tull et al. 2001, Stock et al. 2016a). Secondly, export of large proteins is feasible, as demonstrated by the export of the 173 kDa Gus-Cts1 fusion protein (Stock et al. 2012). Thirdly, Cts1 has been shown to tightly bind chitin, as demonstrated by a Gfp-nanobody-Cts1 fusion protein that was used for a Gfp pulldown on chitin magnetic beads, making it a potentially integrated purification and immobilization tag, next to its use as a carrier (Terfrüchte et al. 2017). Besides reporters like Gus or LacZ this has led to the expression and secretion of several biotechnologically relevant proteins like scFvs, a nanobody against botulinum toxin A and bacterial polygalacturonases via Cts1 hitchhiking (Sarkari et al. 2014,

Terfrüchte et al. 2017, Stoffels et al. 2020). However, the huge drawback of the system has thus far been its low secretory yield.

Towards a competitive expression platform several strategies to optimize unconventional protein secretion in *U. maydis* have been applied. On the genetic side strong constitutive promoters were introduced to increase transcript levels of secretion targets (Sarkari et al. 2014). Additionally, proteolytic activity was reduced by deletion of pre-pro-protease convertase *kex2,* however, this resulted in severe growth defects (Sarkari et al. 2014). Thus, instead, up to eight proteases in a single AB33 strain were deleted, resulting in strong yield improvements (Sarkari et al. 2014, Terfrüchte et al. 2018). Furthermore, an inducible secretion system based on transcriptional and translational regulation of Don3, reconstituting the deletion phenotype of *don3* both in morphology and secretion upon Don3 induction, was developed (Hussnätter et al. 2021). Genetic engineering efforts were supported by studies in process engineering. Through the use of online monitoring media conditions were optimized and through the use of buffered media, pH could be kept stable in expression cultures, thus preventing activity of extracellular proteases at low pH and increasing secretory yield and protein stability (Terfrüchte et al. 2018). Furthermore, an auto induction process was developed for the Don3 based inducible secretion system (Hussnätter et al. 2021). However, while yields could be improved significantly, reaching up to 140 µg/L for αBonTA-nanobody-Cts1, they are still not competitive.

1.5 Aim of this thesis

The biotechnological potential of *U. maydis* for production of heterologous proteins, especially biopharmaceuticals, has previously been demonstrated (Stock et al. 2012, Terfrüchte et al. 2017). Furthermore, the system has been thoroughly optimized by both genetic and process engineering tools and by elucidation of the underlying mechanism (Terfrüchte et al. 2018, Reindl et al. 2019, Hussnätter et al. 2021). Immobilization of the export carrier Cts1 via chitin binding was demonstrated, allowing for the use of the carrier as a built-in immobilization-tag (Terfrüchte et al. 2017). However, these findings and optimizations have not yet let to either a competitive yield nor a suitable application strategy for *U. maydis* derived biopharmaceuticals. Therefore, two main goals were set for this thesis:

i. First, anchoring factor Jps1 should be characterized as a potential new carrier for unconventional protein export. Jps1 was shown to co-localize with Cts1 in the fragmentation zone in the late stages of cytokinesis and to be exported into the culture supernatant, making it an ideal candidate to potentially increase yields of the system.
ii. Second, the production of biopharmaceuticals and the immobilization of Cts1 should be combined into a functional application. Therefore, a chitin-based ELISA type antigen test should be established, if possible, utilizing direct detection of the antigen via a functionalized nanobody.

2 A novel secretion carrier

A novel potent carrier for unconventional protein export in *Ustilago maydis*

Magnus Philipp[1], Kai. P. Hussnätter[1], Michèle Reindl[1], Kira Müntjes[1], Michael Feldbrügge[1] and Kerstin Schipper[1,*]

[1] Institute for Microbiology, Heinrich Heine University Düsseldorf, Universitätsstraße 1, 40225 Düsseldorf, Germany

*** Correspondence:**

Kerstin Schipper

kerstin.schipper@uni-duesseldorf.de (KS)

Keywords: Luciferase, Sars-CoV2, sybody, unconventional secretion, *Ustilago maydis*.

Abstract

Recombinant proteins are ubiquitously applied in fields like research, pharma, diagnostics or the chemical industry. To provide the full range of useful proteins, novel expression hosts need to be established for proteins that are not sufficiently produced by the standard platform organisms. Unconventional secretion in the fungal model *Ustilago maydis* is an attractive novel option for export of heterologous proteins without *N*-glycosylation using chitinase Cts1 as a carrier. Recently, a novel factor essential for unconventional Cts1 secretion termed Jps1 was identified. Here, we show that Jps1 is unconventionally secreted using a fusion to bacterial β-glucuronidase as an established reporter. Interestingly, the experiment also demonstrates that the protein functions as an alternative carrier for heterologous proteins, showing about 2-fold higher reporter activity than the Cts1 fusion in the supernatant. In addition, Jps1-mediated secretion even allowed for efficient export of functional firefly luciferase as a novel secretion target which could not be achieved with Cts1. As an application for a relevant pharmaceutical target, export of functional bi-specific synthetic nanobodies directed against the SARS-CoV2 spike protein was demonstrated. The establishment of an alternative efficient carrier thus constitutes an excellent expansion of the existing secretion platform.

2.1 Introduction

The market for recombinant proteins like biopharmaceuticals is steadily increasing (Walsh 2018). As one example, the number of monoclonal antibody therapeutics entering phase 3 clinical trials has risen from 39 in 2014 to 88 in 2020 (Reichert 2015, Kaplon and Reichert 2021). Protein secretion into the culture broth is an excellent strategy for the production of recombinant proteins because it supports straightforward and inexpensive downstream processing (Nicaud et al. 1986, Flaschel and Friehs 1993). In eukaryotes, proteins are mostly targeted via the endomembrane system by N-terminal signal peptides for secretion (Viotti 2016). By contrast, the term unconventional secretion describes protein export that does not occur via the classical endomembrane system including endoplasmic reticulum and Golgi apparatus (Nickel 2010). Various routes for such alternative secretion events exist, including direct transfer across the plasma membrane via transporters or self-sustained translocation or vesicular pathways where membrane vesicles are hitchhiked for export (Nickel 2010, Rabouille 2017).

Unconventional export of chitinase Cts1 in yeast cells of the fungal model *Ustilago maydis* is coupled to cytokinesis in a lock-type mechanism (Reindl et al. 2019). Upon formation of the daughter cell at one growth pole of the cigar shaped mother cell, Cts1 is targeted to the so-called fragmentation zone delimited at the mother-daughter neck by consecutive formation of two septa (Langner et al. 2015). Here, the chitinase participates in separation of the two cells likely by degrading the remnant cell wall (Langner et al. 2015). Two septation factors, guanine nucleotide exchange factor (GEF) Don1 and kinase Don3, are essential for formation of the secondary septum and for Cts1 secretion (Weinzierl et al. 2002, Aschenbroich et al. 2019). Furthermore, a recently identified potential anchoring factor, Jps1, is crucial for chitinase localization and export (Reindl et al. 2020b).

Importantly, unconventional Cts1 secretion can be exploited for co-export of heterologous proteins (Stock et al. 2012). Circumventing the classical secretion system is advantageous for the production of distinct proteins, because it avoids post-translational modifications like *N*-glycosylation occurring in the endomembrane system. In addition, there is no apparent size limitation (Stock et al. 2012). Successful examples are secretion of functional enzymes like β-glucuronidase or β-galactosidase, and antibody formats like scFvs or nanobodies (Stock et al. 2012, Sarkari et al. 2014, Terfrüchte et al. 2017, Reindl et al. 2020b). While the secretion system is operational for several target proteins, low yields in the µg per liter range are currently limiting its applicability (Terfrüchte et al. 2017). Recently, major improvements were achieved by the generation of protease-deficient

production strains, usage of strong constitutive promoters and medium optimization (Sarkari et al. 2014, Terfrüchte et al. 2018). However, novel strategies to further advance the system are needed.

In the present study we demonstrate that Jps1 is a novel potent carrier for co-export of heterologous proteins. We observed improved overall yields of secreted protein and export of firefly luciferase that was not functionally secreted via Cts1-fusions. As a proof-of-principle for pharmaceutical proteins we exported functional nanobodies directed against the receptor-binding domain (RBD) of the SARS-CoV2 spike protein. The novel carrier thus constitutes an important improvement of our expression system towards a competitive production platform.

2.2 Results

2.2.1 Jps1 is a potent new carrier for unconventional protein export

Previous experiments had shown that Jps1 co-localizes with Cts1 in the fragmentation zone (Reindl et al. 2020b), suggesting that it might also be unconventionally secreted. To study this, we applied the well-established β-glucuronidase (Gus) reporter system (Fig. 2.1 A, B). This bacterial enzyme is largely inactivated upon secretion through the eukaryotic endomembrane system. By contrast, it is released in a functional state via unconventional secretion in yeast cells of *U. maydis* (Stock et al. 2012). To assay unconventional secretion of Jps1, a strain expressing a Gus-Jps1 fusion protein was generated in the background of the octuple protease-deletion laboratory strain AB33P8Δ (Fig. 2.1 A) (Terfrüchte et al. 2018). Microscopic analysis revealed that yeast cells expressing Gus-Jps1 did not show any morphological differences as compared to the progenitor (Sup. Fig. 2.1, 2.2). The Gus-Jps1 fusion did also not disturb Cts1 function as detected by determining extracellular chitinase activity of AB33P8Δ/Gus-Jps1 which was similar to the activity detected in a strain expressing Gus-Cts1 (Sup. Fig. 2.1). Subsequently, intra- and extracellular Gus activity was determined (Fig. 2.1 C, D). The progenitor strain AB33P8Δ was used as a negative control, while a strain expressing intracellular Gus served as a lysis control (AB33 Gus^{cyt}) (Stock et al. 2012). High Gus activity was present in cell extracts of all strains harboring the Gus enzyme but not in the progenitor AB33P8Δ lacking the enzyme (Fig. 2.1 C). Importantly, Gus activity was also detected in the supernatant of Gus-Jps1 expressing strains but not for the lysis control, confirming unconventional secretion of Jps1 (Fig. 2.1 D). At the same time, this experiment demonstrates, that Jps1 – similar to Cts1 - is able to act as a carrier for heterologous proteins. Notably, extracellular Gus activity levels were increased by about 2-fold in culture supernatants of Gus-Jps1 compared to Gus-Cts1 expressing

strains (Fig. 2.1 D), suggesting that Jps1 might constitute a more effective carrier than Cts1. Both strains were also compared in terms of growth speed and strain fitness using online monitoring in a BioLector device (m2p-labs, Baesweiler, Germany) (Funke et al. 2010). The progenitor strain AB33P8Δ as well as AB33P8Δ/Gus-Cts1 and AB33P8Δ/Gus-Jps1 showed similar proliferation patterns and doubling times of about 3 h during the exponential growth phase when incubated in CM medium supplemented with 1% glucose (Sup. Fig. 2.2). Thus, Jps1 constitutes a promising candidate for a novel potent carrier for heterologous proteins.

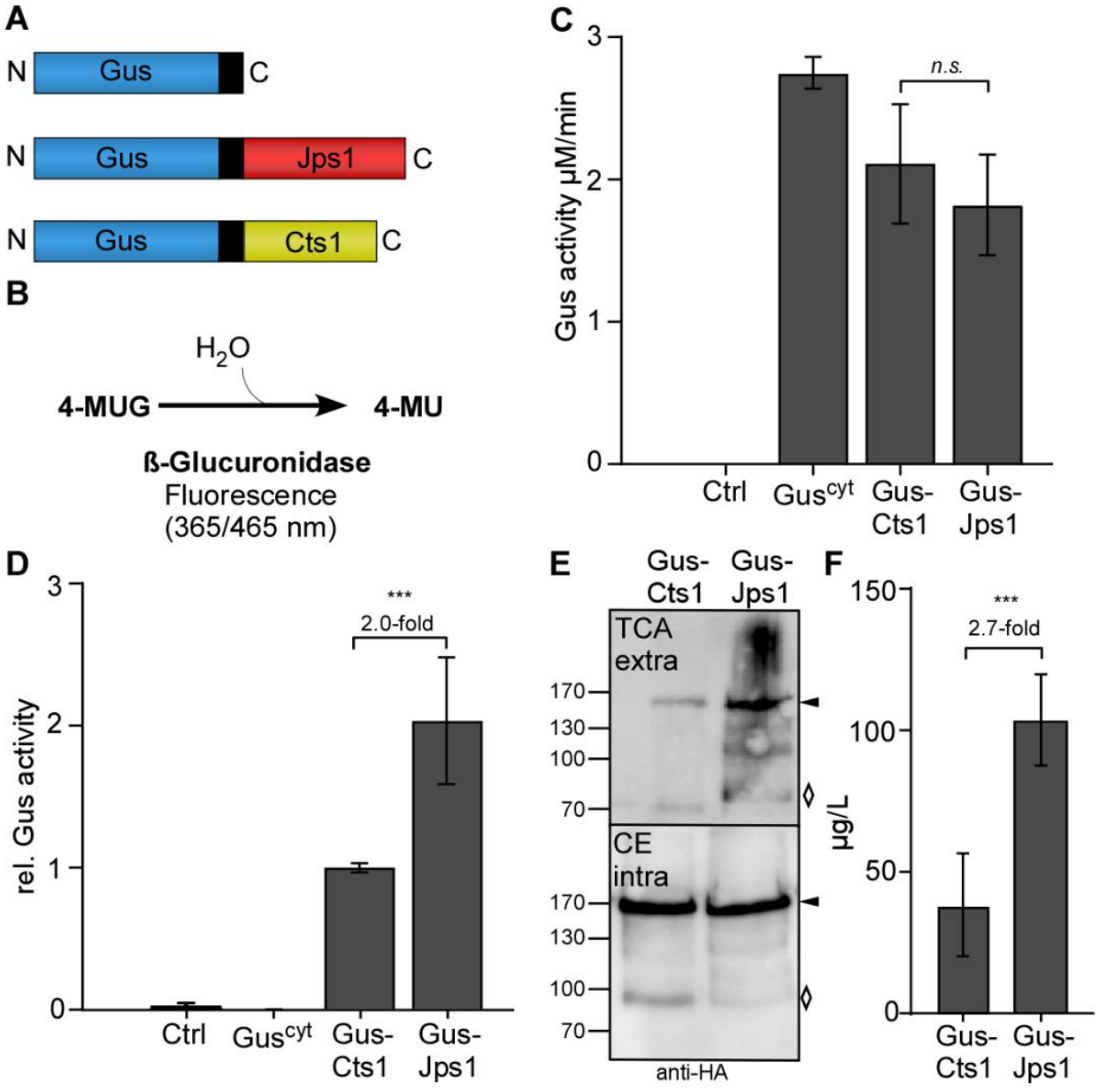

Figure 2.1: Jps1 is unconventionally secreted and serves as an alternative carrier for Gus export.
Schematic display of the proteins expressed to study unconventional secretion. Cytoplasmic Gus (Gus^{cyt}) is used as a lysis control (top). Gus-Jps1 (middle) and Gus-Cts1 (bottom) harbor the respective carrier proteins at the C-terminus. All proteins carry an SHH (double Strep, ten times His, triple HA) tag indicated in black (Sarkari et al. 2014). All schemes are drawn to scale. **(B)** Enzymatic reaction mediated by β-glucuronidase. 4-methyl-umbeliferyl-β-D-glucuronide (4-MUG) and H_2O are converted to 4-methyl-umbelliferone which is a fluorescent molecule (365 nm excitation/ 465 nm emission). **(C)** Determination of intracellular Gus activity. Progenitor strain AB33P8Δ (Ctrl) and AB33 Gus^{cyt} expressing cytoplasmic Gus were included as controls. The experiment was conducted in three biological replicates. **(D)** Comparative extracellular Gus activity of strains using either Cts1 or Jps1 as a carrier. Enzyme activities were normalized to average values of the strain secreting Gus-Cts1. AB33P8Δ and AB33 Gus^{cyt} were used as a negative and lysis controls, respectively. The experiment was conducted in three biological replicates. **(E)** Representative Western blot analysis of Gus-Cts1 and Gus-Jps1 secretion. Extracellular protein was enriched from culture supernatants by TCA precipitation. Intracellular protein levels were visualized by cell extracts. Western blots show 1 ml of precipitated supernatants (TCA) and 10 µg cell extract (CE). Full length protein signal indicated by arrows, degradation bands with a rhombus. **(F)** Quantification of secreted protein using Western blot analysis. Supernatants of strains producing Gus-Jps1 or Gus-Cts1 were enriched by TCA precipitation and subjected to Western blot analysis. Signal intensities were compared to defined protein amounts of Multiple Tag protein (GenScript Piscataway, NJ, USA) included in the same gel. Bars show extrapolated protein amounts in µg/L. Western blots used for the analysis, see Fig. S3. Three biological replicates are shown; error bars in figures **(C)**, **(D)**, and **(F)** indicate standard deviation. Definition of statistical significance (***): p-value < 0.05. p-value derived from students unpaired t-test.

To assay secretion on the protein level, Western blot analyses were conducted. These experiments showed that extracellular amounts of Gus-Jps1 were markedly increased as compared to Gus-Cts1, while intracellular levels were comparable. This confirms that Jps1 is secreted with enhanced efficiency in relation to Cts1 (Fig. 2.1 E, Sup. Fig. 2.3). To quantify this result distinct amounts of Multiple Tag protein (GenScript Biotech, Piscataway, NJ, USA) were included (Sup. Fig. 2.4). Quantification of the Western blot signals revealed that Gus-Cts1 levels in the supernatant reach concentrations of 38 µg/L while Gus-Jps1 is present at about 103 µg/L (about 2.7-fold increase; Fig. 2.1 F). In summary, these results demonstrate that Jps1 can deal as a powerful carrier for heterologous proteins with elevated levels in comparison to Cts1.

2.2.2 *don3* induced secretion further enhances Gus-Jps1 secretion

Recently, we have established a system that allows for the induction of unconventional secretion via regulation of kinase Don3, a gatekeeper of the fragmentation zone (Hussnätter et al. 2021). To this end we used a arabinose-inducible promoter to control *don3* expression, which is prerequisite for

secondary septum formation (Weinzierl et al. 2002). Unconventional secretion is only functional with a functional fragmentation zone consisting of two septa (Aschenbroich et al. 2019). Here we reproduced these findings using Jps1 as a carrier as demonstrated by a strain which carried genetic modifications for transcriptional induction of *don3* and expressed the Gus-Jps1 reporter as read-out (Fig. 2.2 A, B) (Hussnätter et al. 2021). Although we observed a slightly higher background activity in arabinose cultures, the induction was more than 18-fold and thus, significantly higher than for using Cts1 as a carrier protein, showing about 12-fold induction (Fig. 2.2 B). Furthermore, Gus-activity was elevated 2.4-fold compared to induced Gus-Cts1 secretion and more than 3-fold compared to regular Gus-Cts1 secretion. Hence, inducible Jps1 constitutes a powerful tool for unconventional secretion of heterologous proteins. Jps1 enables export of functional firefly luciferase

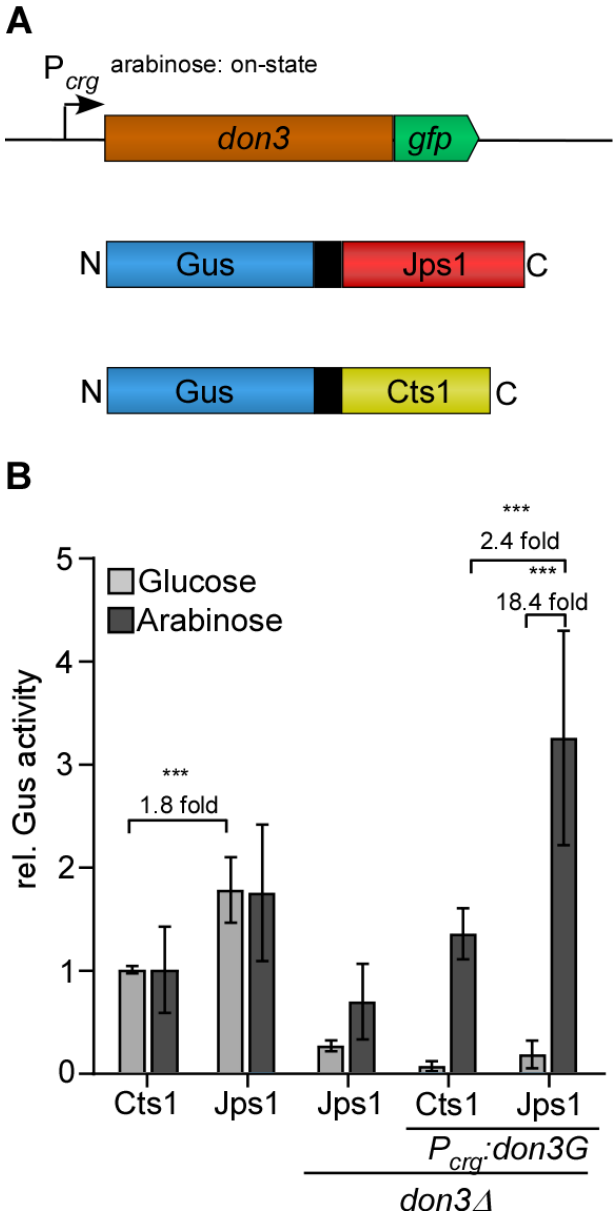

Figure 2.2: Inducible secretion of Gus-Jps1 via transcriptional regulation of *don3*. (A) Schematic display of the inducible secretion system. *don3-gfp* is expressed under control of the arabinose-inducible promoter $P_{crg.}$ Under glucose conditions the promoter is in its "off state", unconventionally secreted proteins under control of P_{oma} are thus expressed but not secreted. Under arabinose condition the promoter is in its "on state" and proteins are secreted. Gus is fused to either Cts1 or Jps1 including an internal SHH tag (double Strep, ten times His, triple HA). **(B)** Gus activity in culture supernatants of AB33 derivatives expressing Gus-Cts1 or Gus-Jps1 and their Δ*don3* variants. Enzymatic activity was normalized to average values of positive controls secreting Gus-Cts1 constitutively. The diagram represents the results of three biological replicates. Error bars depict standard deviation. Fold change of induced cultures depicted over brackets. Definition of statistical significance (***): p-value < 0.05. p-value derived from students unpaired t-test.

2.2.3 Jps1 enables export of functional firefly luciferase

Photinus pyralis luciferase FLuc was recently established for intracellular use in *U. maydis* (Müntjes et al. 2020). Bioluminescence would be a straight-forward alternative read-out for unconventional secretion because the signal can be detected directly from the culture broth while the established reporters Gus and β-galactosidase (LacZ) require more elaborate biochemical assays. Further advantages are low background signals and the use of the inexpensive substrate D-luciferin (Miska and Geiger 1987). To test bioluminescence as a read-out for unconventional secretion, an expression strain producing FLuc-Cts1 was generated in the background of the octuple protease deletion strain (AB33P8Δ/FLuc-Cts1). Similarly, a FLuc-Jps1 expressing strain was generated (AB33P8Δ/FLuc-Jps1) to evaluate the effect of the alternative carrier (Fig. 2.3 A). AB33 producing intracellular luciferase ($FLuc^{Cyt}$) was used as a positive control in all assays (Müntjes et al. 2020). Monitoring of proliferation revealed that growth speed was slightly reduced in AB33P8Δ/FLuc-Jps1 with a doubling time of 3.5 h, compared to the progenitor strain AB33P8Δ and AB33P8Δ/FLuc-Cts1 showing doubling times of 3 h in the exponential growth phase (Sup. Fig. 2.2). The slight reduction might eventually be caused by a minor increase in the number of abnormal cells growing in clusters in the FLuc-Jps1 expressing strain (Sup. Fig. 2.2 C). Luciferase assays showed that intracellular activity was very low in the FLuc-Cts1 expressing strain compared to the strain producing cytoplasmic FLuc, while levels of Fluc-Jps1 expressing strains were comparable to the cytoplasmic control showing significant activity (Fig. 2.3 C). Importantly, in culture supernatants the observed effect was even more pronounced and extracellular FLuc activity for the strain producing FLuc-Jps1 was about 48-fold higher than activity of FLuc-Cts1 secreting cells for which no significant difference to the control strain could be observed (Fig. 2.3 D). These results were confirmed in Western blot analyses. While intracellular levels of FLuc-Cts1 were reduced in comparison to FLuc-Jps1 which showed an about 1.8-fold higher signal intensity, only FLuc-Jps1 was detectable in supernatants (Fig. 2.3 E; Sup. Fig. 2.3). This demonstrates that not only expression of FLuc-Cts1 was impaired, but also detectable Cts1 based secretion was absent. The reason for the differential performance of the Cts1 and Jps1 fusions with FLuc remains unclear. The size of the FLuc-Cts1 fusion protein is likely not affecting its unconventional secretion, since larger fusions had been successfully exported in earlier studies (Stock et al. 2012). Eventually, structural interferences or other unknown features of this particular fusion led

to reduced protein production or its instability. These results further emphasize the advantage of having a second carrier for the unconventional secretion system at hands.

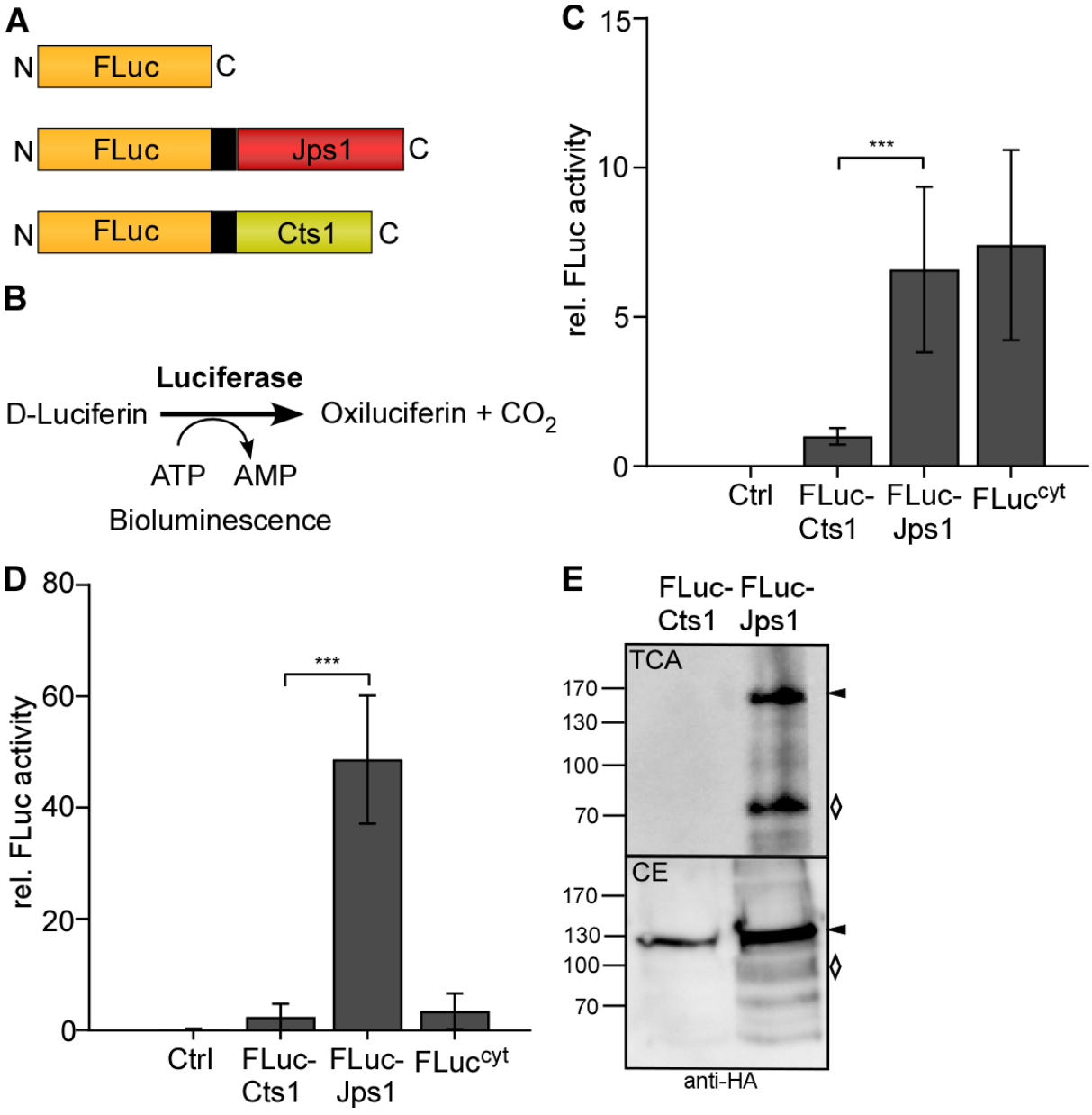

Figure 2.3: Efficient Jps1-mediated export of firefly luciferase as a new reporter for unconventional secretion. (A) Schematic display of the proteins expressed to study unconventional secretion. Cytoplasmic FLuc ($FLuc^{cyt}$) was used as a lysis control (top). FLuc-Jps1 (middle) and FLuc-Cts1 (bottom) harbor the respective carrier proteins at the C-terminus. All proteins carry an SHH tag indicated in black (Sarkari et al. 2014). All schemes are drawn to scale. **(B)** Enzymatic reaction mediated by firefly luciferase: D-Luciferin and ATP are converted to oxiluciferin, AMP and CO_2. During this reaction excited intermediates emit energy in the form of light that can be detected as bioluminescence. **(C)** Comparison of intracellular FLuc activity of the strains AB33P8Δ/FLuc-Cts1 and AB33P8Δ/FLuc-Jps1. Enzymatic activity was normalized to average values of strain secreting FLuc-Cts1. The progenitor strain AB33P8Δ was used as a negative control. Strain AB33 $FLuc^{cyt}$ with intracellular FLuc expression dealt as positive control. Three biological replicates are shown. **(D)**

Comparison of extracellular FLuc activity of strains harboring either Cts1 or Jps1 as a carrier. Enzymatic activity was normalized to average values of strain secreting FLuc-Cts1. Strain AB33 $FLuc^{cyt}$ with intracellular FLuc expression dealt as lysis control**.** Three biological replicates are shown. Error bars in figures **(C)** and **(D)** indicate standard deviation. Definition of statistical significance (***): p-value < 0.05. p-value was derived from students unpaired t-test. **(E)** Representative Western blot of FLuc-Cts1 and FLuc-Jps1. Secreted protein was enriched from the supernatant by TCA precipitation. Intracellular protein levels were visualized by cell extracts. Western blots show 1 ml of precipitated supernatants (TCA) and 10 µg cell extracts (CE). Full length protein signals indicated by arrows, degradation bands with a rhombus.

2.2.4 Unconventional secretion of functional antibodies against Sars-CoV2-RBD

Next, we tested unconventional secretion of nanobodies directed against the SARS-CoV2 spike protein receptor binding domain (RBD) as a timely example of pharmaceutically relevant targets. Therefore, strains were generated in which two synergistic synthetic nanobodies (sybodies) directed against the Sars-CoV2 spike-RBD were combined (Walter et al. 2020). The bi-specific sybody was tagged with a 10× His-linker for purification and fused to either Cts1 or Jps1 for unconventional secretion (AB33P8Δ/$Sy^{68/15}$-Cts1 and AB33P8Δ/$Sy^{68/15}$-Jps1) (Fig. 4 A). Western blot analyses confirmed that both fusion proteins were synthesized. However, $Sy^{68/15}$-Cts1 was produced at a lower level compared to $Sy^{68/15}$-Jps1. The latter showed stronger degradation than observed for other Jps1 fusion proteins (see above). In supernatants only a very faint signal was present for $Sy^{68/15}$-Cts1 while for $Sy^{68/15}$-Jps1 a stronger signal and less degradation than in cell extracts was detected (Fig. 4 C). Quantification revealed an increase of about 18-fold in signal intensity for the Jps1 full-length fusion compared to the Cts1 full-length fusion (Sup. Fig. 3). Subsequently, the antigen-binding activity of the sybody was determined via direct confrontation with spike-RBD immobilized on ELISA plates and subsequent detection with an antibody sandwich. Immobilized bovine serum albumin (BSA) dealt as a negative control. ELISA experiments using cell extracts demonstrated that both sybody-fusion proteins were functional in detecting the cognate antigen. While the activity of $Sy^{68/15}$-Cts1 was only slightly above baseline, $Sy^{68/15}$-Jps1 showed strong volumetric activity (Fig. 4 E). Next, sybody- fusion proteins were IMAC purified from culture supernatants and applied to ELISA in up to 10-fold concentrated solutions. While no activity could be observed for $Sy^{68/15}$-Cts1, $Sy^{68/15}$-Jps1 showed volumetric binding activity on the antigen, confirming the secretion of the functional sybody fusion

protein. Thus, pharmaceutically relevant nanobodies were exported in their functional form using Jps1 as a carrier for unconventional secretion.

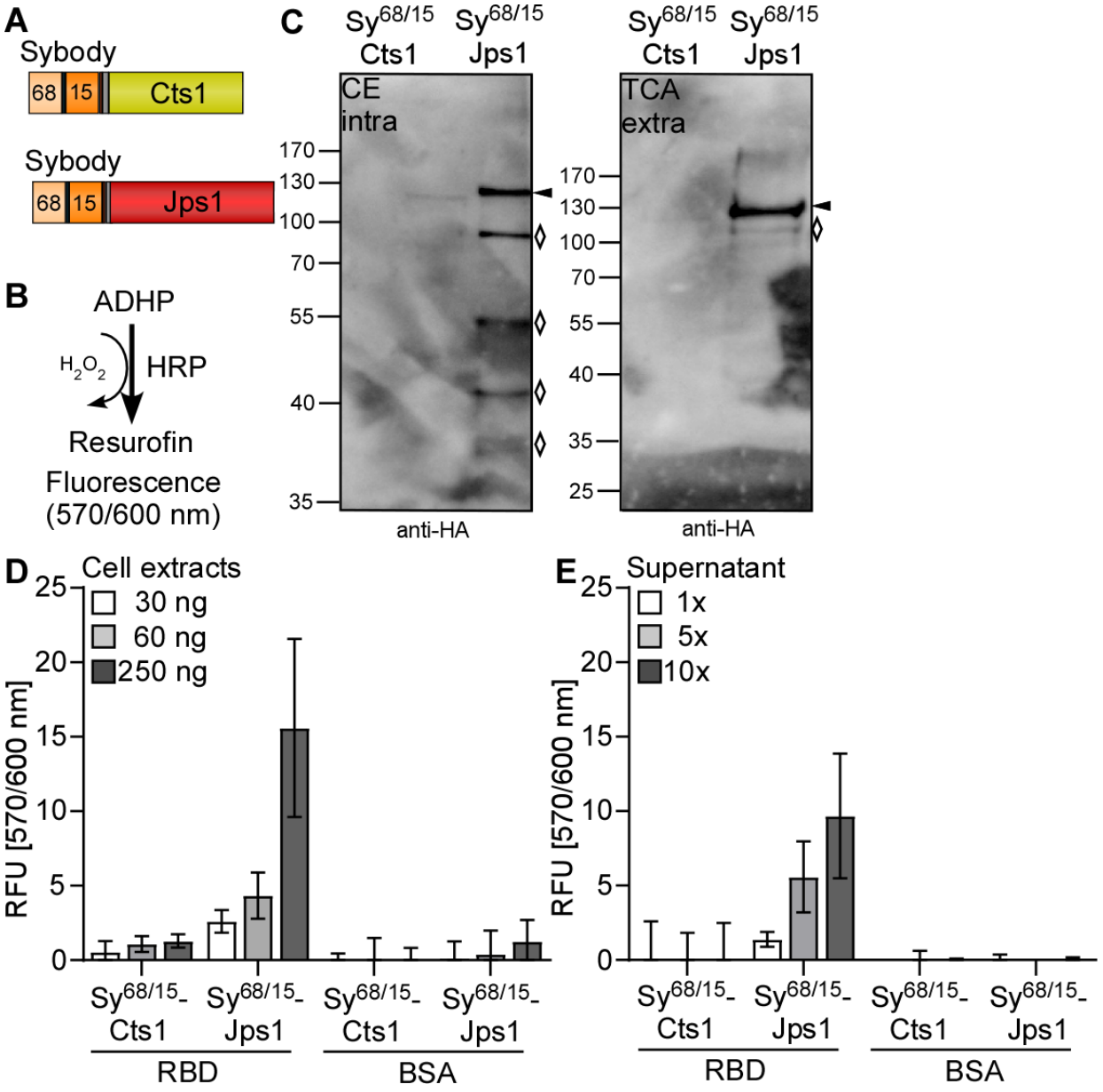

Figure 2.4: Export of functional bi-specific Sars-CoV2 sybodies using Jps1 as a carrier for unconventional secretion. **(A)** Bi-specific anti SARS-CoV2 spike-RBD sybodies sy#15 and sy#68 (Walter et al. 2020) were tagged with a 10x His tag and fused to either Cts1 (top) or Jps1 (bottom) via a TEV protease cleavage site and an HA-tag. **(B)** Detection reaction for ELISA: Colorless 10-acetyl-3,7-dihydrophenoxazine (ADHP) is converted by horseradish peroxidase (HRP) using H_2O_2 to resurofin, a purple substance that emits strong fluorescence (excitation 570 nm, emission 600 nm). **(C)** Representative Western blot analyses of $Sy^{68/15}$-Cts1 and $Sy^{68/15}$-Jps1. Secreted protein was enriched from the supernatant by TCA precipitation. Intracellular protein levels were visualized by cell extracts. Western blots show 1 ml of precipitated supernatants (TCA) and 10 µg cell extracts (CE). Full length protein signals indicated by arrows, degradation bands with rhombi. **(D)** ELISA of cell extracts: 1 µg of RBD was immobilized per well. 1 µg BSA dealt as a negative control. Baseline was established by a well coated with RBD and only treated with anti-HA and anti-mouse-HRP. Serial dilutions of *U.*

maydis cell extracts (30 ng, 60 ng, 250 ng per well) were applied in technical triplicates both to RBD and BSA coated wells. Detection was carried out with the before mentioned anti-HA-mouse and anti-mouse-HRP antibodies. Three biological replicates are shown. Error bars indicate standard deviation of biological replicates. **(E)** ELISA of protein purified from supernatants: ELISA wells were coated, and reactions detected as described in **(D)**. Culture supernatants containing sybody-fusion proteins were subjected to $Nickel^{2+}$-NTA IMAC and subsequently concentrated up to 10-fold. Serial dilutions of supernatants (1-fold, 5-fold, 10-fold concentrated supernatant) were mixed with blocking solution and added to ELISA wells in technical triplicates. Three biological replicates are shown. Error bars indicate standard deviation for biological replicates.

2.3 Discussion

Here we successfully evaluated the potential anchoring factor Jps1 as a novel carrier for the export of heterologous proteins by unconventional secretion in *U. maydis*. Carrier proteins are ubiquitously used in fungal protein expression systems based on conventional secretion (Fleissner and Dersch 2010). This is mainly due to the observation that homologous proteins like hydrolytic enzymes are secreted with very high titers compared to heterologous targets (Nevalainen and Peterson 2014). In our system, similar to the previously used carrier chitinase Cts1, Jps1 was fused to the C-terminus of heterologous target proteins to mediate their export via the fragmentation zone. Of note, one exception identified during this study was the reporter enzyme LacZ: Here, a LacZ-Cts1 fusion is functional and unconventionally secreted (Reindl et al. 2020b) while strains producing the respective LacZ-Jps1 fusion showed growth retardation and were lacking detectable LacZ activity and LacZ-Jps1 protein in the culture supernatant (results not shown). We anticipate that this could be related to the formation of tetramers by LacZ which interfere with Jps1 but not with Cts1 secretion; however, this hypothesis needs to be verified. Nevertheless, the discovery of a second carrier for unconventional secretion in *U. maydis* is a very favorable addition to our expression system (Reindl et al. 2019, Wierckx et al. 2021): The choice between the two fusion proteins, Cts1 and Jps1, will greatly enhance the repertoire of our secretion targets. Jps1 proofed valuable for the export of proteins that were not secreted at significant levels as Cts1 fusions and showed promising secretion levels for these targets. This is for example true for the firefly luciferase FLuc or the bi-specific sybodies that were only secreted efficiently when fused to Jps1. As a positive side effect, the FLuc-Jps1 fusion protein is a valuable alternative that allows a quick and inexpensive quantification of unconventional secretion via Jps1 in future studies (Wider and Picard 2017, Branchini et al. 2018). On the contrary, the intrinsic feature of chitin binding of Cts1 is very attractive as a tool which can be developed for efficient *in situ* protein purification from culture

broth (Terfrüchte et al. 2017). Hence, both carriers show distinct advantages that can be exploited depending on the actual demands.

In line with our results, different carriers show varying efficiencies in other fungal systems. For example, glycoamylase or α-amylase have been described as a powerful tool for heterologous protein secretion in filamentous fungi like Aspergilli (Ward et al. 1990, Nakajima et al. 2006). Similarly, the choice of the conventional signal peptide for efficient entry into the endoplasmic reticulum has been described as a key factor for improving conventional secretion (Xu et al. 2018, Wang et al. 2020b). While existence of a signal peptide remains elusive for lock-type unconventional secretion (Stock et al. 2012), it is conceivable that other unconventionally secreted proteins are still to be discovered that might constitute even more powerful carriers. Currently, we do not have a precise idea on why Jps1 mediates export of heterologous proteins more effectively than Cts1. Further studies on the molecular roles of Jps1 during Cts1 secretion might resolve this question in the future. Notably, unconventional secretion was also observed for septation factor Don3 (Aschenbroich et al. 2019) which may thus serve as such alternative carrier. However, Gus activity levels of unconventionally secreted Gus-Don3 are minute compared to Gus-Cts1, suggesting that it does not constitute a promising alternative (Aschenbroich et al. 2019). Hence, it is important to further study the mechanism of lock-type secretion and in particular, to identify further players that localize to the fragmentation zone for export during cytokinesis (Reindl et al. 2019, Wierckx et al. 2021).

The successful synthesis and functional export of nanobodies directed against the RBD of the surface spike protein of the SARS-CoV2 virus is a timely new addition to the repertoire of secreted targets. The current pandemics situation underpinned that it is important to develop novel methodology for quick, specific, and sensitive detection and treatment of viral infections in the future. On the one hand nanobodies are potent proteins for antigen detection (Muyldermans 2013) and thus very promising tools in the context of SARS-CoV2 detection. On the other hand, antibody-based pharmaceuticals like Casirivimab and Imdevimab are already used to treat COVID-19 infection (Sun and Ho 2020b). Therefore, besides application in virus diagnostics, nanobodies directed against SARS-CoV2 could potentially even become novel pharmaceutical targets for therapeutic approaches (Dubey et al. 2020). The unique system of unconventional secretion in *U. maydis* now offers new possibilities for nanobody production without the risk of undesired modifications by *N*-glycosylation (Stock et al. 2012). This would eliminate the necessity to humanize llama derived nanobodies for safe use as pharmaceuticals to avoid allergic reaction in patients (Vincke et al. 2009, Dong et al. 2020). To achieve this, both the unconventional secretion system and specifically the production and application of

nanobodies via this system have to be optimized, for example by further multimerization to increase valency and affinity (Wichgers Schreur et al. 2020, König et al. 2021). By the establishment of a new carrier and export of functional SARS-CoV2 nanobodies we have thus laid a solid foundation for further exploitation and application of lock-type unconventional secretion.

2.4 Material and methods

2.4.1 Molecular biology methods

All plasmids (pUMa/pUx vectors) generated in this study were obtained using standard molecular biology methods established for *U. maydis* including Golden Gate and Gibson cloning (Brachmann et al. 2004, Gibson et al. 2009, Gibson 2011, Terfrüchte et al. 2014). All plasmids were verified by restriction analysis and sequencing. Oligonucleotides applied for cloning are listed in Table 1. Genomic DNA of *U. maydis* strain UM521 was used as template for PCR reactions. The genomic sequence for this strain is stored at the EnsemblFungi database (EnsemblFungi). The generation of plasmids pUMa3329_Δupp1_P_{crg}-eGfp-T_{nos}-natR, pUMa2113_pRabX1-P_{oma}_gus-SHH-cts1, pUMa2240_Ip_Poma-his-αGfpllama-ha-Cts1-CbxR and pUMa3771_Δupp3_Potef_FLuc_NatR has been described previously (resulting strains, see Table 2). For the generation of pUMa3012_Ip_Poma_Gus-SHH-Jps1_CbxR the *jps1 gene* (*umag_03776*) was amplified from genomic DNA using primers oMB372 and oMB373 with AscI and ApaI hydrolyzation sites. Subsequently, the backbone of pUMa2113_Ip_Poma_Gus-SHH-Cts1_CbxR was used for restriction ligation cloning and *jps1* was inserted into the backbone instead of *cts1*. pUMa4131_Ip_Poma_FLuc-SHH-Cts1_CbxR was generated by amplification of the *U. maydis* dicodon-optimized *P. pyralis fluc* gene from pUMa3771_Δupp3_Potef_FLuc_NatR using oAB297 and oAB298 with BamHI and SfiI hydrolyzation sites. pUMa2113_Ip_Poma_Gus-SHH-Cts1_CbxR was then hydrolyzed with BamHI and SfiI and *fluc* was inserted into the backbone instead of *gus* via restriction/ligation cloning. A restriction/ligation cloning approach was applied for pUMa4566_Ip_Poma_FLuc-SHH-Jps1_CbxR. *jps1* was excised from pUMa3012_Ip_Poma_Gus-SHH-Jps1_CbxR using AscI and ApaI and inserted into pUMa4131_Ip_Poma_FLuc-SHH-Cts1_CbxR, also hydrolyzed with AscI and ApaI. pUx1_Ip_Poma-Sy#68-his-Sy#15-ha-Cts1-CbxR was generated by amplification of genes $sy^{\#68}$ and $sy^{\#15}$ (Walter et al. 2020) from a synthetic gBlock (Integrated DNA Technology, Coralville, Iowa, USA) using primers oAB908 and oAB909 for $sy^{\#15}$ adding BamHI and SpeI hydrolyzation sites and

oCD234 and oCD235 for *sy*$^{\#68}$ with complementary overhangs for Gibson cloning. Subsequently, pUMa2240_Ip_Poma-his-αGfpllama-ha-Cts1-CbxR (Terfrüchte et al. 2017) was hydrolyzed with BamHI and SpeI and gene *sy*$^{\#15}$ was inserted via restriction ligation cloning, replacing *αgfpllama* and thereby generating pUMa4678. pUMa4678 was then hydrolyzed with BamHI and the sequence encoding for sy$^{\#68}$ was inserted via Gibson cloning (Gibson et al. 2009), generating pUx1. For the generation of pUx8 *jps1* was excised from pUMa3012 using AscI and ApaI and inserted into the AscI and ApaI hydrolyzed backbone of pUx1.

2.4.2 Strain generation

U. maydis strains used in this study were obtained by homologous recombination yielding genetically stable strains (Bösch et al. 2016) (Table 2). For genomic integrations at the *ip* locus, integrative plasmids were used (Stock et al. 2012). These plasmids contained the *ip*^{r} allele, promoting carboxin resistance. For integration, plasmids were linearized within the *ip*^{r} allele to allow for homologous recombination with the *ip*^{s} locus. For transformation, integrative plasmids were hydrolyzed within the *ip*^{r} locus using the restriction endonuclease SspI, resulting in a linear DNA fragment. For genetic modifications in other loci, plasmids with about 1 kb flanking regions and a resistance cassette were generated (Brachmann et al. 2004, Terfrüchte et al. 2014). For transformation, the insertion cassette was excised from the plasmid backbone using SspI or SwaI (Terfrüchte et al. 2014). For all genetic manipulations, *U. maydis* protoplasts were transformed with linear DNA fragments for homologous recombination. All strains were verified by Southern blot analysis (Southern 1974). For *in locus* modifications the flanking regions were amplified as probes. For *ip* insertions, the probe was obtained by PCR using the primer combination oMF502/oMF503 and the template pUMa260 (Keon et al. 1991, Brachmann et al. 2004). Primer sequences are listed in Table 1.

2.4.3 Cultivation

U. maydis strains were grown at 28 °C in complete medium supplemented with 1% (w/v) glucose (CM-glc) or with 1% (w/v) arabinose (CM-ara) if not described differently (Holliday 1974a, Tsukuda et al. 1988). Solid media were supplemented with 2% (w/v) agar agar. Growth phenotypes were evaluated using the BioLector microbioreactor (m2p-labs, Baesweiler, Germany) (Funke et al. 2010). MTP-R48-B(OH) round plates were inoculated with 1.5 ml culture per well and incubated at 1,000 rpm at 28 °C. Backscatter light with a gain of 25 or 20 was used to determine biomass.

2.4.4 Quantification of unconventional secretion using the Gus reporter

Extracellular Gus activity was determined to quantify unconventional Cts1 secretion using the specific substrate 4-methylumbelliferyl β-D galactopyranoside (MUG, bioWORLD, Dublin, OH, USA)) (Koepke et al. 2011, Stock et al. 2012, Stock et al. 2016b). Cell-free culture supernatants were mixed 1:1 with 2× Gus assay buffer (10 mM sodium phosphate buffer pH 7.0, 28 µM β-mercaptoethanol, 0.8 mM EDTA, 0.0042% (v/v) lauroyl-sarcosin, 0.004% (v/v) Triton X-100, 2 mM MUG, 0.2 mg/ml (w/v) BSA) in black 96-well plates. Relative fluorescence units (RFUs) were determined using a plate reader (Tecan, Männedorf, Switzerland) for 100 min at 28 °C with measurements every 5 minutes (excitation/emission wavelengths: 365/465 nm, gain 60). For quantification of conversion of MUG to the fluorescent product 4-methylumbelliferone (MU), a calibration curve was determined using 0, 1, 5, 10, 25, 50, 100, 200 µM MU.

2.4.5 Determination of extracellular Cts1 activity

Extracellular Cts1 activity was analyzed using 4-methylumbelliferyl β-D cellobioside (MUC, Sigma-Aldrich, Billerica, MA, USA) as a substrate (Koepke et al. 2011). Whole cell cultures were mixed 3:7 with KHM Buffer (110 mM CH_3CO_2K, 20 mM HEPES, 2 mM $MgCl_2$, 2 mM MUC) in black 96 well plates. Relative fluorescence units were determined using a plate reader (Tecan, Männedorf, Switzerland) by fluorescence measurement at 28°C for 100 min every 2 min (360 nm excitation and 450 nm emission, gain 100).

2.4.6 Quantification of unconventional secretion using luciferase reporter

Extra- and intracellular luciferase activity was determined using D-luciferin (Biosynth Carbosynth, Compton, UK). Cell-free supernatants or whole cell cultures in CM medium were mixed 8:2 with luciferin substrate mix (20 mM tricine, 2.67 mM $MgSO_4 \times 7H_2O$, 0.1 mM EDTA×2 H_2O, 33.3 mM DTT, 0.524 mM ATP, 0.269 mM acetyl-CoA, 0.467 mM D-luciferin, 5 mM NaOH, 0.264 mM $MgCO_3 \times 5H_2O$) in white 96-well plates. Relative photon count (RPC) was determined using a Mithras LB 940 plate reader (Berthold technologies, Bad Wildbad, Germany) for 20 min with measurements every 20 s.

2.4.7 Quantification of unconventional secretion

Gus-Cts1 and Gus-Jps1 secretion was analyzed by trichloroacetic acid (TCA) precipitation of culture broths. 1 ml of cell-free supernatants of cultures grown in Verduyn medium (55.5 mM Glucose, 74.7 mM NH_4Cl, 0.81 mM $MgSO_4 \times 7H_2O$, 0.036 mM $FeSO_4 \times 7H_2O$, 36.7 mM KH_2PO_4, 100 mM MES pH 6.5, 0.051 mM EDTA, 0.025 mM $ZnSO_4 \times 7H_2O$, 0.041 mM $CaCl_2$, 0.016 mM H_3bBO_3, 6.7 µM $MnCl_2 \times 2H_2O$, 2.3 µM $CoCl_2 \times 6H_2O$, 1.9 µM $CuSO_4 \times 5H_2O$, 1.9 µM $Na_2MoO_4 \times 2H_2O$, 0.6 µM KI) to an OD_{600} of 3 were chilled on ice and mixed with 400 µl 50 % (v/v) TCA solution and incubated on ice at 4 °C overnight. Subsequently, precipitated protein pellets were harvested by centrifugation at 11,000 x g at 4 °C for 30 min. Supernatants were discarded and pellets were washed with 300 µl of -20 °C acetone followed by centrifugation at 11,000 × g at 4 °C for 20 min twice. Pellets were dried at room temperature and resuspended in Laemmli buffer containing 0.12 M NaOH. Resuspended pellets were denatured at 95 °C for 10 min and then subjected to SDS-PAGE and Western blot analysis. To determine protein concentration obtained by TCA precipitation a standard ladder of 50, 100, 200 and 500 ng of Multiple Tag protein (GenScript Biotech, Piscataway, NJ, USA) was loaded onto the SDS-PAGE next to obtained samples. Western blot signals were quantified using image studio lite version 5.2 (Li-Cor Biosciences, Lincoln, NE, USA) and the standard curve obtained by quantification of Multiple Tag protein signals was used to determine protein concentrations in culture supernatants.

2.4.8 SDS PAGE and Western blot analysis

To verify protein production and secretion in cell extracts and supernatants, respectively, Western Blot analysis was used. 20 ml cultures were grown to an OD_{600} of 1.0 and harvested at 1,500 × g for 5 min in centrifugation tubes. Until further preparation, pellets were stored at -20 °C. For preparation of cell extracts, cell pellets were resuspended in 1 mL cell extract lysis buffer (100 mM sodium phosphate buffer pH 8.0, 10 mM Tris/HCl pH 8.0, 8 M urea, 1 mM DTT, 1 mM PMSF, 2.5 mM benzamidine, 1 mM pepstatin A, 2× complete protease inhibitor cocktail (Roche, Sigma/Aldrich, Billerica, MA, USA) and cells were crushed by agitation with glass beads at 2,500 rpm for 12 min at 4 °C. After centrifugation (11,000 × g for 30 min at 4 °C), the supernatant was separated from cell debris and was transferred to a fresh reaction tube. Protein concentration was determined by Bradford assay (BioRad, Hercules, CA, USA) (Bradford 1976) and 10 µg total protein was used for SDS-PAGE. SDS-PAGE was conducted using 10% (w/v) acrylamide gels. Subsequently, proteins were transferred to methanol activated PVDF membranes using semi-dry Western blotting. SHH-tagged Gus-Cts1 was detected using a primary anti-HA (1:3,000, Millipore/Sigma, Billerica, USA). An anti-mouse IgG-

horseradish peroxidase (HRP) conjugate (1:3,000 Promega, Fitchburg, USA) was used as secondary antibody. HRP activity was detected using the Amersham ™ ECL ™ Prime Western Blotting Detection Reagent (GE Healthcare, Chalfont St Giles, UK) and a LAS4000 chemiluminescence imager (GE Healthcare Life Sciences, Freiburg, Germany).

2.4.9 IMAC purification of supernatants

For the purification of recombinant unconventionally secreted protein from *U. maydis*, cells were grown in CM-glucose (1% w/v) medium buffered with 0.05 M MES pH 6.5. 200 ml of culture supernatants were harvested at and OD_{600} of 0.8 by centrifugation at 5,000 × g for 3 min. Harvested supernatants were chilled to 4 °C and treated with a protease inhibitor tablet of cOmplete protease inhibitor (Roche, Sigma/Aldrich, Billerica, MA, USA). 2 ml of $Nickel^{2+}$-NTA matrix was equilibrated with 50 ml lysis buffer (10 mM imidazole 50 mM NaH_2PO_4, 300 mM NaCl, pH 8.0). 22 ml of 10 times concentrated lysis buffer were added to the supernatants and subsequently $Nickel^{2+}$-NTA matrix was added to the supernatant. The mixture was batched by gentle stirring on a magnetic stirrer at 4 °C for 1 h. Following batching supernatant flow-through was discarded via a PD-10 column. Matrix was collected in the PD-10 column during the process. Collected matrix was washed with 50 ml of wash buffer (lysis buffer, 20 mM Imidazole) and protein was eluted with 2 ml elution buffer (lysis buffer, 250 mM imidazole). In the last step supernatants were concentrated via Amicon Ultra 50 k 0.5 ml centrifugal filter devices (Merck Millipore, Burlington, Massachusetts, USA) and the buffer exchanged to PBS (137 mM NaCl, 2.7 mM KCl, 10 mM Na_2HPO_4, 1.8 mM KH_2PO_4, pH 7.2) and applied for ELISA.

2.4.10 Enzyme-linked immunosorbent assay (ELISA)

For detection of nanobody binding activity protein adsorbing 384-well microtiter plates (Nunc® Maxisorp™, ThermoFisher Scientific, Waltham, MA, USA) were used. Wells were coated with 1 µg commercially available Sars-CoV2 spike-RBD-domain protein (GenScript Biotech, Piscataway, NJ, USA). 1 µg BSA per well dealt as negative control (NEB, Ipswich, MA, USA). Samples were applied in a final volume of 100 µl coating buffer (100 mM Tris-HCL pH 8, 150 mM NaCl, 1 mM EDTA) per well at 4 °C for at least 16 h. Blocking was conducted for at least 4 h at 4 °C with 5% (w/v) skimmed milk in coating buffer. Subsequently, 5% (w/v) skimmed milk in PBS was added to defined protein amounts of nanobody samples from cell extracts or purified from culture

supernatants and respective controls. 100 µl of sample was added to wells coated with Sars-CoV2 spike-RBD and BSA. The plate was incubated with samples and controls over night at 4 °C. After 3x PBS-T (PBS supplemented with 0.05% (v/v) Tween-20, 100 µl per well) washing, a mouse anti-HA antibody (Millipore/Sigma, Billerica, USA) 1: 5,000 diluted in PBS supplemented with skimmed milk (5% w/v) was added (100 µl per well) and incubated for 2 h at room temperature. Then wells were washed again three times with PBS-T (100 µl per well) and incubated with an anti-mouse IgG-horseradish peroxidase (HRP) conjugate (Promega, Fitchburg, USA) (50 µl per well) for 1 h at room temperature (1: 5,000 in PBS supplemented with skimmed milk (5% w/v)). Subsequently wells were washed three times with PBS-T and three times with PBS and incubated with Quanta Red™ enhanced chemifluorescent HRP substrate (50:50:1, 50 µl per well) (ThermoFisher Scientific, Waltham, MA, USA) at room temperature for 15 min. The reaction was stopped with 10 µl per well Quanta RedTM stop solution and fluorescence readout was performed at 570 nm excitation and 600 nm emission using an Infinite M200 plate reader (Tecan, Männedorf, Switzerland).

2.4.11 Microscopic analyses

Microscopic analyses were performed with immobilized early-log phase budding cells on agarose patches (3% w/v) using a wide-field microscope setup from Zeiss (Oberkochen, Germany) Axio Imager M1 equipped with a Spot Pursuit CCD camera (Diagnostic Instruments, Sterling Heights, USA) and the objective lenses Plan Neofluar (40×, NA 1.3), Plan Neofluar (63×, NA 1.25) and Plan Neofluar (100×, NA 1.4). The microscopic system was controlled by the software MetaMorph (Molecular Devices, version 7, Sunnyvale, USA). Image processing including rotating and cropping of images, scaling of brightness, contrast and fluorescence intensities as well as insertion of scale bars was performed with MetaMorph. Arrangement and visualization were performed with Canvas 12 (ACD Systems).

2.5 Acknowledgements

We are thankful to B. Axler for excellent technical support of the project. We gratefully acknowledge support in microscopic imaging and analysis by N. Heßler. K.P.H. was supported by the CLIB-Competence Center Biotechnology (CKB) funded by the European Regional Development Fund ERDF (34.EFRE-0300096). K.S. and M.R. received funding from the Deutsche

Forschungsgemeinschaft (DFG, German Research Foundation) - Projektnummer 267205415 - SFB 1208.

2.6 Conflict of interest

The authors declare that the research was conducted in the absence of any commercial or financial relationships that could be construed as a potential conflict of interest.

2.7 Author contributions

M.P., K.P.H. and M.R. designed the experiments. M.P. and K.P.H. conducted the experiments. K.S., K.M. and M.F. supervised the project. K.S., M.P. and K.M. prepared the manuscript with input from all co-authors. M.P. and K.P.H. prepared figures and tables.

2.8 Tables

Table 1. DNA oligonucleotides used in this study.

Designation	**Nucleotide sequence (5´- 3´)**
oMB372_jps1_fw	TTAGGCGCGCCATGCCAGGCATCTCC
oMB373_jps1_rev	TTAGGGCCCTTAGGATTCCGCATCGATTGGGG
oMF502_ip_fw	ACGACGTTGTAAAACGACGGCCAG
oMF503_ip_rev	TTCACACAGGAAACAGCTATGACC
oAB297_fluc_fw	AAATTGGATCCATGGAGGACGCCAAGAACATCAAG
oAB298_fluc_rev	AATAGGCCGCGTTGGCCACGGCGATCTTGCCACCCTT
oAB908_sy$^{\#15}$_fw	ATATAGGATCCATGGCGGCCCATCACCACCATCACCACCATCACCACCATCATATG CAGGTGCAGCTCG
oAB909_sy$^{\#15}$_rev	ATATAACTAGTCGAGACGGTGACCTGGGTGC
oCD234_sy$^{\#68}$_fw	CTACCTTACTCTATCAGGATCATGCAGGTGCAGCTCGTCG
oCD235_sy$^{\#68}$_rev	GGTGATGGGCCGCCATGGATCCCGAGACGGTGACCTGGGTGC

Table 2. *U. maydis* strains used in this study.

Strains	Relevant genotype/ Resistance	Strain collection no. (UMa[1])	Plasmids transformed / Resistance[2]	Manipulated locus	Progenitor (UMa[1])	Reference
AB33	*a2 P$_{nar}$bW2bE1* PhleoR	133	pAB33	*b*	FB2 (55)	(Brachmann et al. 2001)
AB33 Gus-Cts1	*a2 P$_{nar}$bW2bE1* PhleoR *ip^{S}[P$_{oma}$gus:shh:cts1]ip^{R}*CbxR	1289	pUMa2113/ CbxR	*ip*	133	(Sarkari et al. 2014)
AB33don3Δ/Gus-Cts1	*a2 P$_{nar}$bW2bE1* PhleoR *ip^{S}[P$_{oma}$gus:shh:cts1]ip^{R}* CbxR *umag_don3Δ*_HygR	1742	pUMa2717/ HygR	*umag_05543 (don3)*	1289	(Aschenbroich et al. 2019)
AB33don3Δ	*a2 P$_{nar}$bW2bE1* PhleoR *umag_don3Δ*_HygR	2028	pUMa2717/HygR	*umag_05543 (don3)*	133	(Aschenbroich et al. 2019)
AB33don3Δ/P$_{crg}$don3-gfp/Gus-Cts1	*a2 P$_{nar}$bW2bE1* PhleoR *ip^{S}[P$_{oma}$gus:shh:cts1]ip^{R}* CbxR *umag_don3Δ*_HygR *upp1::[P$_{crg}$don3:gfp]* NatR	2302	pUMa3330/ NatR	*umag_02178* (*upp1*)	1742	(Aschenbroich et al. 2019)
AB33P8ΔGus-Cts1	*a2 P$_{nar}$bW2bE1* PhleoR *FRT10[um04641Δ::hyg] FRT11[um03947Δ] FRT6[um03975Δ] FRT5[um04400Δ] FRT3[um11908Δ] FRT2[um00064Δ] FRTwt[um02178Δ] FRT1[um04926Δ]* HygR *ip^{S}[P$_{oma}$gus:shh:cts1]ip^{R}* CbxR	2418	pUMa2113	*Ip*	2413	(Terfrüchte et al. 2018)

AB33don3Δ/ Gus-Jps1	*a2 P$_{nar}$bW2bE1* PhleoR *ip^{S}[P$_{oma}$gus:shh:cts1]ip^{R}* CbxR *umag_don3Δ*_HygR	2734	pUMa3012	*Ip*	2028	This study
AB33don3Δ/ P$_{crg}$don3-gfp/Gus-Jps1	*a2 P$_{nar}$bW2bE1* PhleoR *ip^{S}[P$_{oma}$gus:shh:cts1]ip^{R}* CbxR *umag_don3Δ*_HygR *upp1::[P$_{crg}$don3:gfp]* NatR	2776	pUMa3330/ NatR	*umag_02178* (*upp1*)	2734	This study
AB33P8ΔGus-Jps1	*a2 P$_{nar}$bW2bE1* PhleoR *FRT10[um04641Δ::hyg] FRT11[um03947Δ] FRT6[um03975Δ] FRT5[um04400Δ] FRT3[um11908Δ] FRT2[um00064Δ] FRTwt[um02178Δ] FRT1[um04926Δ]* HygR *ip^{S}[P$_{oma}$gus:shh:jps1]ip^{R}* CbxR	2900	pUMa3012	*Ip*	2413	this study
AB33P8Δ FLuc-Cts1	*a2 P$_{nar}$bW2bE1* PhleoR *FRT10[um04641Δ::hyg] FRT11[um03947Δ] FRT6[um03975Δ] FRT5[um04400Δ] FRT3[um11908Δ] FRT2[um00064Δ] FRTwt[um02178Δ] FRT1[um04926Δ]* HygR *ip^{S}[P$_{oma}$fluc:shh:cts1]ip^{R}* CbxR	3151	pUMa4131	*Ip*	2413	this study
AB33P8Δ FLuc-Jps1	*a2 P$_{nar}$bW2bE1* PhleoR *FRT10[um04641Δ::hyg] FRT11[um03947Δ] FRT6[um03975Δ] FRT5[um04400Δ] FRT3[um11908Δ] FRT2[um00064Δ] FRTwt[um02178Δ] FRT1[um04926Δ]* HygR *ip^{S}[P$_{oma}$fluc:shh:jps1]ip^{R}* CbxR	3214	pUMa4566	*ip*		this study
AB33P8ΔSy#68 /#15-Cts1	*a2 P$_{nar}$bW2bE1* PhleoR *FRT10[um04641Δ::hyg] FRT11[um03947Δ] FRT6[um03975Δ]*	Ux1	pUx1	*ip*	2413	this study

	FRT5[um04400Δ] *FRT3[um11908Δ]* *FRT2[um00064Δ]* *FRTwt[um02178Δ]* *FRT1[um04926Δ]* HygR *ip^{S}[P$_{oma}$antirbdsybody#68:his:antirbdsybody#15:ha:cts1]ip^{R}* CbxR					
AB33P8ΔSy#68 /#15-Jps1	*a2 P$_{nar}$bW2bE1* PhleoR *FRT10[um04641Δ::hyg]* *FRT11[um03947Δ]* *FRT6[um03975Δ]* *FRT5[um04400Δ]* *FRT3[um11908Δ]* *FRT2[um00064Δ]* *FRTwt[um02178Δ]* *FRT1[um04926Δ]* HygR *ip^{S}[P$_{oma}$antirbdsybody#68:his:antirbdsybody#15:ha:jps1]ip^{R}* CbxR	Ux8	pUx8	*ip*	2413	this study

[1] Internal strain collection numbers (UMa/Ux codes)

[2] Plasmids generated in our working group are integrated in a plasmid collection and termed pUMa or pUx plus a number as 4-digit number as identifier.

2.9 Supplementary material

The supplementary material contains supplementary figures 1-3.

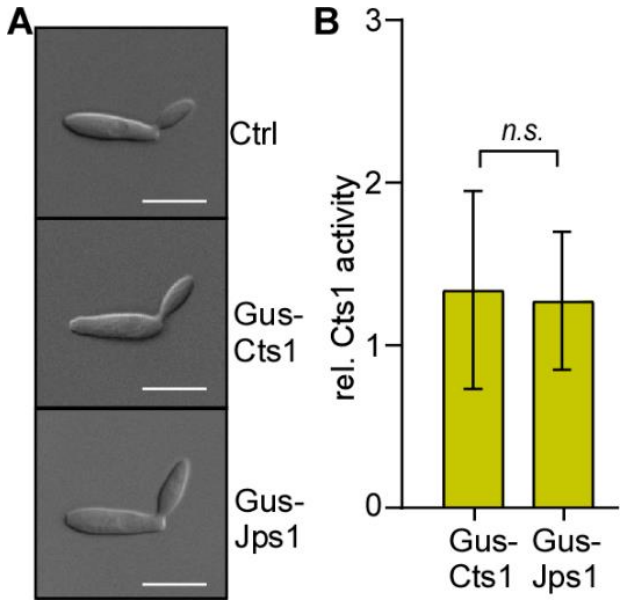

Supplementary Figure 1: Cell morphology and Cts1 activity of Gus-Cts1 and Gus-Jps1 producing strains. (A) Microscopic morphology of Gus-Cts1 and Gus-Jps1 expressing strains during yeast-like growth. The progenitor strain AB33P8Δ dealt as reference (Ctrl). Scale bars represent 10 µm. **(B)** Determination of extracellular Cts1 activity in Gus-Jps1 and Gus-Cts1 expressing strains. For determination of extracellular Cts1 activity yeast like growing cultures were incubated with 4-methylumbelliferyl β-D cellobioside. The changes in the relative fluorescence at 360 nm excitation and 450 nm emission was monitored for 90 min. The experiment was conducted in three biological replicates.

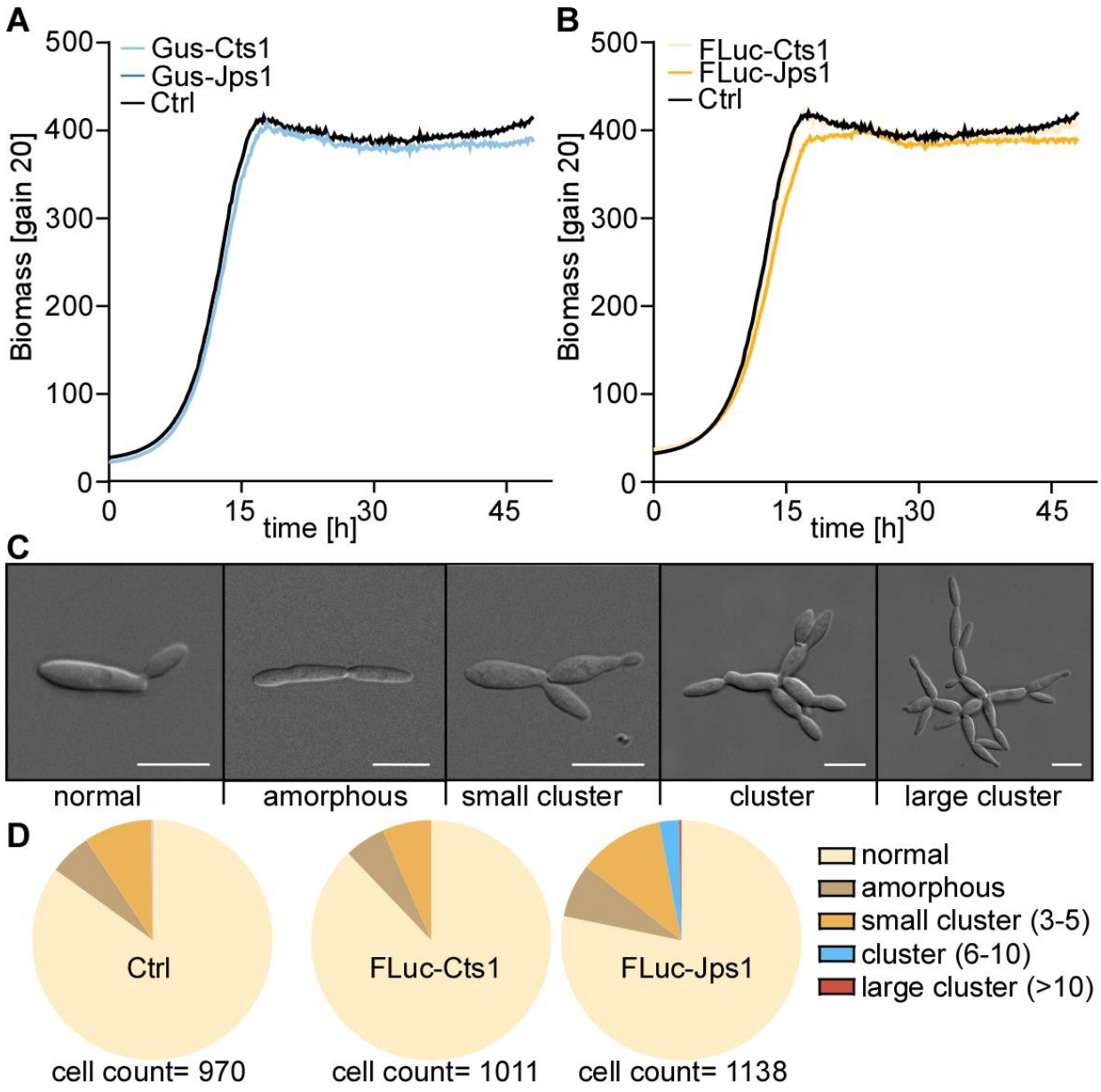

Supplementary Figure 2: Morphology and fitness of strains exporting firefly luciferase FLuc. (A) Proliferation of strains secreting Gus-Cts1, and Gus-Jps1 was compared to the progenitor strain AB33P8Δ (Ctrl) in a BioLector online monitoring device (m2p-labs, Baesweiler, Germany). The Gus-Cts1 producing strains and the progenitor entered exponential growth phase after a 7 h lag phase and entered stationary phase after 17 h. During exponential growth phase all strains exhibited a doubling time of 3 h. **(B)** Proliferation of strains secreting FLuc-Cts1, and FLuc-Jps1 was compared to the progenitor strain AB33P8Δ (Ctrl) in a BioLector online monitoring device. The FLuc-Jps1 producing strain entered exponential growth phase after 8 h and entered stationary phase after 17 h. Overall biomass was slightly reduced to the progenitor and FLuc-Cts1. Doubling time for Fluc-Jps1 was 3.5 h. **(C)** Representative DIC pictures of different occuring morphologies during yeast-like growth. Left to right: normal cell, amorphous cell, small cluster (3-5 cells), cluster (6-10 cells), large cluster (>10 cells). Scale bars represent 10 µm. **(D)** Morphological quantification of the FLuc-Cts1 and FLuc-Jps1 expressing strains according to morphologies depicted in **(C)**. Progenitor AB33P8Δ dealt as control (Ctrl).

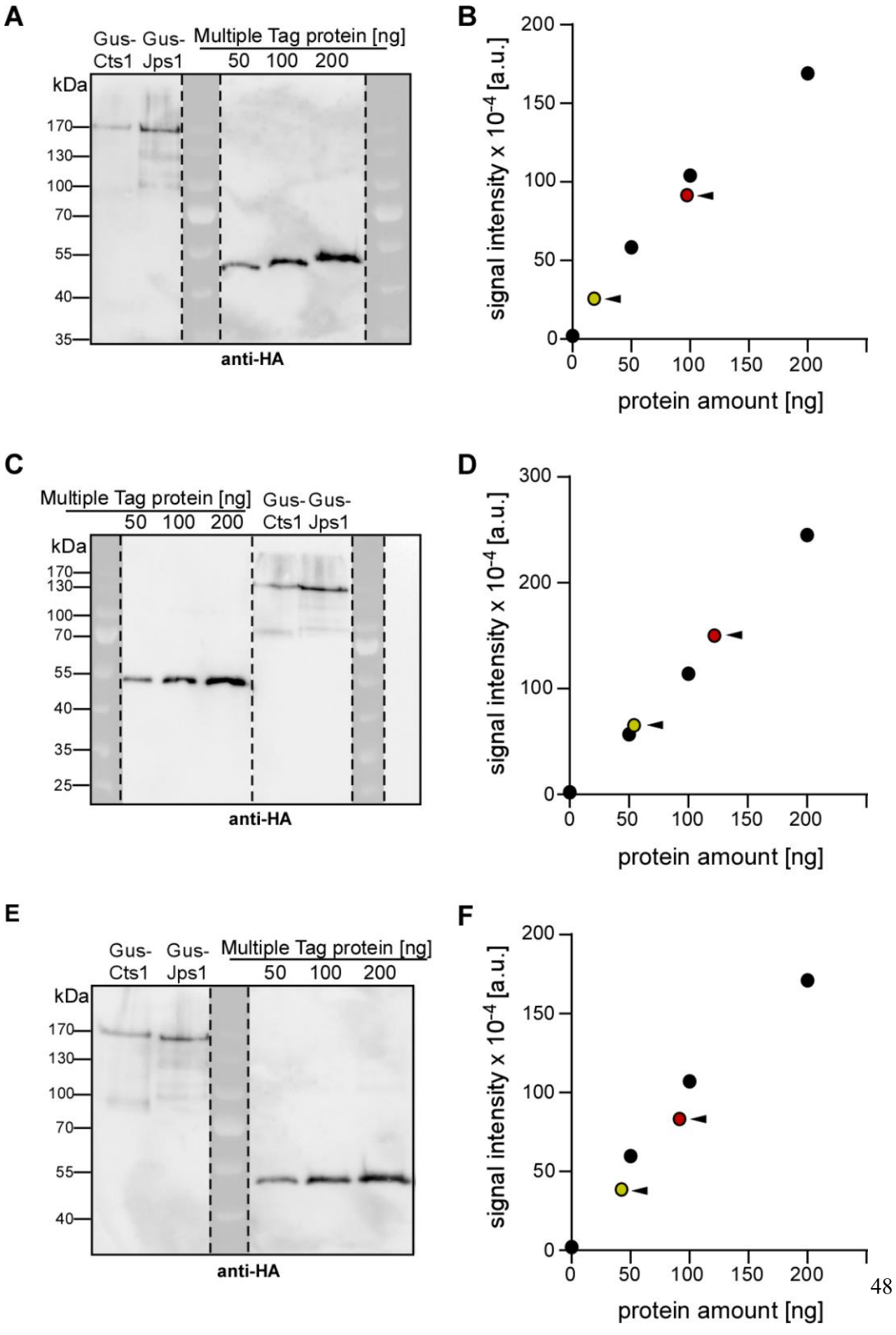
A
Gus-Cts1
Gus-Jps1
Multiple Tag protein [ng]
50 100 200
kDa
170
130
100
70
55
40
35
anti-HA
B
signal intensity x 10-4 [a.u.]
protein amount [ng]
C
Multiple Tag protein [ng]
50 100 200
Gus-Cts1
Gus-Jps1
kDa
170
130
100
70
55
40
35
25
anti-HA
D
signal intensity x 10-4 [a.u.]
protein amount [ng]
E
Gus-Cts1
Gus-Jps1
Multiple Tag protein [ng]
50 100 200
kDa
170
130
100
70
55
40
anti-HA
F
signal intensity x 10-4 [a.u.]
protein amount [ng]

Supplementary Figure 3: Quantitative Western blot analysis of Gus-Cts1 and Gus-Jps1 secretion. (A, C, E) Total extracellular protein was concentrated via TCA precipitation from 1 ml of supernatant of Gus-Jps1 and Gus-Cts1 producing strains and subjected to SDS-PAGE and subsequent Western blot analysis using antibodies directed against the HA tag. Standards of Multiple Tag protein (GenScript Biotech, Piscataway, NJ, USA)) were loaded onto the gels equalling amounts of 50, 100, 200 and 500 ng. Expected protein sizes: Gus-Cts1, 134 kDa; Gus-Jps1, 145 kDa. **(B, D, F)** Western blot signals of Multiple Tag protein standards were quantified using Image Studio Lite (LI-COR Biosciences, Lincoln, NE, USA) and used to extrapolate protein amounts of Gus-Jps1 and Gus-Cts1 in the supernatant. Standard curve derived from signal strenghts of the Multiple Tag protein is depicted by black dots, yellow dots indicate signals obtained and cognate protein amounts calculated from linear regression for Gus-Cts1, red dots indicate signal obtained and cognate protein amount calculated from linear regression for Gus-Jps1. Figure pairs **(A/B; C/D; E/F)** each depict Western blot and derived quantification curves of one replicate.

3 A chitin-based antigen test

A novel strategy for Sars-CoV2 detection utilizing a chitin surface and components derived from the fungal microorganism *Ustilago maydis*

Magnus Philipp[1], Kai P. Hussnätter[1], Lisa Müller[2], Kerstin Schipper[1], Heiner Schaal[2] and Michael Feldbrügge[1,*]

[1] Institute for Microbiology, Heinrich Heine University Düsseldorf, Universitätsstraße 1, 40225 Düsseldorf, Germany

[2] Institute for Virology, Heinrich Heine University Düsseldorf, Universitätsstraße 1, 40225 Düsseldorf, Germany

[*] Corresponding author:
Michael Feldbrügge
E-mail: feldbrue@uni-duesseldorf.de

Running Header: **An alternative unconventional virus detection system**
Keywords: Nanobody, Sars-CoV2, chitin, chitinase, *Ustilago maydis*.

Abstract

The COVID-19 pandemic has greatly impacted the global economy and health care systems. The need for quick and inexpensive responses to a pandemic threat like COVID-19 in the form of vaccines and antigen tests has become very clear in the last two years. The causative agent of COVID-19 is Sars-CoV2. It harbors a Spike protein on its surface that interacts with the human angiotensin-converting enzyme (ACE2) via the so-called receptor binding domain (RBD) and thereby facilitates virus to cell fusion. This RBD is become of great research interest, as it represents a target for vaccines, therapeutic antibodies and for antigen test systems. Currently, antigen testing is generally done by either flow chromatography using antibodies or via ELISA-type assays. Both are costly due to the use of expensive materials like gold or latex particles and protein adhesive polymers. In this study we present an alternative ELISA approach using inexpensive materials and permitting quick detection based on components from the microbial model organism *Ustilago maydis*. In this fungus, chitinase Cts1 is

unconventionally secreted via a lock-type mechanism and importantly, heterologous proteins like biopharmaceuticals can be co-exported and bound to chitin via the chitinase for purification or immobilization. Here, we produced different mono- and bivalent Sars-CoV2 nanobodies directed against the viral RBD as Cts1 fusions and screened their RBD binding affinity *in vitro* and *in vivo.* We present a straightforward strategy for an antigen test based on a chitin surface with immobilized nanobody-Cts1 fusions forming an RBD-trap. The developed strategy provides a solid basis for establishment of a novel, inexpensive antigen test utilizing an effective RBD-trap based on nanobodies produced by unconventional secretion and a biodegradable surface.

3.1 Introduction

The current COVID-19 pandemic impacts not only global healthcare systems and economies but has also highlighted the need for novel versatile strategies to fight viral pandemics. Several major innovations have already been driven by the pandemic. One example is the prompt development of mRNA-based vaccines like BNT162b2 by Biontech/Pfizer and mRNA-1237 by Moderna (Kudlay and Svistunov 2022). Furthermore, the adaptation of monoclonal antibody therapeutics formerly mostly used in cancer patients for the treatment of COVID-19 in the form of biopharmaceuticals like Casirivimab and Imdevimab represented an important step (Sun and Ho 2020a, Bierle et al. 2021).

COVID-19 is caused by Sars-CoV2, which has become a target of great interest for the research community and the structure of the virus has been elucidated both on RNA (Jain et al. 2020) and protein level (Korber et al. 2020, Ou et al. 2020, Walls et al. 2020, Wrapp et al. 2020b). The spike protein complex was identified as one of the most important research targets, as it is not only openly displayed on the virus capsid surface but also facilitates the docking of the virus to the human Angiotensin receptor 2 (Ace2) (Wang et al. 2020a). This mechanism has also been observed for other beta Corona viruses like Sars-CoV. Generally, the spike proteins of these viral species consist of the two main subunits S2 and S1. S2 mainly serves as the anchor of the protein in the viral membrane (Hulswit et al. 2016). The S1 part on the other hand is responsible for binding of ACE2 (Wang et al. 2020a). Corona virus S1 proteins are generally organized into four domains of which domains A and B form the receptor binding domain (RBD) which directly facilitates this binding process (Li et al. 2003, Wang et al. 2020a). The B subdomain of the RBD carries an extended loop that is highly variable among coronavirus species and therefore also referred to as a hypervariable region (Kirchdörfer et al. 2016). This hypervariable region is also of interest in Sars-CoV2 as all variants of concern that have been

structurally elucidated to date (B.1.1.7 Alpha, B.1.351 Beta and B.1617 Delta) carry mutations within the RBD domain that are assumed to play a role in infectivity and transmissibility of the virus (Baral et al. 2021).

Therefore, the spike protein and especially its RBD domain are in the focus for the development of therapeutics and vaccines, with the majority of vaccines cleared for use to date using a template of the spike protein to evoke an immune response (Callaway 2020, Fernandes et al. 2022). However, since it was realized that even vaccinated persons can still be infected with and spread Sars-CoV2, there is a strong pressure to further develop test systems and therapeutics to form a multi-layered defense which is needed to treat COVID-19 and to control the spread Sars-CoV2. Antibodies are key to both test systems and drug development. *Camelidae* and shark derived single heavy chain antibodies or nanobodies are emerging as potent antibody alternatives in the field (Muyldermans 2013, Salvador et al. 2019). *Camelidae* type antibodies only carry a heavy chain on their IgG scaffold as opposed to the light- and heavy chain of regular mammalian antibodies (Muyldermans 2013). This heavy chain alone can be easily adapted to novel targets such as Sars-CoV2 and upscaling of production e in microbial hosts is easily achieved in contrast to the complex form of conventional monoclonal antibodies (Muyldermans et al. 2009, Wrapp et al. 2020a). Nanobodies have been shown to bind ligands in the nano molar range and to be stable under conditions of chemical and heat induced stress (Muyldermans 2013) which makes them promising molecules for widespread antigen testing. To his end several Sars-CoV2 nanobodies have been generated, both synthetically via phage display or directly by immunization of llamas, alpacas, and sharks (Custodio et al. 2020, Gauhar et al. 2021, König et al. 2021).

We utilize the microbial model organism *Ustilago maydis* to produce heterologous proteins including alternative antibody formats like scFvs and nanobodies (Sarkari et al. 2014, Terfrüchte et al. 2017). Production in the yeast form of this fungus provides several advantages over other fungal protein expression hosts. The fungus uses a lock-type unconventional secretion mechanism for export of chitinase Cts1 during cytokinesis (Reindl et al. 2019). This pathway circumvents potentially harmful post translational modifications such as *N*-glycosylation which could lead to strong reactions in patients when proteins are applied as biopharmaceuticals (Stock et al. 2012). Of note, Cts1 has previously been shown to exhibit chitin binding activity making it a potential build-in immobilization- and purification tag (Terfrüchte et al. 2017). Since yields are yet limiting, tailor made tools have been employed to enhance this secretory pathway. These include protease deficient expression strains and strains capable of inducible secretion utilizing transcriptional or post-translational regulation of kinase Don3 which is

crucial for unconventional protein export (Terfrüchte et al. 2018, Aschenbroich et al. 2019, Hussnätter et al. 2021). The newly identified potential anchoring factor Jps1 was established as an alternative carrier with enhanced export capacities for distinct proteins. Based on these grounds, we recently applied unconventional secretion for the production of functional synthetic anti-Sars-CoV2 nanobodies as a proof-of-principle for protein biopharmaceuticals (Reindl et al. 2019, Philipp et al. 2021).

3.2 Results

3.2.1 Functional comparison of different Sars-CoV2 nanobodies produced by unconventional secretion

Previously, we for the first time demonstrated expression and unconventional secretion of functional Sars-CoV2 nanobodies in *U. maydis* (Philipp et al. 2021). In this study we used Jps1 as an effective novel carrier for a synthetic bivalent nanobody directed against the receptor binding domain of the Sars-CoV2 spike protein (RBD). However, nanobody export mediated by Cts1 is also of great interest due to the ability of the chitinase to bind chitin. This property might potentially act as a build in immobilization tag for the expressed nanobody. In the present study, we aimed on testing this and initially screened six nanobody-Cts1 fusions for their expression, unconventional secretion and binding activity against Sars-CoV2 RBD. To this end four different nanobody versions were fused to Cts1. The nanobody versions comprised two synthetic nanobodies generated by Wagner et al. (2020) and two llama derived nanobodies generated by König et al. (2021), all directed against the Sars-CoV2 RBD. Towards more versatile and stronger binders, not only single VHHE and VHHV domains but also bivalent versions of these nanobodies were generated, pairing VHHE with VHHV, since these were shown to display synergistic activity (König et al. 2021). Additionally, a double VHHE version was generated to test for enhanced binding capability without bivalence. *U. maydis* expression strains were generated for all protein versions, using the background AB33P8Δ lacking eight extracellular proteases to optimize secretory yield. Previously described functional nanobody fusions $Sy^{68/15}$-Cts1 and $Sy^{68/15}$-Jps1 (Philipp et al. 2021) dealt as controls (Fig. 3.1 A). Expression and secretion of all versions was investigated via Western blot analysis. In cell extracts signals at expected sizes were obtained for all candidates. However, expression of Sy^{68}-Cts1, VHHVE-Cts1 and $Sy^{68/15}$-Cts1 was weaker than that of other constructs. Western blot with precipitated culture supernatants confirmed secretion for Sy^{15}-Cts1, VHHE-Cts1, VHHV-Cts1 and VHHEE-Cts1. (Fig. 3.1 B; Supp. Fig. 3.1 A, B). By contrast, only faint or no signals were obtained for all other variants, suggesting that these are not exported in significant amounts. To test for RBD binding activity, the different variants were

subjected to direct ELISA assays. Cell extracts of derivatives of the protease deficient strain AB33P8Δ producing Sy^{15}-Cts1, Sy^{68}-Cts1, VHHE-Cts1, VHHV-Cts1, VHHEE-Cts1 or VHHVE-Cts1 were added to ELISA plates coated with commercial RBD protein (GenScript Biotech, Piscataway, USA). The previously established derivatives secreting $Sy^{68/15}$-Cts1 and $Sy^{68/15}$-Jps1 were used as negative and positive controls, respectively. Wells coated with BSA dealt as additional negative controls (Sup. Fig. 3.1 C). Interaction was detected using an HA-antibody (mouse) and anti-mouse-HRP antibody sandwich. Interestingly, VHHEE-Cts1 showed the strongest binding with signals reaching 21 RFUs after a detection time of 10 min, closely followed by $Sy^{68/15}$-Jps1 and VHHE-Cts1, while Sy^{15}-Cts1, Sy^{68}-Cts1, $Sy^{68/15}$-Cts1 and VHHV-Cts1 showed almost no volumetric binding activity. The lack of binding activity was particularly unexpected for VHHV-Cts1 which showed the strongest Western blot signal in culture supernatants. All in all, binding activity could be shown for 3 of 8 nanobody variants and binding capabilities of nanobodies were improved in the multimerized variant of VHHEE-Cts1 (Fig. 3.1 C). Based on these results VHHEE-Cts1, VHHE-Cts1 and $Sy^{68/15}$-Jps1 were chosen for further analysis.

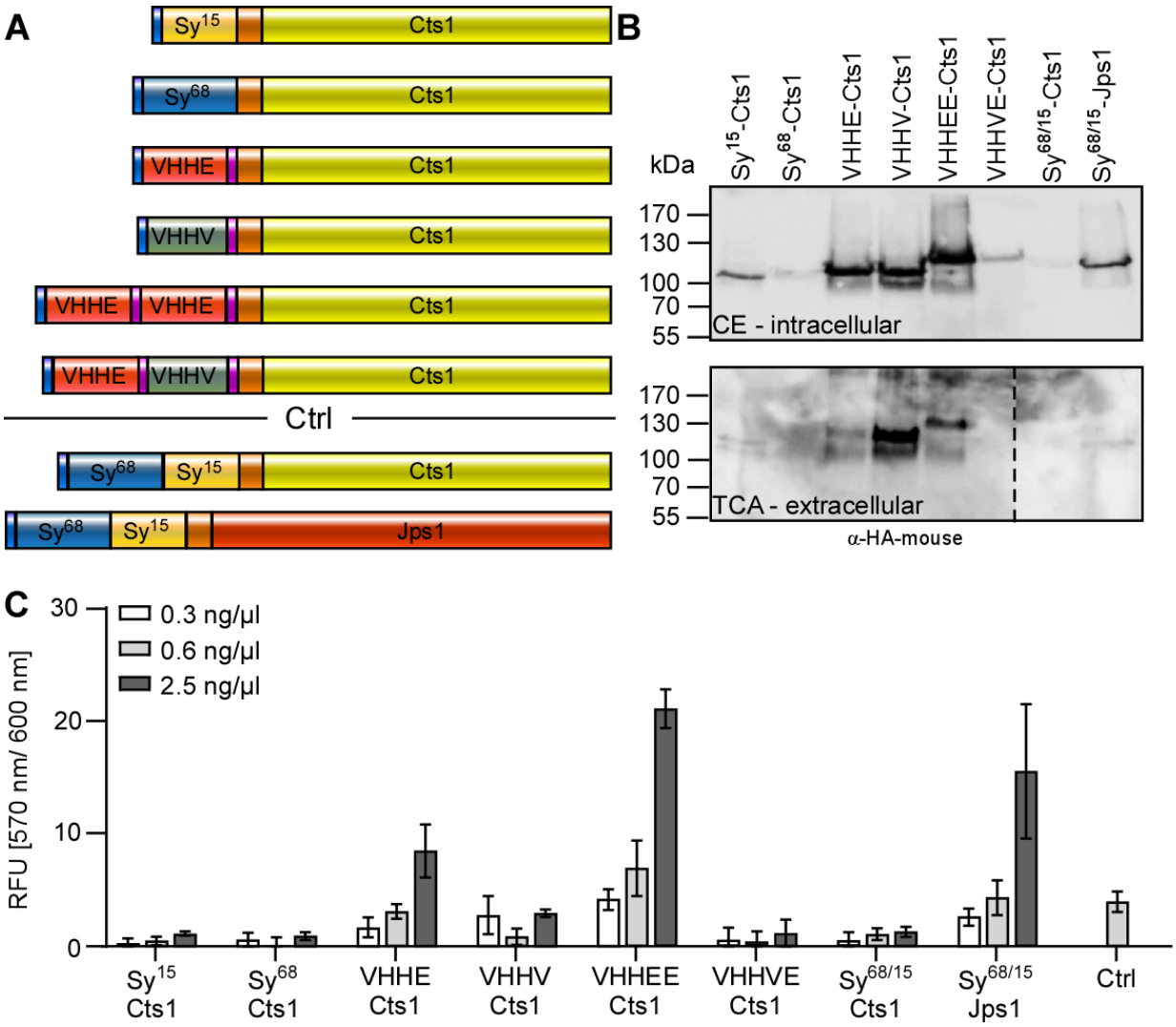

Figure 3.1: Initial screen of anti-Sars-CoV2 nanobody-Cts1 fusions. (A) Schematic representation of nanobody protein variants fused to the carriers Cts1 or Jps1. Sy^{15}, Sy^{68}, VHHE, VHHV and VHHV with VHHE as well as double VHHE were fused to Cts1 (yellow) via an HA-tag (orange) for detection. An N-terminal His-tag (blue) was added for purification. In the case of the VHHE and VHHV nanobodies GS-linkers (purple) introduced by (König et al. 2021) were placed between individual nanobodies and between the nanobodies and Cts1. $Sy^{68/15}$-Cts1 and $Sy^{68/15}$-Jps1 (Philipp et al., 2021) dealt as controls. **(B)** Western blot analysis of nanobody expression and secretion levels. 10 µg of cell extracts were subjected to Western blot analysis. Nanobody-Cts1 fusions were detected using an Ha-mouse antibody. Nanobodies were detected slightly above their expected sizes around 100 kDa. Nanobody-Cts1 fusions were enriched from the supernatant via TCA precipitation, the HA tag was used for detection. **(C)** Direct ELISA of nanobody-Cts1 fusions against 1 µg/well of RBD domain coated to ELISA plate and detected by a sandwich of anti-Ha (mouse) and an anti-mouse-HRP conjugate. Cell extracts of expression strains were added to wells in serial dilutions of 0.3 ng/µl, 0.6 ng/µl and 2.5 ng/µl. Experiment was carried out in three biological replicates comprising three technical replicates each. Error bars depict standard deviation of biological replicates.

3.2.2 *In vivo* activity of nanobody-Cts1 fusions

To determine if *in vitro* binding to Sars-CoV2 RBD would translate to binding or even virus neutralization *in vivo,* standardized medical neutralization assays, normally used to test sera of vaccinated or recovered patients for Sars-CoV2 neutralization, were used. The assays were conducted in cooperation with the Institute for Medical Microbiology, Heinrich Heine University Düsseldorf (Dr. Lisa Müller). To this end, serial dilutions of Sars-CoV2 viral particles were pre-incubated with the purified nanobodies VHHE-Cts1, VHHEE-Cts1 and $Sy^{68/15}$-Jps1 at a concentration of 0.5 mg/ml and subsequently used to infect human lung cell cultures displaying the ACE2 receptor on their surface. Three days' post infection, cells were screened for infection via microscopic analysis. Infection is characterized by cytopathic effects in the form of darkened plaques, while non-infected cells appear clear. In the case of VHHE-Cts1 all sampled cells were infected, even with the lowest viral load of tissue culture infection dose50 ($TCLD_{50}$) 12.5, suggesting that this nanobody version is not able to prevent infection. By contrast, VHHEE-Cts1 showed full neutralization of the lowest viral load and seemingly reduced infection at the second lowest viral load of $TCLD_{50}$ 25. Interestingly, $Sy^{68/15}$-Jps1 fully neutralized Sars-CoV2 at $TCLD_{50}$ 12.5 and 25 and seemingly achieved partial neutralization at $TCLD_{50}$ 50, despite showing a slightly weaker signal than VHHEE-Cts1 in direct ELISA (Fig 3.2 A).

To further confirm these results, qPCR analysis of infected cells was carried out for each replicate prior to infection and after infection at the time microscopic images were taken. Therefore, Sars-CoV2 RNA was reverse translated and oligonucleotides specific for the virus were used for detection. qPCR results are represented by difference in Ct value. Expectedly, differences in Ct value between time points t0 and t3 were high for VHHE-Cts1 for every concentration of viral particles, confirming visual analysis results. VHHEE-Cts1 showed identical Ct value between time points for $TCLD_{50}$ 12.5 and only slight deviation at $TCLD_{50}$ 25 thus confirming partial neutralization of this viral concentration. However, from $TCLD_{50}$ 50 onwards difference in Ct value was comparable to VHHE-Cts1, indicating the lack Sars-CoV2 neutralization. Interestingly, $Sy^{68/15}$-Jps1 showed full neutralization of $TCLD_{50}$ 12.5 and 25 with no difference in Ct value. At $TCLD_{50}$ 50 partial neutralization was confirmed but at the highest viral concentration no neutralization occurred (Fig 3.2 B). Given that binding does not necessarily reflect neutralization, but neutralization definitely includes binding, it could be determined that VHHEE-Cts1 and $Sy^{68/15}$-Jps1 were indeed capable of binding Sars-CoV2 *in vivo*.

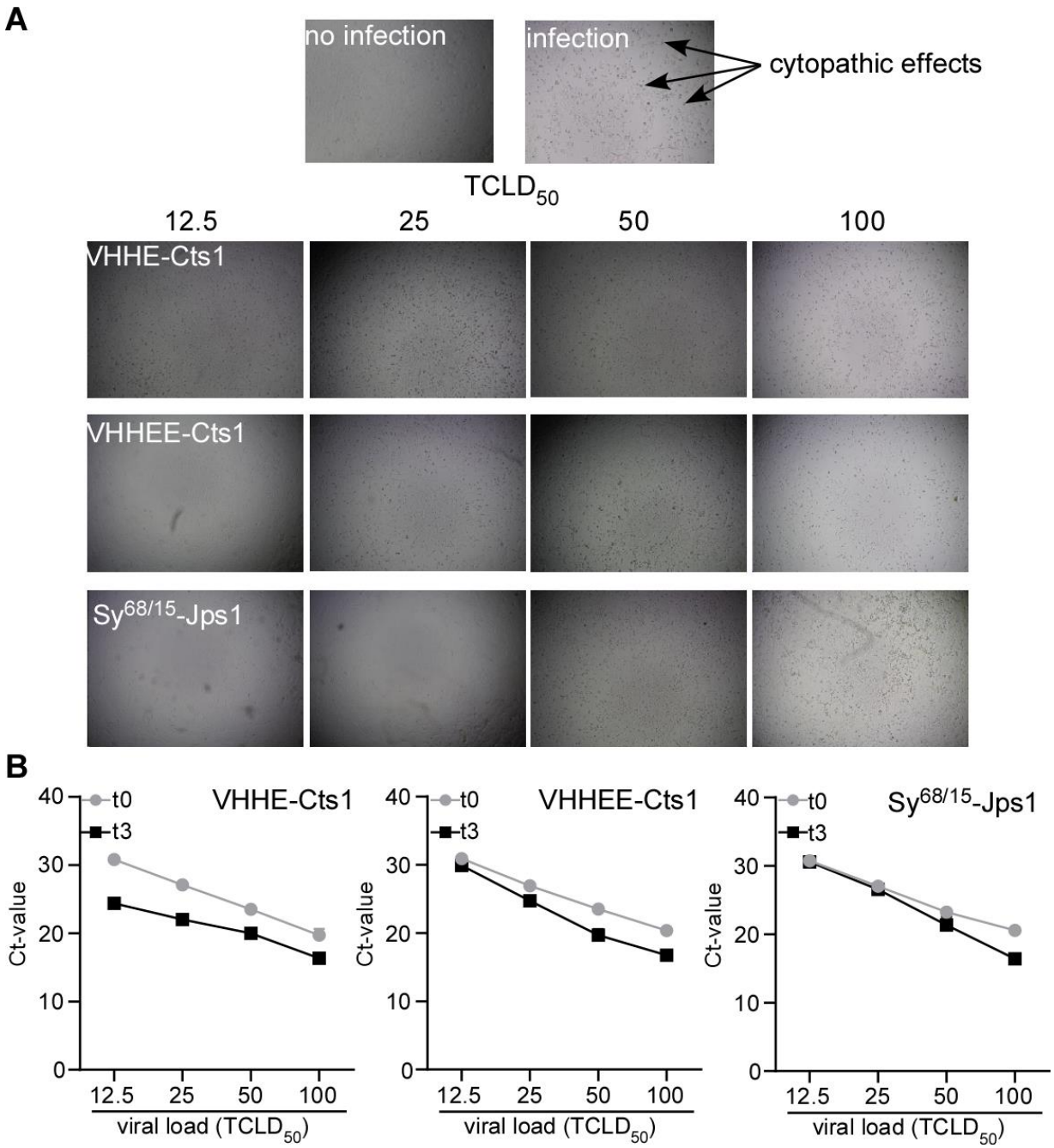

Figure 3.2: Neutralization assays conducted with nanobody fusions against Sars-CoV2. (A) Visual inspection of human lung cell cultures infected with Sars-CoV2 after viral particles were treated with respective nanobody fusion protein indicated in the upper left. Viral load administered for infection is depicted at the top of the images. Formation of dark plaques indicate viral infection. No infection was observed for VHHEE-Cts1 and $Sy^{68/15}$-Jps1 at viral loads of $TCLD_{50}$ 12.5 and 12.5 and 25, respectively. **(B)** qPCR analysis to detect viral abundance in cell cultures treated with nanobody/Sars-CoV2 mixtures. Ct values of samples prior to infection (t0) and three days' post infection (t3) are depicted for each viral load and each nanobody. Strong difference between Ct values of t0 and t3 indicate infection. All cell cultures where viral particles were treated with VHHE-Cts1 were infected. Viral particles were fully neutralized at $TCLD_{50}$ 12.5 and partially neutralized at $TCLD_{50}$ 25 by VHHEE-Cts1. Full neutralization was observed at $TCLD_{50}$ 12.5 and 25, and partial neutralization was observed for $TCLD_{50}$ 50 for $Sy^{68/15}$-Jps1. Mean values of three biological replicates are depicted.

3.2.3 Characterization of Cts1 chitin binding and immobilization

Cts1 is capable of binding to chitin-coated surfaces without degrading the polymer (Terfrüchte et al. 2017). This observation could be developed into a strategy for a novel antigen test using an inexpensive surface based on bulk chitin obtained from crab shell or insects for immobilization of Cts1-nanobody fusions. To recapitulate chitin binding, Cts1 was recombinantly expressed in *E. coli* and binding efficiency was monitored via SDS-PAGE. Purified protein was coated to chitin beads, bound protein was eluted by boiling and subjected to SDS-PAGE (Fig 3.3 A). Roughly 50% of the protein bound to the beads. While losses during washing steps were minimal most of the unbound protein was lost in the flow-through, suggesting that the part that is bound, remains stably connected to the surface, confirming previous results (Terfrüchte et al. 2017) (Fig. 3.3 B). Next, *U. maydis* derived β-glucuronidase (Gus)-Cts1 fusion protein was used to confirm these findings and to further characterize the binding capacity of unconventionally secreted fusion proteins. Gus-Jps1 which is not able to bind to chitin was used as a negative control (Fig. 3.3 C). Chitin beads were coated with 5 µg of protein purified from *U. maydis* while washing and elution procedures were kept consistent to experiments carried out with *E. coli* derived Cts1. Gus-Cts1 bound to chitin beads at slightly higher efficiency compared to *E. coli* derived Cts1 while no binding was observed for Gus-Jps1, confirming results obtained from *E. coli* derived recombinant protein and showing binding of N-terminal Cts1 fusion proteins to chitin surfaces (Fig. 3.3 D). To assay if the fusion protein is functional after immobilization, Gus activity was determined on chitin beads previously incubated with 50 µg of raw cell extracts from strains expressing Gus-Cts1 and Gus-Jps1. While only background activity was observed for chitin beads treated with Gus-Jps1, assays with beads incubated with Gus-Cts1 reached activities of up to 2.5 µM/min. This does not only confirm that Cts1 binding to chitin is specific and that bound fusion proteins remain active, but also that direct immobilization of Cts1 fusion protein from raw cell extract on chitin could be achieved (Fig. 3.3 E).

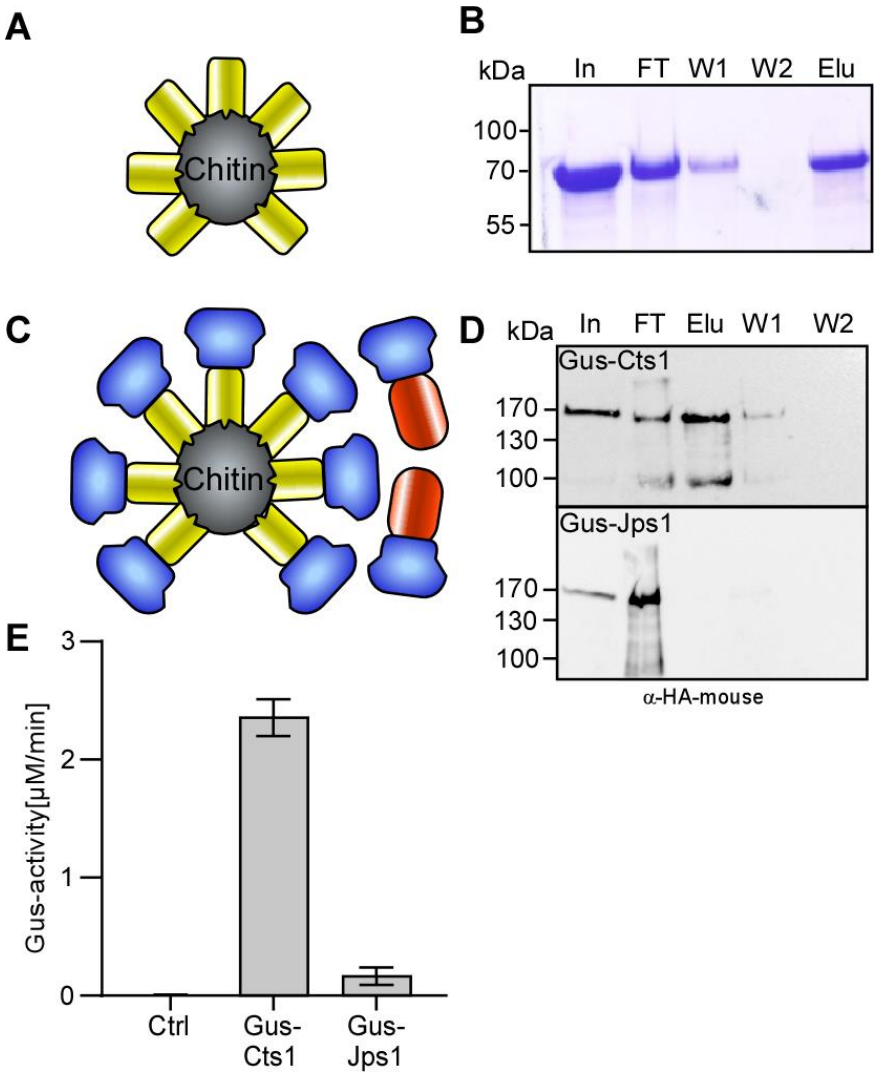

Figure 3.3: Chitin banding capacity of Cts1. (A) Experimental setup for initial Cts1 chitin binding experiments. *E. coli* derived, purified, recombinant Cts1 (yellow) was coated to magnetic chitin beads, washed and subsequently eluted by boiling. **(B)** Coomassie-stained SDS-PAGE of binding fractions: input (In), flow-through (FT), wash (W1 and W2) and elution (Elu) fractions of the experiment. Roughly 50 % of the Cts1 input were lost in the flow-through while 50 % remained stably attached to the beads. **(C)** Experimental setup for Cts1 chitin binding experiments using *U. maydis* derived N-terminal Cts1-fusion proteins. Gus-Cts1 (blue-yellow) was coated to chitin beads, while a second set of beads treated with Gus-Jps1 (blue-red) dealt as a negative control. **(D)** Western blot analysis of input (In), flow-through (FT), wash (W1 and W2) and elution (Elu) fractions of purified Gus-Cts1 and Gus-Jps1 fusion protein incubated with chitin beads. More than 50% of Gus-Cts1 remained coated to chitin beads while the entire Gus-Jps1 fraction was lost in the flow-through. **(E)** On-bead Gus assays conducted with cell extracts of Gus-Cts1 and Gus-Jps1. Beads were treated with Gus-Cts1 and Gus-Jps1. After washing a Gus activity assay was conducted. Conversion from 4-MUG to 4-MU was monitored for 1 h. Empty beads dealt as a blank, Gus-Jps1 and cell extracts of the progenitor strain (Ctrl) dealt as a negative control. Gus-Cts1 remained active when coated to chitin beads. Mean values of three biological replicates are shown. Error bars depict standard deviation.

3.2.4 Assessing the potential of nanobody-Cts1 fusions for RBD capture and chitin binding

To determine the capture capability of the most promising nanobody variants VHHE-Cts1 and VHHEE-Cts1, sandwich ELISAs were conducted both on ELISA plates and non-classically on chitin beads. $Sy^{68/15}$-Jps1 dealt as a control for both assays as it should show activity in plate-based ELISA but not on a chitin surface. Therefore, VHHE-Cts1, VHHEE-Cts1 and $Sy^{68/15}$-Jps1 were coated to ELISA plates, incubated with serial dilutions of RBD and subsequently detected by a sandwich of commercial RBD antibody (mouse) and an anti-mouse-HRP conjugate (Fig. 3.4 A). In plate-based ELISA all three nanobody variants were capable of binding RBD domain, however, only VHHEE-Cts1 and $Sy^{68/15}$-Jps1 showed volumetric activity for serial RBD dilutions. As observed in the direct ELISA screen before, VHHEE-Cts1 showed the strongest binding capability reaching RFUs of 4199 and significant activity at the lowest RBD concentration of 0.1 ng/µl and 11062 at the highest concentration of 5 ng/µl after an incubation time of 10 min, showing significantly stronger binding than VHHE-Cts1 (Fig. 3.4 B). To determine if detection of RBD domain was possible and if results from direct and sandwich ELISAs were comparable to experiments conducted on a chitin surface, chitin beads were incubated with 2 µg of purified VHHE-Cts1, VHHEE-Cts1 and $Sy^{68/15}$-Jps1 and subsequently treated with 2.5 ng/µl RBD. (Fig. 3.4 C). In contrast to all controls, activity was obtained for both VHHE-Cts1 and VHHEE-Cts1, while no significant signal could be detected for $Sy^{68/15}$-Jps1. As observed before, signals for VHHEE-Cts1 were roughly twice as strong as those for VHHE-Cts1 (Fig. 3.4 D). These results show the potential of chitin-based ELISA using Sars-CoV2 nanobody-Cts1 fusions and its specificity to the anchor Cts1 without unwanted binding of either unspecific antibodies or the sample itself to the chitin surface. Thus, these experiments provide the basis for designing a chitin-based antigen trap for the Sars-CoV2 virus.

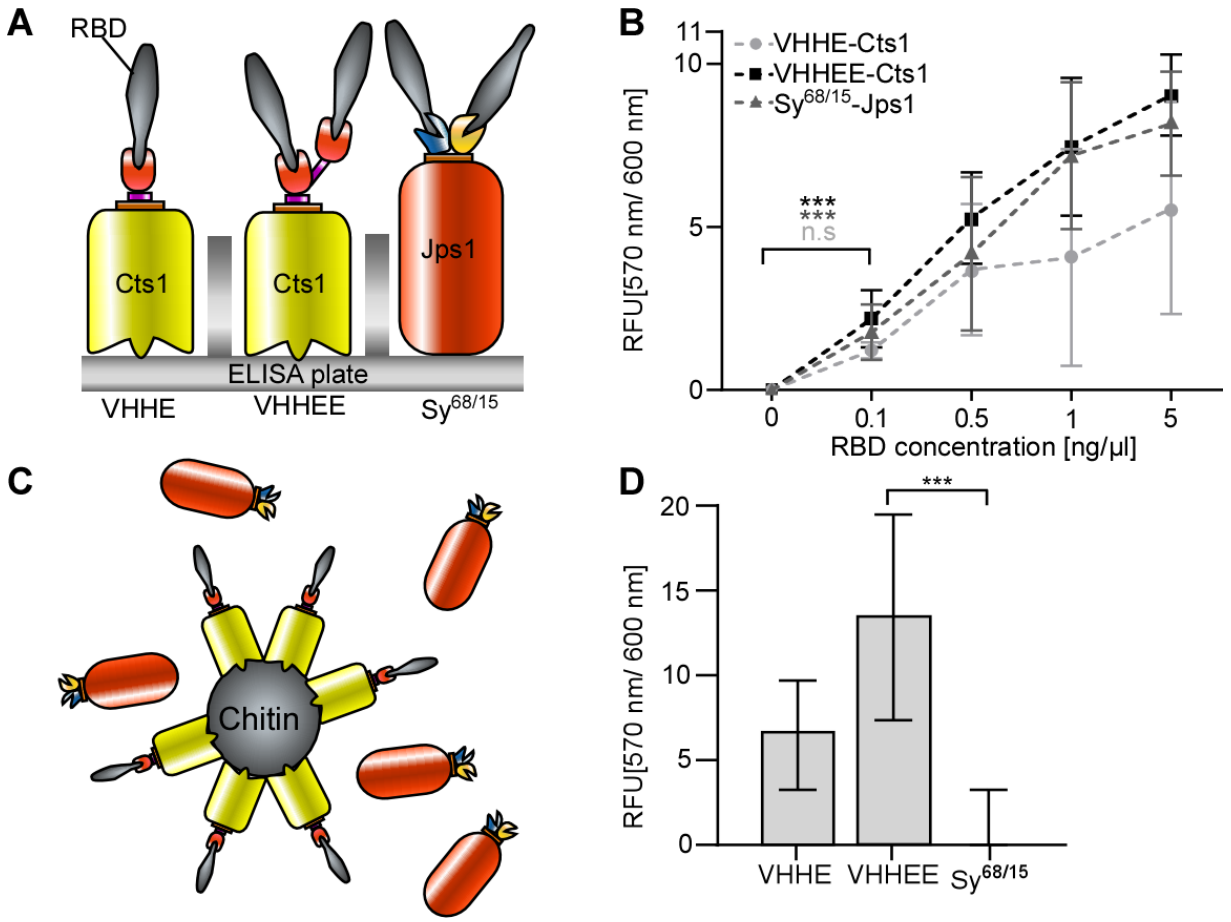

Figure 3.4: Plate-and chitin-based sandwich ELISAs of nanobody fusions for detection of Sars-CoV2 RBD. (A) Experimental setup of plate-based sandwich ELISA. Nanobody-Cts1 fusions were used as capture antibodies for serial dilutions of Sars-CoV2 RBD. **(B)** Quantitative results of plate-based sandwich ELISA. RBD was detected using an anti-RBD-(mouse) antibody and an anti-mouse-HRP conjugate. Strongest RBD binding was observed for VHHEE-Cts1, followed by $Sy^{68/15}$-Jps1 and VHHE-Cts1. Mean values of three biological replicates are shown. Error bars depict standard deviation. Definition of statistical significance (***) p-value < 0.05. **(C)** Experimental setup of chitin-based sandwich ELISA test. Nanobody-Cts1 fusions were coated to chitin beads to serve as capture nanobodies, while $Sy^{68/15}$-Jps1 dealt as negative control because it is unable to bind chitin. **(D)** Quantitative results of chitin-based sandwich ELISA. RBD was detected using an anti-RBD (mouse) antibody and anti-mouse-HRP conjugate. $Sy^{68/15}$-Jps1 dealt as a negative control. Similar to the plate-based sandwich ELISA, VHHEE-Cts1 showed stronger RBD binding than VHHE-Cts1. $Sy^{68/15}$-Jps1 did not show any activity opposed to plate-based ELISA. Mean values of three biological replicates are shown. Error bars depict standard deviation.

To characterize the RBD capturing capabilities of a chitin-based detection system, volumetric binding activity of the system was determined. Based on previous results both in plate based volumetric sandwich ELISA and a non-volumetric chitin-based screen of VHHE-Cts1, VHHEE-Cts1 and $Sy^{68/15}$-Jps1, VHHEE-Cts1 was chosen as capture nanobody. To this end, chitin beads were coated with purified VHHEE-Cts1, subsequently incubated with commercially available RBD domain in serial

dilutions for 2 h and detected with a commercial antibody sandwich as described above (Fig. 3.5 A). A colorimetric reaction was visible within a timeframe of two minutes. While the empty control (0 ng/µl) and lower RBD concentrations of 0.5 ng/µl and 1 ng/µl developed weak signals, intensity strongly increased from 5 to 20 ng/µl RBD (Fig. 3.5 B). These results could be elucidated in quantitative fluorescence measurements of the same samples. Activity was detectable from 0.5 ng/µl RBD onwards and steadily increased until saturation between 10 and 20 ng/µl (Fig. 3.5 C). These results demonstrate that volumetric detection of Sars-CoV2-RBD on a chitin surface is possible, sensitive in the nanomolar range and in the given setup even faster than on a conventional ELISA plate.

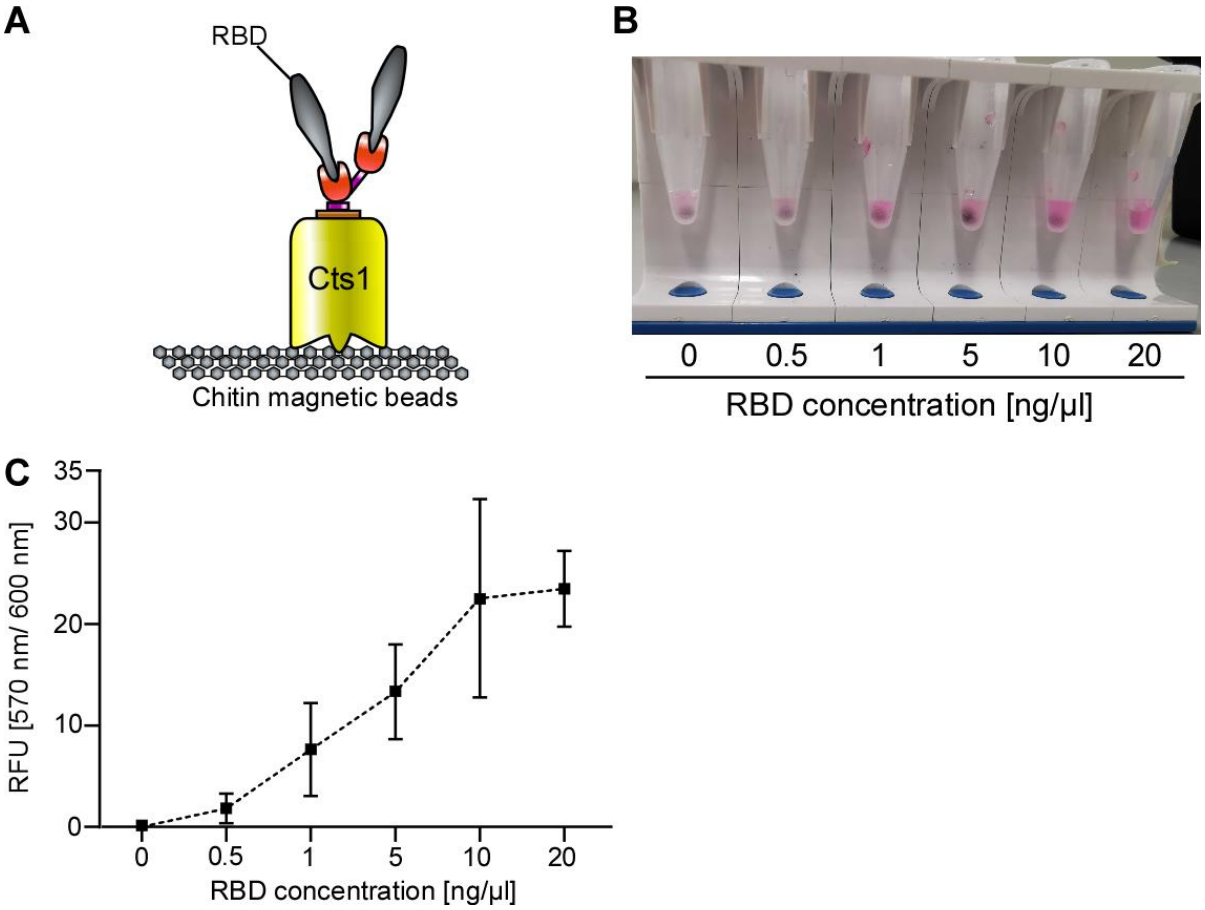

Figure 3.5: Chitin-based antigen test. (A) Setup of chitin-based ELISA. VHHEE-Cts1 was coated to the chitin surface and used as capture antibody for Sars-CoV2 RBD. **(B)** RBD was added to VHHEE-Cts1 coated magnetic chitin beads in serial dilutions and subsequently detected using anti RBD (mouse) and anti-mouse-HRP antibodies. Picture depicts one representative replicate of colorimetric reaction in reaction tubes. **(C)** Quantitative readout of fluorescence measurements from chitin beads coated with VHHEE-Cts1, treated with serial dilutions of Sars-CoV2 RBD. Mean values of three biological replicates are shown. Error bars depict standard deviation.

3.2.5 Further functionalization of an anti-Gfp nanobody using peroxidase Apex2

A key improvement of the chitin based Sars-CoV2 detection system would be a faster and more direct detection without losing sensitivity. Therefore, functionalization of the *U. maydis*-derived nanobodies for direct detection was tested. As a proof of principle, a well characterized anti-Gfp nanobody (αGfpNB) (Terfrüchte et al. 2017) fused to Cts1 and the peroxidase Apex2 were merged into fusion proteins. The latter enzyme, an engineered ascorbate peroxidase, was previously shown to be active, when expressed in *U. maydis* and secreted as a Cts1 fusion (Reindl 2016). To this end Apex2 was attached both N- and C-terminally to αGfpNB. In both cases Cts1 was fused to the C-terminus of the fusion protein. The previously established Cts1 fusions αGfpNB-Cts1 and Apex2-Cts1 dealt as controls in the following assays (Reindl 2016, Terfrüchte et al. 2017) (Fig. 3.6 A). Initially, Apex2 activity assays were conducted with supernatants and cell extracts from strains producing αGfpNB-Cts1, Apex2-Cts1, αGfpNB-Apex2-Cts1 and Apex2-αGfpNB-Cts1 with cell extracts of the background strain dealing as baseline control. While no signal was obtained from supernatants of any tested strain (data not shown), cell extracts revealed Apex2 activity as determined by a plate reader. When 0.1, 0.5 and 1 µg of cell extract were used, peroxidase activity was detected for αGfpNB-Apex2-Cts1 and Apex2-Cts1. Unexpectedly, αGfpNB-Apex2-Cts1 extracts showed much stronger activity than Apex2-Cts1. By contrast, Apex2-αGfpNB-Cts1 expressing cells showed no activity at all (Fig 3.6 B.). Due to its lack in peroxidase activity the Apex2-αGfpNB-Cts1 expressing strains was not further investigated. To further elucidate the difference in signal strengths between αGfpNB-Apex2-Cts1 and Apex2-Cts1 the assay was repeated with higher total protein amounts. Surprisingly, activity slightly diminished when 1 µg to 2 µg of cell extract was applied and strongly diminished with increasing amounts of cell extract used for both variants while controls remained at baseline level independent of the used amount. Furthermore, it could be confirmed that cell extracts of αGfpNB-Apex2-Cts1 are twice as active as their Apex2-Cts1 counterparts (Fig. 3.6 C.). To determine expression and secretion levels of αGfpNB-Apex2-Cts1, Western blot analyses of both cell extracts and TCA precipitated supernatants were conducted, confirming both expression and secretion of the construct. Bands were visible slightly above their expected sizes at 130 kDa (Fig. 3.6 D). After peroxidase activity conveyed by Apex2 as well as secretion of the fusion protein mediated by Cts1 were confirmed, binding activity of αGfpNB was determined to investigate the influence of the huge tags on the nanobody. Therefore, recombinant Gfp purified from *E. coli* was coated to ELISA plates as an antigen. Cell extracts of both αGfpNB-Cts1 and αGfpNB-Apex2-Cts1 were added in serial dilutions and detected with a commercial

antibody sandwich. BSA coated wells dealt as negative controls. Binding capacity of αGfpNB-Apex2-Cts1 was reduced by roughly 50% compared to αGfpNB-Cts1 but still significant after a detection time of 10 min (Fig. 3.6 E). To determine if direct detection of Gfp with αGfpNB-Apex2-Cts1 was feasible, total protein amounts of the cell extract were strongly increased to compensate for the multiplication effect obtained by the binding of a three-antibody sandwich to the cognate antigen. Apex2-Cts1 dealt as control for unspecific retention, while αGfpNB-Cts1 and Apex2-αGfpNB-Cts1 dealt as negative controls. Activity for αGfpNB-Apex2-Cts1 compared to controls was clearly detectable after 2 min starting from 50 ng/µl to 200 ng/µl of cell extract. No unwanted retention of Apex2-Cts1 or unspecific signal development in other negative controls was observed (Fig. 3.6 F). These results clearly show that direct detection based on a nanobody-Apex2-Cts1 fusion is possible for high input of the fusion protein and even results in less background activity and a quicker detection when compared to the use of a commercial antibody sandwich for the detection of the antigen.

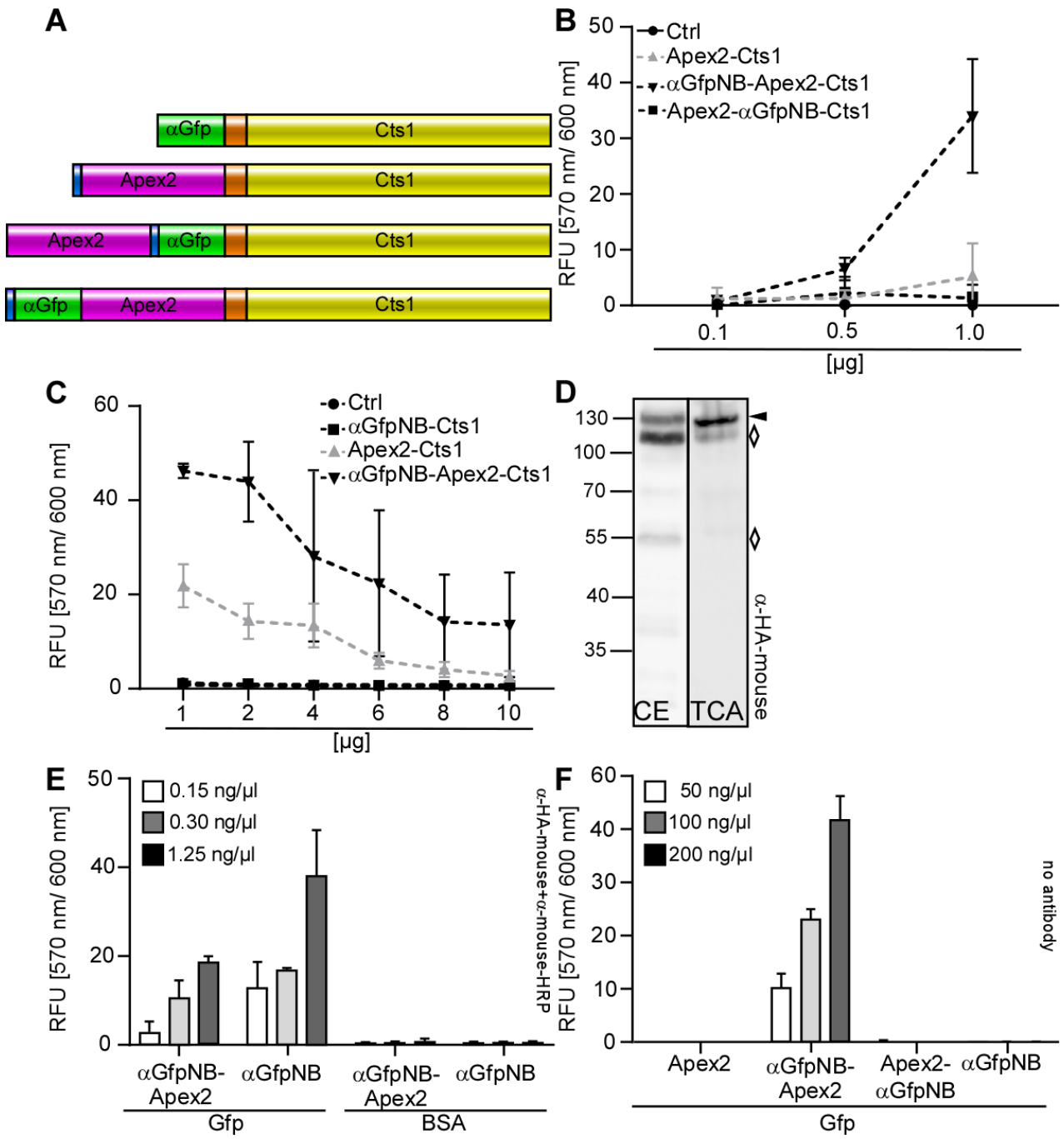

Figure 3.6: Characterization of a functionalized αGfpNB. (A) Representation of nanobody Apex2 fusion variants for unconventional secretion mediated by Cts1. αGfpNB-Cts1 and Apex2-Cts1 dealt as controls for all experiments. Apex2 was fused to αGfpNB either at the N- or C-terminus and expressed as Cts1 fusion. **(B)** Apex2 activity assay. Indicated amounts of cell extracts were diluted in PBS buffer and mixed 1:1 with fluorescent ELISA substrate. Activity was determined 30 min after reaction start. Apex2-Cts1 and αGfpNB-Apex2-Cts1 both showed activity. For Apex2-αGfpNB-Cts1 and the progenitor strain control no activity could be determined. Mean values of three biological replicates are shown. Error bars depict standard deviation. **(C)** Apex2 activity assay with increased amounts of cell extracts. Indicated amounts of cell extract were diluted in PBS buffer and mixed 1:1 with florescent ELISA substrate. Activity was determined 30 min after reaction start. Apex2-Cts1 and αGfpNB-Apex2-Cts1 both displayed activity, however αGfpNB-Apex2-Cts1 exhibits

stronger peroxidase activity, than Apex2-Cts1. Apex2-αGfpNB-Cts1 and the progenitor strain control showed no activity. Mean values of three biological replicates are shown. Error bars depict standard deviation. **(D)** Western blot analysis of αGfpNB-Apex2-Cts1 expression and secretion levels. 10 µg of cell extracts were subjected to Western blot analysis. αGfpNB-Apex2-Cts1 was detected using an Ha-mouse antibody (left lane; cell extracts, CE). Signals were detected slightly above the expected size of 125 kDa. Secreted protein was enriched from the supernatant via TCA precipitation and detected in Western blot via an Ha-mouse antibody (right lane; trichloroacetic acid precipitation, TCA). Full length protein is indicated by arrow, degradation products by rhombus. **(E)** Direct ELISA of αGfpNB-Apex2-Cts1 and αGfpNB-Cts1 against Gfp as an antigen coated to the plate. Indicated serial dilutions of cell extracts were added to wells coated with Gfp and activity was detected with a sandwich of anti-HA and anti-mouse-HRP. BSA coated wells dealt as negative control. Binding activity of αGfpNB-Cts1 was increased roughly 2-fold compared to αGfpNB-Apex2-Cts1. Mean values of three biological replicates are shown. Error bars depict standard deviation. **(F)** Direct ELISA of αGfpNB-Apex2-Cts1 to determine direct enzymatic detection via Apex2. Amounts of cell extract were increased and αGfpNB-Apex2-Cts1 was detected directly after incubation by addition of ELISA substrate. Apex2-Cts1, αGfpNB-Cts1 and Apex2-αGfpNB-Cts1 dealt as negative controls. Activity could only be determined for αGfpNB-Apex2-Cts1. No background was observed in negative controls. Mean values of three biological replicates are shown. Error bars depict standard deviation.

3.2.6 Functionalization of an anti-Sars-CoV2-RBD nanobody

Next, the strategy for direct detection of αGfpNB-Apex2-Cts1 should be transferred to a Sars-CoV2-RBD nanobody. Of note, the carrier protein was changed from Cts1 to Jps1 due to two reasons: i) Jps1 had proven to be a more effective carrier for $Sy^{68/15}$ (Philipp et al. 2021) and ii) Cts1 is not suitable as a carrier protein for a nanobody that might be used for detection in a chitin based antigen test in the future, due to its interaction with the chitin surface. Based on previous results Apex2 was attached to the C-terminus of $Sy^{68/15}$ and VHHE. Jps1 was linked to the C-terminus of Apex2 via an Ha-tag (Fig. 3.7 A). Apex2 assays were repeated as described above with Apex2-Cts1 dealing as positive control and the progenitor strain as negative control. In stark contrast to αGfpNB-Apex2-Cts1 the peroxidase activity of VHHE-Apex2-Jps1 and $Sy^{68/15}$-Apex2-Jps1 was not elevated but severely diminished. For VHHE-Apex2-Jps1 activity was completely undetectable, while $Sy^{68/15}$-Apex2-Jps1 showed roughly 10-fold decreased activity compared to Apex2-Cts1 (Fig. 3.7 B). From this point onward VHHE-Apex-Jps1 was not further investigated. To determine if this effect was based on expression level or activity of the incorporated Apex2, Western blot analyses of TCA precipitated supernatants and cell extracts of strains producing $Sy^{68/15}$-Apex2-Jps1 were conducted. Interestingly, the protein was both expressed and secreted in expected amounts, suggesting that the low peroxidase activity was linked to inactive Apex2 and not to the expression level of the fusion protein (Fig. 3.7 C). To determine RBD binding activity of $Sy^{68/15}$-Apex2-Jps1, RBD coated wells were incubated with

serial dilutions of the purified fusion protein and detected with a commercial antibody-sandwich. 0.15 ng/µl of $Sy^{68/15}$-Jps1 already resulted in a strong signal and saturation was achieved at 0.30 and 1.25 ng/µl, indicating that the binding capacity of $Sy^{68/15}$ was still intact (Fig. 3.7 D). Attempts for direct detection using cell extracts resulted in no activity even at amounts of up to 500 ng/µl protein per well (data not shown). Thus, purified protein was used for direct detection as well. In this case 5.0 ng/µl were necessary for a weak signal above the detection threshold with activity volumetrically rising but not saturating with increased amounts of $Sy^{68/15}$-Apex2-Jps1 up to 40 ng/µl (Fig 3.7 E). While these results indicated that high amounts of $Sy^{68/15}$-Apex2-Jps1 would be necessary for detection, it could be deduced that direct detection of RBD with this construct was still possible albeit far less effectively compared to αGfpNB-Apex2-Cts1.

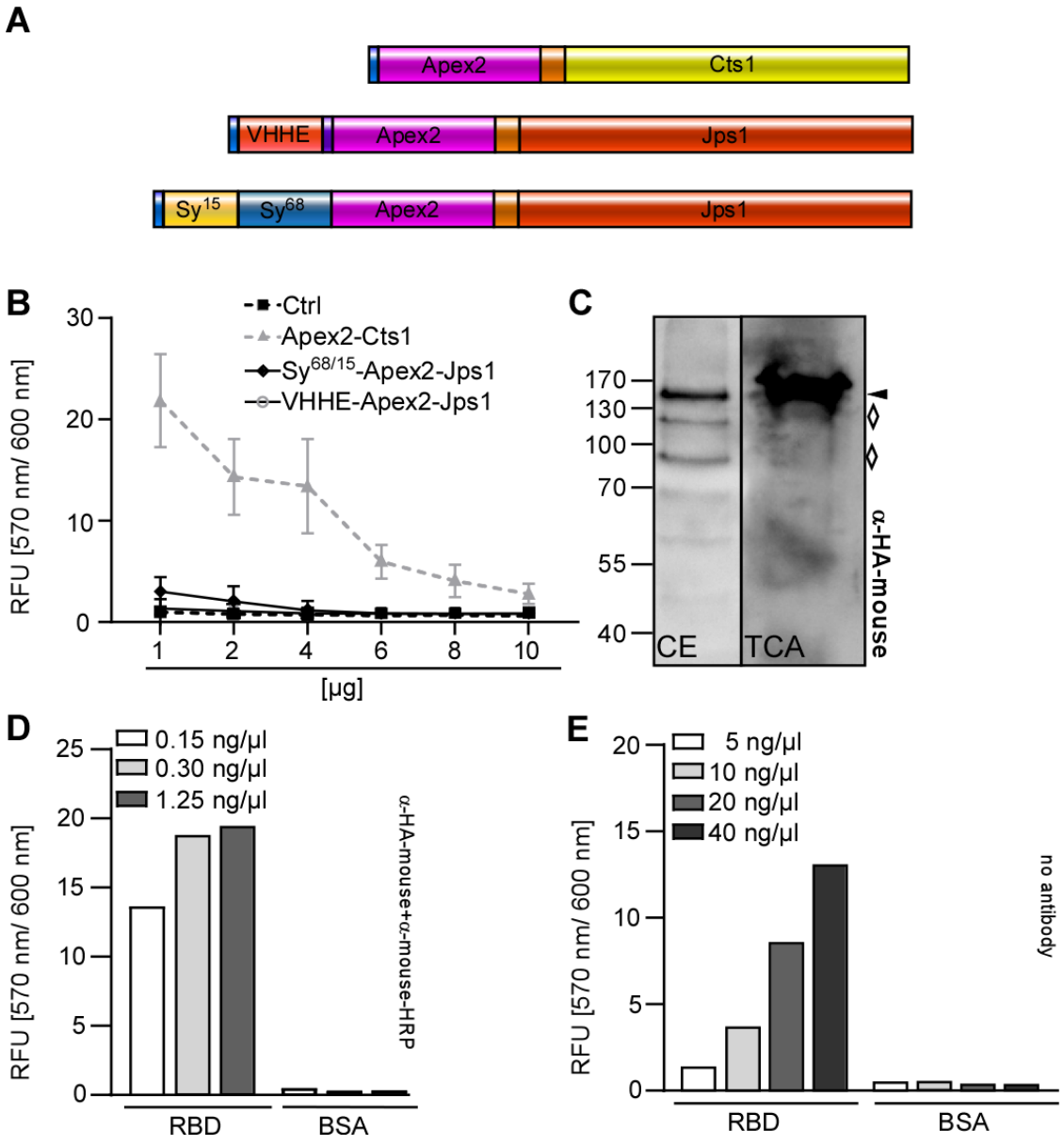

Figure 3.7: Characterization of a functionalized anti Sars-CoV2 nanobody. (A) Representation of nanobody Apex2 fusion constructs. Apex2-Cts1 dealt as control for all activity assays. Apex2 was fused to either $Sy^{68/15}$ or VHHE at the C-terminus and expressed as Jps1 fusion. **(B)** Apex2 activity assay. Indicated amounts of cell extract were diluted in PBS buffer and mixed 1:1 with fluorescent ELISA substrate. Activity was determined 30 min after reaction start. The control strain producing Apex2-Cts1 shows elevated activity compared to the control. Low signal intensities could be observed for $Sy^{68/15}$-Apex2-Jps1. No activity was detected for VHHE-Apex2-Jps1 and the negative control. Mean values of three biological replicates are shown. Error bars depict standard deviation. **(C)** Western blot analysis of $Sy^{68/15}$-Apex2-Jps1 expression and secretion levels. 10 µg of cell extracts were subjected to Western blot analysis. $Sy^{68/15}$-Apex2-Jps1 was detected using an anti-Ha (mouse) antibody. Signals were detected slightly above the expected size at ~150 kDa. Secreted protein was enriched from the supernatant via TCA precipitation and detected in Western blot via an anti-Ha (mouse) antibody. Full length protein is indicated by arrow, degradation products by rhombus **(D)** Direct ELISA of $Sy^{68/15}$-Apex2-Jps1 on Sars-CoV2 RBD coated wells. Indicated serial dilutions of purified protein were added to wells and activity was detected with a sandwich of anti-HA (mouse) and anti-mouse-HRP. BSA coated wells dealt as negative control. Strong activity was detected at 0.15 ng/µl and reaction saturated at 0.3 ng/µl. One representative replicate is shown. **(E)** Direct ELISA of $Sy^{68/15}$-Apex2-Jps1 against Sars-CoV2 RBD coated to plate. Indicated serial dilutions of purified protein were added to wells coated with RBD and activity was detected directly using only the Apex2 activity of the protein fusion. Activity was detectable from 5 ng/µl onward but reaction did not saturate, even at 40 ng/µl. One representative replicate is shown.

3.2.7 Direct detection of sandwich type ELISA using $Sy^{68/15}$-Apex2-Jps1

Final experiments were conducted to determine if direct detection of RBD in sandwich ELISA with $Sy^{68/15}$-Apex2-Jps1 was feasible despite its generally low peroxidase activity. To this end, VHHE-Cts1, VHHEE-Cts1 and $Sy^{68/15}$-Jps1 were coated to ELISA plates and incubated with serial dilutions of Sars-CoV2 RBD as described before. RBD was then directly detected with 40 ng/µl $Sy^{68/15}$-Apex2-Jps1 instead of the previously used conventional antibody sandwich (Fig. 3.8 A). Sandwich ELISAs revealed that direct detection resulted in clear volumetric activity when VHHEE-Cts1 was used as capture nanobody. RBD binding was detectable for VHHE-Cts1 as well, however activity peaked at 1 ng/µl RBD and diminished for 5 ng/µl and 10 ng/µl respectively, not showing a clear volumetric relation between activity and amount of RBD used. Interestingly, the strongest signals were obtained when $Sy^{68/15}$-Jps1 was used as capture nanobody. However, for this capture nanobody the baseline was heavily elevated, and activity did not follow a volumetric correlation to amounts of RBD used (Fig 3.8 B). This might indicate self-interaction of $Sy^{68/15}$-Jps1 due to Jps1 dimerization. Due to the low signal strength obtained by using VHHE-Cts1 as capture nanobody and the elevated baseline of $Sy^{68/15}$-Jps1, VHHEE-Cts1 was chosen for more in-depth analysis. When baseline values were subtracted the

combination of VHHEE-Cts1 and Sy$^{68/15}$-Apex2-Jps1 revealed a volumetric regression curve similar to that obtained with a commercial antibody sandwich (see Fig 3.4 B for comparison), clearly demonstrating that direct detection with components obtained from *U. maydis* is feasible in plate based indirect ELISAs directed against Sars-CoV2 RBD (Fig 3.8 C). In a final experiment chitin-based sandwich ELISAs were repeated with VHHEE-Cts1 as capture nanobody but in this iteration with Sy$^{68/15}$-Apex2-Jps1 as detector. While results in plate-based ELISA had been solid with this combination, chitin based ELISAs did not show proper signals. A weak fluorimetric signal was obtained but colorimetric changes could not be observed. In addition to the weak signal intensity standard deviations between assays were massive and no volumetric relation between activity and RBD concentration could be determined. In conclusion, direct detection of Sars-CoV2 RBD is possible using only Sy$^{68/15}$-Apex2-Jps1 both in direct and sandwich plate-based ELISA. Furthermore, VHHEE-Cts1 is functional as a capture nanobody in both plate-based and chitin-based sandwich ELISA but the combination of VHHEE-Cts1 and Sy$^{68/15}$-Apex2-Jps1 is far less active on chitin than on plate.

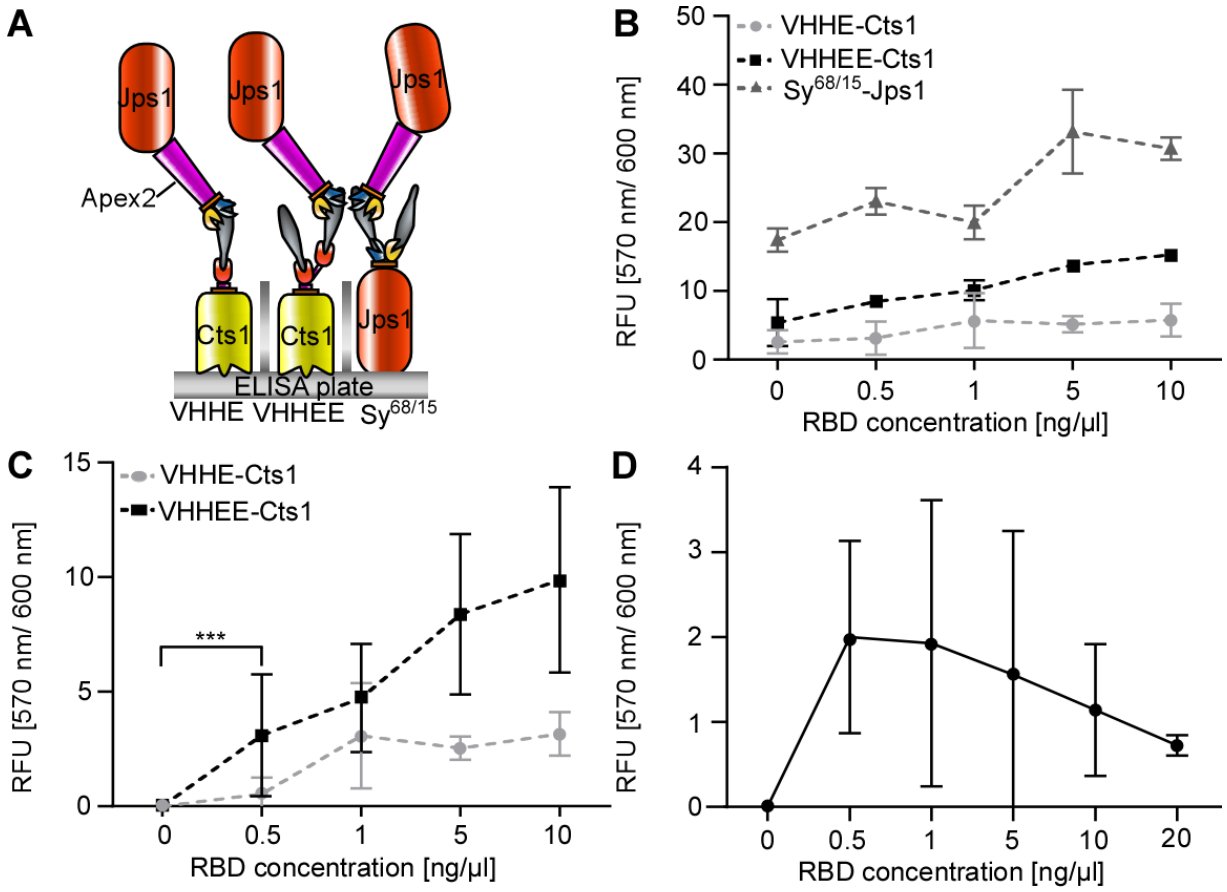

Figure 3.8: Sy$^{68/15}$-Apex2-Jps1 based direct RBD detection in Sandwich ELISA. (A) Experimental setup of plate-based sandwich ELISA. Nanobody-Cts1 fusions were coated to ELISA plates and used as capture antibodies for serial dilution

of Sars-CoV2 RBD. RBD was detected using $Sy^{68/15}$-Apex2-Jps1 in all cases. **(B)** Quantitative results of plate-based sandwich ELISA. To visualize high background activity of $Sy^{68/15}$-Jps1, baseline values were not subtracted. Strongest RBD binding was observed for VHHEE-Cts1. For VHHE-Cts1 and $Sy^{68/15}$-Jps1 direct detection with $Sy^{68/15}$-Apex2-Jps1 did not result in volumetric activity. Mean values of three biological replicates are shown. Error bars depict standard deviation. **(C)** Quantitative results of plate-based sandwich ELISA. For clarification the identical dataset as in panel B is depicted. However, baseline values have been subtracted and $Sy^{68/15}$-Jps1 has been omitted. Clear volumetric activity with VHHEE-Cts1 as capture nanobody is visible. Mean values of three biological replicates are shown. Error bars depict standard deviation. Definition of statistical significance (***) p-value < 0.05. **(D)** Quantitative results of chitin bead-based sandwich ELISA. VHHEE-Cts1 was used as capture nanobody. RBD was detected directly using $Sy^{68/15}$-Apex2-Jps1. While all samples treated with RBD showed activity above baseline, activity was very low and no volumetric correlation between RBD concentration and activity was visible. Mean values of three biological replicates are shown. Error bars depict standard deviation.

3.3 Discussion

Here we demonstrate the successful expression, secretion and functionalization of monovalent, multivalent and multimerized nanobody fusion proteins via unconventional secretion for Sars-CoV2 detection on a chitin surface. This was achieved by C-terminal fusion of Cts1 to the target nanobody and subsequent immobilization on chitin. Cts1 was thus exploited in a dual use strategy for both export of the heterologous protein and as an immobilization tag. The second, recently established carrier for unconventional secretion, Jps1, was applied for exporting the detection nanobody. The use of carrier proteins is a common practice in fungal hosts (Fleissner and Dersch 2010). As observed in other studies, different combinations of nanobody and carrier resulted in varying levels of expression and activity. This was evident by the high expression and secretion level but inactivity of VHHV-Cts1 or the comparatively low expression and secretion levels of Sy^{15}-Cts1 and Sy^{68}-Cts1 and constructs like VHHEE-Cts1 being both highly expressed and highly active. While this underlines the necessity of a screening step of several constructs for each target oriented nanobody expression process, it is in line with results obtained in other carrier based secretion systems (Wang et al. 2020b). Importantly, we did not only verify the applicability of the nanobodies in virus detection but also successfully tested the neutralization of Sars-CoV2 *in vivo*. This does on the one hand side constitutes an important confirmation of nanobody binding of the entire virus as opposed to only the RBD domain *in vitro*, necessary for antigen test application. On the other hand, it also enables further research towards drug development using unconventionally secreted proteins from *U. maydis.* Nanobodies are currently discussed as novel drug targets due to ease of production, prolonged shelf life compared to conventional antibodies and favorable *in vivo* attributes, such as improved tissue penetration and

decreased immunogenicity (Bannas et al. 2017, Salvador et al. 2019). Furthermore, the main drawback of nanobodies *in vivo,* their quick clearance from the bloodstream, has been addressed by fusion of larger proteins such as album-binding domain (Xenaki et al. 2021). Here, an application of Sars-CoV2 nanobodies derived from *U. maydis*, where the non-glycosylated carrier protein would carry out the stabilizing function would be an interesting target for further investigation. This is further underlined by Sars-CoV2 nanobodies effectively neutralizing Sars-CoV2 *in vivo* in hamster models (Esparza et al. 2021). Furthermore, using the carrier protein directly for immobilization in conventional immunoassays is not a common practice. Protein immobilization is generally achieved via protein adhesive polymers and not by specific protein-molecule interaction (Lin 2015, Andryukov 2020). Moreover, direct immobilization of Cts1 fusion proteins was shown from cell extracts in this study. Building upon these results could enable direct purification from the supernatant, thus greatly easing the purification process and thereby production costs of biopharmaceuticals. Similar non chromatography purification processes have already been applied using GST, biotin and streptavidin coated magnetic particles to purify protein from *E. coli cell* lysates (Franzreb et al. 2006) and supernatants (Fernandes et al. 2016) but also from human serum plasma (Santos et al. 2020). While nanobody immobilization on chitin via Cts1 has previously been shown (Terfrüchte et al. 2017), its application for virus detection constitutes a novelty. The use of bio-based polymers for immobilization is of high interest since it allows for reduction of antigen test pricing and use of sustainable and inexpensive resources. To this end a similar study achieved Sars-CoV2 detection based on nanobody immobilization on cellulose, albeit without using the immobilization tag for export at the same time (Sun et al. 2022). Importantly, both systems based on chitin and cellulose showed similar capture capabilities in the low nanomolar range and are thus well within described limits for other Sars-CoV2 Spike RBD detection systems (Baker et al. 2020). Hence protein-based immobilization of nanobodies for target capture and detection as shown in this study constitutes an important step towards new technologies for antigen testing.

Functionalization of nanobodies in this study was not only achieved by immobilization but also by enzymatic fusion for direct detection. Fusion of peroxidase Apex2 to αGfpNB-Cts1 enabled fast, efficient and resource-saving detection of the cognate antigen. Functionalization of antibodies for detection of antigens using enzymes such as HRP or alkaline phosphatase is a common practice (Gillet et al. 1993, Lequin 2005). Use of Apex2 for nanobody functionalization and ELISA detection on the other hand is not as widespread but has been demonstrated before (Sherwood and Hayhurst 2022). Furthermore, Apex2 outperformed HRP for direct antigen detection, when fused to αGfpNB-Cts1 and

secreted unconventionally (Terfrüchte 2016). Tandem use of Cts1 for immobilization and antigen capture and Jps1 for detection of the antigen demonstrates the versatility of components derived from the *U. maydis* unconventional secretion system and enabled one-step-detection of Sars-CoV2 RBD in plate-based sandwich ELISA. Nonetheless, reduced Apex2 activity prevented detection of Sars-CoV2 RBD on chitin. To this end future studies will be focused on the design of improved detectors. Up to this point, conventional detection methods can be applied as shown in this study.

All in all, we demonstrated Sars-CoV2 detection and neutralization by unconventionally secreted, multimerized nanobodies derived from *U. maydis.* Furthermore, we demonstrated that capture capability of nanobody-Cts1 fusions is transferable from a typical polymer surface to chitin, thus enabling a chitin based Sars-CoV2 antigen detection system. This builds a solid foundation for future development of a versatile virus detection cassette, for example on the level of a biohybrid Cts1-binding surface on a micro fluidic chip to form a "lab-on-a-chip" (Zhuang et al. 2020).

3.4 Materials and methods

3.4.1 Molecular biology methods

All plasmids (pUMa/pUx vectors) generated in this study were obtained using standard molecular biology methods established for *U. maydis* including restriction ligation and Gibson cloning (Gibson et al. 2009). Enzymes for cloning were purchased from NEB (Ipswich, MA, USA). For the generation of pUMa4678 and 4679 *αgfpnb* was excised from pUMa2240 (Terfrüchte et al. 2017) by hydrolyzation with BamHI and SpeI. DNA sequences encoding for Sy^{15} and Sy^{68} (Walter et al. 2020) were amplified from synthetic gene blocks (IDT Coralville, IA, USA) using oligonucleotide pairs oAB908/oAB909 and oAB910/oAB911, respectively. Subsequently PCR products were hydrolyzed with BamHI and SpeI and inserted into the backbone of pUMa2113 via restriction ligation cloning to generate pUMa4678 and 4679. pUMa4774 was generated by hydrolyzation of the pUMa2240 backbone with AscI (NEB) and amplification of Apex2 from the backbone of pUMa2798 (Reindl 2016) with oCD293 and oCD153 which was subsequently inserted via Gibson cloning. Generation of pUx4 and pUx5 was achieved by excision of *αgfpnb* from pUMa2240 with BamHI and SpeI and amplification of *vhhe* and *vhhv* with BamHI and SpeI restriction sites from synthetic gene blocks using oligo pairs oCD359/oCD360 and oCD363 /oCD364, respectively. These sequences were subsequently hydrolyzed with BamHi and SpeI and inserted into the backbone of pUMa2240 via restriction ligation cloning, thereby generating pUx4 and pUx5. pUx6 was generated in a similar manner. However, after

the hydrolyzation of the pUMa2240 backbone *vhhe* was amplified once with a BamHI and EcoRI and once with an EcoRI and SpeI hydrolyzation sites. After hydrolyzation two sequences for *vhhe* were inserted into the open reading frame via restriction ligation cloning, thereby encoding for fusion protein VHHEE-Cts1. For the generation of pUx7 this process was repeated but instead of using two *vhhe* sequences with differing hydrolyzation sites, the first *vhhe* sequence with BamHI and EcoRI hydrolyzation sites was exchanged for *vhhv* with corresponding hydrolyzation sites. pUx8 and pUx4 were hydrolyzed using AscI and used as backbone for pUx30 and pUx31, respectively. *Apex2* was amplified from pUMa4774 with oligonucleotides oCD293 and oCD611 and inserted into the pUx8 and pUx4 backbones via Gibson cloning respectively, thereby generating pUx30 and pUx31.

Table 4.1. DNA oligonucleotides used in this study.

Designation	**Nucleotide sequence (5´- 3´)**
oMB372_jps1_fw	TTAGGCGCGCCATGCCAGGCATCTCC
oMB373_jps1_rev	TTAGGGCCCTTAGGATTCCGCATCGATTGGGG
oAB908_Sy15_fw	ATATAGGATCCATGGCGGCCCATCACCACCATCACCACCATCACCACCA TCATATGCAGGTGCAGCTCG
oAB909_Sy15_rev	ATATAACTAGTCGAGACGGTGACCTGGGTGC
oAB910_Sy68_fw	TATAGGATCCATGGCGGCCCATCACCACCATCACCACCATCACCACCAT CATATGCAGGTGCAGCTCGTCGAG
oAB911_sy68_rev	ATATATACTAGTCGAGACGGTGACCTGGGTGC
oCD153_Apex2_Asc_rev	CGACGTGCCCGACTATAGGGCGCATGGGCGGTGGTGGCAAGTCG
oCD154_Apex2_Bam_fw	CCAAACATTCTAGAGGCGCGGTCGGCGAAGCCGAGCTCG
oCD155_Apex2_Bam_rev	CAACTACCTTACTCTATCAGATGGGCGGTGGTGGCAAGTCG
oCD293_Apex2_Asc_fw	CGACGTGCCCGACTATAGGATGGGCGGTGGTGGCAAGTCG
oCD359_VHHE_fw	ATATAGGATCCATGGCGGCCCATCACCACCATCACCACCATCACCACCA TCATATGCAGGTGCAGCTCGTCG
oCD360_VHHE_rev	ATATGAATTCATGCAGGTGCAGCTCGTCG
oCD361_VHHE_linker	ATATACTAGTAGAGCCACCACCACCAGAGCCACCACCACCAGAGCCACC ACCACCCGACGAGACGGTGACGAGCG
oCD362_VHHE_linker	ATATGAATTCAGAGCCACCACCACCAGAGCCACCACCACCAGAGCCACC ACCACCCGACGAGACGGTGACGAGC
oCD363_VHHV_fw	ATATAGGATCCATGGCGGCCCATCACCACCATCACCACCATCACCACCA TCATATGCAGGTGCAGCTCGTCG
oCD364_VHHV_rev	ATATACTAGTAGAGCCACCACCACCAGAGCCACCACCACCAGAGCCACC ACCACCCGACGAGACGGTGACCTGG

oCD365_VHHV_linker	ATATGAATTCAGAGCCACCACCACCAGAGCCACCACCACCAGAGCCACC ACCACCCGACGAGACGGTGACCTG
oCD611_Apex2Jps1_rev	GGCTTCTTGGAGATGCCTGGCATGGCGCGGTCGGCGAAGCCGAGCTCG

3.4.2 Strain generation

U. maydis strains used in this study were obtained by homologous recombination yielding genetically stable strains (Table 4.2). For genomic integrations at the *ip* locus, integrative plasmids were used (Stock et al. 2012). For genomic integration at the *ip* locus, integrative plasmids contained the ip^r allele, promoting carboxin (Cbx) resistance. Thus, plasmids were linearized within the ip^r allele using restriction enzymes SspI and SwaI to allow for homologous recombination with the ip^s locus. For all genetic manipulations, *U. maydis* protoplasts were transformed with linear DNA fragments. All strains were verified by Southern blot analysis. For *in locus* modifications the flanking regions were amplified as probes. For *ip* insertions, the probe was obtained by PCR using the primer combination oMF502/oMF503 and the template pUMa260. Primer sequences are listed in Table 1.

Table 4.2. *U. maydis* strains used in this study.

Strains	**Relevant genotype/ Resistance**	**Strain collection no. (UMa[1])**	**Plasmids transformed / Resistance[2]**	**Manipulated locus**	**Pro-genitor (UMa[1])**	**Reference**
AB33P8Δ	*a2 P$_{nar}$bW2bE1* PhleoR *FRT10[um04641Δ::hyg] FRT11[um03947Δ] FRT6[um03975Δ] FRT5[um04400Δ] FRT3[um11908Δ] FRT2[um00064Δ] FRTwt[um02178Δ] FRT1[um04926Δ]* HygR	2413		*um04926*		Terfrüchte et al. 2018
AB33P8Δ Gus-Cts1	*a2 P$_{nar}$bW2bE1* PhleoR *FRT10[um04641Δ::hyg] FRT11[um03947Δ] FRT6[um03975Δ] FRT5[um04400Δ] FRT3[um11908Δ] FRT2[um00064Δ] FRTwt[um02178Δ]*	2418	pUMa2113	*ip*	2413	Terfrüchte et al. 2018

	FRT1[um04926Δ] HygR *ip^{S}[P$_{oma}$gus:shh:cts1]ip^{R}*CbxR					
AB33P8ΔGus-Jps1	*a2 P$_{nar}$bW2bE1* PhleoR *FRT10[um04641Δ::hyg]* *FRT11[um03947Δ]* *FRT6[um03975Δ]* *FRT5[um04400Δ]* *FRT3[um11908Δ]* *FRT2[um00064Δ]* *FRTwt[um02178Δ]* *FRT1[um04926Δ]* HygR *ip^{S}[P$_{oma}$gus:shh:jps1]ip^{R}*CbxR	2900	pUMa3012	*ip*	2413	Philipp et al. 2022
AB33P8Δ Sy^{15}-Cts1	*a2 P$_{nar}$bW2bE1* PhleoR *FRT10[um04641Δ::hyg]* *FRT11[um03947Δ]* *FRT6[um03975Δ]* *FRT5[um04400Δ]* *FRT3[um11908Δ]* *FRT2[um00064Δ]* *FRTwt[um02178Δ]* *FRT1[um04926Δ]* HygR *ip^{S}[P$_{oma}$his:sybody#15:ha:cts1]ip^{R}*CbxR	3360	pUMa4678	*ip*	2413	This study
AB33P8Δ Sy^{68}-Cts1	*a2 P$_{nar}$bW2bE1* PhleoR *FRT10[um04641Δ::hyg]* *FRT11[um03947Δ]* *FRT6[um03975Δ]* *FRT5[um04400Δ]* *FRT3[um11908Δ]* *FRT2[um00064Δ]* *FRTwt[um02178Δ]* *FRT1[um04926Δ]* HygR *ip^{S}[P$_{oma}$his:sybody#68:ha:cts1]ip^{R}*CbxR	3361	pUMa4679	*ip*	2413	This study
AB33P8Δ αGfpNB-Apex2-Cts1	*a2 P$_{nar}$bW2bE1* PhleoR *FRT10[um04641Δ::hyg]* *FRT11[um03947Δ]* *FRT6[um03975Δ]* *FRT5[um04400Δ]* *FRT3[um11908Δ]* *FRT2[um00064Δ]* *FRTwt[um02178Δ]* *FRT1[um04926Δ]* HygR	3414	pUMa4774	*ip*	2413	This study

	*ip^{S}[P$_{oma}$his:*αgfpnb*:Apex2:ha:cts1]ip^{R}* CbxR					
*AB33P8*Δ *Apex2-*αGfpNB*-Cts1*	*a2 P$_{nar}$bW2bE1* PhleoR *FRT10[um04641Δ::hyg] FRT11[um03947Δ] FRT6[um03975Δ] FRT5[um04400Δ] FRT3[um11908Δ] FRT2[um00064Δ] FRTwt[um02178Δ] FRT1[um04926Δ]* HygR *ip^{S}[P$_{oma}$his:Apex2:*αgfpnb*:ha:cts1]ip^{R}* CbxR	3415	pUMa4775	*ip*	2413	This study
*AB33P8*Δ *Sy$^{68/15}$-Cts1*	*a2 P$_{nar}$bW2bE1* PhleoR *FRT10[um04641Δ::hyg] FRT11[um03947Δ] FRT6[um03975Δ] FRT5[um04400Δ] FRT3[um11908Δ] FRT2[um00064Δ] FRTwt[um02178Δ] FRT1[um04926Δ]* HygR *ip^{S}[P$_{oma}$sybody#68:his:sybody#15:ha:cts1]ip^{R}*CbxR	Ux1	pUx1	*ip*	2413	Philipp et al. 2022
*AB33P8*Δ *VHHE-Cts1*	*a2 P$_{nar}$bW2bE1* PhleoR *FRT10[um04641Δ::hyg] FRT11[um03947Δ] FRT6[um03975Δ] FRT5[um04400Δ] FRT3[um11908Δ] FRT2[um00064Δ] FRTwt[um02178Δ] FRT1[um04926Δ]* HygR *ip^{S}[P$_{oma}$his:vhhe:gs:ha:cts1]ip^{R}*CbxR	Ux4	pUx4	*ip*	2413	This study
*AB33P8*Δ *VHHV-Cts1*	*a2 P$_{nar}$bW2bE1* PhleoR *FRT10[um04641Δ::hyg] FRT11[um03947Δ] FRT6[um03975Δ] FRT5[um04400Δ] FRT3[um11908Δ] FRT2[um00064Δ] FRTwt[um02178Δ] FRT1[um04926Δ]* HygR	Ux5	pUx5	*ip*	2413	This study

	*ip^{S}[P$_{oma}$his:vhhv:gs:ha:cts1]ip^{R}*CbxR					
AB33P8Δ VHHEE-Cts1	*a2 P$_{nar}$bW2bE1* PhleoR *FRT10[um04641Δ::hyg] FRT11[um03947Δ] FRT6[um03975Δ] FRT5[um04400Δ] FRT3[um11908Δ] FRT2[um00064Δ] FRTwt[um02178Δ] FRT1[um04926Δ]* HygR *ip^{S}[P$_{oma}$his:vhhe:gs:vhhe:gs:ha:cts1]ip^{R}*CbxR	Ux6	pUx6	*ip*	2413	This study
AB33P8Δ VHHVE-Cts1	*a2 P$_{nar}$bW2bE1* PhleoR *FRT10[um04641Δ::hyg] FRT11[um03947Δ] FRT6[um03975Δ] FRT5[um04400Δ] FRT3[um11908Δ] FRT2[um00064Δ] FRTwt[um02178Δ] FRT1[um04926Δ]* HygR *ip^{S}[P$_{oma}$his:vhhv:gs:vhhe:gs:ha:cts1]ip^{R}*CbxR	Ux7	pUx7	*ip*	2413	This study
AB33P8Δ Sy$^{68/15}$-Jps1	*a2 P$_{nar}$bW2bE1* PhleoR *FRT10[um04641Δ::hyg] FRT11[um03947Δ] FRT6[um03975Δ] FRT5[um04400Δ] FRT3[um11908Δ] FRT2[um00064Δ] FRTwt[um02178Δ] FRT1[um04926Δ]* HygR *ip^{S}[P$_{oma}$sybody#68:his:sybody#15:ha:jps1]ip^{R}*CbxR	Ux8	pUx8	*ip*	2413	Philipp et al. 2022
AB33P8Δ^{5} VHHE-Apex2-Jps1	*a2 P$_{nar}$bW2bE1* PhleoR *FRT10[um04641Δ::hyg] FRT11[um03947Δ] FRT6[um03975Δ] FRT5[um04400Δ] FRT3[um11908Δ] FRT2[um00064Δ] FRTwt[um02178Δ] FRT1[um04926Δ]* HygR	Ux22	pUx31	*ip*	2413	This study

	*ip^{S}[P$_{oma}$vhhe:apex2:ha:jps1]ip^{R}*CbxR					
AB33P8Δ Sy$^{68/15}$-Apex2-Jps1	*a2 P$_{nar}$bW2bE1* PhleoR *FRT10[um04641Δ::hyg] FRT11[um03947Δ] FRT6[um03975Δ] FRT5[um04400Δ] FRT3[um11908Δ] FRT2[um00064Δ] FRTwt[um02178Δ] FRT1[um04926Δ]* HygR *ip^{S}[P$_{oma}$sybody#68:his:sybody#15:apex2:ha:jps1]ip^{R}*CbxR	Ux23	pUx30	*Ip*	2413	This study

[1] Internal strain collection numbers (UMa/Ux codes)

[2] Plasmids generated in our working group are integrated in a plasmid collection and termed pUMa or pUx plus a 4-digit number as identifier.

3.4.3 Cultivation

U. maydis strains were grown at 28 °C in complete medium supplemented with 1% (w/v) glucose (CM-glc) if not described differently. Solid media were supplemented with 2% (w/v) agar agar. Growth phenotypes were evaluated using the BioLector microbioreactor (m2p-labs). MTP-R48-B(OH) round plates were inoculated with 1.5 ml culture per well and incubated at 1,000 rpm at 28 °C. Backscatter light with a gain of 25 or 20 was used to determine biomass.

3.4.4 Quantification of Gus activity on chitin beads

Gus activity was determined to quantify chitin binding of Gus-Cts1 using the specific substrate 4-methylumbelliferyl β-D galactopyranoside (MUG, Sigma–Aldrich). To his end 50 µg of *U. maydis* cell extracts were diluted in chitin binding buffer to a final volume of 500 µl. 50 µl chitin magnetic beads (New England Biolabs, Ipswich, MA, USA) were washed with 500 µl water, equilibrated with 500 µl chitin binding buffer (500 mM NaCl, 50 mM Tris-HCl buffer pH 8.0, 0,05 % Tween-20 (v/v)) and subsequently incubated with cell extracts in binding buffer at 4 °C on a stirring wheel for 16 h. Subsequently, chitin beads were washed with 500 µl chitin binding buffer and 500 µl of water, taken up in 2× Gus assay buffer (10 mM sodium phosphate buffer pH 7.0, 28 µM β-mercaptoethanol, 0.8 mM EDTA, 0.0042% (v/v) lauroyl-sarcosin, 0.004% (v/v) Triton X-100, 2 mM MUG, 0.2 mg/ml (w/v) BSA) and transferred to black 96-well plates. Relative fluorescence units (RFUs) were determined using a plate reader (Tecan, Männedorf, Switzerland) for 100 min at 28 °C with measurements every

5 minutes (excitation/emission wavelengths: 365/465 nm, gain 60). For quantification of conversion of MUG to the fluorescent product 4-methylumbelliferone (MU), a calibration curve was determined using 0, 1, 5, 10, 25, 50, 100, 200 µM MU.

3.4.5 Trichloroacetic acid precipitation

Gus-Cts1 and Gus-Jps1 secretion was analyzed by TCA precipitation of culture broths. Therefore, 2 ml of cultures grown in Verduyn medium (55.5 mM Glucose, 74.7 mM NH_4Cl, 0.81 mM $MgSO_4 \times 7H_2O$, 0.036 mM $FeSO_4 \times 7H_2O$, 36.7 mM KH_2PO_4, 100 mM MES pH 6.5, 0.051 mM EDTA, 0.025 mM $ZnSO_4 \times 7H_2O$, 0.041 mM $CaCl_2$, 0.016 mM H_3bBO_3, 6.7 µM $MnCl_2 \times 2H_2O$, 2.3 µM $CoCl_2 \times 6H_2O$, 1.9 µM $CuSO_4 \times 5H_2O$, 1.9 µM $Na_2MoO_4 \times 2H_2O$, 0.6 µM KI) to an OD_{600} of 3 were harvested by centrifugation at 11.000 × g and supernatant was transferred to a fresh reaction tube. 1 ml of cell free supernatants of cultures were chilled on ice, mixed with 400 µl 50 % (v/v) TCA solution and incubated on ice at 4 °C overnight. Subsequently, protein pellets were harvested by centrifugation at 11.000 × g at 4 °C for 30 min. Supernatants were discarded and pellets were washed with 300 µl of -20 °C acetone followed by centrifugation at 11.000 × g at 4 °C for 20 min two times. Pellets were dried at room temperature and resuspended in Laemmli buffer containing 0.12 M NaOH. Resuspended pellets were denatured at 95 °C for 10 min and then subjected to SDS-PAGE and Western blot analysis.

3.4.6 Generation of cell extracts

For the verification of protein production via Western blot or further IMAC purification, cultures were grown to an OD_{600} of 1.0 and harvested at 5000 × g for 5 min in centrifugation tubes. Until further use, pellets were stored at −20°C. For preparation of cell extracts, cell pellets were resuspended in 1 ml cell extract lysis buffer (100 mM sodium phosphate buffer pH 8.0, 10 mM Tris/HCl pH 8.0, 8 M urea, 1 mM DTT, 1 mM PMSF, 2.5 mM benzamidine, 1 mM pepstatin A, 2× complete protease inhibitor cocktail (Roche, Sigma/Aldrich, Billerica, MA, United States) and cells were crushed by agitation with glass beads at 2,500 rpm for 12 min at 4°C. After centrifugation (11,000 × g for 30min at 4°C), the supernatant was separated from cell debris and was transferred to a fresh reaction tube. For direct use protein concentration was determined by Bradford assay (BioRad, Hercules, CA, United States) (Bradford 1976). Otherwise cell extracts were subjected to IMAC purification.

3.4.7 SDS PAGE and Western blot analysis

To assay protein production and secretion, 10 µg of cell extract or TCA precipitated samples were subjected to SDS-PAGE. SDS-PAGE was conducted using 10% (w/v) acrylamide gels. Subsequently, proteins were transferred to methanol activated PVDF membranes using semi-dry Western blotting. Nanobody fusion proteins were detected using a primary anti-HA (mouse; 1:3,000, Sigma-Aldrich, St. Louis, MO, USA). An anti-mouse IgG-horseradish peroxidase (HRP) conjugate (1:3,000 Promega, Fitchburg, United States) was used as secondary antibody. HRP activity was detected using the Amersham ™ ECL ™ Prime Western Blotting Detection Reagent (GE Healthcare, Chalfont St Giles, United Kingdom) and a LAS4000 chemiluminescence imager (GE Healthcare Life Sciences, Freiburg, Germany).

3.4.8 IMAC purification of His-tagged protein

Purification of *U. maydis* derived nanobody fusion proteins was achieved by generation of cell extracts from 400 ml of *U. maydis* culture harvested at an OD_{600} of 1.0 and subsequent $Nickel^{2+}$-NTA purification. Therefore, culture harvested at 5000 × g for 5 min was resuspended in 8 ml lysis buffer (10 mM imidazole, 50 mM NaH_2PO_4, 300 mM NaCl, pH 8.0), 1.6 ml glass beads were added to cell suspension and cells were crushed by agitation with glass beads at 2,500 rpm at 4 °C for 12 min. Subsequently, cell debris was removed by centrifugation at 11,000 × g at 4 °C for 30 min. $Nickel^{2+}$-NTA matrix was settled in empty columns and after flow-through of ethanol, equilibrated with 10 column volumes of lysis buffer. Subsequently, matrix was dissolved in cleared cell extracts and the mixture was incubated on a stirring wheel at 4 °C for 1 h. Subsequently, flow-through was discarded and matrix was washed with 5 column volumes of washing buffer (20mM imidazole 50mM NaH_2PO_4, 300mM NaCl, pH 8.0). Protein was eluted in two fractions of 2 ml each using elution buffer 1 (lysis buffer, 150 mM imidazole) and elution buffer 2 (lysis buffer, 250 mM imidazole). For application in ELISA elution fractions were pooled via Amicon Ultra-15 50k centrifugal filter units (Merck Millipore, Burlington, MA, USA). Elution buffer was chosen for the intended application (coating buffer for sandwich ELISA, chitin binding buffer for chitin ELISA, PBS-T for direct detection, see chapters 3.4.10, 3.4.11, 3.4.12 for buffer composition).

3.4.9 *In vivo* neutralization assays

Nanobodies were IMAC purified and stored at 4 °C prior to incubation with Sars-CoV2. Nanobodies at concentration of 0.5 mg/ml in PBS-buffer were incubated with Sars-CoV2 particles in serial dilutions for 1 h at 37 °C. Subsequently, human lung cell cultures displaying ACE2 (Vero cell line) were incubated with pre incubated samples. After three days of incubation visual microscopic analysis was conducted to observe cytopathic effects and thus determine if infection had occurred. qPCR analysis was conducted using anti-Sars-CoV2 primer pairs validated for analytic use.

3.4.10 Direct ELISA

For detection of nanobody binding activity protein adsorbing 384-well microtiter plates (Nunc® Maxisorp™, ThermoFisher Scientific, Waltham, MA, USA) were used. Wells were coated with 1 µg Gfp for anti-GfpNB or 1 µg commercially available Sars-CoV2 Spike-RBD-domain protein for Sars-CoV2 nanobody-Cts1 fusion proteins (Invitrogen, Waltham Massachusetts, USA). Recombinant Gfp was produced in *E. coli* and purified by Ni^{2+}-chelate affinity chromatography as described earlier (Terfrüchte et al. 2017). 1 µg BSA per well dealt as negative control (NEB, Ipswich, MA, USA). Samples were applied in a final volume of 100 µl coating buffer (100 mM Tris-HCL pH 8, 150 mM NaCl, 1 mM EDTA) per well at room temperature for at least 16 h. Blocking was conducted for at least 4 h at room temperature with 5% (w/v) skimmed milk in coating buffer. Subsequently, 5% (w/v) skimmed milk in PBS (137 mM NaCl, 2.7 mM KCl, 10 mM Na_2HPO_4, 1.8 mM KH_2PO_4, pH 7.2) were added to defined protein amounts of nanobody fusion protein samples purified from culture supernatants or cell extracts via Ni^{2+}-NTA gravity flow and respective controls. 100 µl of sample was added to wells coated with the cognate antigen and BSA. The plate was incubated with samples and controls over night at 4 °C. After 3× PBS-T (PBS supplemented with 0.05% (v/v) Tween-20, 100 µl per well) washing, a primary anti-Ha antibody (mouse, Sigma-Aldrich, St. Louis, MO, USA) 1: 5,000 diluted in PBS supplemented with skimmed milk (5% w/v) was added (100 µl per well) and incubated for 2 h at room temperature. Then wells were washed again three times with PBS-T (100 µl per well) and incubated with a secondary mouse-HRP antibody (goat, Promega, Madison, WI, USA) (50 µl per well) for 1 h at room temperature (1: 5,000 in PBS supplemented with skimmed milk (5% w/v)). Subsequently, wells were washed three times with PBS-T and three times with PBS and incubated with Quanta Red™ enhanced chemifluorescent HRP substrate (50:50:1, 50 µl per well, ThermoFisher Scientific, Waltham, MA, USA) at room temperature for 15 min. The reaction was stopped with 10 µl

Quanta Red™ stop solution per well and fluorescence readout was performed at 570 nm excitation and 600 nm emission using an Infinite M200 plate reader (Tecan, Männerdorf, Switzerland).

3.4.11 Sandwich ELISA

To determine nanobody-Cts1 fusion capabilities to act as capture antibody for an antigen test application, a mixture of 0.5 µg of IMAC purified protein and 0.5 µg BSA (New England Biolabs, Ipswich, MA, USA) in 100 µl of coating buffer per well was added to 384-well microtiter plates (1 µg without BSA for direct detection). Coating was conducted for 16 h at 4 °C. Subsequently, plates were blocked with 5 % skimmed milk in coating buffer for 2 h at room temperature. RBD samples were added in serial dilutions in a volume of 100 µl sample buffer (5 % skimmed milk powder in PBS-T) and incubated for 2 h at room temperature. Subsequently plates were washed 3 times with PBS-T and primary antibody (anti-RBD-mouse, R&D systems, Minneapolis, MN, USA) was added in a dilution of 1: 5,000 in sample buffer and incubated for 2 h at room temperature. Afterwards wells were washed again with PBS-T thrice and incubated with secondary mouse-HRP antibody (goat, Promega, Fitchburg, WI, United States) was added in a dilution of 1: 5,000 in 50 µl sample buffer and incubated for 1 h at room temperature. Prior to detection plates were washed thrice with 100 µl PBS-T and three times with 100 µl PBS per well. Detection was carried out using Quanta Red™ enhanced chemifluorescent HRP substrate (50:50:1, 50 µl per well, ThermoFisher Scientific, Waltham, MA, USA) at room temperature for 10 min. The reaction was stopped with 10 µl Quanta Red™ stop solution per well and fluorescence readout was performed at 570 nm excitation and 600 nm emission using an Infinite M200 plate reader (Tecan, Männedorf, Switzerland).

3.4.12 Chitin based sandwich ELISA

For chitin-based sandwich ELISA 50 µl of chitin magnetic beads (New England Biolabs, Ipswich, MA, USA) were transferred into a 1.5 ml reaction tube, washed with 500 µl of water and equilibrated in 500 µl of chitin binding buffer (500 mM NaCl, 50 mM Tris-HCl buffer pH 8.0, 0,05 % Tween-20 (v/v)). Subsequently 2 µg of IMAC purified protein was added in a final volume of 500 µl chitin binding buffer. Coating was conducted on a stirring wheel at 4 °C for 16 h. Afterwards chitin beads were blocked with 5 % skimmed milk powder in chitin binding buffer on a stirring wheel at room temperature for 2 h. In the next step chitin beads were washed thrice with PBS-T, RBD samples were added in serial dilutions in a volume of 100 µl ELISA sample buffer and incubated on a stirring wheel at room temperature for 2 h. After removal of the sample buffer chitin magnetic beads were

taken up in 100 µl PBS-T, transferred to a fresh reaction tube and subsequently washed three times with 500 µl PBS-T before addition of primary antibody (R&D systems, Minneapolis, MN, USA) 1:5000 in 200 µl sample buffer. The primary antibody was incubated with chitin magnetic beads on a stirring wheel at room temperature for 2 h. Subsequent to primary antibody removal chitin magnetic beads were washed three times with PBS-T and incubated with secondary mouse-HRP antibody (goat, Promega, Fitchburg, United States) 1:5000 in 100 µl sample buffer on a stirring wheel at room temperature for 1 h. For detection chitin magnetic beads were washed three times with 500 µl PBS-T and three times with 500 µl PBS before being taken up in 100 µl Quanta Red™ enhanced chemifluorescent HRP substrate (50:50:1, 50 µl per well, ThermoFisher Scientific, Waltham, MA, USA) and transferred to a black 96-well microtiter plate. Fluorescence readout was performed 2 min after addition of the substrate at 570 nm excitation and 600 nm emission using an Infinte M200 plate reader (Tecan, Männedorf, Switzerland) after stopping of the reaction with 10 µl QuantaRed™ stop solution.

3.5 Author contributions

M.P., L.M. and K.P.H designed the experiments. K.P.H. conducted initial chitin binding experiments (Fig. 3.3 C). L.M. conducted neutralization experiments and RT-PCR (Fig. 3.2). M.P. purified nanobodies for neutralization experiments and conducted all other experiments. M.P. designed and prepared the figures and tables. K.S., H.S. and M.F. supervised the project. M.P. prepared the manuscript with advice from K.S.

3.6 Supplementary Material

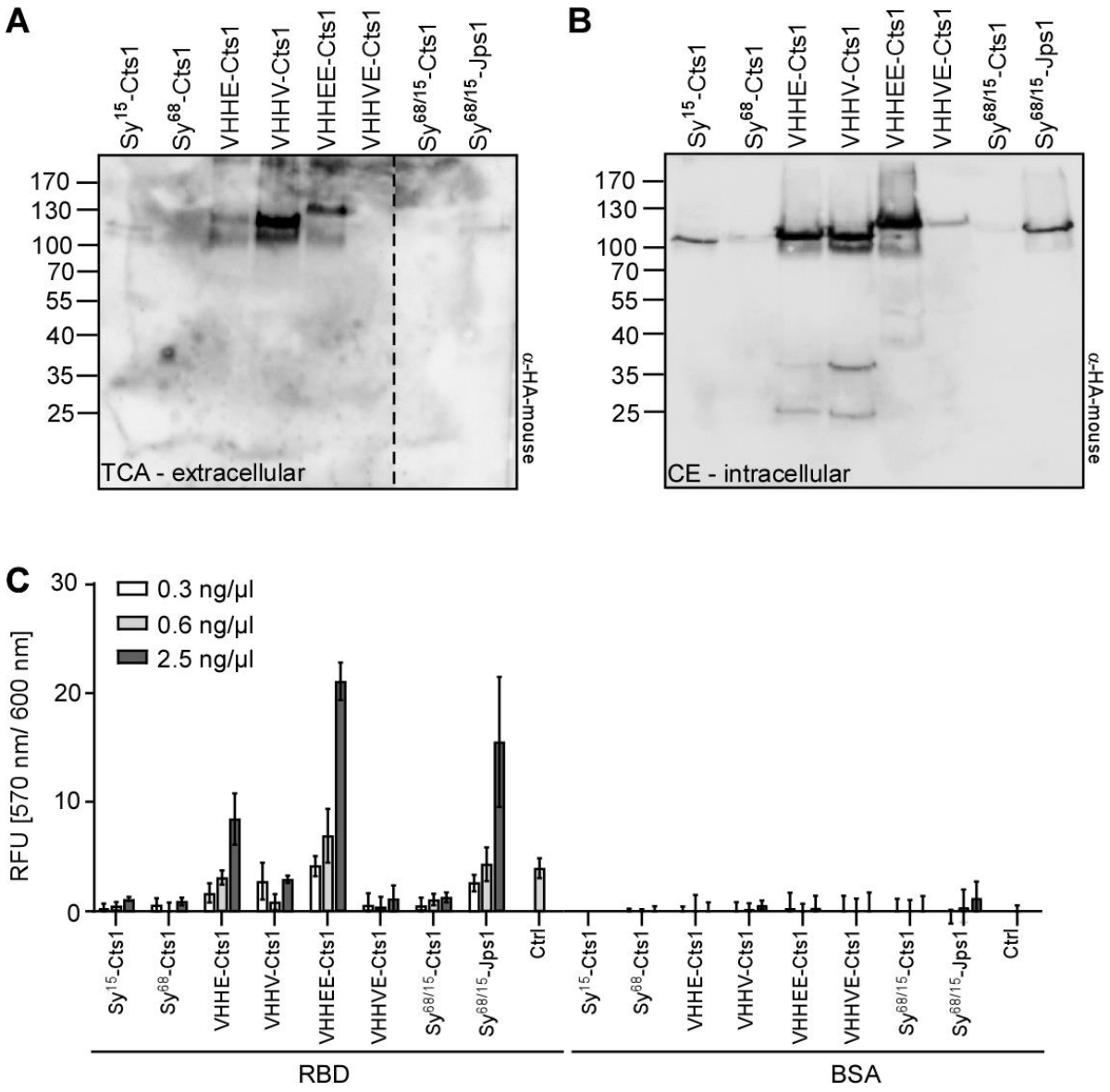

Supplementary Figure 3.1: Full western blots and ELISA of the initial nanobody screen. (A, B) Western blot analysis of nanobody expression and secretion levels. 10 µg of cell extracts were subjected to Western blot analysis. Nanobody-Cts1 fusions were detected using an Ha-mouse antibody. Nanobodies were detected slightly above their expected sizes around 100 kDa. For VHHE-Cts1 and VHHV-Cts1 degradation bands are observable at 35 and 25 kDa. Nanobody-Cts1 fusions were enriched from the supernatant via TCA precipitation, the HA tag was used for detection. **(C)** Direct ELISA of nanobody-Cts1 fusions against 1 µg/well of RBD domain coated to ELISA plate and detected by a sandwich of anti-Ha (mouse) and an anti-mouse-HRP conjugate. Cell extracts of expression strains were added to wells coated either with BSA or RBD in serial dilutions of 0.3 ng/µl, 0.6 ng/µl and 2.5 ng/µl. Experiment was carried out in three biological replicates comprising three technical replicates each. Error bars depict standard deviation of biological replicates.

4 Final Discussion

4.1 Jps1 – a new export carrier for unconventional secretion

Unconventional secretion of Jps1 was confirmed using the Gus-reporter system in the same way, as Cts1 secretion was confirmed before (Stock et al. 2012, Reindl 2020b). Interestingly, supernatant activity was about two-fold increased compared to Gus-Cts1. This result could be confirmed when secretion levels were compared by quantitative Western blot analysis, thus proving that the increased activity is due to higher Gus-Jps1 amounts in the supernatants and not due to changes in Gus activity that might arise from the fusion with the different carriers. Interestingly, intracellular levels of Gus-Cts1 and Gus-Jps1 appear to be similar. However, more sensitive Gus activity assays performed with cell extracts revealed slightly reduced activity in the Gus-Jps1 strain, compared to Gus-Cts1. Thus, the increased extracellular protein levels are likely a direct result of more efficient translocation to the supernatant and not only linked to a higher expression level. There are two possible hypotheses that could explain the more efficient secretion mode. A first possibility is the retention of Cts1 on the cell surface. All enzymatic assays and TCA precipitations in chapter 2 were carried out with cell free supernatants. However, due to its chitin binding capability it is likely that a portion of Cts1 is retained on the cell surface, while only part is freely available in the supernatant. This for example is evident by the fact that Cts1 activity can be measured directly on the cell surface (Stock et al. 2012). Jps1, in contrast, is not predicted to stick to chitin, suggesting that all protein is released into the supernatant. Secondly, Jps1 was shown to form homo dimers *in vitro* (Reindl 2020a). Hence it is possible that the effect is of a stoichiometric nature with two Jps1 molecules in form of a homo dimer entering the fragmentation zone for one single Cts1 molecule, resulting in a fragmentation zone loaded with a higher amount of Jps1 as opposed to Cts1 and thus in higher overall secretion. This theory could be further underlined by the effect observed for Jps1-mediated secretion of LacZ. The reason for impaired strain fitness and LacZ-Jps1 secretion might be linked to lacZ tetramers interfering with Jps1 dimerization and thus secretion.

As apparent from the above discussed points, understanding the cellular role of Jps1 is crucial to fully elucidate its mode of secretion and the differences to that of Cts1. The protein is discussed as an anchoring factor for Cts1 in the lock-type secretion mechanism (Reindl et al. 2020b, Wierckx et al. 2021). In line with that, Jps1 was shown to weakly interact with Cts1 in yeast-two hybrid and co-purification experiments (Hussnätter 2016). This was further underlined by direct detection experiments depicted in chapter 3.8 where no significant background that could have been caused by

Jps1-Cts1 interaction by VHHEE-Cts1 and $Sy^{68/15}$-Apex2-Jps1 was detected, while self-interaction between $Sy^{68/15}$-Jps1 and $Sy^{68/15}$-Apex2-Jps1 was observed. Nonetheless, Jps1 is crucial for Cts1 localization and secretion, since deletion of the respective gene completely negated Cts1 secretion (Reindl et al. 2020b). Furthermore, Jps1 was shown to bind phosphatidyl-inositol-phosphates, specifically Ptldn(4,5)P_2 (Reindl et al. 2020b), hence possibly interacting with the inner layer of the cell membrane (Di Paolo and De Camilli 2006). This could give several hints at its function during unconventional secretion. First it has been described that accumulation of membranous vesicles occurs after formation of the primary septum during formation of the fragmentation zone (Weinzierl et al. 2002) which could be interaction partners for Jps1. Secondly, the N-terminal domain of Jps1 is predicted to form amphipathic helices (Reindl 2020a). These are shown to be involved in sensing or induction of membrane curvature (Jensen et al. 2011) which would fit the localization of Jps1 before and during cell separation. Another hint towards Jps1 function is the prediction of structural similarities to DNA- and RNA polymerases by PredictProtein and RaptorX software (Reindl 2020a). This mode of binding was later confirmed in an individual-nucleotide resolution UV crosslinking and immunoprecipitation (iCLIP) experiment (Reindl 2020a). The significance of this observations is yet unclear. However, these results point towards a complex and diverse intracellular function of Jps1 besides Cts1 localization, but do not allow for a clear understanding of its secretory mechanism. Thus, further studies will be needed to understand the crucial differences in Cts1 and Jps1 secretion and allow for manipulation of the pathway. One approach in this direction, that is already being taken is the identification of interaction partners via Jps1-Gfp pulldown and MS analysis (Reindl 2020a). This has yielded the potential interaction partners *umag_10123*, *umag_04320*, *umag_00582* and *umag05906* which are currently under detailed investigation by generation of deletion strains and their phenotyping (Sanchi Dali, pers. commun.).

The observation that Jps1 can act as a potent new carrier for the export of heterologous proteins is a very important step for the development of the expression system. Importantly from a biotechnological standpoint, Jps1 secretion could be manipulated by inducible Don3 expression in a similar manner to Cts1, further enhancing the secretory yield obtained for Gus by more than 3-fold compared to the non-inducible Gus-Cts1 expression strain. This constitutes the strongest increase in secretion for a target protein that is efficiently expressed and secreted by both Cts1 and Jps1.

Interestingly, Gus was the only target protein that functioned well in tandem with both carriers, even though Jps1 was more efficient in Gus secretion than Cts1. Both FLuc and $Sy^{68/15}$ could not be effectively produced as Cts1 fusion proteins, but were effective, when Jps1 was used as export carrier.

This underlines the advantage of multiple carriers for the *U. maydis* secretion system, as it enables the expansion of the repertoire of secretory targets, ultimately making the secretion system more effective and versatile. The need for a variety of export carriers has been widely described in literature, as there is no one-size-fits-all carrier available for any secretion system yet and reasons for differing carrier performance can be numerous (Wang et al. 2020b). For example, the *S. cerevisiae* Matα signal sequence is regularly used for protein export in *P. pastoris* (He et al. 2012). However, the sequence has a Kex2 cleavage site (KR or RR) by which it is processed for efficient secretion, thus proteins that themselves harbor such a cleavage site, cannot be secreted at full length utilizing the Matα sequence (Govindappa et al. 2014). Another example is the efficient secretion of Gus mediated by xylanase XYNA but not by xylanases XYNB and XYNC in the filamentous fungus *Penicillium funiculosum* (Alcocer et al. 2003). Furthermore, similar effects have been observed on several occasions for fusions of target proteins to cell wall display proteins in filamentous fungi and yeasts. Where correct pairing of anchor and display target has been described as crucial for correct function, export and display of both proteins (Urbar-Ulloa et al. 2019). Further insights into this topic could be gained by crystallization studies of Jps1 and Cts1 to on the one hand further investigate the single and homo-dimer structure of Jps1, but also on the other hand detect differences in N-terminal folding, since it forms the link to secretion targets (McPherson 2017).

The successful secretion of a bivalent Sars-CoV2 nanobody via Jps1 further underlines the advantage of an additional carrier and constitutes a novel biopharmaceutical target for *U. maydis* as a protein production platform, which was built upon in chapter 3.

Thus, the addition of Jps1 as a novel carrier for unconventional secretion constitutes an important step towards diversifying the target range of the system. However, yield increases for the Gus reporter in the range of 2-3-fold are not yet sufficient to make the secretion system competitive compared to established systems such as *P. pastoris*, *S. cerevisiae*, *A. niger,* mammalian or bacterial systems which would require a 10-20-fold increase. Therefore, more steps besides use of Jps1 as a novel carrier, need to be taken in the future to enhance unconventional secretion yield in *U. maydis*.

A strategy to enhance unconventional secretion based on this study would be to build on the recently established inducible secretion system that in combination with Jps1 resulted in the highest increase in unconventional Gus secretion in this study. The system is based on transcriptional or translational regulation of kinase Don3 (Hussnätter et al. 2021) and thus far build on either transcriptional induction via the arabinose sensitive promoter P*crg* or post-translational regulation using the bulky ATP analogue NA-PP1. P*crg* is repressed when glucose, which is preferably metabolized by *U. maydis*

(Müller et al. 2018), is present in the cell and activated when arabinose is metabolized as single carbon source (Brachmann et al. 2004). Thus activating *don3* transcription in the inducible secretion system (Hussnätter et al. 2021). This limits induction speed and requires a carbon source switch for induction, which usually relies on exchanging the growth medium. However, exchange of the growth medium could be circumvented by development of an auto induction process. In case of NA-PP1 the binding pocket of Don3 is blocked by the ATP analogue and the septation factor cannot fulfil its function within the cell (Böhmer et al. 2008, Böhmer et al. 2009). Upon removal of NA-PP1, induction of secretion occurs significantly faster compared to transcriptional induction, since no additional protein biosynthesis is required (Hussnätter et al. 2021). However, a switch of the growth medium is required. This system might be enhanced in two ways: First, the mode of induction could be changed from chemically controlled induction towards less invasive methods, like optogenetics. Optogenetic systems give the possibility to control biological processes by light without the need for invasive use of chemicals or changes of carbon source (Christie and Zurbriggen 2021). These systems are based on photosensitive proteins that can be excited by a wide variety of wavelengths. This generally leads to a conformational change in the light sensitive protein that can be exploited to induce gene transcription or alter protein function. These changes range from red light inducible dimerization of phytochromes like the PHYB/PIF3 complex (Legris et al. 2016), to blue light inducible oligomerization of cryptochromes (Christie et al. 2015) but also UV light sensitive proteins like UVR8 (Christie et al. 2012). These can be used to spatiotemporally separate or bring together proteins of interest fused to these interaction partners upon light induction. Another class of optogenetic switch exists in the form of a blue light inducible conformational change of light-oxygen-voltage (LOV) domains, that can be used to cage attached proteins of interest in darkness and release them upon light induction (Wu et al. 2009). Optogenetic systems have been shown to be a great tool for non-invasive induction of protein expression. This has been demonstrated for example for the induction of a luciferase reporter in plant protoplasts by PHYB-PIF6 interaction. Here a VP16 transactivation domain and a nuclear targeting domain were added to PHYB, while PIF6 was fused to an E DNA binding domain. Upon red light induction, the two interaction partners formed a heterodimer that could act as a transcription factor for the minimal promoter controlling luciferase transcription which resulted in 400-fold induction of luciferase expression (Müller et al. 2014). Furthermore, activity of already expressed protein can also be controlled, as has been shown by the light dependent control of peroxisomal trafficking of a Gfp reporter in mammalian cells. Here a peroxisomal targeting sequence (PTS) was fused to an LOV-domain and Gfp. In darkness the PTS remained caged by the LOV domain and the reporter remained

in the cytosol, while it was targeted to the peroxisome upon light induction due to uncaging of the PTS from the LOV domain (Spiltoir et al. 2016). Enabling optogenetic induction of *don3* transcription or more favorably engineering a caged version of Don3 that can be activated with a light pulse could greatly enhance the system. Secondly, if more core factors for unconventional secretion have been identified, a gene or protein that shows a less severe phenotype than *don3* upon deletion or abolishment of function, respectively, could be incorporated into the system, since the large tree-like like structures that are formed by *don3* deletion strains are generally difficult to work with and are susceptible to harsh mechanical stress. Establishment of such a switch has already been attempted using an arabinose inducible version of Jps1, since *jps1* deletion also abolishes Cts1 secretion. However, this resulted in Jps1 mis-localization and only weak induction of Cts1 secretion (Hussnätter et al. 2021). Hence, identifying another gene that like *don3* controls both Cts1 and Jps1 secretion but shows a less severe phenotype when applied as induced version, might greatly benefit the system.

4.2 The potential of bivalent nanobodies produced by unconventional secretion

An important aim of this work was to produce functional anti-Sars-CoV2 RBD nanobodies as Cts1 fusions. Expression and secretion of VHHE-Cts1 and VHHEE-Cts1 was successful, and both variants were capable of detecting Sars-CoV2 RBD domain in ELISA assays, thus showing their functionality. Furthermore, VHHEE-Cts1 did at least partially neutralize Sars-CoV2 *in vivo*, matching the in *vivo* binding of VHHEE to Sars-CoV2 spike as described by König et al. (2021). However, it was unexpected that VHHV, VHHVE, Sy^{15} and Sy^{68} showed no antigen binding activity when expressed in fusion with Cts1, although VHHE and VHHEE were active. All nanobodies were chosen for their binding capacity described in König et al. (2021) and Walter et al. (2020), and activity of Sy^{15} and Sy^{68} in tandem could be demonstrated in this work, when Jps1 was used as a carrier (chapter 2). Finding a suitable carrier or even signal peptide for the export of a target protein can be difficult both in filamentous fungi and yeast systems and thus far several matches and mismatches between carrier and target have been described (Govindappa et al. 2014, Wang et al. 2020b) (see chapter 4.1). Especially in the case of larger export carriers, the reason for this is often based on structural inhibition of either the targets activity by the carrier or *vice versa*. Nonetheless, in case of structurally similar and small proteins, such as nanobodies, this is an unexpected result that needs to be further investigated. Towards a more elegant design for future target screening, structure prediction using software like PredictProtein or AlphaFold2 (Berhofer et al. 2021, Jumper et al. 2021) could be employed before expression and secretion of certain constructs are attempted. The next step would be crystallization studies of present

fusion proteins, especially in presence of the antigen to elucidate the position and availability of the complementary determining region (McPherson 2017). Crystallization of complex fusion proteins might prove difficult however, thus crystallization of carrier and nanobody independently could also give important insight. Similar studies have been undertaken to determine the structure of nanobodies and their respective antigen to reveal the exact mode of binding for example for Sars-CoV2 RBD, human PD-L1 and epidermal growth factor receptor nanobodies (Schmitz et al. 2013, Zhang et al. 2017, Huo et al. 2021). This could yield vital information for the choice of further nanobody/carrier combinations in future research, enabling a more elegant design of constructs, replacing or complementing crude screening approaches, as conducted in this study.

Overall, the successful expression and secretion of two multimerized nanobodies described in chapters 2 and 3 demonstrates that these molecules are promising novel biopharmaceutical targets for unconventional secretion in *U. maydis*. Importantly, both multimerized nanobody versions clearly outperformed single nanobodies with regard to antigen binding and viral neutralization. These results are perfectly in line with literature, as it has been shown on several occasions that multimerized nanobodies can far exceed the binding capacity of individual proteins (Els Conrath et al. 2001, Cortez-Retamozo et al. 2002, König et al. 2021). Furthermore, the potential use of bi- or multivalent nanobodies, binding more than one antigen or epitope might be an excellent tool especially for targeting viruses like Sars-CoV2 (Dubey et al. 2020). It has been described that the spike protein of the new Sars-CoV2 variant B.1.1.529 (Omicron) is changed in such a way that previously used antibodies such as casirivimab can no longer neutralize the virus and show severely decreased binding (VanBlargan et al. 2022). While the effect is most severe in B.1.1.529, diminished binding activity and increased immue evasion has previously been reported for other variants of concern as well (Liu et al. 2021b, Planas et al. 2021). Hence, a multivalent nanobody, binding different epitopes of the spike protein could potentially compensate this effect. To this end, several studies have demonstrated neutralization of Sars-CoV2 and variants of concern for example by bivalent constructs (Weinstein et al. 2022) and nanobody trimers, directly targeting the RBD-ACE2 interface (Xu et al. 2021). However, these studies are not limited to Sars-CoV2 alone and bi- and trivalent nanobodies have been used to neutralize HIV and equine enciphalitis virus, respectively, but also to target cancer therapy proteins of interest like vegetative growth factor 1 (VEGF1) and tumor necrosis factor (TNF) (Beirnärt et al. 2017, Weiss and Verrips 2019, Sadeghi et al. 2020, Liu et al. 2022). These examples demonstrate the versatility of the nanobody scafffold. A further advantage of multivalent nanobodies is the possibility to streamline production. Antibody therapeutics are usually employed in the form of cocktails containing several

antibodies to achive virus neutralization or to stop tumor proliferation in patients (Marrocco et al. 2019, Sun and Ho 2020a, Weinreich et al. 2021). This strategy has also been employed for nanobodies to neutralize Sars-CoV2 in mice models (Pymm et al. 2021). However, in the same study it was shown that bivalent versions of the nanobodies employed in the cocktails were also able to neutralize Sars-CoV2 on their own (Pymm et al. 2021). Similar effects have been observed for single domain and bivalent nanobodies in hamster models (Esparza et al. 2021, Huo et al. 2021). This strategy of employing single antibody drugs based on a multimerization as opposed to conventional antibody cocktails would allow for easier bulk production of one single polypeptide chain in contrast to several indivdual ones, thus streamlining drug production, allowing for greater product yield and thereby increasing availability and lowering prices.

In terms of production *U. maydis* might infact constitute a great host for multivalent nanobodies. While single nanobodies are simple, small and easy to produce in bacteria such as *E. coli* (Muyldermans et al. 2009), fusion proteins of several nanobodies might prove a challenge for bacterial expression systems, as it was shown before that fungal systems outperform bacteria when it comes to the production of larger, more complex proteins (Wang et al. 2020b). Given the efficiency of bivalent nanobodies produced in this study, larger multivalent nanobody versions are interesting targets for the future, especially considering the capability to secrete large proteins during unconventional secretion (Stock et al. 2012). The fact that nanobody-Cts1/Jps1 fusions are secreted to the supernatant is another advantage of the system, as secretion is favorable for biotechnological applications due to easier downstream processing (Nicaud J.-M. 1986, Flaschel and Friehs 1993). Furthermore, since indivdual nanobodies are mostly screened in *in vitro* and/or bacterial systems (Salvador et al. 2019) it is beneficial if they are produced without eukaryotic *N*-glycosylation via unconventional secretion, hence avoiding alteration to the respective nanobodies properties. For example, it has been shown that high mannose type *N*-glycans can negatively affect pharmacokinetics and stability of therapeutic mAbs and even increase cytotoxicity (Mastrangeli et al. 2020).

In summary, the unique properties of the system support the generation of multimerized nanobody pharmaceuticals, which will be of high interest in the future.

4.3 Evaluation of a chitin-based antigen test

One of the key aims of the study depicted in chapter 3 was to utilize the chitin binding capacity of Cts1 to engineer a chitin based Sars-CoV2 detection system. Results of chitin binding pre-experiments were

in line with previously performed chitin binding experiments, including *E. coli* derived Cts1 binding to chitin magnetic beads and a Gfp-nanobody-Cts1 based Gfp pulldown assay, described in Terfrüchte et al. (2017). The interesting part of these experiments was a seemingly higher binding rate for *U. maydis* derived Gus-Cts1 fusion protein when compared to *E. coli* derived heterologous Cts1 and the fact, that active Gus-Cts1 could be directly immobilized on chitin magnetic beads from raw cell extracts. The first result has to be further investigated in the future with additional characterization of the chitin binding kinetics. The second result constitutes a further proof of concept for direct purification of Cts1 from a raw cell extract utilizing chitin. This result is in line with that of similar experiments that resulted in immobilization of an anti-Gfp nanobody from *U. maydis* cell extracts on chitin (Terfrüchte et al. 2017) and further demonstrates the potential for future *in situ* purification of unconventionally secreted protein.

Immobilization of VHHE-Cts1 and VHHEE-Cts1 on chitin in an active form that resulted in detection of Sars-CoV2 RBD was an important step towards a chitin-based antigen test. Furthermore, binding capacity of VHHEE, showing signal at 0.1 ng/µl (2.6 nM) in a plate-based ELISA and 0.5 ng/µl (12.8 nM) on chitin was well within previously described binding parameters of nanobodies, despite the crude nature of the proof of principle chitin ELISA. Generally, nanobodies are described to bind their respective antigen in the nanomolar to picomolar range (Muyldermans 2013). For example, a Sars-CoV2 nanobody shown to be capable of neutralizing both Sars-CoV2 and variants of concern showed dissociation constants of 5.82 to 32.52 nM to the RBD (Weinstein et al. 2022). Another potent Sars-CoV2 RBD nanobody was shown to have dissociation constants to RBD of 4-6 nM (Huo et al. 2020), while VHHEE in its native form showed dissociation constants to Sars-CoV2 of 0.9 nM (König et al. 2021). In this case the difference in binding capacity between VHHEE in König et al. (2021) and the Cts1 fusion described in this study can likely be explained by different experimental methodology and a slight reduction in nanobody binding activity, due to the fusion of the nanobody to the much larger Cts1. A comparison to commercially available lateral flow tests is difficult, as detection quality of these tests varies heavily (Somborac Bacura et al. 2021). However, detection capabilities of professional lateral flow tests that have been described are in the range of 5 ng/µl for the spike protein (Baker et al. 2020) and 0.65 pg/µl for the nucleocapsid protein (Grant et al. 2020), placing the detection capability of the VHHEE-Cts1 – chitin based detection system within the range of these described limits. A comparison is difficult though, as methodologies are vastly different. Despite both assays being based on antibody sandwich formation, the ELISA type assays are generally more sensitive (Hsiao et al. 2021). Nonetheless, these results demonstrate that chitin can be exploited as a novel

surface for viral antigen detection. This postulates several advantages besides a potential ease of purification of Cts1 fusion proteins from culture broth, as discussed above. Chitin is the second most abundant biopolymer next to cellulose and produced in a large variety of organisms, reaching from shell fish to molluscs, insects and fungi (Brine and Austin 1981). Applications for chitin already in use include a wide variety of biomedical applications in treatment of neurological, cardiovascular and respiratory diseases, such as its use as a nanotube scaffold for the enhancement of neural growth (Singh et al. 2016, Satitsri and Muanprasat 2020). Due to this reason valorization of chitin is generally well understood. Chitin is most often obtained from the shells of crustaceans, a waste product during food generation, by deproteinization at alkaline conditions and demineralization in acidic conditions (Younes and Rinaudo 2015). Additionally, more environmentally friendly options for chitin valorization in the form of using deep eutectic solvents and extraction of more easily available insect shell chitin are being developed (Vicente et al. 2020, Zainol Abidin et al. 2020). This makes it an inexpensive, bio-based resource that is not interfering with food production which is often the case for cellulose when used for example as a source for biofuel generation (Tenenbaum 2008). Hence, chitin in combination with Cts1 nanobody fusions constitutes a valuable building block towards more economic and ecologic antigen testing systems in the future that no longer rely on petrol based, expensive protein adhesive polymers, as is still the case for state of the art ELISA (Lequin 2005). The need for these tests has been made clear by the increasing number of zoonotic disease outbreaks in the recent past and the massive numbers of tests conducted during the Sars-CoV2 pandemic (McArthur 2019, Rahman et al. 2020, BfRAM 2022). This has been underlined by other studies also trying to valorize biopolymers for antigen testing, such as a recently published study on a Sars-CoV2 capture system based on immobilization of nanobodies on cellulose (Sun et al. 2022). However, while chitin constitutes a great building block for future antigen tests in combination with Cts1 nanobody fusion proteins, engineering of a proper chitin surface in form of a flow assay or a “lab-on-a-chip” (Zhuang et al. 2020), will be key to fully utilize the potential of the proof of principle presented in this study.

Another important step towards a more economic antigen test was the simplification of detection, which was attempted in this study by functionalization of nanobodies utilizing peroxidase Apex2. While the most widely employed enzymes for functionalization of secondary antibodies used in applications such as ELISA and Western blot are HRP and alkaline phosphatase (Gillet et al. 1993, Freeman 2013, Lin 2015) Apex2 was shown to be secreted at higher amounts and with increased activity when unconventionally produced in *U. maydis* compared to HRP (Reindl 2016). Results obtained for αGfpNB-Apex2-Cts1 confirmed this result, lowering the required amount of

functionalized nanobody for direct Gfp detection by 5-fold, when compared to a previously used HRP fusions of the same nanobody (Terfrüchte, 2016). When applied to a bivalent Sars-CoV2 nanobody and the novel carrier Jps1, however, Apex2 activity was reduced massively, preventing direct detection of Sars-CoV2 RBD trapped by VHHEE-Cts1 on a chitin surface. As discussed above (chapters 4.1 and 4.2) this might very well be a structural effect either based on the link of Apex2 and the bivalent nanobody or Apex2 and the carrier protein Jps1. A possibility to improve the constructs, would be the use of flexible linkers, such as glycine-serine (3x GGGGS) and glycine (6-8x G) linkers or a rigid linker such as Alanine-Proline (5-17x AP) which have been shown to enhance stability and folding as well as improve biological activity in fusion proteins (Huston et al. 1988, McCormick et al. 2001, Sabourin et al. 2007). In case this approach should fail further insights into the folding of the fusion protein and a new round of nanobody and detector screening would be required. However, the chosen detector is largely dependent on the assay it is used for and beyond the enzymatic proof of principle utilizing peroxidase Apex2 in this assay, further detection methods could be utilized instead of enzymatic detection. Technologies used in commercially available antigen tests such as conjugated metal-based nanoparticles, latex particles or fluorophores could be used to simplify detection (Hsiao et al. 2021).

In summary the aim of generating a chitin-based Sars-CoV2 detection system derived from components of *U. maydis* was accomplished. The most important proof of principle - immobilization of a nanobody-Cts1 fusion on a chitin surface and subsequent trapping and detection of Sars-CoV2 RBD domain even at low nanomolar concentrations was demonstrated. Additionally, two functionalized detector nanobodies against Gfp and the Sars-CoV2 RBD could be generated. Although direct detection of RBD trapped on a chitin surface was not possible with the functionalized nanobody, these constructs still serve as a proof of principle and starting point for future studies on generation of functionalized nanobody fusions for unconventional secretion in *U. maydis*. Thus, the new detection system constitutes a combination of chitin, Cts1 and anti-Sars-CoV2 nanobodies that form a stable trapping surface for Sars-CoV2, while direct and fast detection and a sophisticated chitin surface need to be further investigated in future studies (Fig. 5.1)

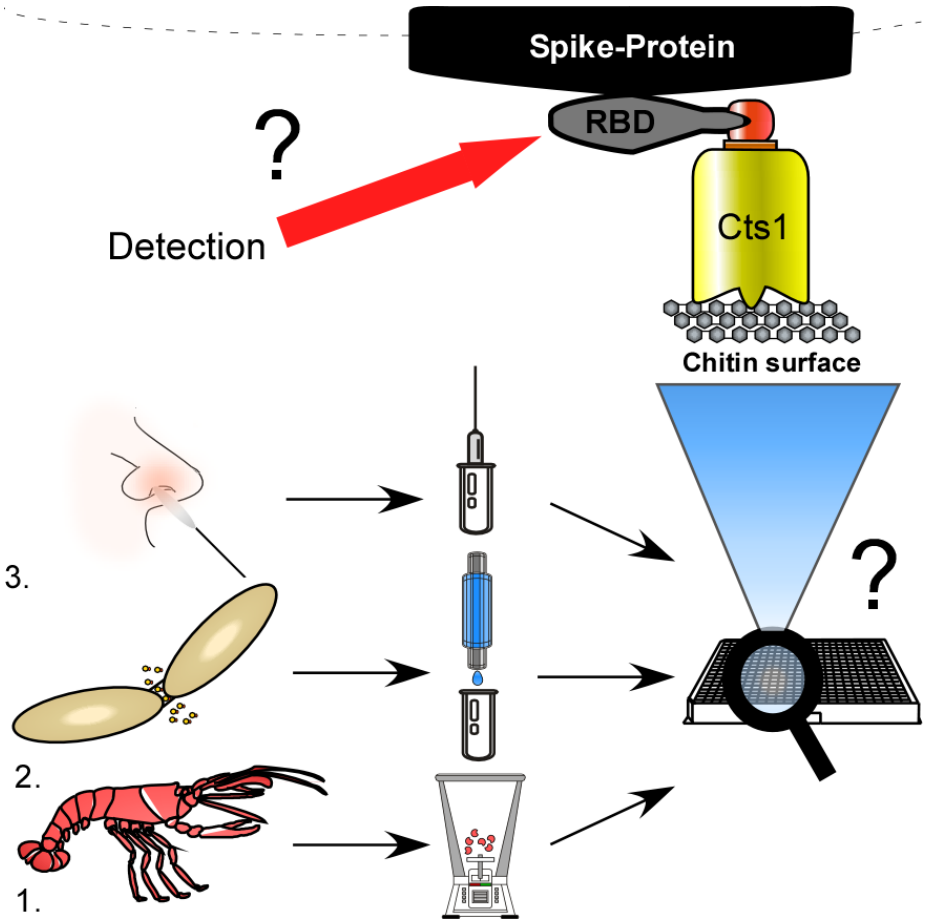

Figure 4.1: Strategy for a novel chitin-based antigen test. Crab shell chitin would be utilized to form a sophisticated chitin surface, for example an ELISA plate or a "lab-on-a-chip". *U. maydis* derived nanobody-Cts1 fusion protein would be purified and immobilized and subsequently used to trap Sars-CoV2 from a patient sample on the chitin surface, which could then subsequently be detected. In this study binding of nanobody VHHEE-Cts1 and $Sy^{68/15}$-Jps1 to Sars-CoV2 *in vivo* was confirmed. Furthermore, RBD domain could be detected on a chitin surface at low nanomolar concentrations, using VHHEE-Cts1 stably bound to the surface. Hence, the missing links towards a novel antigen test are a convenient and stable chitin surface, and a quick, inexpensive and easy method of detection. Missing links are indicated by question marks (?).

4.4 Possible future applications for *U. maydis* derived biopharmaceuticals

Engineering a detection interface between chitin and the Sars-CoV2 virus with components derived from unconventional secretion constitutes a solid biopharmaceutical application for *U. maydis*. In the even future this interface might have further implications. It is well known that antigen detection assays in the form of ELISA or lateral flow technology can be used to detect a multitude of antigens (Lequin 2005, Andryukov 2020). Since nanobodies against three different targets, namely Gfp, botulinum toxin A and the Sars-CoV2 RBD have already been adapted (Terfrüchte et al. 2017, Philipp et al. 2021), screening of novel nanobodies against varied targets and adaption to this type of interface

should be straight forward. This would allow for a quick adaption of the system in case of a new pandemic.

Furthermore, Cts1-chitin interaction in conjunction with nanobodies could also be used to enhance existing antigen detection technologies not as a novel immobilization interface but for antigen detection. Colloidal nanoparticles coated with antibodies have been shown to greatly enhance detection capacity of ELISA assays (Billingsley et al. 2017), however, these are usually manufactured from gold (Oldenburg et al. 1998), which is a rather expensive resource. Chitin on the other hand is inexpensive and is already used in for engineering of nanocrystals, hydrogel scaffolds and nanofibrils (Xu et al. 2020b, Zhu et al. 2020b, Gu et al. 2021). Combination of chitin nanocrystals or nanoparticles coated with nanobody-Cts1 fusions could thus be tested in future studies to replace antibody coated, gold-based nanoparticles.

Moreover, the neutralization of Sars-CoV2 *in vivo* by VHHEE-Cts1 and $Sy^{68/15}$-Jps1 demonstrates the applicability of *U. maydis* derived biopharmaceuticals as potential novel drug targets in the future. Thus far, antibody based therapeutics are almost exclusively based on mAbs (Walsh 2018). However, nanobodies are currently tested for medical application due to their small size, stability, long shelf life and solubility (Kijanka et al. 2015, Salvador et al. 2019). To this end nanobodies targeting cancer targets such as epidermal and hepatocyte growth factor receptors, chemokine receptor CRCX7 and hepatocyte growth factor have been targeted with nanobodies *in vivo* (Roovers et al. 2007, Vosjan et al. 2012, Maussang et al. 2013, D'Huyvetter et al. 2014). Similar approaches have been taken with application of anti Sars-CoV2 nanobodies in hamster and mice models (Esparza et al. 2021, Huo et al. 2021, Pymm et al. 2021). Hence, nanobodies from *U. maydis* might be suited for similar applications, especially due to their lack of *N*-glycosylation (Stock et al. 2016a). Nonetheless, the large attached carrier proteins Cts1 or Jps1 might interfere with nanobody properties especially *in vivo*. However, in case of nanobodies, unconventional secretion could prove an advantage for drug application in the future. First, it was shown that nanobodies clear fast from the blood stream and are able to cross the blood brain barrier (Ingram et al. 2018, Salvador et al. 2019), which is not desirable for all applications. Hence, nanobodies have been conjugated with albumin binding domain, Fc fragments of conventional Abs and multimerized, to increase *in vivo* stability (Bannas et al. 2017, Sadeghi et al. 2020, Xenaki et al. 2021). As it has been demonstrated in this study, that complex fusions of carrier, nanobody and additional proteins can be exported in an active state, unconventionally secreted nanobodies could be unconventionally secreted with a stabilizer like album binding domain attached and employed directly after carrier removal by proteolytic cleavage, which has already been demonstrated (Terfrüchte 2016).

Secondly, first studies on the use of drug loaded chitin scaffolds for are currently undertaken, with first results showing growth inhibition of *Staphylococcus aureus* by a decamethoxine loaded chitin scaffold in agar diffusion assays (Kovalchuk et al. 2019). Such chitin scaffolds could be loaded with stably bound nanobody-Cts1 fusions and used in future applications. Similar technologies utilizing nanobodies but not chitin are currently developed and include display of nanobodies on phages, motif-mediated formation of pentabodies by self-assembly and the use of nanobody coated nanoparticles (Wang et al. 2016). Overall, the potential future applications for nanobody based biopharmaceuticals from *U. maydis* are numerous and offer unique advantages due to chitin immobilization for use in immunoassays or transport and lack of *N*-glycosylation as opposed to other fungal hosts.

4.5 Future strategies to further enhance unconventional secretion

Range and applicability of *U. maydis* derived biopharmaceuticals have been demonstrated and discussed in this study, however, the feasibility of the unconventional secretion system as a whole will ultimately depend on overcoming the bottleneck that is formed by its low secretory yield.

The classical secretion pathway in yeasts and filamentous fungi is well understood and genetic engineering has been applied in several ways to drastically increase yields. These engineering steps include the generation of protease deficient strains, co-expression of ER resident chaperones and cytosolic translocation factors, use of strong promoters to raise transcript levels and general manipulation of the unfolded protein response (UPR) pathway (Heimel 2015, Wang et al. 2020b). While some but not all of these strategies can be and have been applied to enhance unconventional secretion, such as generation of protease deficient strains and use of strong promoters, not all manipulation methods are feasible for unconventional secretion (Sarkari et al. 2014, Terfrüchte et al. 2018). Thus, alternative strategies have to be identified for optimizing unconventional lock-type secretion.

Manipulation of the unfolded protein response, either by upregulation of ER resident chaperones or by upregulation of the UPR inducing transcription factor Cib1 would likely not enhance unconventional secretion, since it is not ER dependent (Stock et al. 2012, Heimel 2015). An approach in a similar direction that might be more interesting however, would be the overexpression of unconventional secretion associated translocation factors. However, the only Cts1 translocation factor known to this date is Jps1. As mentioned above, the detailed characterization of the lock-type secretion pathway is crucial to identify further important proteins relevant for unconventional export. Interestingly, Jps1

overexpression did already result in increased Cts1 secretion by about 1.3-fold (Reindl 2020a). For broader application of a strategy involving upregulation of accessory secretion components, identification of more core-translocation factors for unconventional secretion would be necessary. The Jps1 interaction targets *umag_10123*, *umag_04320*, *umag_00582* and *umag05906* discussed in chapter 4.1 might be interesting candidates in this regard.

Further progress could be achieved by further widening the repertoire of applicable carriers. Don3 was already shown to be unconventionally secreted using the Gus reporter, albeit at minute levels (Aschenbroich et al. 2019). Thus, it might not be a choice of interest but underlines the possibility to find more unconventional carriers next to Cts1 and Jps1. Further elucidation of Jps1 interaction targets might reveal such carriers in the future. One target however, that is already known to be unconventionally secreted is the peroxisomal sterol carrier protein 2 (Scp2) (Krombach et al. 2018). Interestingly, similar to Gus-Cts1 it was shown that Scp2 was not active, meaning it could not fulfil its virulence function, when it was conventionally secreted (Krombach et al. 2018). However, Scp2 is postulated to be secreted via peroxisomes and not via lock-type unconventional secretion (Krombach et al. 2018). Thus careful screening steps would have to be conducted to check for its capability of acting as an export carrier and to see if exported targets show the same properties such as lack of *N*-glycosylation as those exported via lock-type unconventional secretion. Such screening steps would include using the Gus reporter and potentially treatment of secreted protein with PNGaseF for deglycosylation and subsequent determination of size differences between treated and untreated samples in Western blot to determine if the protein is *N*-glycosylated or not (Takahashi 1983, Stock et al. 2012, Stoffels et al. 2020).

In general, one clear bottleneck can be identified for lock-type unconventional secretion. Besides yet unknown protein factors and expression levels of the respective carrier used for export, lock-type unconventional secretion is dependent on two things: The fragmentation zone and cell cycle. It has been shown in several studies that high amount of expressed protein remains in the cell instead of being unconventionally secreted (Terfrüchte et al. 2017, Philipp et al. 2021). This is especially true, when strong promoters are used to enhance the amount of produced protein. Thus, the fragmentation zone likely constitutes a bottleneck in lock-type unconventional secretion. Hence strategies to either prolong the time the fragmentation zone stays intact or to enlarge the size of the fragmentation zone, might be very beneficial to overcome this bottleneck. Strategies to enlarge organelles, such as the ER have been successfully implemented in *S. cerevisiae* (Arendt et al. 2017). However, the fragmentation zone is a dynamic structure that is formed and broken down during the cell cycle, and not a stable cell organelle.

Also, the regulation of its formation is complex and not fully understood, yet (Weinzierl et al. 2002, Hlubek et al. 2008, Schink and Bölker 2009). It has been described that formation of the fragmentation zone requires formation of two septa and formation of an actomyosin ring. The known key proteins involved in this process are Cdc42, Don1 and Don3. Cdc42 is a GTP binding protein that is a crucial factor for cytoskeletal organisation and cell separation (Schink and Bölker 2009). It has been shown that guanine nucleotide exchange factor Don1 crucial for its activity and signalling specificity (Hlubek et al. 2008). Ste20-like kinase Don3 on the other hand acts independently of Cdc42 in the rearrangement of septin structures and thereby secondary septum formation, however, both are required for formation of the fragmentation zone (Böhmer et al. 2008, Böhmer et al. 2009). Hence, enlarging its size would require intricate engineering of the septin cytosceleton and transport machinery as well as its key players, such as Don1, Don3 and Cdc42. This, however, might lead to heavy growth or cell morphology defects (Böhmer et al. 2008, Hlubek et al. 2008, Schink and Bölker 2009, Zander et al. 2016, Aschenbroich et al. 2019). On the other hand, increasing the time the fragmentation zone remains stable, would most likely require extensive engineering of the cell cycle at the very end of the G1 phase (Perez-Martin et al. 2006), directly before cell separation, but when the fragmentation zone is already intact. Cell cycle engineering is a rising topic in synthetic biology but thus far it has mostly been used to link transcription of certain genes to the cell cycle, for example to generate biological oscillators (Li and Yang 2018). Further research is conducted towards generation of synthetic cells with deep consideration given to the generation of an entirely synthetic cell cycle, but this research is mainly directed towards generation of synthetic bacterial systems due to their simpler cellular structure and organization as opposed to more complex fungal cells (Olivi et al. 2021). To this end, engineering of the fragmentation zone bottleneck is an interesting topic that could be addressed in the future, when further breakthroughs towards in depth understanding of cell cycle regulation and fragmentation zone formation have been made.

One last approach to increase yields would be the implementation of genetic screening, similar to the screen conducted to identify Jps1 (Reindl et al. 2020b) but with the aim to find candidates that secrete higher amounts of Cts1 and Jps1 as opposed to strains incapable of unconventional secretion. Random mutagenesis screening, most often conducted using UV mutagenesis, is a well-studied practice in metabolic engineering, either when genetic engineering options have been exhausted or when strains for non-GMO applications are required (Anderson 1995, Kun et al. 2019). Indeed, a first round of screening has already been conducted and has resulted in up to 6-fold increased Gus-Cts1 secretion in the best candidates. However, identification of the exact causative mutation had not been successful,

yet (Hussnätter, 2021). Nonetheless, evaluation and replication of this mutagenesis approach under optimized conditions might yield valuable insight into the unconventional secretion mechanism and significantly increase yield at the same time.

Finally, another way to make unconventional lock-type secretion more economically feasible would be a co-culture approach. While Co-cultivation with one or more other organisms would not necessarily positively impact product titers, it could lead to the use of more economically, sustainable and ecologically beneficial carbon sources, thus making the final product more environmentally friendly and less expensive. Co-cultivation of different *U. maydis* strains has already been demonstrated and led to effective growth on polygalacturonic acid (Stoffels et al. 2020). Furthermore, *U. maydis* strains capable of breaking down xylan, cellobiose and carboxymethyl cellulose (Geiser et al. 2016b), could be applied in combination with a production strain to produce biopharmaceuticals via unconventional secretion utilizing cellulosic plant biomass. Indeed, an approach towards product generation from cellulose via a co-culture approach has already been successfully implemented. A co-culture process using *T. reesei* to break down cellulose and *U. maydis* to produce itaconic acid yielded 34 g/L itaconic acid (Schlembach et al. 2020). However, using either filamentous fungi or *U. maydis* as a co-culturing partner for a production strain might not be a wise strategy for biopharmaceutical protein production, as both are known to produce high amounts of extracellular proteases (Ward 2012, Terfrüchte et al. 2018). Furthermore, production of biopharmaceuticals on plant biomass would impede downstream processing due to non-homogenous media. Hence, a more promising approach for biopharmaceutical protein production would be co-cultivation of *U. maydis* with cyanobacteria for direct valorization of CO_2 and sunlight. Co-cultivation of cyanobacteria as carbon source donors with other organisms is a rising research topic and several co-cultivation processes have been established thus far. These include co-cultures of cyanobacteria and algae, that are currently engineered towards the production of biodiesel (Satpati and Pal 2021) as well as co-cultures of *E. coli* and *Synchecoccus elongatus* for the production of isoprene (Liu et al. 2021a) among others. Furthermore, first steps towards co-cultivation of cyanobacteria and fungi were successfully established, for example a co-culture between the cyanobacterium *Nostoc* sp. PCC6720 and filamentous fungus *Aspergillus nidulans* (Jiang et al. 2020). Cyanobacteria like *Synechocystis sp.* and *Synechococcus elongatus* are known to produce sucrose via photosynthesis and are capable of sucrose secretion (Du et al. 2013), while *U. maydis* is capable of metabolizing sucrose, likely by direct uptake and/or extracellularly cleavage of sucrose via the transporter Srt1 (*umag_02374*) (Wahl et al. 2010) and secreted invertase Suc2 (*umag_01945)* (Horst et al. 2008), respectively. Towards a successful co-culture between cyanobacteria and *U. maydis*,

several factors would have to be considered. The first would be sufficient sucrose supply from the cyanobacterial side to ensure sufficient *U. maydis* biomass accumulation and efficient product production. To this end, given the high interest in cyanobacterial co-cultures, engineered strains that show increased rates of sucrose production of both *S. elongatus* and *Synechocystis sp.* are available (Kirsch et al. 2018, Lin et al. 2020). Secondly, the sucrose cleavage and uptake machinery of *U. maydis* would have to be fine-tuned in order to allow efficient uptake. *srt1* transcription would have to be activated by a constitutive promoter, as it is only transcriptionally induced during pathogenic development (Wahl et al. 2010, Lanver et al. 2018). *suc2* on the other hand is transcribed at a basal level in axenic culture (Lanver et al. 2018).

Thus, *U. maydis* can be engineered and applied in a multitude of ways including identification and genetic engineering of novel translocation components, identification and establishment of new export carriers, further engineering of inducible secretion, mutagenesis screening for over secretors and co-culture with cyanobacteria, to increase the competitiveness of unconventional secretion.

5 Conclusion

The characterization of Jps1 led to a broadened repertoire of functionally secreted targets of unconventional secretion in *U. maydis* and a significant increase in secretory yield for the Gus reporter enzyme and bivalent synthetic Sars-CoV2-RBD nanobodies. The secretion of a bivalent nanobody construct also represented a proof-of-principle for a novel biopharmaceutical target. However, increase in secretory yield was not significant enough to make *U. maydis* competitive as a protein production platform. Thus, the research depicted in chapters 2 constitutes an important step in the right direction, but further research to enhance secretory yield for example by the use of novel carriers or further strain engineering, as discussed above, will be essential.

Application of biopharmaceuticals in the form of a chitin based antigen test was mostly successful as well. The repertoire of unconventionally secreted biopharmaceuticals could be expanded by the secretion of a single and multimerized version of a functional llama derived Sars-CoV2 nanobody. As a proof of principle the chitin based ELISA depicted in chapter 3 demonstrates detection of Sars-CoV2 RBD at low nanomolar concentrations, even in a crude assay, which is in range of published binding and detection capacities for other Sars-CoV2 nanobodies and available antigen tests. Confirmed neutralization of the Sars-CoV2 virus constitutes the first *in vivo* application of *U. maydis* derived

biopharmaceuticals, marking an important albeit early step towards potential drug development. Functionalization of nanobodies utilizing Apex2 as detector in the αGfp-Apex-Cts1 variant clearly improved direct detection of Gfp compared to the earlier application of HRP. While the ultimate aim of a direct RBD detection in a chitin-based antigen test could not be achieved yet, direct detection of the Sars-CoV2 RBD domain could at least be observed in sandwich ELISA by $Sy^{68/15}$-Apex2-Jps1. In combination with the excellent detection capabilities of αGfp-Apex-Cts1, this demonstrates the potential for functionalization of unconventionally secreted nanobodies.

Overall, this work serves as a proof of principle that the repertoire of unconventionally secreted biopharmaceuticals can be further expanded by screening for novel targets, as well as use of new carriers and that these biopharmaceuticals have unique properties for application. However, while the potential variety and applicability of *U. maydis* derived biopharmaceuticals in the future is high, success of the system will ultimately rely on improvement of secretory yields to a competitive standard

6 Appendix

6.1 References

Abrahamsen H, Stenmark H. (2010). Protein secretion: unconventional exit by exophagy. *Curr Biol*. May 11;**20**:R415-418 DOI: 10.1016/j.cub.2010.03.011

Al-Kindi S, Zidar DA. (2022). COVID-lateral damage: cardiovascular manifestations of SARS-CoV-2 infection. *Transl Res*. Mar;**241**:25-40. Epub 20211112 DOI: 10.1016/j.trsl.2021.11.005

Alcocer MJ, Furniss CS, Kroon PA, Campbell M, Archer DB. (2003). Comparison of modular and non-modular xylanases as carrier proteins for the efficient secretion of heterologous proteins from Penicillium funiculosum. *Appl Microbiol Biotechnol*. Feb;**60**:726-732. Epub 20021221 DOI: 10.1007/s00253-002-1184-4

Anderlei T, Zang W, Papaspyrou M, Büchs J. (2004). Online respiration activity measurement (OTR, CTR, RQ) in shake flasks. *Biochemical Engineering Journal* **17** 184-194

Anderson P. (1995). Mutagenesis. *Methods Cell Biol*.**48**:31-58 DOI: https://www.ncbi.nlm.nih.gov/pubmed/8531732

Andryukov BG. (2020). Six decades of lateral flow immunoassay: from determining metabolic markers to diagnosing COVID-19. *AIMS Microbiol*.**6**:280-304. Epub 20200826 DOI: 10.3934/microbiol.2020018

Arbabi Ghahroudi M, Desmyter A, Wyns L, Hamers R, Muyldermans S. (1997). Selection and identification of single domain antibody fragments from camel heavy-chain antibodies. *FEBS Lett*. Sep 15;**414**:521-526 DOI: 10.1016/s0014-5793(97)01062-4

Arendt P, Miettinen K, Pollier J, De Rycke R, Callewaert N, Goossens A. (2017). An endoplasmic reticulum-engineered yeast platform for overproduction of triterpenoids. *Metab Eng*. Mar;**40**:165-175. Epub 20170216 DOI: 10.1016/j.ymben.2017.02.007

Arnold CE, Wittrup KD. (1994). The stress response to loss of signal recognition particle function in Saccharomyces cerevisiae. *J Biol Chem*. Dec 2;**269**:30412-30418 DOI: https://www.ncbi.nlm.nih.gov/pubmed/7982955

Asaadi Y, Jouneghani FF, Janani S, Rahbarizadeh F. (2021). A comprehensive comparison between camelid nanobodies and single chain variable fragments. *Biomark Res*. Dec 4;**9**:87. Epub 20211204 DOI: 10.1186/s40364-021-00332-6

Aschenbroich J, Hussnätter KP, Stoffels P, Langner T, Zander S, Sandrock B, Bölker M, Feldbrügge M, Schipper K. (2019). The germinal centre kinase Don3 is crucial for unconventional secretion of chitinase Cts1 in *Ustilago maydis*. *Biochim Biophys Acta Proteins Proteom*. Dec;**1867**:140154. Epub 2018/10/15 DOI: 10.1016/j.bbapap.2018.10.007

Astuti I, Ysrafil. (2020). Severe Acute Respiratory Syndrome Coronavirus 2 (SARS-CoV-2): An overview of viral structure and host response. *Diabetes Metab Syndr*. Jul - Aug;**14**:407-412. Epub 20200418 DOI: 10.1016/j.dsx.2020.04.020

Baker AN, Richards SJ, Guy CS, Congdon TR, Hasan M, Zwetsloot AJ, Gallo A, Lewandowski JR, Stansfeld PJ, Straube A, et al. (2020). The SARS-COV-2 Spike Protein Binds Sialic Acids and Enables Rapid Detection in a Lateral Flow Point of Care Diagnostic Device. *ACS Cent Sci*. Nov 25;**6**:2046-2052. Epub 20200923 DOI: 10.1021/acscentsci.0c00855

Bannas P, Hambach J, Koch-Nolte F. (2017). Nanobodies and Nanobody-Based Human Heavy Chain Antibodies As Antitumor Therapeutics. *Front Immunol*.**8**:1603. Epub 20171122 DOI: 10.3389/fimmu.2017.01603

Banuett F. (1992). *Ustilago maydis*, the delightful blight. *Trends Genet*. May;**8**:174-180 DOI: 10.1016/0168-9525(92)90220-x

Banuett F, Herskowitz I. (1989). Different a alleles of *Ustilago* maydis are necessary for maintenance of filamentous growth but not for meiosis. *Proc Natl Acad Sci U S A*. Aug;**86**:5878-5882 DOI: 10.1073/pnas.86.15.5878

Baral P, Bhattarai N, Hossen ML, Stebliankin V, Gerstman BS, Narasimhan G, Chapagain PP. (2021). Mutation-induced changes in the receptor-binding interface of the SARS-CoV-2 Delta variant B.1.617.2 and implications for immune evasion. *Biochem Biophys Res Commun*. Oct 15;**574**:14-19. Epub 20210815 DOI: 10.1016/j.bbrc.2021.08.036

Becker F, Stehlik T, Linne U, Bölker M, Freitag J, Sandrock B. (2021). Engineering *Ustilago maydis* for production of tailor-made mannosylerythritol lipids. *Metab Eng Commun*. Jun;**12**:e00165. Epub 20210206 DOI: 10.1016/j.mec.2021.e00165

Becker J, Hosseinpour Tehrani H, Gauert M, Mampel J, Blank LM, Wierckx N. (2020). An *Ustilago* maydis chassis for itaconic acid production without by-products. *Microb Biotechnol*. Mar;**13**:350-362. Epub 20191227 DOI: 10.1111/1751-7915.13525

Beirnaert E, Desmyter A, Spinelli S, Lauwereys M, Aarden L, Dreier T, Loris R, Silence K, Pollet C, Cambillau C, et al. (2017). Bivalent Llama Single-Domain Antibody Fragments against Tumor Necrosis Factor Have Picomolar Potencies due to Intramolecular Interactions. *Front Immunol*.**8**:867. Epub 20170731 DOI: 10.3389/fimmu.2017.00867

Belouzard S, Chu VC, Whittaker GR. (2009). Activation of the SARS coronavirus spike protein via sequential proteolytic cleavage at two distinct sites. *Proc Natl Acad Sci U S A*. Apr 7;**106**:5871-5876. Epub 20090324 DOI: 10.1073/pnas.0809524106

Belouzard S, Millet JK, Licitra BN, Whittaker GR. (2012). Mechanisms of coronavirus cell entry mediated by the viral spike protein. *Viruses*. Jun;**4**:1011-1033. Epub 20120620 DOI: 10.3390/v4061011

Benham AM. (2012). Protein secretion and the endoplasmic reticulum. *Cold Spring Harb Perspect Biol*. Aug 1;**4**:a012872. Epub 20120801 DOI: 10.1101/cshperspect.a012872

Berhofer M, Dallago C, Karl T, Satagopam V, Heinziger M, Littmann M, Olenyi T, Qiu J, Schütze K, Yachdav G, et al. (2021). PredictProtein – Predicting Protein Structure and Function for 29 Years. *bioRxiv*. DOI: 10.1101/2021.02.23.432527

Berlec A, Strukelj B. (2013). Current state and recent advances in biopharmaceutical production in Escherichia coli, yeasts and mammalian cells. *J Ind Microbiol Biotechnol*. Apr;**40**:257-274. Epub 2013/02/07 DOI: 10.1007/s10295-013-1235-0

BfRAM.Antigen-Tests auf SARS-CoV-2 zur professionellen Anwendung. Available from https://antigentest.bfarm.de/ords/antigen/r/antigentest/liste-der-antigentests (last accessed: 02/22/2022)

Bierle DM, Ganesh R, Razonable RR. (2021). Breakthrough COVID-19 and casirivimab-imdevimab treatment during a SARS-CoV-2 B1.617.2 (Delta) surge. *J Clin Virol*. Dec;**145**:105026. Epub 20211108 DOI: 10.1016/j.jcv.2021.105026

Billingsley MM, Riley RS, Day ES. (2017). Antibody-nanoparticle conjugates to enhance the sensitivity of ELISA-based detection methods. *PLoS One*.**12**:e0177592. Epub 20170511 DOI: 10.1371/journal.pone.0177592

Böhmer C, Böhmer M, Bölker M, Sandrock B. (2008). Cdc42 and the Ste20-like kinase Don3 act independently in triggering cytokinesis in *Ustilago maydis*. *J Cell Sci*. Jan 15;**121**:143-148. Epub 20071218 DOI: 10.1242/jcs.014449

Böhmer C, Ripp C, Bölker M. (2009). The germinal centre kinase Don3 triggers the dynamic rearrangement of higher-order septin structures during cytokinesis in *Ustilago* maydis. *Mol Microbiol*. Dec;**74**:1484-1496. Epub 20091110 DOI: 10.1111/j.1365-2958.2009.06948.x

Bölker M, Genin S, Lehmler C, Kahmann R. (1995). Genetic regulation of mating and dimorphism in *Ustilago maydis*. *Canadian Journal of Botany*.**73** DOI: 10.1139/b95-262

Bösch K, Frantzeskakis L, Vranes M, Kamper J, Schipper K, Gohre V. (2016). Genetic Manipulation of the Plant Pathogen *Ustilago maydis* to Study Fungal Biology and Plant Microbe Interactions. *J Vis Exp*. Sep 30. Epub 20160930 DOI: 10.3791/54522

Brachmann A, Konig J, Julius C, Feldbrügge M. (2004). A reverse genetic approach for generating gene replacement mutants in *Ustilago maydis*. *Mol Genet Genomics*. Sep;**272**:216-226. Epub 2004/08/19 DOI: 10.1007/s00438-004-1047-z

Brachmann A, Weinzierl G, Kamper J, Kahmann R. (2001). Identification of genes in the bW/bE regulatory cascade in *Ustilago maydis*. *Mol Microbiol*. Nov;**42**:1047-1063. Epub 2001/12/12 DOI: 10.1046/j.1365-2958.2001.02699.x

Bradford MM. (1976). A rapid and sensitive method for the quantitation of microgram quantities of protein utilizing the principle of protein-dye binding. *Anal Biochem*. May 7;**72**:248-254. Epub 1976/05/07 DOI: 10.1006/abio.1976.9999

Branchini BR, Southworth TL, Fontaine DM, Kohrt D, Florentine CM, Grossel MJ. (2018). A Firefly Luciferase Dual Color Bioluminescence Reporter Assay Using Two Substrates To Simultaneously Monitor Two Gene Expression Events. *Sci Rep*. Apr 16;**8**:5990. Epub 2018/04/18 DOI: 10.1038/s41598-018-24278-2

Brefort T, Döhlemann G, Mendoza-Mendoza A, Reissmann S, Djamei A, Kahmann R. (2009). *Ustilago maydis* as a Pathogen. *Annu Rev Phytopathol*.**47**:423-445 DOI: 10.1146/annurev-phyto-080508-081923

Brine CJ, Austin PR. (1981). Chitin variability with species and method of preparation. *Comparative Biochemistry and Physiology*.283–286 DOI: 10.1016/0305-0491(81)90242-X

Bürth C, Kovacic F, Stock J, Terfruchte M, Wilhelm S, Jäger KE, Feldbrügge M, Schipper K, Ernst JF, Tielker D. (2014). Uml2 is a novel CalB-type lipase of Ustilago maydis with phospholipase A activity. *Appl Microbiol Biotechnol*. Jun;**98**:4963-4973. Epub 20140128 DOI: 10.1007/s00253-013-5493-6

Bui N, Strub K. (1999). New insights into signal recognition and elongation arrest activities of the signal recognition particle. *Biol Chem*. Feb;**380**:135-145 DOI: 10.1515/BC.1999.021

Callaway E. (2020). COVID vaccine excitement builds as Moderna reports third positive result. *Nature*. Nov;**587**:337-338 DOI: 10.1038/d41586-020-03248-7

Chang HC, Samaniego F, Nair BC, Buonaguro L, Ensoli B. (1997). HIV-1 Tat protein exits from cells via a leaderless secretory pathway and binds to extracellular matrix-associated heparan

sulfate proteoglycans through its basic region. *AIDS*. Oct;**11**:1421-1431 DOI: 10.1097/00002030-199712000-00006

Cheng CM. (2020). Small-volume point-of-care analytical methods. *Sci Rep*. Aug 27;**10**:14230. Epub 20200827 DOI: 10.1038/s41598-020-70903-4

Chirico WJ, Waters MG, Blobel G. (1988). 70K heat shock related proteins stimulate protein translocation into microsomes. *Nature*. Apr 28;**332**:805-810 DOI: 10.1038/332805a0

Christensen JJ. (1963). Corn smut Caused by *Ustilago maydis*. *American Phytopathology Society*.**Monograph No. 2**:1-41

Christie JM, Blackwood L, Petersen J, Sullivan S. (2015). Plant flavoprotein photoreceptors. *Plant Cell Physiol*. Mar;**56**:401-413. Epub 20141215 DOI: 10.1093/pcp/pcu196

Christie JM, Gawthorne J, Young G, Fraser NJ, Roe AJ. (2012). LOV to BLUF: flavoprotein contributions to the optogenetic toolkit. *Mol Plant*. May;**5**:533-544. Epub 20120319 DOI: 10.1093/mp/sss020

Christie JM, Zurbriggen MD. (2021). Optogenetics in plants. *New Phytol*. Mar;**229**:3108-3115. Epub 20201128 DOI: 10.1111/nph.17008

Cohen MJ, Chirico WJ, Lipke PN. (2020). Through the back door: Unconventional protein secretion. *Cell Surf*. Dec;**6**:100045. Epub 20200915 DOI: 10.1016/j.tcsw.2020.100045

Corman VM, Landt O, Kaiser M, Molenkamp R, Meijer A, Chu DK, Bleicker T, Brunink S, Schneider J, Schmidt ML, et al. (2020). Detection of 2019 novel coronavirus (2019-nCoV) by real-time RT-PCR. *Euro Surveill*. Jan;**25** DOI: 10.2807/1560-7917.ES.2020.25.3.2000045

Cortez-Retamozo V, Lauwereys M, Hassanzadeh Gh G, Gobert M, Conrath K, Muyldermans S, De Baetselier P, Revets H. (2002). Efficient tumor targeting by single-domain antibody fragments of camels. *Int J Cancer*. Mar 20;**98**:456-462 DOI: 10.1002/ijc.10212

Cruz-Garcia D, Curwin AJ, Popoff JF, Bruns C, Duran JM, Malhotra V. (2014). Remodeling of secretory compartments creates CUPS during nutrient starvation. *J Cell Biol*. Dec 22;**207**:695-703. Epub 20141215 DOI: 10.1083/jcb.201407119

Csala M, Kereszturi E, Mandl J, Banhegyi G. (2012). The endoplasmic reticulum as the extracellular space inside the cell: role in protein folding and glycosylation. *Antioxid Redox Signal*. May 15;**16**:1100-1108. Epub 20120223 DOI: 10.1089/ars.2011.4227

Cui J, Li F, Shi ZL. (2019). Origin and evolution of pathogenic coronaviruses. *Nat Rev Microbiol*. Mar;**17**:181-192 DOI: 10.1038/s41579-018-0118-9

Curwin AJ, Brouwers N, Alonso YAM, Teis D, Turacchio G, Parashuraman S, Ronchi P, Malhotra V. (2016). ESCRT-III drives the final stages of CUPS maturation for unconventional protein secretion. *Elife*. Apr 26;**5**. Epub 20160426 DOI: 10.7554/eLife.16299

Custodio TF, Das H, Sheward DJ, Hanke L, Pazicky S, Pieprzyk J, Sorgenfrei M, Schroer MA, Gruzinov AY, Jeffries CM, et al. (2020). Selection, biophysical and structural analysis of synthetic nanobodies that effectively neutralize SARS-CoV-2. *Nat Commun*. Nov 4;**11**:5588. Epub 20201104 DOI: 10.1038/s41467-020-19204-y

D'Huyvetter M, Vincke C, Xavier C, Aerts A, Impens N, Baatout S, De Raeve H, Muyldermans S, Caveliers V, Devoogdt N, et al. (2014). Targeted radionuclide therapy with A 177Lu-labeled anti-HER2 nanobody. *Theranostics*.**4**:708-720. Epub 20140425 DOI: 10.7150/thno.8156

Davies NG, Abbott S, Barnard RC, Jarvis CI, Kucharski AJ, Munday JD, Pearson CAB, Russell TW, Tully DC, Washburne AD, et al. (2021). Estimated transmissibility and impact of SARS-CoV-2 lineage B.1.1.7 in England. *Science*. Apr 9;**372**. Epub 20210303 DOI: 10.1126/science.abg3055

De Greve H. (2022). Production of Designer VHH-Based Antibodies in Plants. *Methods Mol Biol*.**2446**:205-230 DOI: 10.1007/978-1-0716-2075-5_10

de Groot RJ, Baker SC, Baric RS, Brown CS, Drosten C, Enjuanes L, Fouchier RA, Galiano M, Gorbalenya AE, Memish ZA, et al. (2013). Middle East respiratory syndrome coronavirus (MERS-CoV): announcement of the Coronavirus Study Group. *J Virol*. Jul;**87**:7790-7792. Epub 20130515 DOI: 10.1128/JVI.01244-13

de Marco A. (2022). Cytoplasmic Production of Nanobodies and Nanobody-Based Reagents by Co-Expression of Sulfhydryl Oxidase and DsbC Isomerase. *Methods Mol Biol*.**2446**:145-157 DOI: 10.1007/978-1-0716-2075-5_7

Delic M, Valli M, Graf AB, Pfeffer M, Mattanovich D, Gasser B. (2013). The secretory pathway: exploring yeast diversity. *FEMS Microbiol Rev*. Nov;**37**:872-914. Epub 20130412 DOI: 10.1111/1574-6976.12020

Di Paolo G, De Camilli P. (2006). Phosphoinositides in cell regulation and membrane dynamics. *Nature*. Oct 12;**443**:651-657 DOI: 10.1038/nature05185

Dinger R, Lattermann C, Flitsch D, Fischer JP, Kosfeld U, Buchs J. (2022). Device for respiration activity measurement enables the determination of oxygen transfer rates of microbial cultures in shaken 96-deepwell microtiter plates. *Biotechnol Bioeng*. Mar;**119**:881-894. Epub 20220107 DOI: 10.1002/bit.28022

Djamei A, Kahmann R. (2012). *Ustilago maydis*: dissecting the molecular interface between pathogen and plant. *PLoS Pathog*.**8**:e1002955. Epub 20121101 DOI: 10.1371/journal.ppat.1002955

Döhlemann G, Wahl R, Vranes M, de Vries RP, Kamper J, Kahmann R. (2008). Establishment of compatibility in the *Ustilago maydis*/maize pathosystem. *J Plant Physiol*. Jan;**165**:29-40. Epub 20071001 DOI: 10.1016/j.jplph.2007.05.016

Dong J, Huang B, Jia Z, Wang B, Gallolu Kankanamalage S, Titong A, Liu Y. (2020). Development of multi-specific humanized llama antibodies blocking SARS-CoV-2/ACE2 interaction with high affinity and avidity. *Emerg Microbes Infect*. Dec;**9**:1034-1036. Epub 2020/05/15 DOI: 10.1080/22221751.2020.1768806

Du L, He Y, Zhou Y, Liu S, Zheng BJ, Jiang S. (2009). The spike protein of SARS-CoV--a target for vaccine and therapeutic development. *Nat Rev Microbiol*. Mar;**7**:226-236. Epub 20090209 DOI: 10.1038/nrmicro2090

Du W, Liang F, Duan Y, Tan X, Lu X. (2013). Exploring the photosynthetic production capacity of sucrose by cyanobacteria. *Metab Eng*. Sep;**19**:17-25. Epub 20130528 DOI: 10.1016/j.ymben.2013.05.001

Dubey A, Dahiya S, Rouse BT, Sehrawat S. (2020). Perspective: Reducing SARS-CoV2 Infectivity and Its Associated Immunopathology. *Frontiers in Immunology*. 2020-October-22;**11** DOI: 10.3389/fimmu.2020.581076

Dütz WA, Rüdi L, Hermann R, O'Connor K, Buchs J, Witholt B. (2000). Methods for intense aeration, growth, storage, and replication of bacterial strains in microtiter plates. *Appl Environ Microbiol*. Jun;**66**:2641-2646 DOI: 10.1128/AEM.66.6.2641-2646.2000

Dumoulin M, Conrath K, Van Meirhäghe A, Meersman F, Heremans K, Frenken LG, Muyldermans S, Wyns L, Matagne A. (2002). Single-domain antibody fragments with high conformational stability. *Protein Sci*. Mar;**11**:500-515 DOI: 10.1110/ps.34602

Duran JM, Anjard C, Stefan C, Loomis WF, Malhotra V. (2010). Unconventional secretion of Acb1 is mediated by autophagosomes. *J Cell Biol*. Feb 22;**188**:527-536. Epub 20100215 DOI: 10.1083/jcb.200911154

Eckert DM, Kim PS. (2001). Mechanisms of viral membrane fusion and its inhibition. *Annu Rev Biochem*.**70**:777-810 DOI: 10.1146/annurev.biochem.70.1.777

Ellgaard L, Ruddock LW. (2005). The human protein disulphide isomerase family: substrate interactions and functional properties. *EMBO Rep*. Jan;**6**:28-32 DOI: 10.1038/sj.embor.7400311

Els Conrath K, Lauwereys M, Wyns L, Muyldermans S. (2001). Camel single-domain antibodies as modular building units in bispecific and bivalent antibody constructs. *J Biol Chem*. Mar 9;**276**:7346-7350. Epub 20001025 DOI: 10.1074/jbc.M007734200

Elshabrawy HA, Coughlin MM, Baker SC, Prabhakar BS. (2012). Human monoclonal antibodies against highly conserved HR1 and HR2 domains of the SARS-CoV spike protein are more broadly neutralizing. *PLoS One*.**7**:e50366. Epub 20121121 DOI: 10.1371/journal.pone.0050366

EnsemblFungi.Available from https://fungi.ensembl.org/Ustilago_maydis/Info/Index (last accessed: 01/25/2022).

Esparza TJ, Chen Y, Martin NP, Bielefeldt-Ohmann H, Bowen RA, Tolbert WD, Pazgier M, Brody DL. (2021). Nebulized delivery of a broadly neutralizing SARS-CoV-2 RBD-specific nanobody prevents clinical, virological and pathological disease in a Syrian hamster model of COVID-19. *bioRxiv*. Nov 12. Epub 20211112 DOI: 10.1101/2021.11.10.468147

EuropeanCommision.Coronavirus response. Available from https://ec.europa.eu/info/live-work-travel-eu/coronavirus-response_en (last accessed 02/24/2022)

EuropeanCommission. (2020). European Economic Forecast, Institutional Paper **132** DOI: 10.2765/828014

Fang H, Wang L, Yang Y. (2020). Human mobility restrictions and the spread of the Novel Coronavirus (2019-nCoV) in China. *J Public Econ*. Nov;**191**:104272. Epub 20200908 DOI: 10.1016/j.jpubeco.2020.104272

Farrel LB, Beachy RN. (1990). Manipulation of β-glucuronidase for use as a reporter in vacuolar targeting studies. *Plant Molecular Biology* **15**:821-825 DOI: 10.1007/BF00039422

Fatal N, Karhinen L, Jokitalo E, Makarow M. (2004). Active and specific recruitment of a soluble cargo protein for endoplasmic reticulum exit in the absence of functional COPII component Sec24p. *J Cell Sci*. Apr 1;**117**:1665-1673. Epub 20040309 DOI: 10.1242/jcs.01019

Feldbrügge M, Bölker M, Steinberg G, Kämper J, Kahmann R. 2006. Regulatory and Structural Networks Orchestrating Mating, Dimorphism, Cell Shape, and Pathogenesis in *Ustilago maydis*. In: The Mycota. p. 375-391.

Feldbrügge M, Kamper J, Steinberg G, Kahmann R. (2004). Regulation of mating and pathogenic development in *Ustilago* maydis. *Curr Opin Microbiol*. Dec;**7**:666-672 DOI: 10.1016/j.mib.2004.10.006

Feldbrügge M, Kellner R, Schipper K. (2013). The biotechnological use and potential of plant pathogenic smut fungi. *Appl Microbiol Biotechnol*. Apr;**97**:3253-3265. Epub 20130302 DOI: 10.1007/s00253-013-4777-1

Feldbrügge M, Zarnack K, Vollmeister E, Baumann S, Koepke J, Konig J, Munsterkotter M, Mannhaupt G. (2008). The posttranscriptional machinery of *Ustilago maydis*. *Fungal Genet Biol*. Aug;**45 Suppl 1**:S40-46. Epub 20080331 DOI: 10.1016/j.fgb.2008.03.013

Fernandes CS, Dos Santos R, Ottengy S, Viecinski AC, Behar G, Mouratou B, Pecorari F, Roque AC. (2016). Affitins for protein purification by affinity magnetic fishing. *J Chromatogr A*. Jul 29;**1457**:50-58. Epub 20160607 DOI: 10.1016/j.chroma.2016.06.020

Fernandes Q, Inchakalody VP, Merhi M, Mestiri S, Taib N, Moustafa Abo El-Ella D, Bedhiafi T, Raza A, Al-Zaidan L, Mohsen MO, et al. (2022). Emerging COVID-19 variants and their impact on SARS-CoV-2 diagnosis, therapeutics and vaccines. *Ann Med*. Dec;**54**:524-540 DOI: 10.1080/07853890.2022.2031274

Flajnik MF, Deschacht N, Muyldermans S. (2011). A case of convergence: why did a simple alternative to canonical antibodies arise in sharks and camels? *PLoS Biol*. Aug;**9**:e1001120. Epub 20110802 DOI: 10.1371/journal.pbio.1001120

Flajnik MF, Kasahara M. (2010). Origin and evolution of the adaptive immune system: genetic events and selective pressures. *Nat Rev Genet*. Jan;**11**:47-59. Epub 20091208 DOI: 10.1038/nrg2703

Flaschel E, Friehs K. (1993). Improvement of downstream processing of recombinant proteins by means of genetic engineering methods. *Biotechnol Adv*.**11**:31-77. Epub 1993/01/01 DOI: 10.1016/0734-9750(93)90409-g

Fleissner A, Dersch P. (2010). Expression and export: recombinant protein production systems for Aspergillus. *Appl Microbiol Biotechnol*. Jul;**87**:1255-1270. Epub 2010/06/10 DOI: 10.1007/s00253-010-2672-6

Franzreb M, Siemann-Herzberg M, Hobley TJ, Thomas OR. (2006). Protein purification using magnetic adsorbent particles. *Appl Microbiol Biotechnol*. May;**70**:505-516. Epub 20060223 DOI: 10.1007/s00253-006-0344-3

Freeman LA. (2013). Western blots. *Methods Mol Biol*.**1027**:369-385 DOI: 10.1007/978-1-60327-369-5_18

Funke M, Buchenauer A, Schnakenberg U, Mokwa W, Diederichs S, Mertens A, Müller C, Kensy F, Buchs J. (2010). Microfluidic biolector-microfluidic bioprocess control in microtiter plates. *Biotechnol Bioeng*. Oct 15;**107**:497-505. Epub 2010/06/03 DOI: 10.1002/bit.22825

Furuhashi M, Saitoh S, Shimamoto K, Miura T. (2014). Fatty Acid-Binding Protein 4 (FABP4): Pathophysiological Insights and Potent Clinical Biomarker of Metabolic and Cardiovascular Diseases. *Clin Med Insights Cardiol*.**8**:23-33. Epub 20150202 DOI: 10.4137/CMC.S17067

Gauhar A, Privezentzev CV, Demydchuk M, Gerlza T, Rieger J, Kungl AJ, Walsh FS, Rutkowski JL, Stocki P. (2021). Single domain shark VNAR antibodies neutralize SARS-CoV-2 infection in vitro. *FASEB J*. Nov;**35**:e21970 DOI: 10.1096/fj.202100986RR

Geiser E, Przybilla SK, Friedrich A, Buckel W, Wierckx N, Blank LM, Bölker M. (2016a). *Ustilago maydis* produces itaconic acid via the unusual intermediate trans-aconitate. *Microb Biotechnol*. Jan;**9**:116-126. Epub 20151207 DOI: 10.1111/1751-7915.12329

Geiser E, Reindl M, Blank LM, Feldbrügge M, Wierckx N, Schipper K. (2016b). Activating Intrinsic Carbohydrate-Active Enzymes of the Smut Fungus *Ustilago maydis* for the Degradation of Plant Cell Wall Components. *Appl Environ Microbiol*. Sep 1;**82**:5174-5185. Epub 2016/06/19 DOI: 10.1128/AEM.00713-16

Geiser E, Wierckx N, Zimmermann M, Blank LM. (2013). Identification of an endo-1,4-beta-xylanase of *Ustilago maydis*. *BMC Biotechnol*. Jul 26;**13**:59. Epub 20130726 DOI: 10.1186/1472-6750-13-59

Gerngross TU. (2004). Advances in the production of human therapeutic proteins in yeasts and filamentous fungi. *Nat Biotechnol*. Nov;**22**:1409-1414 DOI: 10.1038/nbt1028

Gibson DG. (2011). Enzymatic assembly of overlapping DNA fragments. *Methods Enzymol*.**498**:349-361. Epub 2011/05/24 DOI: 10.1016/B978-0-12-385120-8.00015-2

Gibson DG, Young L, Chuang RY, Venter JC, Hutchison CA, 3rd, Smith HO. (2009). Enzymatic assembly of DNA molecules up to several hundred kilobases. *Nat Methods*. May;**6**:343-345. Epub 2009/04/14 DOI: 10.1038/nmeth.1318

Gillet D, Ezan E, Ducancel F, Gaillard C, Ardouin T, Istin M, Menez A, Boulain JC, Grognet JM. (1993). Enzyme immunoassay using a rat prolactin-alkaline phosphatase recombinant tracer. *Anal Chem*. Jul 1;**65**:1779-1784 DOI: 10.1021/ac00061a023

Göhre V, Jones AM, Sklenar J, Robatzek S, Weber AP. (2012). Molecular crosstalk between PAMP-triggered immunity and photosynthesis. *Mol Plant Microbe Interact*. Aug;**25**:1083-1092 DOI: 10.1094/MPMI-11-11-0301

Govindappa N, Hanumanthappa M, Venkatarangaiah K, Periyasamy S, Sreenivas S, Soni R, Sastry K. (2014). A new signal sequence for recombinant protein secretion in Pichia pastoris. *J Microbiol Biotechnol*. Mar 28;**24**:337-345 DOI: 10.4014/jmb.1308.08085

GrandViewResearch.Biotechnology Market Size, Share & Trends Analysis Report By Technology (DNA Sequencing, Nanobiotechnology), By Application (Health, Bioinformatics), By Region, And Segment Forecasts, 2021 - 2028 Grand view research: Grand view research Available from https://www.grandviewresearch.com/industry-analysis/biotechnology-market (last accessed 02/22/2022)

Grant BD, Anderson CE, Williford JR, Alonzo LF, Glukhova VA, Boyle DS, Weigl BH, Nichols KP. (2020). SARS-CoV-2 Coronavirus Nucleocapsid Antigen-Detecting Half-Strip Lateral Flow Assay Toward the Development of Point of Care Tests Using Commercially Available Reagents. *Anal Chem*. Aug 18;**92**:11305-11309. Epub 20200805 DOI: 10.1021/acs.analchem.0c01975

Grieve AG, Rabouille C. (2011). Golgi bypass: skirting around the heart of classical secretion. *Cold Spring Harb Perspect Biol*. Apr 1;**3**. Epub 20110401 DOI: 10.1101/cshperspect.a005298

Gross E, Kastner DB, Kaiser CA, Fass D. (2004). Structure of Ero1p, source of disulfide bonds for oxidative protein folding in the cell. *Cell*. May 28;**117**:601-610 DOI: 10.1016/s0092-8674(04)00418-0

Gu S, Tian Y, Liang K, Ji Y. (2021). Chitin nanocrystals assisted 3D printing of polycitrate thermoset bioelastomers. *Carbohydr Polym*. Mar 15;**256**:117549. Epub 20201220 DOI: 10.1016/j.carbpol.2020.117549

Hale T, Angrist N, Goldszmidt R, Kira B, Petherick A, Phillips T, Webster S, Cameron-Blake E, Hallas L, Majumdar S, et al. (2021). A global panel database of pandemic policies (Oxford COVID-19 Government Response Tracker). *Nat Hum Behav*. Apr;**5**:529-538. Epub 20210308 DOI: 10.1038/s41562-021-01079-8

Hamers-Casterman C, Atarhouch T, Muyldermans S, Robinson G, Hamers C, Songa EB, Bendahman N, Hamers R. (1993). Naturally occurring antibodies devoid of light chains. *Nature*. Jun 3;**363**:446-448 DOI: 10.1038/363446a0

Harmsen MM, van Hagen-van Setten M, Willemsen PTJ. (2022). Small-Scale Secretory VHH Expression in Saccharomyces cerevisiae. *Methods Mol Biol*.**2446**:159-179 DOI: 10.1007/978-1-0716-2075-5_8

Hartmann HA, Kruger J, Lottspeich F, Kahmann R. (1999). Environmental signals controlling sexual development of the corn Smut fungus *Ustilago maydis* through the transcriptional regulator Prf1. *Plant Cell*. Jul;**11**:1293-1306 DOI: 10.1105/tpc.11.7.1293

He Z, Huang Y, Qin Y, Liu Z, Mo D, Cong P, Chen Y. (2012). Comparison of alpha-factor preprosequence and a classical mammalian signal peptide for secretion of recombinant xylanase xynB from yeast Pichia pastoris. *J Microbiol Biotechnol*. Apr;**22**:479-483 DOI: 10.4014/jmb.1109.09031

Heimel K. (2015). Unfolded protein response in filamentous fungi-implications in biotechnology. *Appl Microbiol Biotechnol*. Jan;**99**:121-132. Epub 20141111 DOI: 10.1007/s00253-014-6192-7

Hewald S, Linne U, Scherer M, Marahiel MA, Kamper J, Bölker M. (2006). Identification of a gene cluster for biosynthesis of mannosylerythritol lipids in the basidiomycetous fungus *Ustilago maydis*. *Appl Environ Microbiol*. Aug;**72**:5469-5477 DOI: 10.1128/AEM.00506-06

Hlubek A, Schink KO, Mahlert M, Sandrock B, Bölker M. (2008). Selective activation by the guanine nucleotide exchange factor Don1 is a main determinant of Cdc42 signalling specificity in *Ustilago maydis*. *Molecular microbiology*.**68**:615-623 DOI: 10.1111/j.1365-2958.2008.06177.x

Holliday R. (1964). The Induction of Mitotic Recombination by Mitomycin C in Ustilago and Saccharomyces. *Genetics*. Sep;**50**:323-335 DOI: 10.1093/genetics/50.3.323

Holliday R. (1974a). *Ustilago maydis*. In: Handbook of Genetics. New York, NY: Plenum Press. p. 575-595.

Holliday R. (1974b). *Ustilago maydis* In: Bacteria, Bacteriophages, and Fungi. Boston, MA: Springer. p. 575-595.

Hood L, Campbell JH, Elgin SC. (1975). The organization, expression, and evolution of antibody genes and other multigene families. *Annu Rev Genet*.**9**:305-353 DOI: 10.1146/annurev.ge.09.120175.001513

Horst RJ, Engelsdorf T, Sonnewald U, Voll LM. (2008). Infection of maize leaves with *Ustilago maydis* prevents establishment of C4 photosynthesis. *J Plant Physiol*. Jan;**165**:19-28. Epub 20070808 DOI: 10.1016/j.jplph.2007.05.008

Hosseinpour Tehrani H, Becker J, Bator I, Saur K, Meyer S, Rodrigues Loia AC, Blank LM, Wierckx N. (2019). Integrated strain- and process design enable production of 220 g L(-1) itaconic acid with *Ustilago maydis*. *Biotechnol Biofuels*.**12**:263. Epub 20191106 DOI: 10.1186/s13068-019-1605-6

Houen G. (2022). Therapeutic Antibodies: An Overview. *Methods Mol Biol*.**2313**:1-25 DOI: 10.1007/978-1-0716-1450-1_1

Hsiao WW, Le TN, Pham DM, Ko HH, Chang HC, Lee CC, Sharma N, Lee CK, Chiang WH. (2021). Recent Advances in Novel Lateral Flow Technologies for Detection of COVID-19. *Biosensors (Basel)*. Aug 25;**11**. Epub 20210825 DOI: 10.3390/bios11090295

Huang C, Wang Y, Li X, Ren L, Zhao J, Hu Y, Zhang L, Fan G, Xu J, Gu X, et al. (2020a). Clinical features of patients infected with 2019 novel coronavirus in Wuhan, China. *Lancet*. Feb 15;**395**:497-506. Epub 20200124 DOI: 10.1016/S0140-6736(20)30183-5

Huang SW, Miller SO, Yen CH, Wang SF. (2020b). Impact of Genetic Variability in ACE2 Expression on the Evolutionary Dynamics of SARS-CoV-2 Spike D614G Mutation. *Genes (Basel)*. Dec 24;**12**. Epub 20201224 DOI: 10.3390/genes12010016

Hulswit RJ, de Haan CA, Bosch BJ. (2016). Coronavirus Spike Protein and Tropism Changes. *Adv Virus Res*.**96**:29-57. Epub 20160913 DOI: 10.1016/bs.aivir.2016.08.004

Huo J, Le Bas A, Ruza RR, Duyvesteyn HME, Mikolajek H, Malinauskas T, Tan TK, Rijal P, Dumoux M, Ward PN, et al. (2020). Neutralizing nanobodies bind SARS-CoV-2 spike RBD and block interaction with ACE2. *Nat Struct Mol Biol*. Sep;**27**:846-854. Epub 20200713 DOI: 10.1038/s41594-020-0469-6

Huo J, Mikolajek H, Le Bas A, Clark JJ, Sharma P, Kipar A, Dormon J, Norman C, Weckener M, Clare DK, et al. (2021). A potent SARS-CoV-2 neutralising nanobody shows therapeutic efficacy in the Syrian golden hamster model of COVID-19. *Nat Commun*. Sep 22;**12**:5469. Epub 20210922 DOI: 10.1038/s41467-021-25480-z

Hussnätter KP. 2016. Studying the role of the novel factor Jps1 during unconventional secretion of the chitinase Cts1 [Master thesis]. Heinrich-Heine University Düsseldorf.

Hussnätter KP, Philipp M, Muntjes K, Feldbrügge M, Schipper K. (2021). Controlling Unconventional Secretion for Production of Heterologous Proteins in *Ustilago maydis* through Transcriptional Regulation and Chemical Inhibition of the Kinase Don3. *J Fungi (Basel)*. Mar 3;**7**. Epub 2021/04/04 DOI: 10.3390/jof7030179

Huston JS, Levinson D, Mudgett-Hunter M, Tai MS, Novotny J, Margolies MN, Ridge RJ, Bruccoleri RE, Haber E, Crea R, et al. (1988). Protein engineering of antibody binding sites: recovery of specific activity in an anti-digoxin single-chain Fv analogue produced in Escherichia coli. *Proc Natl Acad Sci U S A*. Aug;**85**:5879-5883 DOI: 10.1073/pnas.85.16.5879

Hwang YC, Lu RM, Su SC, Chiang PY, Ko SH, Ke FY, Liang KH, Hsieh TY, Wu HC. (2022). Monoclonal antibodies for COVID-19 therapy and SARS-CoV-2 detection. *J Biomed Sci*. Jan 4;**29**:1. Epub 20220104 DOI: 10.1186/s12929-021-00784-w

Ingram JR, Schmidt FI, Ploegh HL. (2018). Exploiting Nanobodies' Singular Traits. *Annual Review of Immunology*.**36**:695-715 DOI: 10.1146/annurev-immunol-042617-053327

Jackson A, Friedman S, Zhan X, Engleka KA, Forough R, Maciag T. (1992). Heat shock induces the release of fibroblast growth factor 1 from NIH 3T3 cells. *Proc Natl Acad Sci U S A*. Nov 15;**89**:10691-10695 DOI: 10.1073/pnas.89.22.10691

Jain J, Gaur S, Chaudhary Y, Kaul R. (2020). The molecular biology of intracellular events during Coronavirus infection cycle. *Virusdisease*. Jun;**31**:75-79. Epub 20200504 DOI: 10.1007/s13337-020-00591-1

Jankowski S, Pohlmann T, Baumann S, Muntjes K, Devan SK, Zander S, Feldbrügge M. (2019). The multi PAM2 protein Upa2 functions as novel core component of endosomal mRNA transport. *EMBO Rep*. Sep;**20**:e47381. Epub 20190724 DOI: 10.15252/embr.201847381

Jensen MB, Bhatia VK, Jao CC, Rasmussen JE, Pedersen SL, Jensen KJ, Langen R, Stamou D. (2011). Membrane curvature sensing by amphipathic helices: a single liposome study using alpha-synuclein and annexin B12. *J Biol Chem*. Dec 9;**286**:42603-42614. Epub 20110927 DOI: 10.1074/jbc.M111.271130

Jeppesen DK, Fenix AM, Franklin JL, Higginbotham JN, Zhang Q, Zimmerman LJ, Liebler DC, Ping J, Liu Q, Evans R, et al. (2019). Reassessment of Exosome Composition. *Cell*. Apr 4;**177**:428-445 e418 DOI: 10.1016/j.cell.2019.02.029

Jiang L, Li T, Jenkins J, Hu Y, Brück CL, Pei H, Betenbaugh MJ. (2020). Evidence for a mutualistic relationship between the cyanobacteria Nostoc and fungi Aspergilli in different environments. *Appl Microbiol Biotechnol*. Jul;**104**:6413-6426. Epub 20200529 DOI: 10.1007/s00253-020-10663-3

Jiang L, Wang N, Zuo T, Shi X, Poon KM, Wu Y, Gao F, Li D, Wang R, Guo J, et al. (2014). Potent neutralization of MERS-CoV by human neutralizing monoclonal antibodies to the viral spike glycoprotein. *Sci Transl Med*. Apr 30;**6**:234ra259. Epub 20140428 DOI: 10.1126/scitranslmed.3008140

Juarez-Montiel M, Ruiloba de Leon S, Chavez-Camarillo G, Hernandez-Rodriguez C, Villa-Tanaca L. (2011). Huitlacoche (corn smut), caused by the phytopathogenic fungus *Ustilago maydis*, as a functional food. *Rev Iberoam Micol*. Apr-Jun;**28**:69-73. Epub 20110223 DOI: 10.1016/j.riam.2011.01.001

Jumper J, Evans R, Pritzel A, Green T, Figurnov M, Ronneberger O, Tunyasuvunakool K, Bates R, Zidek A, Potapenko A, et al. (2021). Highly accurate protein structure prediction with AlphaFold. *Nature*. Aug;**596**:583-589. Epub 20210715 DOI: 10.1038/s41586-021-03819-2

Kalies KU, Gorlich D, Rapoport TA. (1994). Binding of ribosomes to the rough endoplasmic reticulum mediated by the Sec61p-complex. *J Cell Biol*. Aug;**126**:925-934 DOI: 10.1083/jcb.126.4.925

Kämper J, Kahmann R, Bölker M, Ma LJ, Brefort T, Saville BJ, Banuett F, Kronstad JW, Gold SE, Müller O, et al. (2006). Insights from the genome of the biotrophic fungal plant pathogen *Ustilago maydis*. *Nature*. Nov 2;**444**:97-101 DOI: 10.1038/nature05248

Kang L, Li Y, Hu S, Chen M, Yang C, Yang BX, Wang Y, Hu J, Lai J, Ma X, et al. (2020). The mental health of medical workers in Wuhan, China dealing with the 2019 novel coronavirus. *Lancet Psychiatry*. Mar;**7**:e14. Epub 20200205 DOI: 10.1016/S2215-0366(20)30047-X

Kaplon H, Reichert JM. (2021). Antibodies to watch in 2021. *MAbs*. Jan-Dec;**13**:1860476. Epub 2021/01/19 DOI: 10.1080/19420862.2020.1860476

Kaye AD, Okeagu CN, Pham AD, Silva RA, Hurley JJ, Arron BL, Sarfraz N, Lee HN, Ghali GE, Gamble JW, et al. (2021). Economic impact of COVID-19 pandemic on healthcare facilities and systems: International perspectives. *Best Pract Res Clin Anaesthesiol*. Oct;**35**:293-306. Epub 20201117 DOI: 10.1016/j.bpa.2020.11.009

Keon JP, White GA, Hargreaves JA. (1991). Isolation, characterization and sequence of a gene conferring resistance to the systemic fungicide carboxin from the maize smut pathogen, *Ustilago maydis*. *Curr Genet*. Jun;**19**:475-481. Epub 1991/06/01 DOI: http://www.ncbi.nlm.nih.gov/pubmed/1879000

Khateeb J, Li Y, Zhang H. (2021). Emerging SARS-CoV-2 variants of concern and potential intervention approaches. *Crit Care*. Jul 12;**25**:244. Epub 20210712 DOI: 10.1186/s13054-021-03662-x

Khrunyk Y, Munch K, Schipper K, Lupas AN, Kahmann R. (2010). The use of FLP-mediated recombination for the functional analysis of an effector gene family in the biotrophic smut fungus *Ustilago maydis*. *New Phytol*. Sep;**187**:957-968. Epub 20100618 DOI: 10.1111/j.1469-8137.2010.03413.x

Kijanka M, Dorresteijn B, Oliveira S, van Bergen en Henegouwen PM. (2015). Nanobody-based cancer therapy of solid tumors. *Nanomedicine (Lond)*. Jan;**10**:161-174 DOI: 10.2217/nnm.14.178

Kijpornyongpan T, Aime MC. (2021). Comparative transcriptomics reveal different mechanisms for hyphal growth across four plant-associated dimorphic fungi. *Fungal Genet Biol*. Jul;**152**:103565. Epub 20210513 DOI: 10.1016/j.fgb.2021.103565

Kirchdörfer RN, Cottrell CA, Wang N, Pallesen J, Yassine HM, Turner HL, Corbett KS, Graham BS, McLellan JS, Ward AB. (2016). Pre-fusion structure of a human coronavirus spike protein. *Nature*. Mar 3;**531**:118-121 DOI: 10.1038/nature17200

Kirsch F, Luo Q, Lu X, Hagemann M. (2018). Inactivation of invertase enhances sucrose production in the cyanobacterium Synechocystis sp. PCC 6803. *Microbiology (Reading)*. Oct;**164**:1220-1228. Epub 20180816 DOI: 10.1099/mic.0.000708

Klionsky DJ, Eskelinen EL, Deretic V. (2014). Autophagosomes, phagosomes, autolysosomes, phagolysosomes, autophagolysosomes... wait, I'm confused. *Autophagy*. Apr;**10**:549-551. Epub 20140317 DOI: 10.4161/auto.28448

König PA, Das H, Liu H, Kummerer BM, Gohr FN, Jenster LM, Schiffelers LDJ, Tesfamariam YM, Uchima M, Würth JD, et al. (2021). Structure-guided multivalent nanobodies block SARS-CoV-2 infection and suppress mutational escape. *Science*. Feb 12;**371**. Epub 2021/01/14 DOI: 10.1126/science.abe6230

Koepke J, Kaffarnik F, Haag C, Zarnack K, Luscombe NM, Konig J, Ule J, Kellner R, Begerow D, Feldbrügge M. (2011). The RNA-binding protein Rrm4 is essential for efficient secretion of endochitinase Cts1. *Mol Cell Proteomics*. Dec;**10**:M111 011213. Epub 2011/08/03 DOI: 10.1074/mcp.M111.011213

Koide A, Tereshko V, Uysal S, Margalef K, Kossiakoff AA, Koide S. (2007). Exploring the capacity of minimalist protein interfaces: interface energetics and affinity maturation to picomolar KD of a single-domain antibody with a flat paratope. *J Mol Biol*. Nov 2;**373**:941-953. Epub 20070821 DOI: 10.1016/j.jmb.2007.08.027

Korber B, Fischer WM, Gnanakaran S, Yoon H, Theiler J, Abfalterer W, Hengartner N, Giorgi EE, Bhattacharya T, Foley B, et al. (2020). Tracking Changes in SARS-CoV-2 Spike: Evidence that D614G Increases Infectivity of the COVID-19 Virus. *Cell*. Aug 20;**182**:812-827 e819. Epub 20200703 DOI: 10.1016/j.cell.2020.06.043

Kovalchuk V, Voronkina A, Binnewerg B, Schubert M, Muzychka L, Wysokowski M, Tsurkan MV, Bechmann N, Petrenko I, Fursov A, et al. (2019). Naturally Drug-Loaded Chitin: Isolation and Applications. *Mar Drugs*. Oct 10;**17**. Epub 20191010 DOI: 10.3390/md17100574

Krombach S, Reissmann S, Kreibich S, Bochen F, Kahmann R. (2018). Virulence function of the *Ustilago maydis* sterol carrier protein 2. *New Phytol*. Oct;**220**:553-566. Epub 20180613 DOI: 10.1111/nph.15268

Kudlay D, Svistunov A. (2022). COVID-19 Vaccines: An Overview of Different Platforms. *Bioengineering (Basel)*. Feb 12;**9**. Epub 20220212 DOI: 10.3390/bioengineering9020072

Kumar S, Chandele A, Sharma A. (2021). Current status of therapeutic monoclonal antibodies against SARS-CoV-2. *PLoS Pathog*. Sep;**17**:e1009885. Epub 20210903 DOI: 10.1371/journal.ppat.1009885

Kun RS, Gomes ACS, Hilden KS, Salazar Cerezo S, Makela MR, de Vries RP. (2019). Developments and opportunities in fungal strain engineering for the production of novel enzymes and enzyme cocktails for plant biomass degradation. *Biotechnol Adv*. Nov 1;**37**:107361. Epub 20190227 DOI: 10.1016/j.biotechadv.2019.02.017

Kwarteng A, Asiedu E, Sakyi SA, Asiedu SO. (2020). Targeting the SARS-CoV2 nucleocapsid protein for potential therapeutics using immuno-informatics and structure-based drug discovery techniques. *Biomed Pharmacother*. Dec;**132**:110914. Epub 20201020 DOI: 10.1016/j.biopha.2020.110914

Kwon S, Rupp O, Brachmann A, Blum CF, Kräge A, Gösmann A, Feldbrügge M. (2021). mRNA Inventory of Extracellular Vesicles from *Ustilago maydis*. *J Fungi (Basel)*. Jul 14;**7**. Epub 20210714 DOI: 10.3390/jof7070562

La Venuta G, Zeitler M, Steringer JP, Müller HM, Nickel W. (2015). The Startling Properties of Fibroblast Growth Factor 2: How to Exit Mammalian Cells without a Signal Peptide at Hand. *J Biol Chem*. Nov 6;**290**:27015-27020. Epub 20150928 DOI: 10.1074/jbc.R115.689257

Langner T, Özturk M, Hartmann S, Cord-Landwehr S, Mörschbacher B, Walton JD, Göhre V. (2015). Chitinases are essential for cell separation in *Ustilago maydis*. *Eukaryot Cell*. Sep;**14**:846-857. Epub 2015/05/03 DOI: 10.1128/EC.00022-15

Lanver D, Müller AN, Happel P, Schweizer G, Haas FB, Franitza M, Pellegrin C, Reissmann S, Altmüller J, Rensing SA, et al. (2018). The Biotrophic Development of *Ustilago maydis* Studied by RNA-Seq Analysis. *Plant Cell*. Feb;**30**:300-323. Epub 20180125 DOI: 10.1105/tpc.17.00764

Lee MC, Miller EA, Goldberg J, Orci L, Schekman R. (2004). Bi-directional protein transport between the ER and Golgi. *Annu Rev Cell Dev Biol*.**20**:87-123 DOI: 10.1146/annurev.cellbio.20.010403.105307

Legris M, Klose C, Burgie ES, Rojas CC, Neme M, Hiltbrunner A, Wigge PA, Schafer E, Vierstra RD, Casal JJ. (2016). Phytochrome B integrates light and temperature signals in Arabidopsis. *Science*. Nov 18;**354**:897-900. Epub 20161027 DOI: 10.1126/science.aaf5656

Lequin RM. (2005). Enzyme immunoassay (EIA)/enzyme-linked immunosorbent assay (ELISA). *Clin Chem*. Dec;**51**:2415-2418. Epub 20050922 DOI: 10.1373/clinchem.2005.051532

Li F. (2016). Structure, Function, and Evolution of Coronavirus Spike Proteins. *Annu Rev Virol*. Sep 29;**3**:237-261. Epub 20160825 DOI: 10.1146/annurev-virology-110615-042301

Li SC, Kane PM. (2009). The yeast lysosome-like vacuole: endpoint and crossroads. *Biochim Biophys Acta*. Apr;**1793**:650-663. Epub 20080813 DOI: 10.1016/j.bbamcr.2008.08.003

Li W, Moore MJ, Vasilieva N, Sui J, Wong SK, Berne MA, Somasundaran M, Sullivan JL, Luzuriaga K, Greenough TC, et al. (2003). Angiotensin-converting enzyme 2 is a functional receptor for the SARS coronavirus. *Nature*. Nov 27;**426**:450-454 DOI: 10.1038/nature02145

Li Z, Yang Q. (2018). Systems and synthetic biology approaches in understanding biological oscillators. *Quant Biol*. Mar;**6**:1-14. Epub 20171102 DOI: 10.1007/s40484-017-0120-7

Lin AV. (2015). Direct ELISA. *Methods Mol Biol*.**1318**:61-67 DOI: 10.1007/978-1-4939-2742-5_6

Lin PC, Zhang F, Pakrasi HB. (2020). Enhanced production of sucrose in the fast-growing cyanobacterium Synechococcus elongatus UTEX 2973. *Sci Rep*. Jan 15;**10**:390. Epub 20200115 DOI: 10.1038/s41598-019-57319-5

Liu H, Cao Y, Guo J, Xu X, Long Q, Song L, Xian M. (2021a). Study on the isoprene-producing co-culture system of Synechococcus elongates-Escherichia coli through omics analysis. *Microb Cell Fact*. Jan 7;**20**:6. Epub 20210107 DOI: 10.1186/s12934-020-01498-8

Liu J, Liu Y, Xia H, Zou J, Weaver SC, Swanson KA, Cai H, Cutler M, Cooper D, Muik A, et al. (2021b). BNT162b2-elicited neutralization of B.1.617 and other SARS-CoV-2 variants. *Nature*. Aug;**596**:273-275. Epub 20210610 DOI: 10.1038/s41586-021-03693-y

Liu JL, Zabetakis D, Gardner CL, Burke CW, Glass PJ, Webb EM, Shriver-Lake LC, Anderson GP, Weger-Lucarelli J, Goldman ER. (2022). Bivalent single domain antibody constructs for effective neutralization of Venezuelan equine encephalitis. *Sci Rep*. Jan 13;**12**:700. Epub 20220113 DOI: 10.1038/s41598-021-04434-x

Liu W, Song H, Chen Q, Yu J, Xian M, Nian R, Feng D. (2018). Recent advances in the selection and identification of antigen-specific nanobodies. *Mol Immunol*. Apr;**96**:37-47. Epub 20180222 DOI: 10.1016/j.molimm.2018.02.012

Liu Y, Huang H. (2018). Expression of single-domain antibody in different systems. *Appl Microbiol Biotechnol*. Jan;**102**:539-551. Epub 20171125 DOI: 10.1007/s00253-017-8644-3

Lu R, Zhao X, Li J, Niu P, Yang B, Wu H, Wang W, Song H, Huang B, Zhu N, et al. (2020). Genomic characterisation and epidemiology of 2019 novel coronavirus: implications for virus origins and receptor binding. *Lancet*. Feb 22;**395**:565-574. Epub 20200130 DOI: 10.1016/S0140-6736(20)30251-8

Mahase E. (2021). Covid-19: Novavax vaccine efficacy is 86% against UK variant and 60% against South African variant. *BMJ*. Feb 1;**372**:n296. Epub 20210201 DOI: 10.1136/bmj.n296

Mambula SS, Calderwood SK. (2006). Heat shock protein 70 is secreted from tumor cells by a nonclassical pathway involving lysosomal endosomes. *J Immunol*. Dec 1;**177**:7849-7857 DOI: 10.4049/jimmunol.177.11.7849

Marra MA, Jones SJ, Astell CR, Holt RA, Brooks-Wilson A, Butterfield YS, Khattra J, Asano JK, Barber SA, Chan SY, et al. (2003). The Genome sequence of the SARS-associated coronavirus. *Science*. May 30;**300**:1399-1404. Epub 20030501 DOI: 10.1126/science.1085953

Marrocco I, Romaniello D, Yarden Y. (2019). Cancer Immunotherapy: The Dawn of Antibody Cocktails. *Methods Mol Biol*.**1904**:11-51 DOI: 10.1007/978-1-4939-8958-4_2

Martin-Sanchez F, Diamond C, Zeitler M, Gomez AI, Baroja-Mazo A, Bagnall J, Spiller D, White M, Daniels MJ, Mortellaro A, et al. (2016). Inflammasome-dependent IL-1beta

release depends upon membrane permeabilisation. *Cell Death Differ*. Jul;**23**:1219-1231. Epub 20160212 DOI: 10.1038/cdd.2015.176

Martinez-Espinoza AD, Garcia-Pedrajas MD, Gold SE. (2002). The Ustilaginales as plant pests and model systems. *Fungal Genet Biol*. Feb;**35**:1-20 DOI: 10.1006/fgbi.2001.1301

Mastrangeli R, Audino MC, Palinsky W, Broly H, Bierau H. (2020). The Formidable Challenge of Controlling High Mannose-Type N-Glycans in Therapeutic mAbs. *Trends Biotechnol*. Oct;**38**:1154-1168. Epub 20200629 DOI: 10.1016/j.tibtech.2020.05.009

Matei A, Doehlemann G. (2016). Cell biology of corn smut disease-*Ustilago maydis* as a model for biotrophic interactions. *Curr Opin Microbiol*. Dec;**34**:60-66. Epub 20160806 DOI: 10.1016/j.mib.2016.07.020

Matsuzaki Y, Kajiwara K, Aoki W, Ueda M. (2022). Production of Single-Domain Antibodies in Pichia pastoris. *Methods Mol Biol*.**2446**:181-203 DOI: 10.1007/978-1-0716-2075-5_9

Maussang D, Mujic-Delic A, Descamps FJ, Stortelers C, Vanlandschoot P, Stigter-van Walsum M, Vischer HF, van Roy M, Vosjan M, Gonzalez-Pajuelo M, et al. (2013). Llama-derived single variable domains (nanobodies) directed against chemokine receptor CXCR7 reduce head and neck cancer cell growth in vivo. *J Biol Chem*. Oct 11;**288**:29562-29572. Epub 20130826 DOI: 10.1074/jbc.M113.498436

McArthur DB. (2019). Emerging Infectious Diseases. *Nurs Clin North Am*. Jun;**54**:297-311. Epub 20190327 DOI: 10.1016/j.cnur.2019.02.006

McCormick AL, Thomas MS, Heath AW. (2001). Immunization with an interferon-gamma-gp120 fusion protein induces enhanced immune responses to human immunodeficiency virus gp120. *J Infect Dis*. Dec 1;**184**:1423-1430. Epub 20011113 DOI: 10.1086/324371

McGrath JP, Varshavsky A. (1989). The yeast STE6 gene encodes a homologue of the mammalian multidrug resistance P-glycoprotein. *Nature*. Aug 3;**340**:400-404 DOI: 10.1038/340400a0

McKeigue PM, McAllister DA, Caldwell D, Gribben C, Bishop J, McGurnaghan S, Armstrong M, Delvaux J, Colville S, Hutchinson S, et al. (2021). Relation of severe COVID-19 in Scotland to transmission-related factors and risk conditions eligible for shielding support: REACT-SCOT case-control study. *BMC Med*. Jun 23;**19**:149. Epub 20210623 DOI: 10.1186/s12916-021-02021-5

McPherson A. (2017). Protein Crystallization. *Methods Mol Biol*.**1607**:17-50 DOI: 10.1007/978-1-4939-7000-1_2

Mercer TR, Salit M. (2021). Testing at scale during the COVID-19 pandemic. *Nat Rev Genet*. Jul;**22**:415-426. Epub 20210504 DOI: 10.1038/s41576-021-00360-w

Millet JK, Whittaker GR. (2014). Host cell entry of Middle East respiratory syndrome coronavirus after two-step, furin-mediated activation of the spike protein. *Proc Natl Acad Sci U S A*. Oct 21;**111**:15214-15219. Epub 20141006 DOI: 10.1073/pnas.1407087111

Miska W, Geiger R. (1987). Synthesis and Characterization of Luciferin Derivatives for Use in Bioluminescence Enhanced Enzyme Immunoassays. New Ultrasensitive Detection Systems for Enzyme Immunoassays, I.**25**:23-30 DOI: doi:10.1515/cclm.1987.25.1.23

Mita T, Furuhashi M, Hiramitsu S, Ishii J, Hoshina K, Ishimura S, Fuseya T, Watanabe Y, Tanaka M, Ohno K, et al. (2015). FABP4 is secreted from adipocytes by adenyl cyclase-

PKA- and guanylyl cyclase-PKG-dependent lipolytic mechanisms. *Obesity (Silver Spring)*. Feb;**23**:359-367. Epub 20141217 DOI: 10.1002/oby.20954

Monegal A, Ami D, Martinelli C, Huang H, Aliprandi M, Capasso P, Francavilla C, Ossolengo G, de Marco A. (2009). Immunological applications of single-domain llama recombinant antibodies isolated from a naive library. *Protein Eng Des Sel*. Apr;**22**:273-280. Epub 20090204 DOI: 10.1093/protein/gzp002

MordorIntelligence.RECOMBINANT PROTEIN MARKET - GROWTH, TRENDS, COVID-19 IMPACT, AND FORECASTS (2022 - 2027). Available from https://www.mordorintelligence.com/industry-reports/recombinant-protein-market (last accessed 02/22/2022)

Mowbray H. (2020). In Beijing, coronavirus 2019-nCoV has created a siege mentality. *BMJ*. Feb 7;**368**:m516. Epub 20200207 DOI: 10.1136/bmj.m516

Müller K, Siegel D, Rodriguez Jahnke F, Gerrer K, Wend S, Decker EL, Reski R, Weber W, Zurbriggen MD. (2014). A red light-controlled synthetic gene expression switch for plant systems. *Mol Biosyst*. Jul;**10**:1679-1688. Epub 20140127 DOI: 10.1039/c3mb70579j

Müller MJ, Stachurski S, Stoffels P, Schipper K, Feldbrügge M, Buchs J. (2018). Online evaluation of the metabolic activity of *Ustilago maydis* on (poly)galacturonic acid. *J Biol Eng*.**12**:34. Epub 20181218 DOI: 10.1186/s13036-018-0128-1

Müntjes K, Devan SK, Reichert AS, Feldbrügge M. (2021). Linking transport and translation of mRNAs with endosomes and mitochondria. *EMBO Rep*. Oct 5;**22**:e52445. Epub 20210817 DOI: 10.15252/embr.202152445

Müntjes K, Philipp M, Hüsemann L, Heucken N, Weidtkamp-Peters S, Schipper K, Zurbriggen MD, Feldbrügge M. (2020). Establishing Polycistronic Expression in the Model Microorganism *Ustilago maydis*. *Front Microbiol*.**11**:1384. Epub 2020/07/17 DOI: 10.3389/fmicb.2020.01384

Muyldermans S. (2013). Nanobodies: natural single-domain antibodies. *Annu Rev Biochem*.**82**:775-797. Epub 2013/03/19 DOI: 10.1146/annurev-biochem-063011-092449

Muyldermans S, Baral TN, Retamozzo VC, De Baetselier P, De Genst E, Kinne J, Leonhardt H, Magez S, Nguyen VK, Revets H, et al. (2009). Camelid immunoglobulins and nanobody technology. *Vet Immunol Immunopathol*. Mar 15;**128**:178-183. Epub 20081017 DOI: 10.1016/j.vetimm.2008.10.299

Nakajima K-i, Asakura T, Maruyama J-i, Morita Y, Oike H, Shimizu-Ibuka A, Misaka T, Sorimachi H, Arai S, Kitamoto K, et al. (2006). Extracellular production of neoculin, a sweet-tasting heterodimeric protein with taste-modifying activity, by Aspergillus oryzae. *Applied and environmental microbiology*. 2006/05//;**72**:3716-3723 DOI: 10.1128/aem.72.5.3716-3723.2006

Nakamura N, Wei JH, Seemann J. (2012). Modular organization of the mammalian Golgi apparatus. *Curr Opin Cell Biol*. Aug;**24**:467-474. Epub 20120620 DOI: 10.1016/j.ceb.2012.05.009

Nevalainen H, Peterson R. (2014). Making recombinant proteins in filamentous fungi- are we expecting too much? *Front Microbiol*.**5**:75. Epub 2014/03/01 DOI: 10.3389/fmicb.2014.00075

Ng DT, Brown JD, Walter P. (1996). Signal sequences specify the targeting route to the endoplasmic reticulum membrane. *J Cell Biol*. Jul;**134**:269-278 DOI: 10.1083/jcb.134.2.269

Nicaud J.-M. MN, Holland I.B. . (1986). Current status of secretion of foreign proteins by microorganisms. *Journal of Biotechnology*.**Volume 3**:255-270 DOI: 10.1016/0168-1656(86)90008-8

Nickel W. (2010). Pathways of unconventional protein secretion. *Curr Opin Biotechnol*. Oct;**21**:621-626. Epub 2010/07/20 DOI: 10.1016/j.copbio.2010.06.004

Nicola M, Alsafi Z, Sohrabi C, Kerwan A, Al-Jabir A, Iosifidis C, Agha M, Agha R. (2020). The socio-economic implications of the coronavirus pandemic (COVID-19): A review. *Int J Surg*. Jun;**78**:185-193. Epub 20200417 DOI: 10.1016/j.ijsu.2020.04.018

Niessing D, Jansen RP, Pohlmann T, Feldbrügge M. (2018). mRNA transport in fungal top models. *Wiley Interdiscip Rev RNA*. Jan;**9**. Epub 20171010 DOI: 10.1002/wrna.1453

Oldenburg SJ, Averitt RD, Westcott SL, Halas NJ. (1998). Nanoengineering of optical resonances. *Chemical Physics Letters*.**288**:234-247

Olgeiser L, Haag C, Börner S, Ule J, Busch A, Koepke J, Konig J, Feldbrügge M, Zarnack K. (2019). The key protein of endosomal mRNP transport Rrm4 binds translational landmark sites of cargo mRNAs. *EMBO Rep*. Jan;**20**. Epub 20181214 DOI: 10.15252/embr.201846588

Olivi L, Berger M, Creyghton RNP, De Franceschi N, Dekker C, Mulder BM, Claassens NJ, Ten Wolde PR, van der Oost J. (2021). Towards a synthetic cell cycle. *Nat Commun*. Jul 26;**12**:4531. Epub 20210726 DOI: 10.1038/s41467-021-24772-8

Oloketuyi S, Bernedo R, Christmann A, Borkowska J, Cazzaniga G, Schuchmann HW, Niedziolka-Jonsson J, Szot-Karpinska K, Kolmar H, de Marco A. (2021). Native llama Nanobody Library Panning Performed by Phage and Yeast Display Provides Binders Suitable for C-Reactive Protein Detection. *Biosensors (Basel)*. Dec 3;**11**. Epub 20211203 DOI: 10.3390/bios11120496

Orfali K. (2020). What Triage Issues Reveal: Ethics in the COVID-19 Pandemic in Italy and France. *J Bioeth Inq*. Dec;**17**:675-679. Epub 20201109 DOI: 10.1007/s11673-020-10059-y

Ou X, Liu Y, Lei X, Li P, Mi D, Ren L, Guo L, Guo R, Chen T, Hu J, et al. (2020). Characterization of spike glycoprotein of SARS-CoV-2 on virus entry and its immune cross-reactivity with SARS-CoV. *Nat Commun*. Mar 27;**11**:1620. Epub 20200327 DOI: 10.1038/s41467-020-15562-9

Padlan EA. (1994). Anatomy of the antibody molecule. *Mol Immunol*. Feb;**31**:169-217 DOI: 10.1016/0161-5890(94)90001-9

Paesani C, Degano AL, Zalosnik MI, Fabi JP, Perez GT. (2021). Enzymatic modification of arabinoxylans from soft and hard Argentinian wheat inhibits the viability of HCT-116 cells. *Food Res Int*. Sep;**147**:110466. Epub 20210531 DOI: 10.1016/j.foodres.2021.110466

Palade G. (1975). Intracellular aspects of the process of protein synthesis. *Science*. Sep 12;**189**:867 DOI: 10.1126/science.189.4206.867-b

Paulino BN, Pessoa MG, Molina G, Kaupert Neto AA, Oliveira JVC, Mano MCR, Pastore GM. (2017). Biotechnological production of value-added compounds by ustilaginomycetous yeasts. *Appl Microbiol Biotechnol*. Nov;**101**:7789-7809. Epub 20170918 DOI: 10.1007/s00253-017-8516-x

Pellis M, Pardon E, Zolghadr K, Rothbauer U, Vincke C, Kinne J, Dierynck I, Hertogs K, Leonhardt H, Messens J, et al. (2012). A bacterial-two-hybrid selection system for one-step

isolation of intracellularly functional Nanobodies. *Arch Biochem Biophys*. Oct 15;**526**:114-123. Epub 20120511 DOI: 10.1016/j.abb.2012.04.023

Perez-Martin J, Castillo-Lluva S, Sgarlata C, Flor-Parra I, Mielnichuk N, Torreblanca J, Carbo N. (2006). Pathocycles: *Ustilago maydis* as a model to study the relationships between cell cycle and virulence in pathogenic fungi. *Mol Genet Genomics*. Sep;**276**:211-229. Epub 20060729 DOI: 10.1007/s00438-006-0152-6

Perez-Nadales E, Nogueira MF, Baldin C, Castanheira S, El Ghalid M, Grund E, Lengeler K, Marchegiani E, Mehrotra PV, Moretti M, et al. (2014). Fungal model systems and the elucidation of pathogenicity determinants. *Fungal Genet Biol*. Sep;**70**:42-67. Epub 20140707 DOI: 10.1016/j.fgb.2014.06.011

Philipp M, Hussnätter KP, Reindl M, Muntjes K, Feldbrügge M, Schipper K. (2021). A Novel Potent Carrier for Unconventional Protein Export in *Ustilago maydis*. *Front Cell Dev Biol*.**9**:816335. Epub 20220110 DOI: 10.3389/fcell.2021.816335

Planas D, Bruel T, Grzelak L, Guivel-Benhassine F, Staropoli I, Porrot F, Planchais C, Buchrieser J, Rajah MM, Bishop E, et al. (2021). Sensitivity of infectious SARS-CoV-2 B.1.1.7 and B.1.351 variants to neutralizing antibodies. *Nat Med*. May;**27**:917-924. Epub 20210326 DOI: 10.1038/s41591-021-01318-5

Pohlmann T, Baumann S, Haag C, Albrecht M, Feldbrügge M. (2015). A FYVE zinc finger domain protein specifically links mRNA transport to endosome trafficking. *Elife*. May 18;**4**. Epub 20150518 DOI: 10.7554/eLife.06041

Potelle S, Klein A, Foulquier F. (2015). Golgi post-translational modifications and associated diseases. *J Inherit Metab Dis*. Jul;**38**:741-751. Epub 20150513 DOI: 10.1007/s10545-015-9851-7

Pramanick I, Sengupta N, Mishra S, Pandey S, Girish N, Das A, Dutta S. (2021). Conformational flexibility and structural variability of SARS-CoV2 S protein. *Structure*. Aug 5;**29**:834-845 e835. Epub 20210430 DOI: 10.1016/j.str.2021.04.006

Prudovsky I, Kumar TK, Sterling S, Neivandt D. (2013). Protein-phospholipid interactions in nonclassical protein secretion: problem and methods of study. *Int J Mol Sci*. Feb 8;**14**:3734-3772. Epub 20130208 DOI: 10.3390/ijms14023734

Pymm P, Adair A, Chan LJ, Cooney JP, Mordant FL, Allison CC, Lopez E, Haycroft ER, O'Neill MT, Tan LL, et al. (2021). Nanobody cocktails potently neutralize SARS-CoV-2 D614G N501Y variant and protect mice. *Proc Natl Acad Sci U S A*. May 11;**118** DOI: 10.1073/pnas.2101918118

Rabouille C. (2017). Pathways of unconventional protein secretion. *Trends Cell Biol*. Mar;**27**:230-240. Epub 2016/12/19 DOI: 10.1016/j.tcb.2016.11.007

Rader RA. (2008). (Re)defining biopharmaceutical. *Nat Biotechnol*. Jul;**26**:743-751 DOI: 10.1038/nbt0708-743

Rahman MT, Sobur MA, Islam MS, Ievy S, Hossain MJ, El Zowalaty ME, Rahman AT, Ashour HM. (2020). Zoonotic Diseases: Etiology, Impact, and Control. *Microorganisms*. Sep 12;**8**. Epub 20200912 DOI: 10.3390/microorganisms8091405

Raj R. (2021). Analysis of non-structural proteins, NSPs of SARS-CoV-2 as targets for computational drug designing. *Biochem Biophys Rep*. Mar;**25**:100847. Epub 20201211 DOI: 10.1016/j.bbrep.2020.100847

Raj VS, Mou H, Smits SL, Dekkers DH, Müller MA, Dijkman R, Muth D, Demmers JA, Zaki A, Fouchier RA, et al. (2013). Dipeptidyl peptidase 4 is a functional receptor for the emerging human coronavirus-EMC. *Nature*. Mar 14;**495**:251-254 DOI: 10.1038/nature12005

Reichert JM. (2015). Antibodies to watch in 2015. *mAbs*. 2015/01/02;**7**:1-8 DOI: 10.4161/19420862.2015.988944

Reichert JM. (2017). Antibodies to watch in 2017. *MAbs*. Feb/Mar;**9**:167-181. Epub 20161214 DOI: 10.1080/19420862.2016.1269580

Reindl M. 2016. Using unconventional secretion for the export of heterologous, cofactor-dependent enzymes in *Ustilago maydis* [Master Thesis]. Heinrich Heine Universität Düsseldorf.

Reindl M. 2020a. A novel core factor for unconventional secretion in *Ustilago maydis* [PhD thesis]. Heinrich-Heine University Düsseldorf.

Reindl M, Hansch S, Weidtkamp-Peters S, Schipper K. (2019). A Potential Lock-Type Mechanism for Unconventional Secretion in Fungi. *Int J Mol Sci*. Jan 22;**20**. Epub 2019/01/27 DOI: 10.3390/ijms20030460

Reindl M, Stock J, Hussnätter KP, Genc A, Brachmann A, Schipper K. (2020b). A Novel Factor Essential for Unconventional Secretion of Chitinase Cts1. *Front Microbiol*.**11**:1529. Epub 2020/08/01 DOI: 10.3389/fmicb.2020.01529

ResearchandMarkets.Global Biopharmaceutical Market (2021-2026) by Product Type, Therapeutic Application, Geography, Competitive Analysis and the Impact of Covid-19 with Ansoff Analysis. Available from https://www.researchandmarkets.com/reports/5397295/global-biopharmaceutical-market-2021-2026-by?utm_source=GNOM&utm_medium=PressRelease&utm_code=zpjtrm&utm_campaign=1581180+-+Global+Biopharmaceutical+Market+Report+2021%3a+Market+is+Expected+to+Reach+%24478.08+Bn+by+2026%2c+from+%24330.7+Bn+in+2021+-+Increasing+Investments+in+R%26D&utm_exec=chdo54prd (last accessed 02/24/2022)

Rettenbacher L. (2021). Microbial protein cell factories fight back? *Trends Biotechnol*. Dec 16. Epub 20211216 DOI: 10.1016/j.tibtech.2021.10.003

Robert B, Dorvillius M, Buchegger F, Garambois V, Mani JC, Pugnieres M, Mach JP, Pelegrin A. (1999). Tumor targeting with newly designed biparatopic antibodies directed against two different epitopes of the carcinoembryonic antigen (CEA). *Int J Cancer*. Apr 12;**81**:285-291 DOI: 10.1002/(sici)1097-0215(19990412)81:2<285::aid-ijc19>3.0.co;2-t

Roovers RC, Laeremans T, Huang L, De Taeye S, Verkleij AJ, Revets H, de Haard HJ, van Bergen en Henegouwen PM. (2007). Efficient inhibition of EGFR signaling and of tumour growth by antagonistic anti-EFGR Nanobodies. *Cancer Immunol Immunother*. Mar;**56**:303-317 DOI: 10.1007/s00262-006-0180-4

Ruigrok VJ, Levisson M, Eppink MH, Smidt H, van der Oost J. (2011). Alternative affinity tools: more attractive than antibodies? *Biochem J*. May 15;**436**:1-13 DOI: 10.1042/BJ20101860

Ruiz-Herrera J, Perez-Rodriguez F, Velez-Haro J. (2020). The signaling mechanisms involved in the dimorphic phenomenon of the Basidiomycota fungus *Ustilago maydis*. *Int Microbiol*. Jan;**23**:121-126. Epub 20200108 DOI: 10.1007/s10123-019-00100-5

Sabino EC, Buss LF, Carvalho MPS, Prete CA, Jr., Crispim MAE, Fraiji NA, Pereira RHM, Parag KV, da Silva Peixoto P, Krämer MUG, et al. (2021). Resurgence of COVID-19 in

Manaus, Brazil, despite high seroprevalence. *Lancet*. Feb 6;**397**:452-455. Epub 20210127 DOI: 10.1016/S0140-6736(21)00183-5

Sabourin M, Tuzon CT, Fisher TS, Zakian VA. (2007). A flexible protein linker improves the function of epitope-tagged proteins in Saccharomyces cerevisiae. *Yeast*. Jan;**24**:39-45 DOI: 10.1002/yea.1431

Sadeghi A, Behdani M, Muyldermans S, Habibi-Anbouhi M, Kazemi-Lomedasht F. (2020). Development of a mono-specific anti-VEGF bivalent nanobody with extended plasma half-life for treatment of pathologic neovascularization. *Drug Test Anal*. Jan;**12**:92-100. Epub 20190912 DOI: 10.1002/dta.2693

Salvador JP, Vilaplana L, Marco MP. (2019). Nanobody: outstanding features for diagnostic and therapeutic applications. *Anal Bioanal Chem*. Mar;**411**:1703-1713. Epub 20190208 DOI: 10.1007/s00216-019-01633-4

Sandrock B, Böhmer C, Bölker M. (2006). Dual function of the germinal centre kinase Don3 during mitosis and cytokinesis in *Ustilago maydis*. *Molecular microbiology*.**62**:655-666 DOI: 10.1111/j.1365-2958.2006.05405.x

Santos RD, Iria I, Manuel AM, Leandro AP, Madeira CAC, Goncalves J, Carvalho AL, Roque ACA. (2020). Magnetic Precipitation: A New Platform for Protein Purification. *Biotechnol J*. Sep;**15**:e2000151. Epub 20200708 DOI: 10.1002/biot.202000151

Saputri DS, Li S, van Eerden FJ, Rozewicki J, Xu Z, Ismanto HS, Davila A, Teraguchi S, Katoh K, Standley DM. (2020). Flexible, Functional, and Familiar: Characteristics of SARS-CoV-2 Spike Protein Evolution. *Front Microbiol*.**11**:2112. Epub 20200917 DOI: 10.3389/fmicb.2020.02112

Saraste J, Prydz K. (2021). Assembly and Cellular Exit of Coronaviruses: Hijacking an Unconventional Secretory Pathway from the Pre-Golgi Intermediate Compartment via the Golgi Ribbon to the Extracellular Space. *Cells*. Feb 26;**10**. Epub 20210226 DOI: 10.3390/cells10030503

Sarkari P, Reindl M, Stock J, Müller O, Kahmann R, Feldbrügge M, Schipper K. (2014). Improved expression of single-chain antibodies in *Ustilago maydis*. *J Biotechnol*. Dec 10;**191**:165-175. Epub 2014/07/06 DOI: 10.1016/j.jbiotec.2014.06.028

Sarkodie SA, Owusu PA. (2021). Global assessment of environment, health and economic impact of the novel coronavirus (COVID-19). *Environ Dev Sustain*.**23**:5005-5015. Epub 20200605 DOI: 10.1007/s10668-020-00801-2

Satitsri S, Muanprasat C. (2020). Chitin and Chitosan Derivatives as Biomaterial Resources for Biological and Biomedical Applications. *Molecules*. Dec 16;**25**. Epub 20201216 DOI: 10.3390/molecules25245961

Satpati GG, Pal R. (2021). Co-Cultivation of Leptolyngbya tenuis (Cyanobacteria) and Chlorella ellipsoidea (Green alga) for Biodiesel Production, Carbon Sequestration, and Cadmium Accumulation. *Curr Microbiol*. Apr;**78**:1466-1481. Epub 20210304 DOI: 10.1007/s00284-021-02426-8

Schink KO, Bölker M. (2009). Coordination of cytokinesis and cell separation by endosomal targeting of a Cdc42-specific guanine nucleotide exchange factor in *Ustilago maydis*. *Mol Biol Cell*. Feb;**20**:1081-1088. Epub 20081210 DOI: 10.1091/mbc.E08-03-0280

Schlembach I, Hosseinpour Tehrani H, Blank LM, Buchs J, Wierckx N, Regestein L, Rosenbaum MA. (2020). Consolidated bioprocessing of cellulose to itaconic acid by a co-culture of Trichoderma reesei and *Ustilago maydis*. *Biotechnol Biofuels*. Dec 14;**13**:207. Epub 20201214 DOI: 10.1186/s13068-020-01835-4

Schmitz KR, Bagchi A, Roovers RC, van Bergen en Henegouwen PM, Ferguson KM. (2013). Structural evaluation of EGFR inhibition mechanisms for nanobodies/VHH domains. *Structure*. Jul 2;**21**:1214-1224. Epub 20130620 DOI: 10.1016/j.str.2013.05.008

Schwarz CK, Landsberg CD, Lenders MH, Smits SH, Schmitt L. (2012). Using an E. coli Type 1 secretion system to secrete the mammalian, intracellular protein IFABP in its active form. *J Biotechnol*. Jun 15;**159**:155-161. Epub 20120217 DOI: 10.1016/j.jbiotec.2012.02.005

Sedykh SE, Prinz VV, Buneva VN, Nevinsky GA. (2018). Bispecific antibodies: design, therapy, perspectives. *Drug Des Devel Ther*.**12**:195-208. Epub 20180122 DOI: 10.2147/DDDT.S151282

Sherwood LJ, Hayhurst A. (2022). Visualizing Filoviral Nucleoproteins Using Nanobodies Fused to the Ascorbate Peroxidase Derivatives APEX2 and dEAPX. *Methods Mol Biol*.**2446**:427-449 DOI: 10.1007/978-1-0716-2075-5_22

Shin JT, Opalenik SR, Wehby JN, Mahesh VK, Jackson A, Tarantini F, Maciag T, Thompson JA. (1996). Serum-starvation induces the extracellular appearance of FGF-1. *Biochim Biophys Acta*. Jun 5;**1312**:27-38 DOI: 10.1016/0167-4889(96)00013-4

Singh N, Chen J, Koziol KK, Hallam KR, Janas D, Patil AJ, Strachan A, J GH, Rahatekar SS. (2016). Chitin and carbon nanotube composites as biocompatible scaffolds for neuron growth. *Nanoscale*. Apr 21;**8**:8288-8299 DOI: 10.1039/c5nr06595j

Skerra A. (1993). Bacterial expression of immunoglobulin fragments. *Curr Opin Immunol*. Apr;**5**:256-262 DOI: 10.1016/0952-7915(93)90014-j

Somborac Bacura A, Dorotic M, Grosic L, Dzimbeg M, Dodig S. (2021). Current status of the lateral flow immunoassay for the detection of SARS-CoV-2 in nasopharyngeal swabs. *Biochem Med (Zagreb)*. Jun 15;**31**:020601 DOI: 10.11613/BM.2021.020601

Song Z, Xu Y, Bao L, Zhang L, Yu P, Qu Y, Zhu H, Zhao W, Han Y, Qin C. (2019). From SARS to MERS, Thrusting Coronaviruses into the Spotlight. *Viruses*. Jan 14;**11**. Epub 20190114 DOI: 10.3390/v11010059

Southern EM. (1974). Detection of specific sequences among DNA fragments separated by gel electrophoresis. *Journal of molecular biology*.**98**:503-517

Spadiut O, Capone S, Krainer F, Glieder A, Herwig C. (2014). Microbials for the production of monoclonal antibodies and antibody fragments. *Trends Biotechnol*. Jan;**32**:54-60. Epub 20131031 DOI: 10.1016/j.tibtech.2013.10.002

Spellig T, Bottin A, Kahmann R. (1996). Green fluorescent protein (GFP) as a new vital marker in the phytopathogenic fungus *Ustilago maydis*. *Mol Gen Genet*. Oct 16;**252**:503-509 DOI: 10.1007/BF02172396

Spiltoir JI, Strickland D, Glotzer M, Tucker CL. (2016). Optical Control of Peroxisomal Trafficking. *ACS Synth Biol*. Jul 15;**5**:554-560. Epub 20151102 DOI: 10.1021/acssynbio.5b00144

Stanley P. (2011). Golgi glycosylation. *Cold Spring Harb Perspect Biol*. Apr 1;**3**. Epub 20110401 DOI: 10.1101/cshperspect.a005199

Steringer JP, Bleicken S, Andreas H, Zacherl S, Laussmann M, Temmerman K, Contreras FX, Bharat TA, Lechner J, Müller HM, et al. (2012). Phosphatidylinositol 4,5-bisphosphate (PI(4,5)P2)-dependent oligomerization of fibroblast growth factor 2 (FGF2) triggers the formation of a lipidic membrane pore implicated in unconventional secretion. *J Biol Chem*. Aug 10;**287**:27659-27669. Epub 20120623 DOI: 10.1074/jbc.M112.381939

Stock J, Sarkari P, Kreibich S, Brefort T, Feldbrügge M, Schipper K. (2012). Applying unconventional secretion of the endochitinase Cts1 to export heterologous proteins in *Ustilago maydis*. *J Biotechnol*. Oct 15;**161**:80-91. Epub 2012/03/27 DOI: 10.1016/j.jbiotec.2012.03.004

Stock J, Terfruchte M, Schipper K. (2016a). A Reporter System to Study Unconventional Secretion of Proteins Avoiding N-Glycosylation in *Ustilago maydis*. *Methods Mol Biol*.**1459**:149-160. Epub 2016/09/26 DOI: 10.1007/978-1-4939-3804-9_10

Stock J, Terfrüchte M, Schipper K. (2016b). A Reporter System to Study Unconventional Secretion of Proteins Avoiding *N*-Glycosylation in *Ustilago maydis*. *Unconventional Protein Secretion: Methods and Protocols Springer Protocols*.**1459**:149-160

Stoffels P, Müller MJ, Stachurski S, Terfruchte M, Schroder S, Ihling N, Wierckx N, Feldbrügge M, Schipper K, Buchs J. (2020). Complementing the intrinsic repertoire of *Ustilago maydis* for degradation of the pectin backbone polygalacturonic acid. *J Biotechnol*. Jan 10;**307**:148-163. Epub 20191109 DOI: 10.1016/j.jbiotec.2019.10.022

Sudre CH, Murray B, Varsavsky T, Graham MS, Penfold RS, Bowyer RC, Pujol JC, Klaser K, Antonelli M, Canas LS, et al. (2021). Attributes and predictors of long COVID. *Nat Med*. Apr;**27**:626-631. Epub 20210310 DOI: 10.1038/s41591-021-01292-y

Sun X, Su X. (2019). Harnessing the knowledge of protein secretion for enhanced protein production in filamentous fungi. *World J Microbiol Biotechnol*. Mar 21;**35**:54. Epub 20190321 DOI: 10.1007/s11274-019-2630-0

Sun X, Yang S, Al-Dossary AA, Broitman S, Ni Y, Guan M, Yang M, Li J. (2022). Nanobody-Functionalized Cellulose for Capturing SARS-CoV-2. *Appl Environ Microbiol*. Mar 8;**88**:e0230321. Epub 20220105 DOI: 10.1128/aem.02303-21

Sun Y, Ho M. (2020a). Emerging antibody-based therapeutics against SARS-CoV-2 during the global pandemic. *Antib Ther*. Dec;**3**:246-256. Epub 2021/04/30 DOI: 10.1093/abt/tbaa025

Sun Y, Ho M. (2020b). Emerging antibody-based therapeutics against SARS-CoV-2 during the global pandemic. *Antibody Therapeutics*.**3**:246-256 DOI: 10.1093/abt/tbaa025

Takahashi N. (1983). [Glycopeptidases releasing intact N-linked oligosaccharides from glycopeptides]. *Seikagaku*. Oct;**55**:1204-1211 DOI: https://www.ncbi.nlm.nih.gov/pubmed/6242677

Teichmann B, Linne U, Hewald S, Marahiel MA, Bölker M. (2007). A biosynthetic gene cluster for a secreted cellobiose lipid with antifungal activity from *Ustilago maydis*. *Mol Microbiol*. Oct;**66**:525-533. Epub 20070910 DOI: 10.1111/j.1365-2958.2007.05941.x

Teichmann B, Liu L, Schink KO, Bölker M. (2010). Activation of the ustilagic acid biosynthesis gene cluster in *Ustilago maydis* by the C2H2 zinc finger transcription factor Rua1. *Appl Environ Microbiol*. Apr;**76**:2633-2640. Epub 20100219 DOI: 10.1128/AEM.02211-09

Tenenbaum DJ. (2008). Food vs. fuel: diversion of crops could cause more hunger. *Environ Health Perspect*. Jun;**116**:A254-257 DOI: 10.1289/ehp.116-a254

Terfrüchte M. 2016. Expression of biopharmaceuticals in *Ustilago maydis* [PhD Thesis]. Heinrich Heine Universität Düsseldorf.

Terfrüchte M, Jöhnk B, Fajardo-Somera R, Braus GH, Riquelme M, Schipper K, Feldbrügge M. (2014). Establishing a versatile Golden Gate cloning system for genetic engineering in fungi. *Fungal Genet Biol*. Jan;**62**:1-10. Epub 2013/11/12 DOI: 10.1016/j.fgb.2013.10.012

Terfrüchte M, Reindl M, Jankowski S, Sarkari P, Feldbrügge M, Schipper K. (2017). Applying Unconventional Secretion in *Ustilago maydis* for the Export of Functional Nanobodies. *Int J Mol Sci*. Apr 29;**18**. Epub 2017/05/05 DOI: 10.3390/ijms18050937

Terfrüchte M, Wewetzer S, Sarkari P, Stollewerk D, Franz-Wachtel M, Macek B, Schleputz T, Feldbrügge M, Buchs J, Schipper K. (2018). Tackling destructive proteolysis of unconventionally secreted heterologous proteins in *Ustilago maydis*. *J Biotechnol*. Oct 20;**284**:37-51. Epub 2018/08/01 DOI: 10.1016/j.jbiotec.2018.07.035

Tölzer C, Gupta K, Yadav SKN, Borucu U, Davidson AD, Kavanagh Williamson M, Shoemark DK, Garzoni F, Staufer O, Milligan R, et al. (2020). Free fatty acid binding pocket in the locked structure of SARS-CoV-2 spike protein. *Science*. Nov 6;**370**:725-730. Epub 20200921 DOI: 10.1126/science.abd3255

Torjesen I. (2021). Covid-19: Omicron may be more transmissible than other variants and partly resistant to existing vaccines, scientists fear. *BMJ*. Nov 29;**375**:n2943. Epub 20211129 DOI: 10.1136/bmj.n2943

Tränkle B, Rothbauer U. (2017). Under the Microscope: Single-Domain Antibodies for Live-Cell Imaging and Super-Resolution Microscopy. *Front Immunol*.**8**:1030. Epub 20170824 DOI: 10.3389/fimmu.2017.01030

Tsukuda T, Carleton S, Fotheringham S, Holloman WK. (1988). Isolation and characterization of an autonomously replicating sequence from *Ustilago maydis*. *Mol Cell Biol*. Sep;**8**:3703-3709. Epub 1988/09/01 DOI: 10.1128/mcb.8.9.3703-3709.1988

Tull D, Gottschalk TE, Svendsen I, Kramhoft B, Phillipson BA, Bisgard-Frantzen H, Olsen O, Svensson B. (2001). Extensive N-glycosylation reduces the thermal stability of a recombinant alkalophilic bacillus alpha-amylase produced in Pichia pastoris. *Protein Expr Purif*. Feb;**21**:13-23 DOI: 10.1006/prep.2000.1348

Turonova B, Sikora M, Schurmann C, Hagen WJH, Welsch S, Blanc FEC, von Bulow S, Gecht M, Bagola K, Horner C, et al. (2020). In situ structural analysis of SARS-CoV-2 spike reveals flexibility mediated by three hinges. *Science*. Oct 9;**370**:203-208. Epub 20200818 DOI: 10.1126/science.abd5223

Urbar-Ulloa J, Montano-Silva P, Ramirez-Pelayo AS, Fernandez-Castillo E, Amaya-Delgado L, Rodriguez-Garay B, Verdin J. (2019). Cell surface display of proteins on filamentous fungi. *Appl Microbiol Biotechnol*. Sep;**103**:6949-6972. Epub 20190729 DOI: 10.1007/s00253-019-10026-7

Valdez-Morales M, Carlos LC, Valverde ME, Ramirez-Chavez E, Paredes-Lopez O. (2016). Phenolic Compounds, Antioxidant Activity and Lipid Profile of Huitlacoche Mushroom (*Ustilago maydis*) Produced in Several Maize Genotypes at Different Stages of Development. *Plant Foods Hum Nutr*. Dec;**71**:436-443 DOI: 10.1007/s11130-016-0572-3

VanBlargan LA, Errico JM, Halfmann PJ, Zost SJ, Crowe JE, Jr., Purcell LA, Kawaoka Y, Corti D, Fremont DH, Diamond MS. (2022). An infectious SARS-CoV-2 B.1.1.529 Omicron virus escapes neutralization by therapeutic monoclonal antibodies. *Nat Med*. Jan 19. Epub 20220119 DOI: 10.1038/s41591-021-01678-y

Vicente FA, Bradic B, Novak U, Likozar B. (2020). alpha-Chitin dissolution, N-deacetylation and valorization in deep eutectic solvents. *Biopolymers*. May;**111**:e23351. Epub 20200312 DOI: 10.1002/bip.23351

Villeneuve J, Bassaganyas L, Lepreux S, Chiritoiu M, Costet P, Ripoche J, Malhotra V, Schekman R. (2018). Unconventional secretion of FABP4 by endosomes and secretory lysosomes. *J Cell Biol*. Feb 5;**217**:649-665. Epub 20171206 DOI: 10.1083/jcb.201705047

Vincke C, Loris R, Saerens D, Martinez-Rodriguez S, Muyldermans S, Conrath K. (2009). General strategy to humanize a camelid single-domain antibody and identification of a universal humanized nanobody scaffold. *J Biol Chem*. Jan 30;**284**:3273-3284. Epub 2008/11/18 DOI: 10.1074/jbc.M806889200

Viotti C. (2016). ER to Golgi-Dependent Protein Secretion: The Conventional Pathway. *Methods Mol Biol*.**1459**:3-29. Epub 2016/09/26 DOI: 10.1007/978-1-4939-3804-9_1

Vollmeister E, Schipper K, Feldbrügge M. (2012). Microtubule-dependent mRNA transport in the model microorganism *Ustilago maydis*. *RNA Biol*. Mar;**9**:261-268. Epub 20120301 DOI: 10.4161/rna.19432

Vosjan MJ, Vercammen J, Kolkman JA, Stigter-van Walsum M, Revets H, van Dongen GA. (2012). Nanobodies targeting the hepatocyte growth factor: potential new drugs for molecular cancer therapy. *Mol Cancer Ther*. Apr;**11**:1017-1025. Epub 20120207 DOI: 10.1158/1535-7163.MCT-11-0891

Vu KB, Ghahroudi MA, Wyns L, Muyldermans S. (1997). Comparison of llama VH sequences from conventional and heavy chain antibodies. *Mol Immunol*. Nov-Dec;**34**:1121-1131 DOI: 10.1016/s0161-5890(97)00146-6

Vuchelen A, O'Day E, De Genst E, Pardon E, Wyns L, Dumoulin M, Dobson CM, Christodoulou J, Hsu ST. (2009). (1)H, (13)C and (15)N assignments of a camelid nanobody directed against human alpha-synuclein. *Biomol NMR Assign*. Dec;**3**:231-233 DOI: 10.1007/s12104-009-9182-4

Wagner HJ, Wehrle S, Weiss E, Cavallari M, Weber W. (2018). A Two-Step Approach for the Design and Generation of Nanobodies. *Int J Mol Sci*. Nov 2;**19**. Epub 20181102 DOI: 10.3390/ijms19113444

Wahl R, Wippel K, Goos S, Kamper J, Sauer N. (2010). A novel high-affinity sucrose transporter is required for virulence of the plant pathogen *Ustilago maydis*. *PLoS Biol*. Feb 9;**8**:e1000303. Epub 20100209 DOI: 10.1371/journal.pbio.1000303

Walls AC, Park YJ, Tortorici MA, Wall A, McGuire AT, Veesler D. (2020). Structure, Function, and Antigenicity of the SARS-CoV-2 Spike Glycoprotein. *Cell*. Apr 16;**181**:281-292 e286. Epub 20200309 DOI: 10.1016/j.cell.2020.02.058

Walsh G. (2018). Biopharmaceutical benchmarks 2018. *Nat Biotechnol*. Dec 6;**36**:1136-1145. Epub 2018/12/07 DOI: 10.1038/nbt.4305

Walter JD, Hutter CZ, I. Wyss, M.; , Earp J, Egloff P, Sorgenfrei MH, L. M. Gonda, I. , Meier G, Remm ST, S. Plattet, P. , Seeger MA. (2020). Sybodies targeting the SARS-CoV-2 receptor-binding domain. *bioRxiv*. DOI: 10.1101/2020.04.16.045419

Walter P, Johnson AE. (1994). Signal sequence recognition and protein targeting to the endoplasmic reticulum membrane. *Annu Rev Cell Biol*.**10**:87-119 DOI: 10.1146/annurev.cb.10.110194.000511

Wang J, Majkova Z, Bever CR, Yang J, Gee SJ, Li J, Xu T, Hammock BD. (2015). One-step immunoassay for tetrabromobisphenol a using a camelid single domain antibody-alkaline phosphatase fusion protein. *Anal Chem*.**87**:4741-4748. Epub 20150422 DOI: 10.1021/ac504735p

Wang Q, Zhang Y, Wu L, Niu S, Song C, Zhang Z, Lu G, Qiao C, Hu Y, Yuen KY, et al. (2020a). Structural and Functional Basis of SARS-CoV-2 Entry by Using Human ACE2. *Cell*. May 14;**181**:894-904 e899. Epub 20200409 DOI: 10.1016/j.cell.2020.03.045

Wang Q, Zhong C, Xiao H. (2020b). Genetic Engineering of Filamentous Fungi for Efficient Protein Expression and Secretion. *Front Bioeng Biotechnol*.**8**:293. Epub 2020/04/24 DOI: 10.3389/fbioe.2020.00293

Wang Y, Fan Z, Shao L, Kong X, Hou X, Tian D, Sun Y, Xiao Y, Yu L. (2016). Nanobody-derived nanobiotechnology tool kits for diverse biomedical and biotechnology applications. *Int J Nanomedicine*.**11**:3287-3303. Epub 20160721 DOI: 10.2147/IJN.S107194

Ward M, Wilson LJ, Kodama KH, Rey MW, Berka RM. (1990). Improved production of chymosin in Aspergillus by expression as a glucoamylase-chymosin fusion. *Biotechnology (N Y)*. May;**8**:435-440. Epub 1990/05/01 DOI: 10.1038/nbt0590-435

Ward OP. (2012). Production of recombinant proteins by filamentous fungi. *Biotechnol Adv*. Sep-Oct;**30**:1119-1139. Epub 20110924 DOI: 10.1016/j.biotechadv.2011.09.012

Wege SM, Gejer K, Becker F, Bölker M, Freitag J, Sandrock B. (2021). Versatile CRISPR/Cas9 Systems for Genome Editing in *Ustilago maydis*. *J Fungi (Basel)*. Feb 18;**7**. Epub 20210218 DOI: 10.3390/jof7020149

Weiermüller J, Akermann A, Laudensack W, Chodorski J, Blank LM, Ulber R. (2021). Brewers' spent grain as carbon source for itaconate production with engineered *Ustilago maydis*. *Bioresour Technol*. Sep;**336**:125262. Epub 20210511 DOI: 10.1016/j.biortech.2021.125262

Weinreich DM, Sivapalasingam S, Norton T, Ali S, Gao H, Bhore R, Musser BJ, Soo Y, Rofail D, Im J, et al. (2021). REGN-COV2, a Neutralizing Antibody Cocktail, in Outpatients with Covid-19. *N Engl J Med*. Jan 21;**384**:238-251. Epub 20201217 DOI: 10.1056/NEJMoa2035002

Weinstein JB, Bates TA, Leier HC, McBride SK, Barklis E, Tafesse FG. (2022). A potent alpaca-derived nanobody that neutralizes SARS-CoV-2 variants. *iScience*. Mar 18;**25**:103960. Epub 20220222 DOI: 10.1016/j.isci.2022.103960

Weinzierl G, Leveleki L, Hassel A, Kost G, Wanner G, Bölker M. (2002). Regulation of cell separation in the dimorphic fungus *Ustilago maydis*. *Mol Microbiol*. Jul;**45**:219-231. Epub 2002/07/09 DOI: 10.1046/j.1365-2958.2002.03010.x

Weiss RA, Verrips CT. (2019). Nanobodies that Neutralize HIV. *Vaccines (Basel)*. Jul 31;**7**. Epub 20190731 DOI: 10.3390/vaccines7030077

Wichgers Schreur PJ, van de Water S, Harmsen M, Bermúdez-Méndez E, Drabek D, Grosveld F, Wernike K, Beer M, Aebischer A, Daramola O, et al. (2020). Multimeric single-domain antibody complexes protect against bunyavirus infections. *eLife*.**9**:e52716 DOI: 10.7554/eLife.52716

Wider D, Picard D. (2017). Secreted dual reporter assay with Gaussia luciferase and the red fluorescent protein mCherry. *PLoS One*.**12**:e0189403. Epub 2017/12/09 DOI: 10.1371/journal.pone.0189403

Wierckx N, Miebach K, Ihling N, Hussnätter KP, Buchs J, Schipper K. (2021). Perspectives for the application of Ustilaginaceae as biotech cell factories. *Essays Biochem*. Jul 26;**65**:365-379. Epub 2021/04/17 DOI: 10.1042/EBC20200141

Wijayanti SD, Sutzl L, Duval A, Haltrich D. (2021). Characterization of Fungal FAD-Dependent AA3_2 Glucose Oxidoreductases from Hitherto Unexplored Phylogenetic Clades. *J Fungi (Basel)*. Oct 17;**7**. Epub 20211017 DOI: 10.3390/jof7100873

Wilkinson B, Gilbert HF. (2004). Protein disulfide isomerase. *Biochim Biophys Acta*. Jun 1;**1699**:35-44 DOI: 10.1016/j.bbapap.2004.02.017

Wrapp D, De Vlieger D, Corbett KS, Torres GM, Wang N, Van Breedam W, Roose K, van Schie L, Team V-CC-R, Hoffmann M, et al. (2020a). Structural Basis for Potent Neutralization of Betacoronaviruses by Single-Domain Camelid Antibodies. *Cell*. May 28;**181**:1004-1015 e1015. Epub 20200505 DOI: 10.1016/j.cell.2020.04.031

Wrapp D, Wang N, Corbett KS, Goldsmith JA, Hsieh CL, Abiona O, Graham BS, McLellan JS. (2020b). Cryo-EM structure of the 2019-nCoV spike in the prefusion conformation. *Science*. Mar 13;**367**:1260-1263. Epub 20200219 DOI: 10.1126/science.abb2507

Wu A, Peng Y, Huang B, Ding X, Wang X, Niu P, Meng J, Zhu Z, Zhang Z, Wang J, et al. (2020). Genome Composition and Divergence of the Novel Coronavirus (2019-nCoV) Originating in China. *Cell Host Microbe*. Mar 11;**27**:325-328. Epub 20200207 DOI: 10.1016/j.chom.2020.02.001

Wu YI, Frey D, Lungu OI, Jaehrig A, Schlichting I, Kuhlman B, Hahn KM. (2009). A genetically encoded photoactivatable Rac controls the motility of living cells. *Nature*. Sep 3;**461**:104-108. Epub 20090819 DOI: 10.1038/nature08241

Xenaki KT, Dorrestijn B, Muns JA, Adamzek K, Doulkeridou S, Houthoff H, Oliveira S, van Bergen En Henegouwen PM. (2021). Homogeneous tumor targeting with a single dose of HER2-targeted albumin-binding domain-fused nanobody-drug conjugates results in long-lasting tumor remission in mice. *Theranostics*.**11**:5525-5538. Epub 20210313 DOI: 10.7150/thno.57510

Xu H, Zhong L, Deng J, Peng J, Dan H, Zeng X, Li T, Chen Q. (2020a). High expression of ACE2 receptor of 2019-nCoV on the epithelial cells of oral mucosa. *Int J Oral Sci*. Feb 24;**12**:8. Epub 20200224 DOI: 10.1038/s41368-020-0074-x

Xu J, Xu K, Jung S, Conte A, Lieberman J, Mücksch F, Lorenzi JCC, Park S, Schmidt F, Wang Z, et al. (2021). Nanobodies from camelid mice and llamas neutralize SARS-CoV-2 variants. *Nature*. Jul;**595**:278-282. Epub 20210607 DOI: 10.1038/s41586-021-03676-z

Xu Y, Wang Y-h, Liu T-q, Zhang H, Zhang H, Li J. (2018). The GlaA signal peptide substantially increases the expression and secretion of α-galactosidase in Aspergillus niger. *Biotechnology letters*. 2018/06/01;**40**:949-955 DOI: 10.1007/s10529-018-2540-5

Xu Y, Xu Y, Bi B, Hou M, Yao L, Du Q, He A, Liu Y, Miao C, Liang X, et al. (2020b). A moldable thermosensitive hydroxypropyl chitin hydrogel for 3D cartilage regeneration in vitro and in vivo. *Acta Biomater*. May;**108**:87-96. Epub 20200405 DOI: 10.1016/j.actbio.2020.03.039

Yang D, Leibowitz JL. (2015). The structure and functions of coronavirus genomic 3' and 5' ends. *Virus Res*. Aug 3;**206**:120-133. Epub 20150228 DOI: 10.1016/j.virusres.2015.02.025

Yau KY, Dubuc G, Li S, Hirama T, Mackenzie CR, Jermutus L, Hall JC, Tanha J. (2005). Affinity maturation of a V(H)H by mutational hotspot randomization. *J Immunol Methods*. Feb;**297**:213-224. Epub 20050120 DOI: 10.1016/j.jim.2004.12.005

Younes I, Rinaudo M. (2015). Chitin and chitosan preparation from marine sources. Structure, properties and applications. *Mar Drugs*. Mar 2;**13**:1133-1174. Epub 20150302 DOI: 10.3390/md13031133

Zainol Abidin NA, Kormin F, Zainol Abidin NA, Mohamed Anuar NAF, Abu Bakar MF. (2020). The Potential of Insects as Alternative Sources of Chitin: An Overview on the Chemical Method of Extraction from Various Sources. *Int J Mol Sci*. Jul 15;**21**. Epub 20200715 DOI: 10.3390/ijms21144978

Zaki AM, van Boheemen S, Bestebrör TM, Osterhaus AD, Fouchier RA. (2012). Isolation of a novel coronavirus from a man with pneumonia in Saudi Arabia. *N Engl J Med*. Nov 8;**367**:1814-1820. Epub 20121017 DOI: 10.1056/NEJMoa1211721

Zander S, Baumann S, Weidtkamp-Peters S, Feldbrügge M. (2016). Endosomal assembly and transport of heteromeric septin complexes promote septin cytoskeleton formation. *J Cell Sci*. Jul 15;**129**:2778-2792. Epub 20160601 DOI: 10.1242/jcs.182824

Zander S, Muntjes K, Feldbrügge M. (2018). RNA Live Imaging in the Model Microorganism *Ustilago maydis*. *Methods Mol Biol*.**1649**:319-335 DOI: 10.1007/978-1-4939-7213-5_21

Zeitler M, Steringer JP, Müller HM, Mayer MP, Nickel W. (2015). HIV-Tat Protein Forms Phosphoinositide-dependent Membrane Pores Implicated in Unconventional Protein Secretion. *J Biol Chem*. Sep 4;**290**:21976-21984. Epub 20150716 DOI: 10.1074/jbc.M115.667097

Zhang F, Wei H, Wang X, Bai Y, Wang P, Wu J, Jiang X, Wang Y, Cai H, Xu T, et al. (2017). Structural basis of a novel PD-L1 nanobody for immune checkpoint blockade. *Cell Discov*.**3**:17004. Epub 20170307 DOI: 10.1038/celldisc.2017.4

Zhou P, Yang XL, Wang XG, Hu B, Zhang L, Zhang W, Si HR, Zhu Y, Li B, Huang CL, et al. (2020). A pneumonia outbreak associated with a new coronavirus of probable bat origin. *Nature*. Mar;**579**:270-273. Epub 20200203 DOI: 10.1038/s41586-020-2012-7

Zhu N, Zhang D, Wang W, Li X, Yang B, Song J, Zhao X, Huang B, Shi W, Lu R, et al. (2020a). A Novel Coronavirus from Patients with Pneumonia in China, 2019. *N Engl J Med*. Feb 20;**382**:727-733. Epub 20200124 DOI: 10.1056/NEJMoa2001017

Zhu Y, Huan S, Bai L, Ketola A, Shi X, Zhang X, Ketoja JA, Rojas OJ. (2020b). High Internal Phase Oil-in-Water Pickering Emulsions Stabilized by Chitin Nanofibrils: 3D Structuring and Solid Foam. *ACS Appl Mater Interfaces*. Mar 4;**12**:11240-11251. Epub 20200220 DOI: 10.1021/acsami.9b23430

Zhuang J, Yin J, Lv S, Wang B, Mu Y. (2020). Advanced "lab-on-a-chip" to detect viruses - Current challenges and future perspectives. *Biosens Bioelectron*. Sep 1;**163**:112291. Epub 20200512 DOI: 10.1016/j.bios.2020.112291

Zimmermann I, Egloff P, Hutter CAJ, Kuhn BT, Brauer P, Newstead S, Dawson RJP, Geertsma ER, Seeger MA. (2020). Generation of synthetic nanobodies against delicate proteins. *Nat Protoc*. May;**15**:1707-1741. Epub 20200408 DOI: 10.1038/s41596-020-0304-x

6.2 Directory of publications

The following chapter provides information on author contributions to individual studies and publications. Information of contributions to individual figures is described in chapter "8.3 Directory of figures". Chapters "1 Introduction" and "4 Discussion" were prepared for this dissertation and are not published elsewhere. Data presented in Chapter "3 A novel strategy for Sars-CoV2 detection utilizing a chitin surface and components derived from the fungal microorganism *Ustilago maydis"* is soon to be published but not submitted yet.

This thesis consists of the following published research articles:

Chapter 2:

A novel potent carrier for unconventional protein export in *Ustilago maydis*

Magnus Philipp, Kai Hußnätter, Michele Reindl, Kira Müntjes, Michael Feldbrügge, Kerstin Schipper (2021). *Frontiers in Cell and Developmental Biology. Section: Membrane Traffic. Special issue: Unconventional protein secretion: From Basic Mechanisms to Dysregulation in Disease.*

MP, KPH and MR designed the experiments. MP and KPH conducted the experiments. KS, KM and MF supervised the project. KS, MP and KM prepared the manuscript with input from all co-authors. MP and KH prepared figures and tables.

Further contributions to publications that are not part of this thesis:

Establishing Polycistronic Expression in the Model Microorganism *Ustilago maydis*

Kira Müntjes, Magnus Philipp, Lisa Hüsemann, Nicole Heucken, Stefanie Weidtkamp-Peters, Kerstin Schipper, Matias D. Zurbriggen, Michael Feldbrügge (2020). *Frontiers in Microbiology.*

MP generated the polycistronic MEL-D(R) production construct and strain, conducted according experiments and designed figure 5. MP gave input to preparation of the manuscript.

Publication summary:

Eukaryotic microorganisms use monocistronic mRNAs to encode proteins. For synthetic biological approaches like metabolic engineering, precise co-expression of several proteins in space and time is advantageous. A straightforward approach is the application of viral 2A peptides to design synthetic polycistronic mRNAs in eukaryotes. During translation of these peptides the ribosome stalls, the peptide chain is released and the ribosome resumes translation. Thus, two independent polypeptide chains can be encoded from a single mRNA when a 2A peptide sequence is placed inbetween the two open reading frames. Here, we establish such a system in the well-studied model microorganism *Ustilago maydis*. Using two fluorescence reporter proteins, we compared the activity of five viral 2A peptides. Their activity was evaluated *in vivo* using fluorescence microscopy and validated using fluorescence resonance energy transfer (FRET). Activity ranged from 20 to 100% and the best performing 2A peptide was P2A from porcine teschovirus-1. As proof of principle, we followed regulated gene expression efficiently over time and synthesised a tri-cistronic mRNA encoding biosynthetic enzymes to produce mannosylerythritol lipids (MELs). In essence, we evaluated 2A peptides *in vivo* and demonstrated the applicability of 2A peptide technology for *U. maydis* in basic and applied science.

Controlling Unconventional Secretion for Production of Heterologous Proteins in *Ustilago maydis* through Transcriptional Regulation and Chemical Inhibition of the Kinase Don3

Kai P. Hussnätter, Magnus Philipp, Kira Müntjes, Michael Feldbrügge, Kerstin Schipper (2021) Journal of Fungi (3;7(3):179)

M.P. generated strains planned by K.P.H. for autoinduction experiment. M.P. assisted in protein purification and conducted ELISA depicted in Fig. 7. M.P. gave input to the preparation of the manuscript.

Publication summary:

Heterologous protein production is a highly demanded biotechnological process. Secretion of the product to the culture broth is advantageous because it drastically reduces downstream processing costs. We exploit unconventional secretion for heterologous protein expression in the fungal model microorganism *Ustilago maydis*. Proteins of interest are fused to carrier chitinase Cts1 for export via the fragmentation zone of dividing yeast cells in a lock-type mechanism. The kinase Don3 is essential for functional assembly of the fragmentation zone and hence, for release of Cts1-fusion proteins. Here, we are first to develop regulatory systems for unconventional protein secretion using Don3 as a gatekeeper to control when export occurs. This enables uncoupling the accumulation of biomass and protein synthesis of a product of choice from its export. Regulation was successfully established at two different levels using transcriptional and post-translational induction strategies. As a proof-of-principle, we applied autoinduction based on transcriptional *don3* regulation for the production and secretion of functional anti-Gfp nanobodies. The presented developments comprise tailored solutions for differentially prized products and thus constitute another important step towards a competitive protein production platform.

A plea for the integration of Green Toxicology in sustainable bioeconomy strategies - Biosurfactants and microgel-based pesticide release systems as examples

Sarah Johann, Fabian G. Weichert, Lukas Schröer, Lucas Stratemann, Christoph Kämpfer, Thomas-Benjamin Seiler, Sebastian Heger, Alexander Töpel, Tim Sassmann, Andrij Pich, Felix Jakob, Ulrich Schwaneberg, Peter Stoffels, Magnus Philipp, Marius Terfrüchte, Anita Loeschke, Kerstin Schipper, Michael Feldbrügge, Nina Ihling, Jochen Büchs, Isabel Bator, Till Tiso, Lars M. Blank, Martina Roß-Nickoll, Henner Hollert (2022). *Journal of Hazardous Materials (426, 127800).*

MP produced and provided MEL samples for toxicology experiments in this study.

Publication summary:

A key aspect of the transformation of the economic sector towards a sustainable bioeconomy is the development of environmentally friendly alternatives for hitherto used chemicals, which have negative impacts on environmental health. However, the implementation of an ecotoxicological hazard

assessment at early steps of product development to elaborate the most promising candidates of lowest harm is scarce in industry practice. The present article introduces the interdisciplinary proof-of-concept project GreenToxiConomy, which shows the successful application of a Green Toxicology strategy for biosurfactants and a novel microgel-based pesticide release system. Both groups are promising candidates for industrial and agricultural applications and the ecotoxicological characterization is yet missing important information. An iterative substance- and application-oriented bioassay battery for acute and mechanism-specific toxicity within aquatic and terrestrial model species is introduced for both potentially hazardous materials getting into contact with humans and ending up in the environment. By applying *in silico* QSAR-based models on genotoxicity, endocrine disruption, skin sensitization and acute toxicity to algae, daphnids and fish, individual biosurfactants resulted in deviating toxicity, suggesting a pre-ranking of the compounds. Experimental toxicity assessment will further complement the predicted toxicity to elaborate the most promising candidates in an efficient pre-screening of new substances.

6.3 Directory of figures

Contribution to design: *****

Contribution in form of generated data: **+**

***Figure 1.1:** domain Schematic representation of mAbs and HcAbs

Figure 1.2: Schematic overview of nanobody generation protocol

***Figure 1.3**: Structure of the Sars-CoV2 Spike

***Figure 1.4:** Known unconventional secretion pathways

Figure 1.5: Model of lock-type unconventional secretion

+*Figure 2.1: Jps1 is unconventionally secreted and serves as an alternative carrier for Gus export.

+*Figure 2.2: Inducible secretion of Gus-Jps1 via transcriptional regulation of *don3.*

+*Figure 2.3: Efficient Jps1-mediated export of firefly luciferase as a new reporter for unconventional secretion.

+*Figure 2.4: Export of functional bi-specific Sars-CoV2 sybodies using Jps1 as a carrier for unconventional secretion.

+*Supplementary Figure 2.1: Cell morphology and Cts1 activity of Gus-Cts1 and Gus-Jps1 producing strains.

+*Supplementary Figure 2.2: Morphology and fitness of strains exporting firefly luciferase FLuc.

+***Supplementary Figure 2.3:** Quantitative Western blot analysis of Gus-Cts1 and Gus-Jps1 secretion.

+***Figure 3.1:** Initial screen of anti-Sars-CoV2 nanobody-Cts1 fusions.

+***Figure 3.2:** In vivo investigation of anti-Sars-CoV2 nanobody-Cts1 fusions.

+***Figure 3.3:** Chitin binding capacity of Cts1.

+***Figure 3.4:** Plate based and chitin bead-based sandwich ELISA of nanobody-Cts1 fusions against Sars-CoV2 RBD.

+***Figure 3.5**: Chitin based antigen test.

+***Figure 3.6:** Characterization of a functionalized anti Gfp nanobody

+***Figure 3.7:** Characterization of a functionalized anti Sars-CoV2 nanobody

+***Figure 3.8:** $Sy^{68/15}$-Apex2-Jps1 based, direct RBD detection in Sandwich ELISA

+***Figure 4.1:** Model for a novel chitin-based antigen test

6.4 Acknowledgements

First of all, on an academic level, I want to thank every single fellow RabXpress PhD student who came before me for bringing the unconventional secretion system to life, as this work was less about discovery of new components and more about connecting loose threads that had been laid out for me.

My first big thanks are addressed to Michael for guiding me on this academic journey. From an open ear and interest for the work of a mere bachelor student in 2015 to enabling “Usti vs. Corona” in 2020 and working through this project with me. Thank you!

I would like to thank Kerstin for great mentorship, allowing me great freedom of research when possible and correcting me when I was straying too far from the path. Your commitment to my work and RabXpress as a whole, despite not just one but two children joining you during the course of my PhD thesis, has been awesome!

I also want to thank Julia Frunzke for great academic guidance from my masters onwards and for taking the time and effort to mentor me during this thesis.

Next, big thanks go out to the entire former and present RabXpress crew! Jan-Peter, thank you for the guidance, as I was taking my first steps in the Lab. Marius, thank you for taking over, teaching me the secret arts of the ELISA and generally being a great labmate! Jörn, Sanchi, Marta, Flippo, Sabrina, Alex, Malte and Lukas thank you for all the fun and great lab atmosphere!
I especially want to highlight Michele, Kai, Silke, Kira and Pesto for forming the core of my PhD experience, providing great fun and friendship between experimental and organizational chaos, and always putting a smile on my face, no matter what happened on any given day. Thank you for great friendship that lasted to this day. Endfit!

Tina! Your attitude and character are awesome and the lab-help you provided during my last year in the lab was invaluable. I could not have done this without you. Thank you so much!

Special thanks also go out to the Südfront! Anton, Lea, Natascha, Kai, Joana, may your blots never be empty, your band sizes correct and your beer always full.

And not to forget the boulder- and Numenera-crews: Joana, Pesto, Kai, Woogie, Nina, Markus, it was a pleasure playing, climbing or both with you all!

I also want to thank Vera, Uli, Senthil, Sri, Sai, Carl, Lilli, Lesley, Summia, Minerva, Ute, Theresa and Simone for the great atmosphere and all the small and big help you provided to me over the years!

Peter und Kai, danke für die ganze Ballerei, von frühen Weihnachtsparties bis zu meiner Hochzeit und darüber hinaus!

Grüße und Liebe gehen raus an die OdbE-Crew! Danke, dass ihr Jungs in dieser Zeit geduldig mit mir wart, meine ewigen Tiraden ertragen habt und einfach von Anfang an immer für mich da wart. Auf viele weitere Jahre zusammen!

Vanessa: Du musstest in den letzten vier Jahren echt ne Menge mit mir durchmachen. Danke, dass du immer bei mir warst und mich immer unterstützt hast, egal wie anstrengend es werden konnte. Ich liebe dich!

Und das Beste zum Schluss: Mama und Papa. Ohne euch wäre ich heute nicht der, der ich bin und ohne eure fortwährende Unterstützung hätte ich es niemals so weit gebracht. Ihr seid das Rückgrat, auf dem jeder einzelne meiner Erfolge gebaut ist. Ich danke Euch.